The role of innate lymphoid cells 1 and natural killer cells during drug induced liver damage

DISSERTATION

submitted to the
Faculty of Chemistry and Biological Chemistry
at the Technische Universität Dortmund
for the degree of
Doctor of Natural Sciences

Sarah Metzler (geb. Schlüter), M. Sc.

Dortmund 2022

First Reviewer: **Prof. Dr. Carsten Watzl**

Second Reviewer: **Prof. Dr. Jan Hengstler**

Eidesstattliche Versicherung (Affidavit)

Name, Vorname
(Surname, first name)

Matrikel-Nr.
(Enrolment number)

Belehrung:

Wer vorsätzlich gegen eine die Täuschung über Prüfungsleistungen betreffende Regelung einer Hochschulprüfungsordnung verstößt, handelt ordnungswidrig. Die Ordnungswidrigkeit kann mit einer Geldbuße von bis zu 50.000,00 € geahndet werden. Zuständige Verwaltungsbehörde für die Verfolgung und Ahndung von Ordnungswidrigkeiten ist der Kanzler/die Kanzlerin der Technischen Universität Dortmund. Im Falle eines mehrfachen oder sonstigen schwerwiegenden Täuschungsversuches kann der Prüfling zudem exmatrikuliert werden, § 63 Abs. 5 Hochschulgesetz NRW.

Die Abgabe einer falschen Versicherung an Eides statt ist strafbar.

Wer vorsätzlich eine falsche Versicherung an Eides statt abgibt, kann mit einer Freiheitsstrafe bis zu drei Jahren oder mit Geldstrafe bestraft werden, § 156 StGB. Die fahrlässige Abgabe einer falschen Versicherung an Eides statt kann mit einer Freiheitsstrafe bis zu einem Jahr oder Geldstrafe bestraft werden, § 161 StGB.

Die oben stehende Belehrung habe ich zur Kenntnis genommen:

Official notification:

Any person who intentionally breaches any regulation of university examination regulations relating to deception in examination performance is acting improperly. This offence can be punished with a fine of up to EUR 50,000.00. The competent administrative authority for the pursuit and prosecution of offences of this type is the chancellor of the TU Dortmund University. In the case of multiple or other serious attempts at deception, the candidate can also be unenrolled, Section 63, paragraph 5 of the Universities Act of North Rhine-Westphalia.

The submission of a false affidavit is punishable.

Any person who intentionally submits a false affidavit can be punished with a prison sentence of up to three years or a fine, Section 156 of the Criminal Code. The negligent submission of a false affidavit can be punished with a prison sentence of up to one year or a fine, Section 161 of the Criminal Code.

I have taken note of the above official notification.

Ort, Datum
(Place, date)

Unterschrift
(Signature)

Titel der Dissertation:
(Title of the thesis):

Ich versichere hiermit an Eides statt, dass ich die vorliegende Dissertation mit dem Titel selbstständig und ohne unzulässige fremde Hilfe angefertigt habe. Ich habe keine anderen als die angegebenen Quellen und Hilfsmittel benutzt sowie wörtliche und sinngemäße Zitate kenntlich gemacht.
Die Arbeit hat in gegenwärtiger oder in einer anderen Fassung weder der TU Dortmund noch einer anderen Hochschule im Zusammenhang mit einer staatlichen oder akademischen Prüfung vorgelegen.

I hereby swear that I have completed the present dissertation independently and without inadmissible external support. I have not used any sources or tools other than those indicated and have identified literal and analogous quotations.

The thesis in its current version or another version has not been presented to the TU Dortmund University or another university in connection with a state or academic examination.*

*Please be aware that solely the German version of the affidavit ("Eidesstattliche Versicherung") for the PhD thesis is the official and legally binding version.

Ort, Datum
(Place, date)

Unterschrift
(Signature)

TABLE OF CONTENTS

SUMMARY

Worldwide, approximately two million deaths per year are caused by different liver diseases. The understanding of the underlying mechanisms causing liver diseases remain incomplete. In the last two decades, the involvement of different immune cells during liver disease progression, regeneration and homeostasis have been closely investigated and offered new therapeutic strategies and targets.

Recently, natural killer (NK) cells have been observed to contribute to the progression of drug induced liver injury (DILI). *In vitro* results of primary human hepatocytes (PHH) and human hepatocyte cell lines pretreated with valproic acid, ketoconazole, promethazine and isoniazid showed enhanced expression of activating NK cell ligands. Moreover, enhanced NK cell activity was observed which was characterized by the higher interferon gamma (IFNγ) production and increased cytotoxicity against the pretreated hepatocytes. In order to validate the *in vivo* relevance of these findings and investigate the DILI mechanism, the first aim was to reproduce the enhanced NK cell activity ligand expression in drug pretreated primary mouse hepatocytes (PMH). The data of drug pretreated PMH revealed higher expression levels of activating NK cell ligands which were more pronounced in combination with tumor necrosis factor alpha (TNFα). In the next step, the aim was to establish a drug induced liver injury mouse model with the most promising drug valproic acid. The attempts to establish a valproic acid induced liver injury mouse model were not successful, since the treatments did not cause increased NK cell numbers in the liver, higher expression of activating NK cell ligands on hepatocytes nor liver damage.

During the last decade, another immune cell type was identified which seem to be involved in liver damage, regenaration and homeostasis: innate lymphoid cell 1 (ILC1). Until today, there is not much known about ILC1s, however they have been described to possess a memory potential. Therefore, another aim of this thesis was to identify and characterize the memory potential of ILC1s after multiple applications of the hepatotoxic compound carbon tetrachloride (CCl_4). After multiple doses of CCl_4 injected in a 30 days interval, memory like ILC1s were discovered which were able to produce more interferon gamma (IFNγ). Further experiments revealed a transient effect of ILC1s in the liver, since higher cell numbers were observed on day one but until day three, the ILC1 cell numbers were again comparable to control cell numbers. Additionally, the memory effect of ILC1s is long-lasting. Nevertheless, the localization and function of memory like ILC1s in the liver need to be further investigated to evaluate the possible contribution to liver disease progression, regeneration and homeostasis.

ZUSAMMENFASSUNG

Weltweit werden circa zwei Millionen Todesfälle pro Jahr durch unterschiedliche Lebererkrankungen verursacht, jedoch bleibt das Verständnis der zugrunde liegenden Mechanismen lückenhaft. In den letzten zwei Jahrzenten wurde die Beteiligung der verschiedenen Immunzellen während des Fortschreitens und der Regeneration einer Leberschädigung, sowie während der Homöostase genauer untersucht. Die daraus gewonnenen Erkenntnisse führten zu möglichen neuen Strategien zur therapeutischen Behandlung von Lebererkrankungen.

Eine dieser kürzlich gewonnenen Erkenntnis bezieht sich auf die natürlichen Killerzellen (NK Zellen), die zum Fortschreiten einer medikamenteninduzierten Leberschädigung (DILI) beitragen. Dabei zeigten in-vitro Ergebnisse, dass primäre humane Hepatozyten und humane Hepatozyten-Zelllinien, die zuvor mit Valproinsäure, Ketoconazol, Promethazin und Isoniazid behandelt wurden, eine höhere Expression von aktivierenden NK Zellliganden aufweisen. Darüber hinaus wurde eine erhöhte NK Zellaktivität beobachtet, die durch eine höhere Interferon gamma (IFNγ)-Produktion und eine erhöhte Zytotoxizität gegenüber den Medikamenten vorbehandelten Hepatozyten gekennzeichnet war. Um die in-vivo Relevanz dieser Ergebnisse zu validieren und den zugrunde liegenden Mechanismus genauer zu untersuchen, war das erste Ziel, die höhere Expression der NK-Zellliganden in medikamenten vorbehandelten primären Maushepatozyten zu reproduzieren. Die Daten von medikamentös vorbehandelter PMH zeigten höhere Expressionsniveaus von aktivierenden NK-Zell-Liganden, die in Kombination mit Tumornekrosefaktor alpha (TNFα) stärker ausgeprägt waren. Im nächsten Schritt sollte ein durch Valproinsäure induziertes Leberschädigungs-Mausmodell etabliert werden**.** Jedoch waren die Versuche zur Etablierung eines Valproinsäure-induzierten Leberschädigungs-Mausmodells nicht erfolgreich, da die Behandlungen weder eine erhöhte NK-Zellzahl in der Leber, eine höhere Expression von aktivierenden NK-Zellliganden auf Hepatozyten noch Leberschäden verursachten.

Während des letzten Jahrzehnts wurde ein weiterer Immunzelltyp identifiziert, der an der Homöostase, Regenerierung und Schädigung der Leber beteiligt zu sein scheint: die angeborene lymphatische Zellen 1 (ILC1). Bis heute ist nicht viel über die ILC1 bekannt, jedoch wird in diesen Zellen ein Gedächtnispotential beschrieben. Daher war ein weiteres Ziel dieser Arbeit, das Gedächtnispotential von ILC1 nach mehrfacher Applikation der hepatotoxischen Substanz Tetrachlormethan (CCl4) zu identifizieren und zu charakterisieren. Nach mehreren Injektionen von CCl_4, welches an jedem 30. Tag injiziert wurde, wurden Gedächtnis-ähnliche ILC1 entdeckt, die mehr IFNγ produzieren konnten. Weitere Experimente zeigten einen transienten Effekt von ILC1 in der Leber, wobei am ersten Tag höhere ILC1 Zellzahlen beobachtet wurden, die jedoch am dritten Tag wieder vergleichbar mit den Kontrollzellzahlen waren. Des weiteren ist der Gedächtnis-Effekt von ILC1 langanhaltend. Dennoch müssen die

Lokalisierung und Funktion von Gedächtnis-ähnlichen ILC1 in der Leber weiter untersucht werden, um den möglichen Beitrag zur Progression und Regeneration der Lebererkrankung sowie während der Homöostase bewerten zu können.

ABBREVIATIONS

%	Percent
°C	Celsius degree
3BP2	3 domain-binding protein-2
α SMA	α-smooth muscle actin
ACK	Ammonium-Chloride-Potassium
Akt	Protein kinase B
ALD	Alcohol liver disease
ALT	Alanine-aminotransferase
AML12	Alpha mouse liver 12
Anti-Asialo GM1	Asialo ganglio-N-tetraosylceramide
APAP	Acetaminophen
APC	Antigen-presenting cell
AREG	Amphiregulin
ASK1	Apoptosis signal-regulating kinase 1
AST	Aspartate-aminotransaminases
ATP	Adenosine triphosphate
BCL	B-cell lymphoma
Blimp-1	B lymphocyte-induced maturation protein-1
bp	Base pairs
BrdU	5-bromo-2´-deoxyuridine
c-Kit	Tyrosine-protein kinase
Ca	Calcium
CCL2	C-C chemokine ligand 2
CCl_4	Carbon tetrachloride
CCR2	C-C chemokine receptor 2
CD	Cluster of differentiation
cDNA	Complementary DNA
CIML	Cytokine induced memory like
CLP	Common lymphoid progenitor
cNK	Circulating NK
CNS1	Conserved non-coding sequence 1
Ct	Cycle threshold
CXCL	C-X-C motif chemokine ligand
CXCR	C-X-C motif chemokine receptor
Cyp2e1	cytochrome P450 enzyme 2e1
DAMP	Damage associated molecular patterns

DAP	DNAX-activation protein
DC	Dendritic cell
DEPC	Diethylpyrocarbonate
dH_2O	Distilled water
DILI	Drug induced liver injury
DNA	Deoxyribonucleic acid
DNAM-1	DNAX accessory molecule-1
DMEM	Dulbecco´s modified Eagle´s medium
DMSO	Dimethyl sulfoxide
DPBS	Dulbecco's phosphate-buffered saline
ECM	Extracellular matrix
EDTA	Ethylenediaminetetraacetic acid
EGTA	Ethylene glycol tetraacetic acid
Eomes	Eomesodermin
ERK	Extracellular signal-regulated kinases
FBS	Fetal bovine serum
FcεRI-γ	Fc receptor for IgE
FCS	Fetal calf serum
FSC	Forward scatter
FSC-A	FSC-Area
FSC-H	FSC-Height
GABA	Gamma-aminobutyric acid
GAPDH	Glyceraldehyde-3-phosphate dehydrogenase
GFP	Green fluorescent protein
Grb2	Growth factor receptor-bound protein 2
H&E	Hematoxylin and eosin
H60	Histocompatibility 60 group proteins
HCMV	Human cytomegalovirus
HGF	Hepatocyte growth factor
HLA-E	Major histocompatibility complex I, E
Hobit	Homolog of Blimp-1 in T-cells
HSC	Hepatic stellate cell
i.p.	Intraperitoneally
iDILI	Idiosyncratic DILI
IL	Interleukin
IL-18Rα	IL-18 receptor alpha
ILC	Innate lymphoid cell

IFNγ	Interferon gamma
IRF9	Interferon regulatory factor 9
ITAM	Immunoreceptor tyrosine-based activation motif
JAK	Janus kinase
JNK	C-Jun N-terminal kinase
KC	Kupffer cell
KIR	Killer immunoglobulin-like receptor
KLRG1	Killer cell lectin like receptor G1
KO	Knock out
LAT	Linker for activation of T cells
LFA-1	Lymphocyte Function-associated Antigen 1
Lin	Lineage
LPS	Lipopolysaccharide
lrNK	Liver resident NK
LSEC	Liver sinusoidal endothelial cell
LTi	Lymphoid tissue inducer
Ly6C	Lymphocyte antigen 6 complex
MAP	Mitogen activated protein
MCMV	Mouse cytomegalovirus
MEK1/2	Mitogen-activated protein kinase kinase
MHC	Major histocompatibility complex
MIC	MHC class I-related chain
MMP	Matrix metalloproteases
MPT	Mitochondrial membrane permeability transition
mRNA	Messenger RNA
MULT1	Mouse UL16-binding protein-like transcript 1
NaCl	Sodium chloride
NAFL	Nonalcoholic fatty liver
NAFLD	Nonalcoholic fatty liver disease
NASH	Nonalcoholic steatohepatitis
NaOH	Sodium hydroxide
NAPQI	N-acetyl-p-benzoquinone imine
NCR	Natural cytotoxicity receptor
NF-κB	Nuclear factor kappa B
NFIL3	Nuclear factor, IL-3 regulated
NK	Natural killer
NKG2D	Activating receptor natural-killer group 2, member D

NPC	Non-parenchymal cells
NTAL	Non-T cell activation linker
PBS	Phosphate buffered saline solution
PCNA	Proliferating cell nuclear antigen
PCR	Polymerase chain reaction
PD1	Programmed cell death protein 1
PDGF	Platelet-derived growth factor
Pen/Strep	Penicillin/ Streptomycin
PHH	Primary human hepatocytes
PI3K	Phosphoinositide 3-kinase
PCR	Polymerase chain reaction
PMH	Primary mouse hepatocytes
qRT-PCR	Quantitative reverse transcription real time PCR
Rae1	Retinoic acid early inducible 1
RAG	Recombination activating gene
RNA	Ribonucleic acid
RORα	Retinoid acid receptor-related orphan receptor
RORγT	Retinoid acid receptor-related orphan receptor gamma t
ROS	Reactive oxygen species
RPMI	Roswell Park Memorial Institute
RT	Reverse transcriptase
RT-PCR	Reverse transcriptase polymerase chain reaction
S1PR1	Sphingosine-1-phosphate receptor-1
SD	Standard diet
SLP-76	Lymphocyte cytosolic protein 2
SMAD4	Small mothers against decapentaplegic homolog 4
SSC	Side scatter
STAT	Signal transducer and activator of transcription
SYK	Spleen tyrosine kinase
T-Bet	T-box transcription factor
TGFβ	Transforming growth factor beta
TCF-1	T cell factor 1
Th	T helper
TIMP	Tissue inhibitor of MMPs
TLR	Toll-like receptors
TNFα	Tumor necrosis factor alpha
TRAIL	Tumor necrosis factor-related apoptosis-inducing ligand

T_{regs}	Regulatory T cells
TSLP	Thymic stromal lymphopoietin
ULBP1-6	Unique long 16-binding proteins
Vav1	Guanine nucleotide exchange factor 1
VPA	Valproic acid
Wnt2	Wingless-type MMTV integration site family, member 2
WD	Western-style diet
WT	Wild type
YINM	Tyrosine-based signaling motif
ZAP70	Zeta chain-associated protein kinase 70
Zbtb32	Zinc finger and BTB domain containing 32

1 INTRODUCTION

1.1 Liver

As the largest gland of the body in vertebrates, the weight of the liver accounts for 2 % to 3 % of the total body weight (Kalra et al., 2022; Ulfig, 2011). Located in the right upper quadrant of the abdominal cavity, the main task of the liver is the synthesis, metabolism, storage and distribution of carbohydrates, lipids and proteins. Moreover, another important function is the detoxification, in which hormones as well as exogenous substances like drugs and toxins are metabolized, degraded and excreted to the bile duct (Aumüller, 2010; Lüllmann-Rauch, 2009; Taub, 2004).

1.2 Liver structure

The liver is supplied with blood by two vessels: portal vein and hepatic artery. Approximately 75 % of the blood supply is nutrient-rich and oxygen-poor, coming from the gastrointestinal tract, spleen and pancreas and is transported to the liver through the portal vein. The remaining 25 % blood provides nutrient-poor and oxygen-rich delivered from the aorta to the liver via the hepatic artery (Abdel-Misih & Bloomston, 2010; Kalra et al., 2022).
In general, the liver consists of four lobes, with the right lobe being the largest in human and the left lobe in mice (Lüllmann-Rauch, 2009; Tortora & Derrickson, 2014). These lobes are further subdivided into functional units called lobules (Kalra et al., 2022; Vernon et al., 2022; Welsch, 2010). The classical liver lobule has a hexagonal shape in cross-section with the central vein in the middle of the hexagon (Fig. 1). Around the central vein, the parenchymal liver cells, also called hepatocytes, are radially arranged as cords. At three corners of the hexagon and the periphery of the lobule, the portal triad can be found consisting of a bile duct, a hepatic artery and a portal vein. The blood flows from the portal vein and the hepatic artery to the central vein through small blood vessels also known as liver sinusoids which are localized between the hepatocytes (Ishibashi et al., 2009; Kalra et al., 2022; Tortora & Derrickson, 2014; Vernon et al., 2022; Welsch, 2010). Based on this blood flow, the liver lobule is clustered into three different zones: periportal (zone 1), midzonal (zone 2) and pericentral zone (zone 3). Within these zones, the hepatocytes express enzymes performing distinct metabolic functions (Fig. 2) (Kietzmann, 2017; LeCluyse et al., 2012; Welsch, 2010).

1.3 Liver cell types

Microscopically, the liver lobules contain two different cell types. 80 % of these cells are parenchymal cells, hepatocytes. The remaining 20 % is comprised by the non-parenchymal cells (NPC) including a heterogeneous group of cells: bile duct epithelia cells (cholangiocytes), hepatic progenitor cells, hepatic stellate cells (HSCs), Kupffer cells (KCs), liver sinusoidal

endothelial cells (LSECs) and pit cells (liver specific natural killer cells) (Fig. 2) (Gebhardt, 1992; LeCluyse et al., 2012).

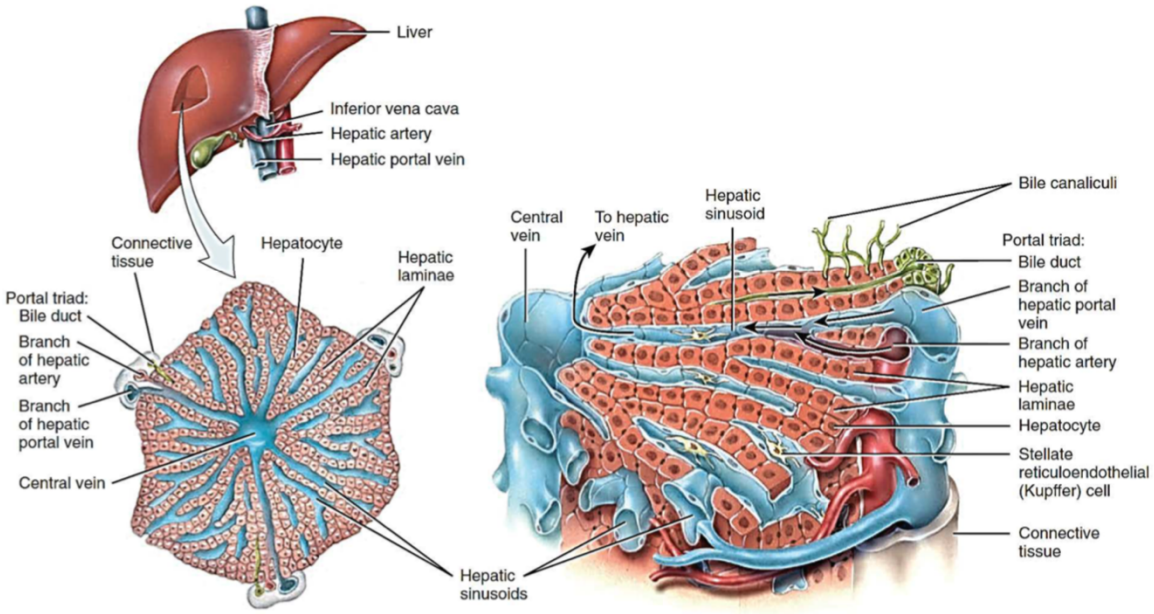

Figure 1. Overview of the structure of a liver lobule.
The liver is supplied with blood via the hepatic artery and the portal vein while the blood leaves the liver through the vena cava to the heart. Divided into smaller functional units, the hepatic lobules have a hexagonal shape and carry blood from the portal triad to the central vein through the sinusoids while the bile flow to the opposite direction. A closer look inside the lobules shows hepatocytes arranged to cords radiating around the central vein (Tortora & Derrickson, 2014).

1.3.1 Hepatocytes

The main type of liver cells are hepatocytes, which belong to one of the largest cell types of the body. These cells are highly polarized and possess three different specific plasma membrane domains having compositional, functional and ultrastructural differences. They are essential for uptake, metabolism and biliary elimination of substances (Krstic, 1997; LeCluyse et al., 2012). One of the domains is the basolateral or also known as sinusoidal domain which constitutes 70 % of the cell surface. The domain faces the liver sinusoids and the perisinusoidal space of Disse and its task is the endo- and exocytosis. Another type is the canalicular or apical domain comprising 15 % of the hepatocyte surface. Together with the apical domain of the opposite hepatocyte, they form the bile canaliculus which are relevant for transport of organic components over the membrane. The last 15 % is comprised by the lateral domain which is localized between the edge of the canalicular domain and the edge of the sinusoidal domain and includes junctional complexes and different cell adhesion molecules (Dufour & Clavien, 2015; Gebhardt, 1992; Krstic, 1997; LeCluyse et al., 2012).

1.3.2 Non-parenchymal cells (NPCs)

Non-parenchymal cells consist of different cell types and most of them are LSECs. LSECs are thin and elongated cells which line the walls of the hepatic sinusoids. These cells are essential for the hepatic homeostasis and hepatic immunity (Gebhardt, 1992; LeCluyse et al., 2012). Firstly, they serve as a selective sieve for different substances like nutrients passing from the blood to the hepatocytes. Secondly, their task is the clearance of blood from macromolecular waste. The involvement in the hepatic immunity is diverse. One of the tasks is to react against foreign pathogens and the induction of immune tolerance to neo-antigens formed during xenobiotic metabolisms. Furthermore, they can also be antigen-presenting cells (APCs) responsible for the induction and proliferation of regulatory T cells and secrete cytokines like interleukin (IL)-1 (Arteta et al., 2010; Caparrós et al., 2020; Dufour & Clavien, 2015; Jenne & Kubes, 2013; Knolle & Wohlleber, 2016; LeCluyse et al., 2012).

Another NPC population, HSCs, is localized in the space of Disse which is between hepatocytes and LSECs (Gebhardt, 1992; LeCluyse et al., 2012). During the non-proliferating, quiescent state, HSCs store retinyl esters (vitamin A) in lipid droplets. Upon activation of HSCs caused by a liver injury, the cells adopt a myofibroblastic phenotype. The phenotype switch results in a loss of vitamin A, production of different types of collagen and various adhesion molecules like fibronectin and laminin. Furthermore, the activated phenotype express α-smooth muscle actin (α SMA) or secrete cytokines like transforming growth factor beta (TGFβ). Because of these features, activated HSCs are the major cell type that contributes to the process of fibrosis in the liver (Jenne & Kubes, 2013; LeCluyse et al., 2012).

Another population of NPCs are cholangiocytes. These intrahepatic bile duct cells are polarized epithelial cells with an apical and basolateral membrane domain. They have several functions like the bile formation and secretion but also the reabsorption of biliary constituents like glucose. Additionally, they also play a role in the immune response by interacting with other immune cells and secretion of cytokines and chemokines (Dufour & Clavien, 2015; LeCluyse et al., 2012).

1.4 Immune cells in the liver

In the hepatic environment, large populations of different immune cells of the adaptive and innate immune system are harbored. They build the first line defense against invading organisms and environmental changes. During inflammation or environmental changes, the liver immune cell population can be dramatically and rapidly changed (Freitas-Lopes et al., 2017; Liaskou et al., 2012).

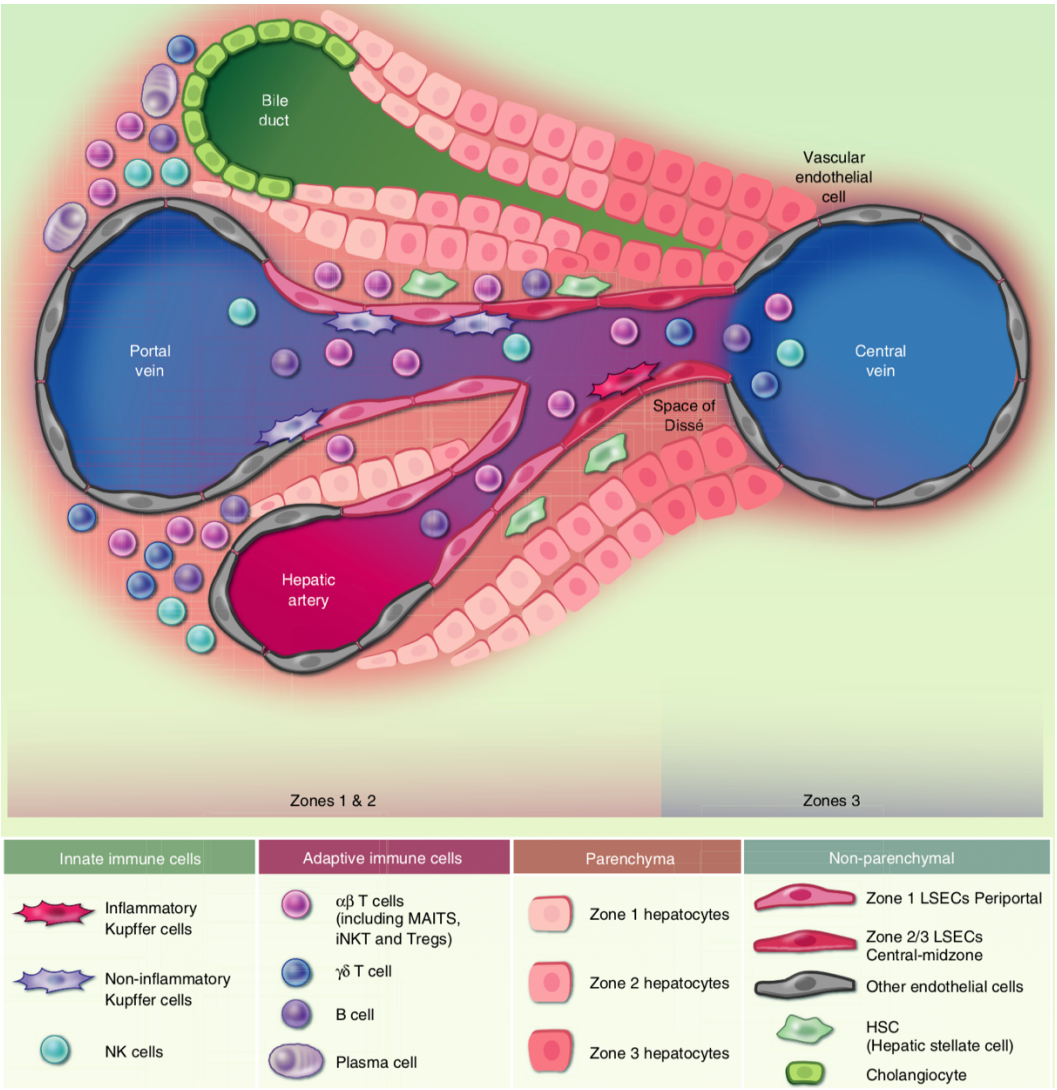

Figure 2. Different cell types in the liver.
Several cell types with different functions are located in the liver. 80 % of the cells are hepatocytes and the remaining 20 % are bile duct epithelia cells (cholangiocytes), hepatic progenitor cells, hepatic stellate cells (HSCs), Kupffer cells (KCs), liver sinusoidal endothelial cells (LSECs) and pit cells (intrahepatic lymphocytes) (Stamataki & Swadling, 2020).

1.4.1 Monocytes and Macrophages

One large immune cell population are the Kupffer cells which belong to the innate immune system. In mice, they are identified as cluster of differentiation (CD) $CD11b^{+}F4/80^{hi}$. Localized within the sinusoids on the lumen side of endothelial cells, the Kupffer cells are liver-resident macrophages. They possess an endocytic and phagocytic capacity removing rapidly and efficiently tissue and cellular debris, bacterial products and endotoxins derived from the gastrointestinal tract from the blood. These macrophages are highly heterogeneous since the KCs in the periportal area are larger and involved in phagocytosis, while centrilobular KCs produce more cytokines and inflammatory responses (Jenne & Kubes, 2013; LeCluyse et al., 2012). Therefore, both KCs types are part of the innate immune response producing proinflammatory cytokines and chemokines like TNFα, C-C chemokine ligand 2 (CCL2), IL-1

and IL-6 and recruit other immune cells (LeCluyse et al., 2012; Stamataki & Swadling, 2020). Furthermore, the activated periportal and centrilobular KCs are necessary for the liver regeneration. Some of these produced cytokines are able to initiate the hepatocyte proliferation, whereas the activated KCs start to produce anti-inflammatory cytokines like IL-10. In addition, the liver fibrosis can also be reversed (Jenne & Kubes, 2013; LeCluyse et al., 2012; Petrasek et al., 2013). However, in most cases, researchers do not precisely distinguish between Kupffer cells, monocytes and monocyte derived macrophages, although these two types of macrophages have different precursor (Markose et al., 2018).

Monocytes are bone marrow-derived leukocytes which maintain in the spleen or circulate in the blood during steady state. They have two different subsets in mice: inflammatory monocytes expressing high levels of lymphocyte antigen 6 complex (Ly6C), and patrolling monocytes which are $Ly6C^{lo}$. Interestingly, $Ly6C^{hi}$ monocytes are the precursors for the more mature $Ly6C^{lo}$ subset (Freitas-Lopes et al., 2017; Robinson et al., 2016; Y. Wang & Zhang, 2019). As the name already reveals, the task of patrolling monocytes is to check the vasculature via the chemokine receptor CX_3CR1 and the integrin Lymphocyte Function-associated Antigen 1 (LFA-1) during steady state. Upon inflammation, $Ly6C^{hi}$ monocytes are recruited from the spleen and bone marrow to the injury site in a C-C chemokine receptor 2 (CCR2) – CCL2-dependent manner (Liaskou et al., 2012; Markose et al., 2018). These recruited, inflammatory monocytes differentiate to monocyte-derived macrophages. In contrast to the $CD11b^{+}F4/80^{hi}$ Kupffer cells, monocyte-derived macrophages are $CD11b^{hi}F4/80^{+}CX_3CR1^{hi}$ and therefore still express the chemokine receptor which is not expressed on Kupffer cells at all (Brempelis & Crispe, 2016; Triantafyllou et al., 2018). Nevertheless, upon injury, the amount of Kupffer cells decrease and the infiltrated $Ly6C^{hi}$ monocyte-derived macrophages aggregate around the injured area. Moreover, these cells have a pro-inflammatory transcriptional profile and it is also described that they may exaggerate hepatic injury. But during the resolution phase, monocyte-derived macrophages acquire a pro-reparative phenotype being $CD11b^{hi}F4/80^{+}Ly6C^{lo}$ and promote angiogenesis, clearance of necrotic area and tissue remodeling (Cheng et al., 2021; Markose et al., 2018; Triantafyllou et al., 2018; Y. Wang & Zhang, 2019).

1.4.2 Dendritic cells

In response to an inflammation, monocytes can not only differentiate to monocyte-derived macrophages but also to dendritic cells (DCs). These cells are located in the portal area of the liver and can be roughly divided into different subsets: myeloid and plasmacytoid DCs (Markose et al., 2018; Robinson et al., 2016). They have several functions like the detection of homeostatic imbalances, cytokine and growth factor secretion and antigen presentation. Therefore, DCs process antigens for T helper (Th) cell presentation to induce T cell activation

and differentiation. Furthermore, in response to antitumoral or antiviral immunity, they present extracellular antigens via major histocompatibility complex (MHC)-I to cytotoxic T cells (Cardoso et al., 2021). In the liver, DCs seem to have regenerative and repair properties by releasing the anti-inflammatory cytokine IL-10 and downregulating the pro-inflammatory IFNγ messenger ribonucleic acid (mRNA) (Markose et al., 2018).

1.4.3 Neutrophils

In the healthy liver, there are relatively low numbers of neutrophils. Upon inflammation, debris of dying hepatocytes and the release of cytokines like TNFα and IL-1 by activated Kupffer cells, activates and recruits neutrophils from the blood circulation into the hepatic sinusoids. The neutrophils accumulate and clear necrotic debris. Nevertheless, these cells exaggerate the inflammation and promote severe liver damage (Liaskou et al., 2012; Markose et al., 2018).

1.4.4 B cells

Up to 50 % of the intrahepatic lymphocytes in mice are B cells. In contrast, human livers comprise only 5 %. Although the murine liver has a lot of B cells, there is not much known about their function in the liver (Freitas-Lopes et al., 2017; Patel et al., 2021). In general, the function of these cells includes antibody production, antigen presentation, cytokine secretion and immune response regulation. A recent study showed, that B cells may contribute through IL-6 production to the differentiation of hepatic stellate cells into myofibroblasts resulting in collagen deposition. Nevertheless, B cells and their role in the liver remains to be further explored (Patel et al., 2021).

1.4.5 NKT cells

NKT cells belong to the lymphocytes and express αβ T cell receptor as well as surface markers of natural killer (NK) cells. In the liver, NKT cells can have diverse and opposing roles. After activation, they can secrete pro- and anti-inflammatory cytokines to attract and stimulate other immune cells like DCs or NK cells. Thus, they have an immunoregulatory role and are involved in liver injury, fibrosis and the maintenance of the immune tolerance (Bandyopadhyay et al., 2016; Freitas-Lopes et al., 2017; Liaskou et al., 2012; Y. Wang & Zhang, 2019).

1.4.6 T cells

There are high numbers of T cells localized in the portal area and parenchyma in healthy liver. Their main task is to maintain the tolerance, but they are also involved in hepatic injury and inflammation. Broadly, T cells can be divided into two subsets: $CD4^+$ (T helper or Th cells) and $CD8^+$ (cytotoxic T cells) cells (Freitas-Lopes et al., 2017). Because of the cytokines released by DCs and macrophages in response to microbes, Th cells can be further differentiated. IL-

12 stimulates $CD4^+$ T cells to differentiate into Th1, IL-4 and IL-13 promote the Th2 phenotype, whereas after IL-1, IL-6 and TGFβ stimulation, they develop to Th17 cells (Liaskou et al., 2012). These different cells can in turn counteract the different types of microbes. Moreover, mouse experiments could demonstrate the involvement of $CD4^+$ and $CD8^+$ cells in the liver regeneration through the lymphotoxin axis. Furthermore, during acetaminophen liver injury, Th17 cells secrete IL-17 resulting in neutrophils recruitment which promotes the inflammation (Markose et al., 2018).

1.4.7 Innate lymphoid cells

Innate lymphoid cells (ILC) are belonging to the lymphocytic lineage of immune cells and are derived from the common lymphoid progenitor (CLP) cell (Diefenbach et al., 2014). In difference to B and T cells, ILCs develop in absence of the recombination activating gene (RAG)- dependent rearranged antigen receptors. Instead, ILCs get activated in response to cytokines, signals from microenvironment and engagement of activating and inhibitory receptors which are exclusively germline-encoded (Seillet et al., 2021; Spits et al., 2013). Another characteristic of these cells is their lack of dendritic and myeloid cell phenotypical markers, called lineage marker-negative cells (Lin^-). Additionally, ILCs have a lymphoid morphology and are mostly tissue resident cells (Y. Shen et al., 2018; Spits et al., 2013; Vivier et al., 2018). Their function is diverse including the early immune responses, homeostasis, tissue tolerance and regeneration. But it is also described that they can contribute to pathologic inflammatory responses, autoimmunity and allergies (Colonna, 2018; Vivier et al., 2018).
ILCs are identified as the innate counterparts of T cells (Bal et al., 2020; Colonna, 2018; Vivier et al., 2018). Based on their developmental pathway and cytokine profile, which is similar to the T cell subsets, the ILCs are divided into five different classes (Bal et al., 2020; Vivier et al., 2018). The first identified ILCs are NK cells which mirror the cytotoxic $CD8^+$ T cells. They are dependent on the transcription factors Eomesodermin (Eomes), nuclear factor, IL-3 regulated (NFIL3) and T-box transcription factor TBX21 (T-Bet). In response to the cytokines IL-12 and IL-18, NK cells produce TNFα and IFNγ. Furthermore, they express Granzyme B and Perforin (Bal et al., 2020; Colonna, 2018; Seillet et al., 2021). One of their main tasks is the tumor defense (An et al., 2020). In contrast to the NK cells which are derived from the NK cell precursors, all other ILCs differentiate from common helper innate lymphoid progenitor cells (Liu & Zhang, 2017; Vivier et al., 2018).

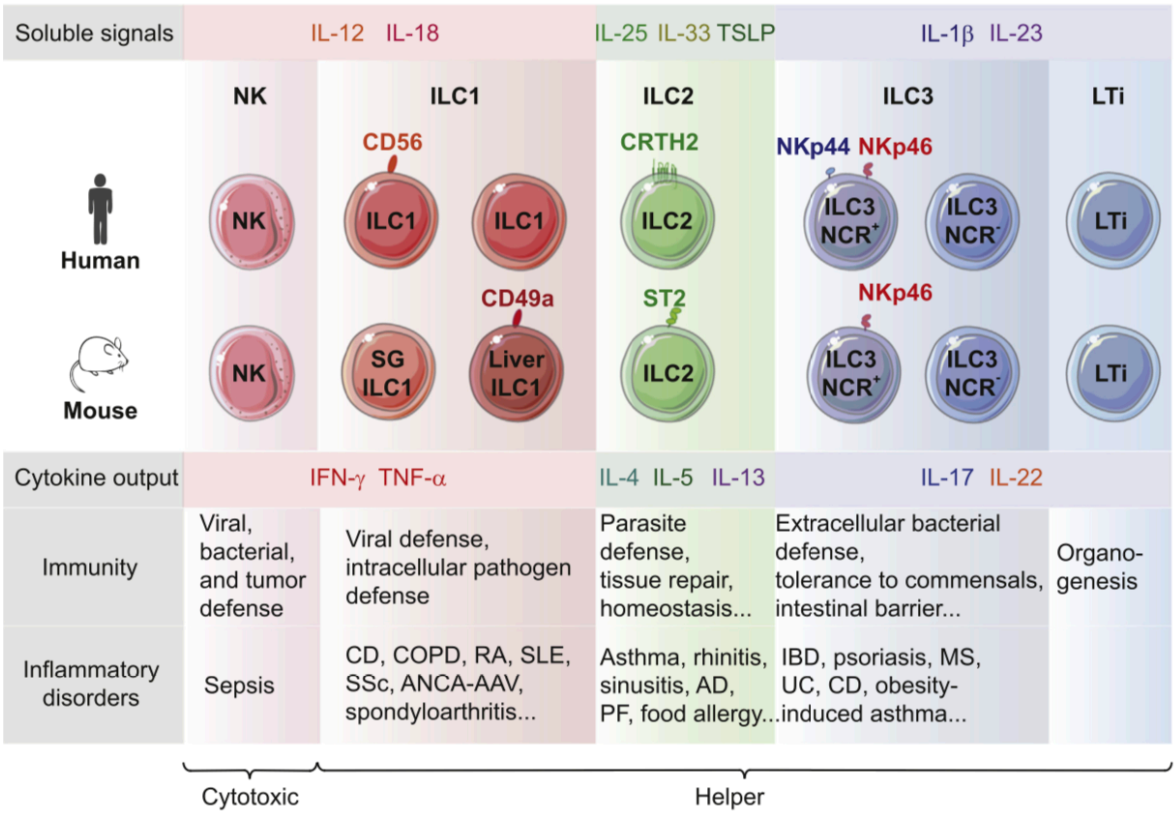

Figure 3. The five different subsets of innate lymphoid cells.
Human and mice have the same subsets of ILCs. But the ILCs do express different markers in different organisms. Nevertheless, the soluble signals and produced cytokines are similar. Furthermore, their task and their impact in inflammatory disorders are similar, too (Guia & Narni-Mancinelli, 2020).

The second subset are the group 1 ILCs (ILC1s) which are phenotypically similar to the NK cells. Like the NK cells, they are dependent on T-Bet but additionally also on the transcription factor homolog of Blimp-1 in T-cells (Hobit). Furthermore, they secrete the same cytokines, whereas the ILC1s produce less perforin. Consequently, they are only weakly cytotoxic and comparable to the Th1 cells. The main differences between NK and ILC1 cells are the tissue residency, the dependence on the transcription factor Eomes, some markers and their development. Their task is the defense against viral and some bacterial infections (Seillet et al., 2021; Vivier et al., 2018).

Group 2 ILCs (ILC2s) produce Th2 associated cytokines IL-4, IL-5, IL-13, IL-9 and amphiregulin (AREG). These cells respond to the cytokines IL-25, IL-33 and thymic stromal lymphopoietin (TSLP) and express large amounts of the transcription factor GATA3 but also low levels of retinoid acid receptor-related orphan receptor alpha (RORα). One of their main tasks is tissue repair (An et al., 2020; Vivier et al., 2018).

Another subset, Group 3 ILCs (ILC3s), are comparable to the T cell subset Th17 depending on the transcription factor retinoid acid receptor-related orphan receptor gamma t (RORγT) (Spits et al., 2013). ILC3s mainly produce IL-22 but a proportion of ILC3s can also produce

IL-17 in response to IL-1β and IL-23 (An et al., 2020; Spits et al., 2013). They are able to mediate the tolerance to chemical toxins (Vivier et al., 2018).

The last subset of ILCs are the lymphoid tissue inducer (LTi) cells. Although these cells are similar to ILC3s regarding the dependence on RORγT and the produced cytokines, ILC3s and LTi have different developmental pathways. The function of LTi cells is the formation of secondary lymphoid organs (An et al., 2020; Vivier et al., 2018).

A special feature of the ILCs is their ability to adopt the phenotype and the function of another ILC population when stimulated with different cytokines. This phenomenon is called plasticity (Fig. 4) (Bal et al., 2020; Vivier et al., 2018).

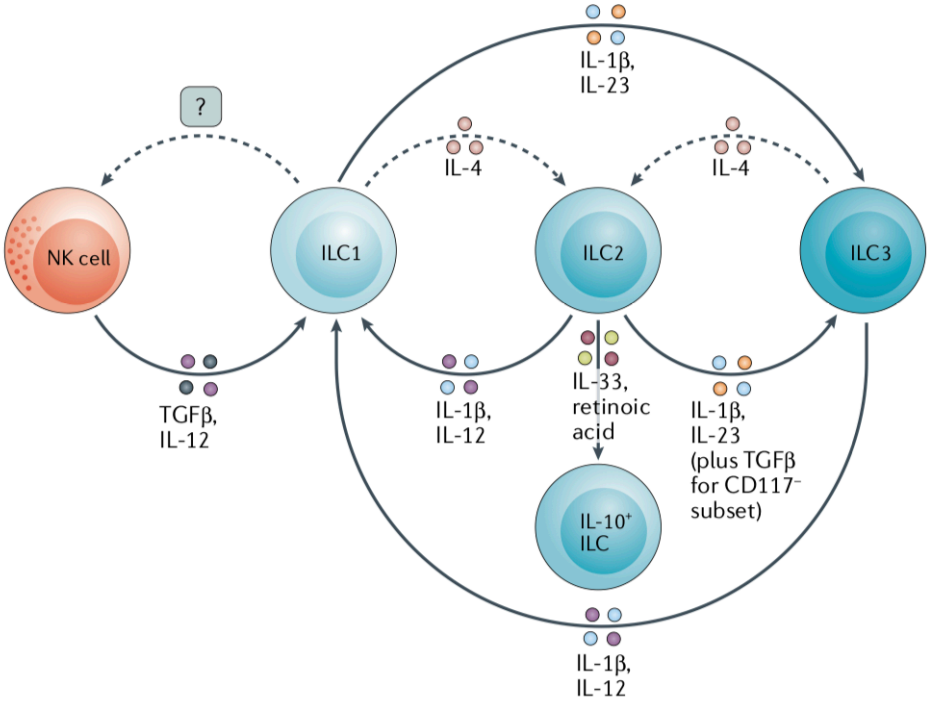

Figure 4. Overview of ILC plasticity.
In response to IL-1β and IL-12, ILC2 and ILC3 can transdifferentiate to ILC1s, whereas IL-1β and IL-23 promote the differentiation of ILC1 and ILC2 to ILC3s. The plasticity of ILC1s and ILC3s into ILC2s can be reversed by IL-4. Additionally, ILC2s can also transdifferentiate into IL-10 producing ILCs driven by IL-33 and retinoic acid. Furthermore, the cytokines TGFβ and IL-12 drive the NK cells to an ILC1-like phenotype but the necessary cytokines for transdifferentiation back to NK cells are not identified yet (Bal et al., 2020).

In general, the different ILC2, ILC3 and NK cells are able to transdifferentiate into ILC1s. Therefore, NKp46$^+$ ILC3s expressing RORγT and T-bet can translate to ILC1s producing IFNγ in response to the pro-inflammatory cytokines IL-1β and IL-12 (Bal et al., 2020; Colonna, 2018; Vivier et al., 2018). This transdifferentiation of ILC3s requires the downregulation of RORγT with parallel upregulation of T-Bet and Notch signaling (Vivier et al., 2018). In response to the cytokines IL-1β, IL-23 and B-cell lymphoma (Bcl)-6 upregulation, ILC1s can be reconverted

into IL-22 producing ILC3s which express again RORγT (Almeida & Belz, 2016; Bal et al., 2020).

Similar to the ILC3 to ILC1 plasticity, also the transdifferentiation of ILC2 to ILC1 producing IFNγ is promoted by IL-1β and IL-12 and is reverted by IL-1β and IL-23. Additionally, IL-4 is necessary for the reversion of IFNγ-producing ex-ILC2s to ILC2s by inducing for example GATA3. The transcription factor GATA3 is able to bind the regulatory element which controls the IFNγ production and therefore the plasticity towards ILC1s (Bal et al., 2020).

The transdifferentiation of NK cells to ILC1s and probably the conversion of ex-ILC1s into NK cells is driven by TGFβ and controlled by the transcription factor small mothers against decapentaplegic homolog 4 (SMAD4) (Cortez et al., 2017). Furthermore, TGFβ and IL-12 are possibly involved in the balance of Eomes and T-Bet expression (Bal et al., 2020; Vivier et al., 2018).

Nevertheless, the different plasticity pathways are not fully understood yet and therefore further investigations are necessary.

1.4.7.1 Natural killer cells in the liver

First identified in the 1970s, NK cells are the first identified ILCs and part of the first line defense against transformed and virally infected cells by mediating cytotoxicity (Tian et al., 2013; Trittel et al., 2019). They are widely distributed through lymphoid and non-lymphoid tissues in which the cells exhibit different phenotypic and functional characteristics (Peng et al., 2016; Yu et al., 2013). In the murine liver, 10-20 % of the total intrahepatic lymphocytes are NK cells which have been originally called pit cells (Peng et al., 2016; Tian et al., 2013). These NK cells can be identified with the marker NK1.1 and can be further divided into circulating NK (cNK) cells and liver resident NK (lrNK) cells based on their expression of the tissue residency marker CD49a and DX5, which is also known as CD49b (Peng et al., 2016; Peng & Tian, 2016). The $CD49a^{-}DX5^{+}$ cNK cells circulate in the blood and can be recruited to the liver. Liver resident NK cells express CD49a but not DX5 and reside in the liver sinusoids. They are known to create a memory-like response and efficiently produce IFNγ, TNFα and GM-CSF. However, the distinction between lrNK cells and ILC1s is difficult, and due to the similarities, the boundaries are blurred. Many publications describe that lrNK are ILC1s, while other researchers are convinced that these are two different cell types (Mikulak et al., 2019; Peng & Tian, 2016). Nevertheless, the distinct roles of the two NK cell subsets during tolerance and diseases in the liver are still under investigation. (Peng & Sun, 2017; Peng & Tian, 2016; Tian et al., 2013; Victorino et al., 2015; Yu et al., 2013).

The bulk analysis of NK cells from the liver indicates a protective as well as a pathogenic role. During homeostasis, NK cells interact with Kupffer cells which can activate NK cells through IL-18. On the other hand, KCs can also suppress NK cells via the anti-inflammatory cytokine IL-10 causing the inhibition of IFNγ expression (Mikulak et al., 2019; Peng & Sun, 2017; Tian

et al., 2013). Moreover, NK cells interact via the inhibitory receptor CD94/ activating receptor natural-killer group 2, member D (NKG2A) with the major histocompatibility complex I, E (HLA-E) on hepatocytes causing the inhibition of NK cells. Additionally, TGFβ is secreted by NK cells which modulates DCs that further induces the expansion of regulatory T cells (T_{regs}). Consequently, T_{regs} produce the immunosuppressive cytokines IL-10 and TGFβ, which further inhibit NK cells and induces a tolerogenic phenotype (Mikulak et al., 2019; Robinson et al., 2016; Tian et al., 2013).

In liver fibrosis, NK cells have a controversial role: they can provide pro- and anti-fibrotic properties (Tosello-Trampont et al., 2017). The anti-fibrotic effect of NK cells focusses on early activated HSCs. These early activated HSC highly express the NKG2D ligand retinoic acid early inducible 1 (Rae1). Consequently, activated NK cells induce apoptosis or cell cycle arrest directly through cell-cell contact or indirectly through IFNγ in HSC-derived myofibroblasts and therefore suppresses the fibrosis. Furthermore, the produced IFNγ recruits more NK cells and causes an increased cytotoxicity against early activated HSCs by upregulation of the tumor necrosis factor-related apoptosis-inducing ligand (TRAIL) (Jeong et al., 2011; Radaeva et al., 2006; Tian et al., 2013; Tosello-Trampont et al., 2017). Additionally, HSCs seem to express an unknown NKp46 ligand. The interaction with the NK cell receptor NKp46 causes the killing of early activated HSCs further underlining the involvement in ameliorating the liver fibrosis (Gur et al., 2012; Krueger et al., 2011; Tosello-Trampont et al., 2017). Nevertheless, quiescent HSCs are resistant to all of these apoptotic signals (Krueger et al., 2011).

In contrast to their anti-fibrotic effect in the liver, some researchers found increasing evidence that NK cells and their released cytokine IFNγ can also be a negative regulator for liver fibrosis (Jeong et al., 2011). The pro-fibrotic effect of NK cells is based on the killing of stressed hepatocytes through the engagement of different receptors like NKG2D and NKp30. In combination with the secreted cytokine IFNγ, which also induces apoptosis, the NK cells lead to the development of liver fibrosis (Beraza et al., 2009; Fasbender et al., 2020; Fernández-Álvarez et al., 2015; Tosello-Trampont et al., 2017).

Another property of NK cells is the contribution to the liver regeneration. By interacting with different cell types in the liver, NK cells can influence the release of cytokines, chemokines and growth hormones contributing the hepatic proliferation. During inflammation, NK cells release the cytokines IL-22 and TNFα which stimulate the proliferation of hepatocytes replacing the dead hepatocytes. Furthermore, the cross talk between NK cells and Kupffer cells promote the regulation of the differentiation of hepatic progenitor cells. Additionally, enhanced recruitment of mesenchymal stem cells, which promote tissue repair, is induced by NK cells and various chemokines such as IL-8 (Li & Hua, 2017; Tosello-Trampont et al., 2017). Taken together, NK cells have several functions in the liver which are contradictory, since they can promote fibrosis progression but also tissue regeneration.

1.4.7.2 NK cell activating receptors NKG2D and NCR

The interaction of NK cells with different cells leads to a variety of signals through two types of natural killer cell receptors: activating and inhibitory receptors (Fig. 5). Depending on the number and strength of each transmitted signal, NK cell reactivity is inhibited or activated (Krueger et al., 2011; Long et al., 2013; Paul & Lal, 2017). Activation of NK cells can be induced by a several activating receptors such as CD16, NKp46, NKG2D and 2B4. Based on their signal mechanism, the activating receptors can be grouped (Watzl, 2014). Since this thesis is focusing just on a few activating receptors and some of their ligands, the following section is mainly concentrating on NKG2D and the natural cytotoxicity receptors (NCR) (Colucci et al., 2002; Krueger et al., 2011).

NKG2D is part of the receptor family NKG2, although it has just little homology to the other family members. The NKG2 family members are C-type lectin-like receptors which are present in humans and mice and are not exclusively expressed on NK cells but also on cytotoxic T cells or macrophages. Usually, NKG2 receptors are forming a heterodimer together with CD94, but unlike to the other family members, NKG2D forms a homodimer. In mice, two NKG2D isoforms are existing which either have a long or a short cytoplasmic tail. While the long-tailed NKG2D isoform only couples with adaptor molecule DNAX-activation protein (DAP) 10, the short-tailed isoform can associate with both DAP10 and DAP12. In humans, only the long-tailed isoform associating with DAP10 is known (Krueger et al., 2011; Paul & Lal, 2017). DAP10 contains a tyrosine-based signaling motif (YINM) while DAP12 is an immunoreceptor tyrosine-based activation motif (ITAM)-containing partner chain (Colucci et al., 2002; Paul & Lal, 2017; Watzl, 2014). Nevertheless, independent of the isoform and the species, the signaling pathway is similar. In the first step, two DAP homodimers non-covalently associate with the NKG2D receptor building a hexameric complex. Next, the cytoplasmic DAP domain containing YINM is phosphorylated by Src family kinases or Janus kinase (Jak) 3 kinases and recruits p85 which is a subunit of the adapter proteins phosphoinositide 3-kinase (PI3K) or growth factor receptor-bound protein 2 (Grb2). The Grb2 phosphorylation results in the phosphorylation of guanine nucleotide exchange factor 1 (Vav1), phospholipase C gamma 2 (PLC-γ2) and lymphocyte cytosolic protein 2 (SLP-76). Furthermore, signaling through PI3K and Grb-Vav1 induces Jak2, signal transducer and activator of transcription 5 (STAT5), protein kinase B (Akt), mitogen-activated protein kinase kinase (MEK1/2) and extracellular signal-regulated kinases (ERK) phosphorylation (Konjević et al., 2017; Krueger et al., 2011; Paul & Lal, 2017; Watzl, 2014). The signaling through DAP12 activates cytotoxicity as well as the secretion of cytokines whereas DAP10 preferentially induces cytotoxicity. Notably, NKG2D expression can be modulated: cytokines like IL-7, IL-12, IL-15 and TNFα increase and IFNγ and TGFβ decrease the expression (Colucci et al., 2002; Diefenbach et al., 2000; Paul & Lal, 2017).

Another difference between human and murine NKG2D are the recognized ligands. Although the ligands are named differently, they are structural homologues of MHCI. In mice, the ligands mouse UL16-binding protein-like transcript 1 (MULT1), Rae1 and histocompatibility 60 group proteins (H60) can be found. The human counterparts of the mouse ligands are the MHC class I-related chain A and B (MICA, MICB) and unique long 16-binding proteins (ULBP1-6) (Fu et al., 2017; Sheppard et al., 2018). However, these ligands are only upregulated and widely expressed in stressed environment especially in tumors and in cells infected with pathogens. Additionally, the soluble forms of the different NKG2D ligands can limit the NK cell activation (Colucci et al., 2002; Diefenbach et al., 2000).

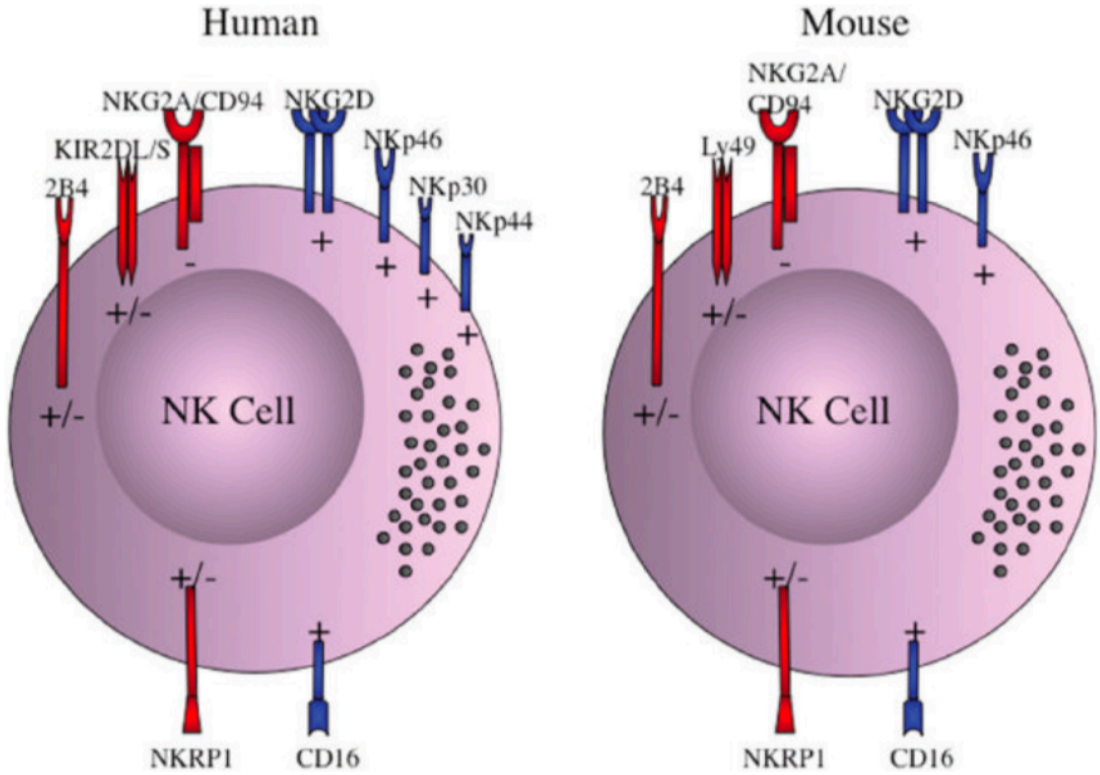

Figure 5. Overview of some activating and inhibitory receptors on human and murine NK cells (Krueger et al., 2011).
NK cells from humans and mice have some of their activating and inhibiting receptors on the surfaces in common. The presented receptors are a selection of activating and inhibiting receptors which the two species share or do not express. The inhibitory (-) receptors are shown in red with long intracellular protein domains and the activating (+) receptors are presented in blue with shorter intracellular protein domains. Both NK cells express the receptors 2B4 and natural killer cell surface protein P1A (NKRP1) which can be activating and inhibiting, promoting the NK cell development. Furthermore, they both have the activating receptors NKG2D, NKp46, CD16 and the inhibitory receptor NKG2A. In contrast to murine NK cells, human NK cells also express the activating receptors NKp30 and NKp44 as well as 15 inhibitory and activating killer cell immunoglobulin-like receptors (KIR). In mice, NK cells have 19 different activating and inhibiting Ly49 receptors instead of the KIR receptors (Konjević et al., 2017; Krueger et al., 2011).

Another group of activating receptors are the natural cytotoxicity receptors. These NCRs are Ig-like transmembrane glycoproteins utilizing an extracellular immunoglobulin-like domain for binding the ligand (Konjević et al., 2017; Paul & Lal, 2017). In human, three types of these

receptors are expressed including NKp46 (NCR1), NKp44 (NCR2) and NKp30 (NCR3). In contrast, murine NK cells only express NKp46 (Paul & Lal, 2017). NKp46 and NKp30 are expressed on resting and activated human NK cells, whereas NKp44 requires IL-2 and therefore restricted to activated NK cells (Konjević et al., 2017). Although NKp46 is considered to be used as a NK-specific marker, the activating receptor is also expressed on ILC1s, a subset of ILC3s and a small subset of T cells (Paul & Lal, 2017). Nonetheless, NCRs are able to recognize several pathogen ligands and also cellular ligands like B7-H6 (NKp30) or proliferating cell nuclear antigen (PCNA, NKp44) (Barrow et al., 2019; Paul & Lal, 2017; Watzl, 2014). In case of NKp46, the only identified cellular ligand is complement factor P (Properdin) (Narni-Mancinelli et al., 2017). Additionally, it is reported that the receptor can recognize surface proteins for example on tumors, HSCs or adipose tissue but for over two decades, the identification of further cellular ligands remains difficult (Barrow et al., 2019; Berhani et al., 2019; Watzl, 2014).

The transmembrane regions of NCRs include positively charged amino acids which associate with ITAM-bearing adapter proteins γ-chain of the high-affinity Fc receptor for IgE (FcεRI-γ) and CD3-ζ for NKp30 or with DAP12 for NKp44 (Walzer et al., 2007). Human NKp46 lacks ITAM but contains a positively charged arginine residue which associates with the negatively charged arginine residue of FcεRI-γ and CD3-ζ whereas the murine NKp46 only couples to the homodimer FcεRI-γ (Barrow et al., 2019; Colucci et al., 2002). However, these different adapter proteins undergo phosphorylation of ITAM by Src-kinases leading to the recruitment and activation of the spleen tyrosine kinase (SYK) and zeta chain-associated protein kinase 70 (ZAP70). This phosphorylation causes another phosphorylation of the transmembrane adapters the linker for activation of T cells (LAT) and non-T cell activation linker (NTAL) and the cytosolic adapters SLP-76 and c-Abl Src homology 3 domain-binding protein-2 (3BP2). In the last step, these kinases recruit, phosphorylate and activate PI3K, PLC-γ1, PLC-γ2 and Vav2, 3 forming signaling complexes causing degranulation, secretion of cytokines and cellular cytotoxicity by cytoskeletal reorganization (Colucci et al., 2002; Konjević et al., 2017; Watzl, 2014).

1.4.7.3 Group 1 innate lymphoid cells in the liver

In 2005, Takeda et al. described a population of liver resident NK cells, which express NK1.1, NKp46, CD49a and TRAIL on their surfaces but no CD49b. These cells were already present in the fetal liver and persist in adults (Takeda et al., 2005). During the following years, these cells were identified as ILC1s and further markers were found to distinguish between hepatic NK cells and ILC1s like CD127, C-X-C motif chemokine receptor CXCR6 and the inhibitory receptor CD200r. Moreover, liver ILC1s can be cytotoxic based on their expression of granzyme B, perforin, TRAIL and IFNγ (Chen & Tian, 2021; Liu & Zhang, 2017). Additionally, hepatic ILC1s are dependent on the transcription factors Hobit and T-Bet while they do not

express Eomes (di Censo et al., 2021). ILC1s were also found in several other organs in which they can express specific markers like CD73 in salivary glands or CD160 in intestine (Seillet et al., 2021). Although a number of single cell RNA sequencing experiments were performed to better distinguish between NK cells and ILC1s and their possible interactions with other cell subsets, the generated knowledge of these results remained limited. One reason for these limited information are the low numbers of ILC1s in different tissues. Nevertheless, liver NK cells and ILC1s differ in many aspects like their developmental pathways, transcriptional programs, function and their plasticity (Jacquelot et al., 2021).

Hepatic ILC1s mainly develop from local hematopoietic progenitors which were enriched in a Lin^- population (Jacquelot et al., 2021). Their differentiation into mature hepatic ILC1s is promoted by other IFNγ producing ILC1s (Takeda et al., 2005). Furthermore, the transcription factors T-Bet as well as Hobit are required for liver ILC1 development (Jacquelot et al., 2021). Additionally, Hobit is necessary for the tissue residential program in lymphoid cells and causes the ILC1 heterogeneity in the liver. This transcription factor also drives the maturation stages from early $CD127^{hi}$T cell factor 1 $(TCF\text{-}1)^{hi}$ ILC1s, producing IFNγ and expressing the tyrosine-protein kinase (c-Kit) and IL-18 receptor alpha (IL-18Rα), into $CD127^-TCF\text{-}1^-$ effector cells which express CD3γ and mainly produce granzyme A and B (Friedrich et al., 2021).

During steady state, nearly 95% of all ILCs in the liver are ILC1 although the total number of these cells is very low compared to other immune cells (Liu & Zhang, 2017). They preferentially localize close to DCs in the perivascular spaces along the portal areas (Chen & Tian, 2021; Liu & Zhang, 2017). However, ILC1s express high levels of NKG2A on their surfaces and through the NKG2A signaling, they can possible control cNK cells. NKG2A signaling inhibits CXCL9 expression and consequently, cNK cells cannot accumulate anymore leading to less IFNγ secretion (Liu & Zhang, 2017). Additionally, NKG2A can further suppress DCs, interrupting the $CD8^+$ T cell priming and thus maintaining the tolerance of the liver (S. Yang et al., 2015).

The role of cNK cells during liver fibrosis is well described. They are able to kill activated HSCs in a TRAIL-dependent manner. But the exact role of ILC1s during liver fibrosis is not clarified until now, although they secrete the antifibrotic cytokine IFNγ, suppress the liver injury and help the hepatocytes to survive in Bcl-2 and Bcl-xL dependency (Nabekura et al., 2020). IFNγ induces apoptosis and the inhibition of proliferation of fibroblasts as well as the inhibition of collagen accumulation and TGFβ production (Liu & Zhang, 2017; Y. Zhang et al., 2016). Furthermore, ILC1 produced IFNγ could also activate NK cells and contribute indirectly to liver damage and fibrosis resolution (S. Yang et al., 2015). However, during liver damage, dying cells, especially hepatocytes, release adenosine triphosphate (ATP) to the extracellular environment (Amaral et al., 2013). This higher extracellular ATP concentration upregulates IL-12 production in DCs which causes the subsequent IFNγ release from hepatic ILC1s amplifying

the liver inflammation (Chen & Tian, 2021). Furthermore, ILC1s also express TRAIL and researchers suggest a contribution to HSC killing and therefore causing the improvement of liver fibrosis. But this hypothesis needs to be further investigated (Liu & Zhang, 2017).
ILC1s can also contribute to liver regeneration. In response to elevated extracellular ATP, ILC1 produce IL-22 and IL-23. The cytokine IL-22 binds to its receptor IL-22R which is expressed on hepatocytes. The binding activates STAT3 and activates the expression of antiapoptotic and proliferation-associated proteins like Bcl-xL or cyclin D1 (Liu & Zhang, 2017). Furthermore, ILC1s showed a destructive response like the clearance of dying cells and debris which is necessary to proceed with the tissue repair and the return to homeostasis (Vivier et al., 2018). Nevertheless, the function of ILC1s during liver homeostasis, fibrosis, regeneration and tissue repair needs to be further investigated since most of the mentioned tasks are hypothesis.

1.4.7.4 Memory like ILC1s and NK cells

Traditionally, the immunological memory was considered part of the adaptive immune system and associated with the B cells and T cells (Gang et al., 2020; Tarannum & Romee, 2021). As the name already says, these memory cells are able to remember a previous pathogen and are able to react faster and even stronger in case of another encounter with the same pathogen (Watzl, 2014). The long-lasting memory of the lymphocytes is based on antigen-dependent clonal proliferation which is achieved by gene arrangement, class switch recombination, isotype switch or somatic hypermutations and these cells have an enhanced capability to proliferate, produce cytokines and are more cytotoxic (Farber et al., 2014; Gang et al., 2020; Williams & Bevan, 2007). During the last years, also other immune cells were described to develop a memory like phenotype: monocytes, macrophages, ILCs and NK cells (Martinez-Gonzalez et al., 2016; Tarannum & Romee, 2021). Memory like ILCs and NK cells have shown to be long-lived cells that can produce higher amount of cytokines, form a larger population of responding cells and even possess antigen specificity. During the last years three different memory like responses of NK cells have been described: hapten-, virus- and cytokine-induced memory (Watzl, 2014).
In order to generate cytokine induced memory like (CIML) NK cells, splenic mouse NK cells were stimulated *in vitro* with the cytokines IL-12, IL-15 and IL-18 overnight. After the adoptive transfer back to RAG-1 deficient mice, the pre-activated NK cells persisted at high numbers for several weeks. Upon restimulation with cytokines or activating receptor engagement *in vitro*, the NK cells showed a higher IFNγ production compared to control NK cells (Pahl et al., 2018). Since this kind of memory cells does not recognize any specific antigens, they have been termed non-specific memory NK cells (X. Wang et al., 2019). The rapid proliferation of CIML NK cells was driven by IL-2 which was produced by $CD4^+$ T cells (Peng & Tian, 2017). However, further experiments revealed that the memory-like property was intrinsic and passed on to daughter generations, although the daughter cells were never exposed to the cytokines.

This finding suggests an epigenetic or transcriptional change in these CIML NK cells. In a later study, a demethylation of conserved non-coding sequence 1 (CNS1) at the *Ifng* locus in CIML NK cells was observed which resulted in the stable IFNγ producing phenotype (Pahl et al., 2018; Peng & Tian, 2017). Additionally, CpG demethylation of PRDM1/BLIMP1 and ZBTB32/TZFP genes and a hypermethylation of FCER1G were also detected, but their contribution to the memory formation or maintenance is not answered till now. The investigation of metabolic regulation revealed elevated oxidative phosphorylation and elevated glycolysis caused by the acetyl-Coenzyme A export through the citrate-malate shuttle (Pahl et al., 2018). Nevertheless, CIML NK cells also expressed higher levels of CD25 (IL-2Rα) and down-regulated TGFβ receptor and the connected signaling pathway. Furthermore, the up-regulation of CD69 and killer cell lectin like receptor G1 (KLRG1) on mature $CD11b^{+}CD27^{-}$ NK cells was observed (Pahl et al., 2018; Peng & Tian, 2017). Similar to the CIML NK cells in mice, human $CD56^{bright}$ and $CD56^{dim}$ NK cells can also create a memory phenotype upon IL-12, IL-15 and IL-18 stimulation. Especially the $CD56^{dim}$ cells had an increased IFNγ production and increased CD94, NKG2A, NKG2C, CD69 and CD25 surface expression while CD57 and killer immunoglobulin-like receptor (KIR) expression was decreased (Peng & Tian, 2017; Watzl, 2014).

The second mentioned memory like NK cells are induced by a viral infection. Virus induced memory like NK cells are generated after infection with mouse cytomegalovirus (MCMV) or the human cytomegalovirus (HCMV) (Watzl, 2014). In mice, the MHC class I-like glycoprotein m157 encoded by MCMV is binding the NK activating receptor Ly49H which is expressed on 50 % of the splenic NK cells (Brillantes & Beaulieu, 2020; Peng & Tian, 2017). As a consequence, the infection triggers the signaling through the adapter protein DAP12 and activation and proliferation of clonal-like expansion of $Ly49H^{+}$ NK cells which also express Ly6C and KLRG1 (Brillantes & Beaulieu, 2020; Peng & Tian, 2017; Sheppard & Sun, 2021). The expansion lasts for about one week and is followed by the contraction phase, after which the remaining cells could persist for several months. These long-lived memory like NK cells exhibit a more mature phenotype and stronger effector functions. *Ex vivo* restimulation of these memory NK cells showed higher response to Ly49H stimulation resulting in increased IFNγ production and degranulation (Gang et al., 2020). Later studies revealed that in total three different signals are involved in the memory generation similar to $CD8^{+}$ T cells. The first signal is the engagement ofLy49H with the antigen m157. The second signal is the co-stimulatory signal DNAX accessory molecule-1 (DNAM-1) and the third signal is the pro-inflammatory cytokine signaling (IL-12, IL-18, IL-33) (Brillantes & Beaulieu, 2020). The pro-inflammatory cytokine IL-12 induces the expression of STAT4 and zinc finger and BTB domain containing 32 (Zbtb32). Zbtb32 antagonizes B lymphocyte-induced maturation protein-1 (Blimp-1) causing the NK cell activation and proliferation, while STAT4 binds to promotor regions and

promotes the expression of Runx1 and Runx3. Especially the transcription factor Runx1 controls the cell cycle of the Ly49H$^+$ NK cells. The other two pro-inflammatory cytokines IL-18 and IL-33 are required for the expansion of the Ly49H$^+$ NK cells (Peng & Tian, 2017; Sheppard & Sun, 2021). Additionally, type I IFNs are critical for the clonal expansion, contraction and memory generation. These anti-inflammatory cytokines are involved in the expression of STAT1, STAT2 and interferon regulatory factor 9 (IRF9) promoting NK cell expansion and survival (Sheppard & Sun, 2021; X. Wang et al., 2019). Furthermore, the autophagic pathway mediated by BNIP and BNIP3L is essential for the memory NK cell persistence since dysfunctional mitochondria are removed during contraction-to-memory phase transition (Peng & Tian, 2017).

In human, HCMV-seropositive individuals express more of the activating receptor complex CD94/ NKG2C$^+$ on NK cells compared to the seronegative individuals. These NKG2C$^+$ NK cells are found to create an adaptive memory response. Although the viral ligand is not identified yet, it has been shown that human leukocyte antigen E (HLA-E) triggers the expansion of NKG2C$^+$ NK cells. Furthermore, HLA-E on infected cells presents HCMV-encoded UL40 peptides to the CD94/ NKG2C complex (Hammer et al., 2018). Thus, the NKG2C-UL40 interaction serves as the first signal. Although the second signal and therefore the co-stimulatory molecule is not yet identified, the third signal is known: IL-12 (Brillantes & Beaulieu, 2020; Peng & Tian, 2017; X. Wang et al., 2019). The cytokine IL-12, which is produced by inflammatory CD14$^+$ monocytes, is required for differentiation, proliferation and expansion through CD25 induction (O'Sullivan et al., 2015). Moreover, these memory NK cells have an enhanced cytotoxicity and IFNγ production (X. Wang et al., 2019). Interestingly, the expansion of NKG2C$^+$ NK cells in HCMV-seropositive individuals is also found after infection with hepatitis B, hepatitis C or hantavirus (Brillantes & Beaulieu, 2020; Watzl, 2014).

The hapten induced memory like NK cells are described to be induced by the contact with chemical haptens like 4-ethoxymethylene-2-phenyloxazol-5-one (oxazolone) resulting in a hypersensitivity upon re-challenging with the same hapten (Min-Oo et al., 2013; Pahl et al., 2018). Previously, it was thought to be mediated by only T cells, but experiments in Rag deficient mice disclosed the impact of NK cells which were accumulated at the site of hapten administration on the skin. Interestingly, only hepatic NK cells, but not splenic NK cells, were found to mediate the memory response restricted to the original sensitizing hapten. These hepatic NK cells were identified as Thy1$^+$CD11b$^+$CD27$^-$ which were capable of long-lived and the antigen-specific memory response. Furthermore, the expression of the receptor CXCR6 as well as the cytokines IFNγ and IL-12 are obligated for NK cell-mediated hapten-specific response (Min-Oo et al., 2013; Paust et al., 2010). These observations revealed that hepatic restricted memory like NK cells are antigen specific. But its´ exact molecular mechanism

remains to be answered since it is actually not reported that NK cells do express antigen-specific receptors (Watzl, 2014).

However, Wang et al., 2018, demonstrated that during the MCMV infection, memory like ILC1s expressing the IL-7 receptor ($CD127^+$) are also generated in the lymph nodes. The skin sensitization with haptens causes the uptake of the hapten or hapten-self protein complex by DCs. Within 24 hours, the DCs migrate to the skin-draining lymph nodes inducing the rapid $CD127^+$ILC1s recruitment in CXCR3-dependency. In the skin-draining lymph nodes, the ILC1s are primed and create the memory potential. Afterwards, the memory like $CD127^+$ILC1s leave the lymph nodes via sphingosine-1-phosphate receptor-1 (S1PR1) and are recruited to the hepatic sinusoids caused by the CXCR6-CXCL16 interaction. In the liver, the memory like ILC1s maintain their longevity through CD127 signaling causing the long-term residency in a BCL-2 dependent manner. Additionally, IL-7, which can be produced by hepatocytes and LSECs, was shown to be essential for the longevity of memory ILC1s. It is hypothesized that IL-7 may support the longevity of ILC1s in a BCL-2 independent manner (X. Wang et al., 2020). Furthermore, these memory like ILC1s are expressing IL-18Rα (Chen & Tian, 2021). In case of a re-challange with the same hapten, the memory like ILC1s migrate to the effector site and mediate an allergic skin inflammation (X. Wang et al., 2018). Nevertheless, the main question remains, if the hapten induced memory effect is based on NK cells, ILC1s or do both cell types have their own contribution to hapten induced memory generation.

1.5 Liver regeneration and the progression to liver fibrosis

The liver has a remarkable capacity to adapt to different situations. In case of an injury of the liver for example caused by hepatitis or hepatotoxicants like a drug, the organ has a rapid response to repair the damaged tissue and achieve the restitution of liver mass (Pellicoro et al., 2014; Zuñiga-Aguilar & Ramírez-Fernández, 2022). As the result of a hepatic insult, hepatocytes become necrotic which lead to the release of inflammatory mediators and the so-called damage associated molecular patterns (DAMPs) including ATP, histones, mitochondrial and deoxyribonucleic acid (DNA) fragments (B. Woolbright, 2017). DAMPs bind to pattern recognition receptors such as Toll-like receptors (TLRs) which are present on KCs. Consequently, the inflammatory mediators mainly recruit KCs to the site of injury. In the next step, the liver macrophages phagocytose dead and apoptotic hepatocytes or other NPCs and generate more pro-inflammatory cytokines like TNFα, IL-6, TFGβ and IL-1β. As a consequence of the secreted cytokines, other immune cells are recruited like monocytes, neutrophils, T cells and NK cells. Furthermore, the KCs activate the nuclear factor kappa B (NF-κB) pathway, which causes the HSC activation, resulting in the synthesis and secretion of more pro-inflammatory cytokines, chemokines, reactive oxygen species (ROS) and nitrogen species (Puengel & Tacke, 2018; B. Woolbright, 2017; B. L. Woolbright & Jaeschke, 2015). The

transiently activated HSCs produce extracellular matrix (ECM) and form a temporary scar at injury site which prevents the wound to collapse. In addition, HSCs stimulate the hepatocyte proliferation through the release of hepatocyte growth factor (HGF) (Forbes & Rosenthal, 2014; K. Shen et al., 2011). Moreover, LSECs upregulate CXCR7 caused by the transcription factor Id1, mitogenic factors like HGF and wingless-type MMTV integration site family, member 2 (Wnt2) which trigger the proliferation of hepatocytes (Böhm et al., 2010; Hoehme et al., 2010). Another cell type which is contributing to the tissue repair are the monocytes. Although the monocytes have an inflammatory phenotype and exacerbate the damage, they change their phenotype to repair-promoting phagocytes after termination of injury (Ding et al., 2014; Puengel & Tacke, 2018). However, it should be mentioned that also other factors support the regeneration of the liver which are not described in this chapter such as insulin secreted from the pancreas (Taub, 2004).

Nevertheless, this rapid respond of tissue repair and regeneration is dependent on the duration of the insult. If the insult is stronger or occurs more often, another kind of wound healing process starts: fibrosis (Pellicoro et al., 2014; Zuñiga-Aguilar & Ramírez-Fernández, 2022). Fibrosis is defined as excessive deposition of ECM, in particular collagen type I, which causes only minor clinical symptoms (Karimzadeh Toosi, 2015; Liedtke et al., 2013). In response to the liver injury and the secreted pro-inflammatory factors TFGβ, IL-6, platelet-derived growth factor (PDGF) and IL-1β, quiescent HSCs transdifferentiate into pro-fibrogenic myofibroblasts. Upon the transdifferentiation, they lose vitamin A and upregulate the synthesis of α-SMA, desmin, type I collagen and inhibit the matrix metalloproteases (MMPs) (Pellicoro et al., 2014; Y. Shen et al., 2018; C.-Y. Zhang et al., 2016; Zuñiga-Aguilar & Ramírez-Fernández, 2022). One member of MMPs are the collagenases which usually cleave the native helix of fibrillar collagen. But the HSCs secrete the tissue inhibitor of MMPs (TIMPs) resulting in the inhibition of MMPs (Campana & Iredale, 2017). Activated HSCs are highly proliferative, contractile, scar producing, migratory, immunomodulatory and phagocytic (Pellicoro et al., 2014; Zuñiga-Aguilar & Ramírez-Fernández, 2022). Sustained fibrogenesis can ultimately lead to liver cirrhosis. The pathological characteristics of a liver cirrhosis include the degeneration of hepatocytes, parenchyma replacement by fibrotic tissue and the loss of liver function marking the irreversible late-stage of the damaged liver. Until today, there are almost no efficient strategies to treat liver cirrhosis so that cirrhosis patients are mostly dependent on a liver transplantation or the cirrhosis may end in hepatocellular cancer (Y. Zhang et al., 2016; Zhou, 2014).

In contrast to the irreversible late-stage cirrhosis, the fibrosis is a bidirectional process (Zhou, 2014). The fibrosis can be reversible but therefore the underlying liver damaging source needs to be removed. The following regression of the fibrosis is accompanied by deceased levels of proinflammatory cytokines such as TFGβ and IL-6 (Pellicoro et al., 2014). Moreover, the TIMP

level drops due to the reduction of activated HSCs. As a consequence, the MMPs activity increases and the degradation of collagen fibers occurs (Campana & Iredale, 2017; Pellicoro et al., 2014; C.-Y. Zhang et al., 2016). Interestingly, the main source for MMPs are the pro-resolution macrophages. These pro-resolution macrophages are not only rich of MMPs but also of the death receptor ligand TRAIL (Pellicoro et al., 2014). Since the activated HSCs express different death receptors such as the TRAIL receptors, the macrophage produced TRAIL can induce apoptosis via the death receptor mediated pathway. But macrophages are not the only source for TRAIL (Campana & Iredale, 2017). Loss of vitamin A, elevated Rae1 and decreased MHC I expression of activated HSCs stimulate NK cells and induce the apoptosis of activated HSCs (Y. Shen et al., 2018). Additionally, NK cells have elevated TRAIL expression and also induce the death receptor mediated pathway or directly decrease the proliferation and activation of HSCs through IFNγ (S. Yang et al., 2015; Y. Zhang et al., 2016). The loss of myofibroblasts is one main mechanism of the fibrosis regression. Besides the two mentioned mechanisms, there are several different mechanisms leading to the apoptosis of HSCs or the reversion to quiescent HSCs (Kisseleva & Brenner, 2021). For the better understanding of the mechanisms in the liver during liver damage, fibrosis, regeneration or drug induced liver injury, different mouse models were designed. The mouse models enable the serial sampling of tissues as well as a detailed study of cellular and molecular mechanisms (Iredale, 2007). In the following chapters, some liver damage mouse models are introduced.

1.6 Drug induced liver injury

Although every single drug has to pass the developmental, preclinical and clinical trials, there are still safety issues with some drugs that have already been approved. Most of these drugs were recalled and, in the end, withdrawn from the market (Craveiro et al., 2020). The most common reason for withdrawing drugs from the market is the drug-induced liver injury (DILI) (Katarey & Verma, 2016). DILI describes the unexpected harm that drugs can cause to the liver like acute liver failure. In general, DILI can be divided into two groups based on their presumed mechanism of action: intrinsic and idiosyncratic (Andrade et al., 2019; McGill & Jaeschke, 2019).

Intrinsic DILI, which is also known as direct or predictable DILI, is dose-dependent, reproducible in mouse models and mostly occurs shortly after exposure. The toxicity of the majority of these intrinsic drugs is based on their chemical properties (McGill & Jaeschke, 2019). The most prominent example of intrinsic DILI is acetaminophen (APAP), which is better known as paracetamol. In the western countries, around 50% of acute liver failure is based on paracetamol, since hepatotoxicity occurs already slightly above the maximum of the daily dose of 4 g (Andrade et al., 2019).

The second group, idiosyncratic DILI (iDILI), is the unpredictable form of DILI. It occurs at recommended therapeutic doses, is dose independent, lacks objective diagnostic markers and therefore makes the diagnosis difficult (Iorga et al., 2017; Yamashita et al., 2017). This type of DILI is unexpected, since the routine animal toxicology fails to identify the possible toxicity (Iorga et al., 2017; Katarey & Verma, 2016). It is characterized by a variable latency, occurs only in a small proportion of exposed individuals causing severe health problems and could be a potential cause for mortality (Iorga et al., 2017). Prominent examples for iDILI drugs are the antibiotic isoniazid and the anti-epileptic drug valproic acid (Yamashita et al., 2017).

During the last decades, several risk factors for DILI were identified. One of the first identified risk factors is the sex. Women are more susceptible probably caused by a hormonal effect. Besides the sex, older patients have a threefold increased risk of developing DILI. Additionally, the duration and drug dose are playing a crucial role in DILI. Pre-existing liver diseases and genetic factors can also increase the susceptibility to DILI. Researchers found out that the specific HLA genotype B*5701 has an eightyfold increased susceptibility (Katarey & Verma, 2016; Uetrecht, 2019; Yamashita et al., 2017).

Until today, physicians classify DILI in immune-mediated or non-immune-mediated. The immune-mediated reaction is comparable to an allergic reaction including fever and autoantibodies. It is defined by a short latency of one up to six weeks whereas the non-immune-mediated reaction occurs after a long latency of around one year and lacks the before mentioned symptoms (Andrade et al., 2019).

Nevertheless, in most DILI cases, the underlying mechanism and pathogenesis is poorly understood especially for iDILI (Iorga et al., 2017). There are many projects ongoing which concentrate on the identification of mechanisms and biomarkers (Tasnim et al., 2021).

In order to identify the underlying mechanisms of DILI, most projects try to work with mouse models. Although there are well established DILI mouse models like APAP and carbon tetrachloride (CCl_4), the introduction of iDILI mouse models poses a greater technical challenge (McGill & Jaeschke, 2019). Indeed, the greatest challenge seems to overcome the liver immune tolerance which appears to be the dominant response to significant liver injury in animals (Metushi et al., 2016). However, in order to achieve an adverse reaction to a known iDILI drug, four different strategies are common: pre-treatment, inflammation, suppression of immune tolerance or genetic manipulation. But all these different strategies have the potential to affect the clinical relevance (McGill & Jaeschke, 2019).

The other main focus of DILI safety and mechanism prediction are biomarkers. Therefore, researchers often use cell lines like the human hepatoma cell line HepG2 or cryopreserved primary human hepatocytes (PHH) and treat them with different DILI drugs. To identify biomarkers for *in vitro* systems predicting toxicity *in vivo*, Grinberg et al., 2014, published toxicotranscriptomics datasets of PHH exposed to different chemicals and integrated other

available data into their biostatistical analysis which in the end summarized key factors of chemically influenced genes. Their analysis revealed an up-regulation of certain activating NK cell ligands on PHH in response to some drugs (Grinberg et al., 2014). In a follow up study performed with drug exposed human hepatocyte cell lines, a co-cultivation with NK cells caused an enhanced NK cell activity resulting in increased cytotoxicity and IFNγ production (Fasbender et al., 2020). Since these experiments were performed *in vitro*, the question of *in vivo* relevance of these findings needs to be answered.

1.6.1 Acetaminophen induced liver damage

In the Western world, the leading cause for acute liver failure is the overdose with the pain-relieving DILI drug acetaminophen (APAP, paracetamol, N-acetyl-para-aminophenol) (Ben-Shachar et al., 2012). The underlying mechanism of APAP induced liver injury is well investigated and can be translated from animals to humans (Vliegenthart et al., 2017). Usually, APAP is predominantly metabolized by sulfotransferase or UDP-glucuronosyltransferase into non-toxic sulfate (APAP-Sul) or glucuronide (APAP-Glu) conjugates, which are easily excreted in the urine. In case of a high dose of APAP, it is converted by the cytochrome P450 enzyme Cyp2E1 and Cyp1A2 to the highly reactive and toxic metabolite N-acetyl-p-benzoquinone imine (NAPQI). NAPQI rapidly reacts with the cysteine sulfhydryl group on glutathione (GSH) via glutathione-S-transferase. Most of the formed APAP-GSH is subsequently converted to APAP-mercapturate (APAP-Mer) and APAP-cysteine (APAP-Cys) conjugates and effectively and safely eliminated. But in case of an APAP dose higher than 4 g/day, the sulfonation reaction becomes saturated and NAPQI completely depletes GSH in the liver. Then, unconjugated NAPQI accumulates in the liver and covalently binds to sulfhydryl groups of proteins and other subcellular structures. Consequently, this leads to oxidative stress, hepatocyte necrosis and acute liver failure (Ben-Shachar et al., 2012; Ramachandran & Jaeschke, 2018; Vliegenthart et al., 2017).

Additionally, mitochondrial proteins are early targets of NAPQI adducts leading to mitochondrial oxidant stress and altered morphology (Ramachandran & Jaeschke, 2018; Vliegenthart et al., 2017). The oxidative stress causes the activation of apoptosis signal-regulating kinase 1 (ASK1) and the mitogen activated protein (MAP) kinase c-Jun N-terminal kinase (JNK). The translocation of JNK from the cytosol into the mitochondria further increases ROS formation. As a consequence, mitochondrial membrane permeability transition (MPT) occurs and the mitochondrial membrane potential collapses. This loss of membrane potential results in cellular ATP depletion (Jaeschke et al., 2013a; Ramachandran & Jaeschke, 2018, 2020). Additionally, the pro-apoptotic Bax protein causes the rupture of the outer mitochondrial membrane and since MPT occurs, mitochondrial endonucleases are released. These released endonucleases translocate to the nucleus leading to nuclear DNA fragmentation and

consequently to cell necrosis (Clemens et al., 2019; Jaeschke et al., 2013a; McGill & Jaeschke, 2013; Ramachandran & Jaeschke, 2020).

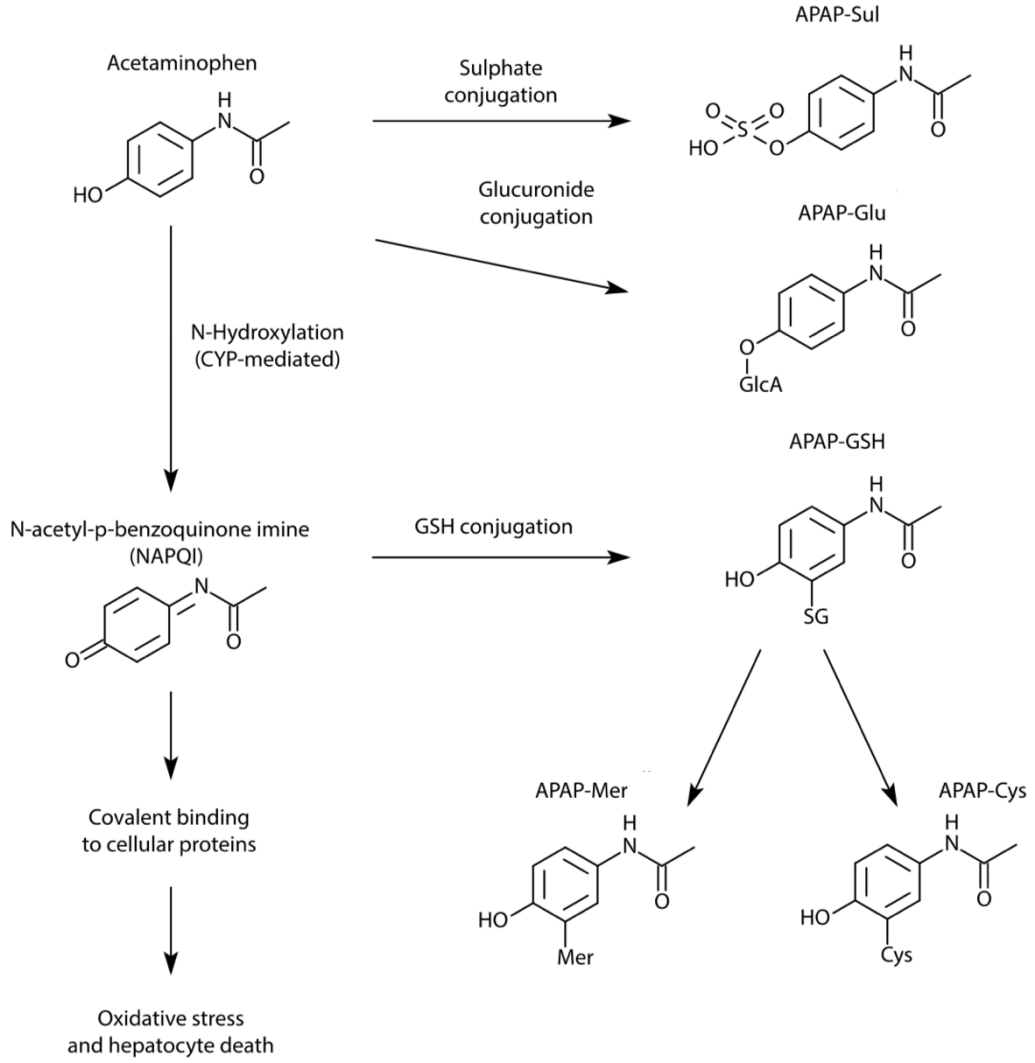

Figure 6. Pathways of APAP metabolism.
Usually, APAP is metabolized into non-toxic sulfate (APAP-Sul) or glucuronide (APAP-Glu) conjugates. But in case of a high dose of APAP, it is converted by cytochrome P450 enzymes to N-acetyl-p-benzoquinone imine (NAPQI). On the one hand, NAPQI can react with the cysteine sulfhydryl group on glutathione (GSH). Subsequently, the formed APAP-GSH is converted to APAP-mercapturate (APAP-Mer) and APAP-cysteine (APAP-Cys) conjugates. On the other hand, in case of an APAP overdose, unconjugated NAPQI accumulates in the liver and bind to proteins and other subcellular structures. The resulting peroxynitrite formation in mitochondria leads to the JNK activation. JNK amplifies the oxidative stress and induces mitochondrial permeability transition. Consequently, endonucleases are released and translocated to the nucleus where they induce DNA damage and cell death (Ramachandran & Jaeschke, 2018; Vliegenthart et al., 2017).

1.6.2 Carbon tetrachloride as a model for liver damage

Carbon tetrachloride (CCl_4) is described to be toxic as well as polluting. Permanent exposure results in severe damage of the liver, kidney, intestine and the central nervous system (Greim H & Dem E, 1996; Jaeschke et al., 2013b). In research, the CCl_4 animal models are popular because of the simple handling and the reproducibility. Moreover, CCl_4 induced liver damage

in animals shows great similarities to human liver damage, fibrosis and its development to cirrhosis (Crespo Yanguas et al., 2016; Jiang, 2004; Tribble et al., 1987).

The metabolism of this hepatotoxic compound shows that CCl_4 itself is not toxic but the metabolized trichloromethyl radical CCl_3^* (Fig. 7). The reductive metabolism of CCl_4 is caused by the cytochrome P450 enzyme CYP2e1 which is localized at the endoplasmic reticulum in the pericentral region of the lobule (Weber et al., 2003). The formed radical CCl_3^* can bind CYP2e1 covalently, thereby causing inactivation of the enzyme and necrosis in the pericentral region. In presence of oxygen, the reactive CCl_3^* radical reacts with the molecular oxygen to form the trichloromethyl peroxy radical CCl_3OO^* which is even more reactive. This reactive radical removes a hydrogen atom from unsaturated fatty acids forming lipid radicals which initiate lipid peroxidation. The resulting lipid radicals form the hydroperoxide while the unsaturated fatty acids disintegrate in malondialdehyde and other products (Fuhrmann G, 2006; Greim H & Dem E, 1996; Weber et al., 2003).

Alternatively, the trichloromethyl radical CCl_3^* does not only react with oxygen, it may also covalently bind proteins and lipids or the radical can directly abstract the hydrogen proton from unsaturated fatty acids. As a result, chloroform and a lipid radical are formed. The fatty acid radical reacts with oxygen forming hydroperoxide which is reduced to malondialdehyde and other products binding DNA and enzymes. Furthermore, chloroform can react with CYP2e1 directly which oxidatively converts chloroform to toxic phosgene (Mehendale, 2010; Vohr, 2010).

Nevertheless, as a result of all metabolism pathways of CCl_4, the membrane barrier is destroyed and the membrane of the endoplasmic reticulum is damaged. Consequently, ATP formation stops, causing membrane pumps to stop working, increasing the free cytosolic calcium (Ca) concentration, catabolic enzymes are activated and the protein synthesis is inhibited (Vohr, 2010). In the end, CCl_4 causes necrosis in hepatocytes and cellular response like inflammation which can increase the damage as well as promote the regeneration of hepatocytes. The regeneration of the tissues, also including wound closure and the reconstitution of the liver architecture, lasts several days, also depending on the administered dose. Continued or high doses of CCl_4 result in irreversible damage in the form of fibrosis or hepatocellular cancer and may cause a leaky gut (Campos et al., 2014; Crespo Yanguas et al., 2016; Jiang, 2004).

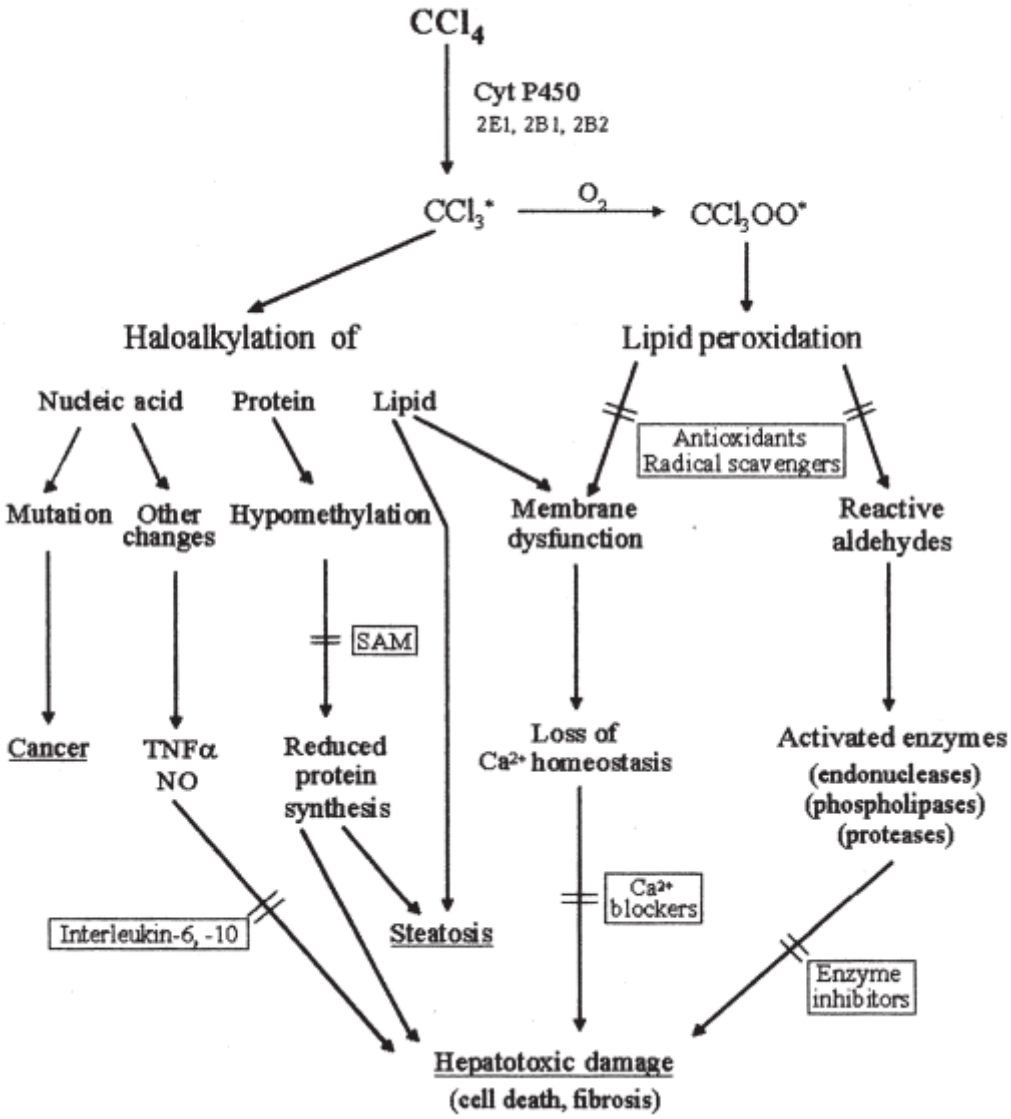

Figure 7. Mechanism of action of CCl4- induced liver damage.
The hepatotoxic compound CCl_4 is metabolized by the cytochrome P450 enzyme CYP2E1. The formed trichloromethyl radical (CCl_3^*) is highly reactive and reacts with different substances such as nucleic acids, proteins and lipids. Furthermore, it also reacts with oxygen, building the even more reactive trichloromethylperoxide (CCl_3OO^*) which in turn results in lipid peroxidation. In the end, it results in hepatotoxic damage (Weber et al., 2003).

1.6.3 Valproic acid

Valproic acid (VPA) is a branched and short-chained fatty acid which is an anticonvulsant drug. It is prescribed for treatment of epilepsy, bipolar disorder, migraine prophylaxis and as mood stabilizer (Bennett & Shad, 2021; Phiel et al., 2001). Although different mechanisms are reported to explain the activity of VPA, the precise mode of action is still not identified. Based on the broad spectrum of VPA, its activity seems to combine different neurochemical and neurophysiological mechanisms (Barthel, 1998). The first identified VPA mechanism causes an increased availability of the synaptic inhibitor gamma-aminobutyric acid (GABA). The inhibitory effect of GABA is enhanced and facilitates the response in special brain regions

(Bennett & Shad, 2021). Furthermore, researchers showed that VPA reduces N-methyl-D-aspartate (NMDA) excitatory responses and consequently reduces the neurotransmission in the medial prefrontal cortex. Additionally, it is described that VPA also has an effect on excitable membranes and probably modulates sodium, calcium and potassium channels (Barthel, 1998; Bennett & Shad, 2021). Although there are some possible mechanisms of VPA, it is also reported that VPA therapy may cause liver injury but the metabolism is unknown. Researchers associated the VPA induced hepatotoxicity with the formation of reactive metabolites, inhibition of mitochondrial β-oxidation pathway or oxidative stress (Bennett & Shad, 2021). Recently, our working group showed that VPA treated PHH and human hepatocyte cell lines are more susceptible to activated NK cells resulting in the killing of the treated hepatocytes and higher IFNγ production (Fasbender et al., 2020; Grinberg et al., 2014). But this finding needs to be further investigated to evaluate the *in vivo* relevance.

1.7. Western diet mouse model

Fatty liver diseases are closely linked with a westernized lifestyle and other diseases like type 2 diabetes mellitus, obesity or metabolic syndrome but also to alcohol (Vancells Lujan et al., 2021). As the name reveals, it is mainly characterized by excessive lipid accumulation inside the hepatocytes. The most common liver disease worldwide is the nonalcoholic fatty liver disease (NAFLD). NAFLD is a term which comprises several liver abnormalities like nonalcoholic fatty liver (NAFL) and nonalcoholic steatohepatitis (NASH) (Friedman et al., 2018; Vancells Lujan et al., 2021). The difference between NAFL and NASH is that NAFL patients only have the fat accumulation and do not have damaged liver tissue or a liver inflammation, whereas NASH patients have both. The inflamed and damaged liver of NASH patients can cause pericellular fibrosis and further lead to cirrhosis or hepatocellular carcinoma (Lin & Fan, 2022; Vancells Lujan et al., 2021; P. Yang et al., 2020).

Although many researchers contribute to the clarification of the pathogenesis of NAFLD the underlying mechanisms and the involvement of especially NK cells and ILC1s remain elusive (P. Yang et al., 2020). In NASH, NK cells are still able to limit fibrosis but on the other hand they seem to promote obesity since NK cell deficient mice showed less fat accumulation and inflammation in the liver (Chen & Tian, 2021). Furthermore, the plasticity of NK cells toward ILC1s mediated by TFGβ was observed, which revealed a protective role and reduced cytotoxicity in NASH (Luci et al., 2019). ILC1s seem to contribute to the homeostasis in adipose tissue and interact with macrophages. Nevertheless, their role in NAFLD needs to be further investigated (Cuff et al., 2019).

1.8 Aim of the current thesis

The liver has always fascinated scientists because of its diverse and important properties, in particular the liver injury caused by different insults and its ability to recover. Various mechanisms describing the injury and recovery were identified and published. However, during the last decades, the different immune cells, their function and interactions have been intensively involved in liver research. But especially the role and function of NK cells and ILC1 cells in different liver diseases is not clarified till now and sometimes seems to be contradictive. Within this thesis, the aim was to investigate NK cells and ILC1s during liver injury *in vivo*. Therefore, the thesis is structured into three parts which focus on different topics:

1. Establishment of a VPA induced liver damage mouse model to investigate the role of NK cells.

This project based on the groundwork of Grinberg, Stöber, et al. and Fasbender et al. Based on the genome wide expression analysis of PHH, which had been exposed to clinically relevant concentrations of 148 drugs, several drugs had a higher expression of activating ligands for different NK cell receptors like B7-H6 and MICA (Grinberg et al., 2014). In the next step, Fasbender et al. took a closer look to the specific role of NK cells in context of drug induced liver injury. Their results showed an enhanced NK cell activity against PHH and human hepatocyte cell lines which were pretreated with the drugs valproic acid, ketoconazole, promethazine and isoniazid. The enhanced NK cell activity was characterized by the higher IFNγ and increased cytotoxicity against hepatocytes (Fasbender et al., 2020).
In order to validate the *in vivo* relevance of these findings, one aim of this current thesis was to establish a drug induced liver injury mouse model. In the first step, the findings of higher expression of activating NK cell ligands needed to be confirmed on primary mouse hepatocytes (PMH), since murine NK cells do not express the same and less activating receptors compared to human NK cells. Therefore, PMH were exposed to valproic acid, isoniazid, promethazine and ketoconazole to identify differently expressed activating NK cell ligands on the surface of PMH. The most promising drug candidate was chosen to establish a DILI mouse model to enable further investigations.

2. Role of immune cells during chemical induced repeated liver damage

In the second part of this thesis, different immune cells during repeated liver injury caused by a chemical compound are investigated. The focus is on a potential memory effect of liver immune cells, since it had already been described that for example lrNK cells possess memory like features in response to haptens. In order to investigate a potential memory effect of immune cells in the liver, we used one of the most common and well investigated intrinsic DILI mouse model: carbon tetrachloride. The identified immune cell fraction, which showed a

memory like feature in the repeatedly CCl_4-induced liver damaging mouse model, was further characterized. To investiagte the function and localization of these memory like immune cells in the liver, the cells were also analyzed in a different mouse strains and in different mouse models.

2 MATERIAL AND METHODS

2.1 Materials

2.1.1 Technical equipment

Table 1. Overview of used technical equipment.

Equipment	Description, Company
Autoclave	5075 ELV, Tuttenauer, Germany
Balance	EW, Kern, Germany
Benches	Hera-Safe, Heraeus, USA
Centrifuge	Centrifuge 5425 R, Eppendorf, Germany
	MiniSpin®/ MiniSpin® plus, Eppendorf, Germany
Centrifuge with cooling function	Heraeus Biofuge fresco, Thermo Fisher, Germany
	5424R, Eppendorf, Germany
Electrophoresis Chamber	Sigma-Aldrich® MSMINIDUO horizontal, Sigma-Aldrich Corp, USA
Freezer	Liebherr (-20 °C), Germany
	Thermo Scientific (-80 °C), USA
Fridge	Siemens, Germany
	Bosch, Germany
Flow cytometer	LSRFortessa™ Cell Analyzer, BD Bioscience, USA
	Aurora, CYTEK®, USA
Gel Documentation Imaging	E-BOW C5, Vilber Lourmat, France
Heating blocks	HTM 130, Haep Labor Consult, USA
	PHMT-PSC20, Grant Instruments, USA
	HX-2, VWR Peqlab, Germany

High Throughput Sampler (HTS)	BD Bioscience, USA
Ice machine	AF 100, Scotsman, USA
Incubators	CO_2 Incubator C150 R Hinge 230, Binder, USA
Laminar Flow Hood	Electronics FAZ 2, Waldner, Germany
Magnetic stirrer	IKAMAG RCT, IKA, Germany
Microscope	Eclipse TS100, Nikon, USA
Microtome	HM 450 Sliding Microtome, Microm, Germany
Microscope CCD-Camera	AxioCam ICm 1, Germany
Minishaker	MS 2, IKA, Germany
Modular tissue embedding center	EC 350, Microm, Germany
Multichannel pipette	Research, Eppendorf, Germany
pH meter	CG 842, Schott, Germany
Piccolo Xpress Analyzer	Abaxis, USA
Pipettes	Research plus, Eppendorf, Germany
	Reference, Eppendorf, Germany
	Pipetman, Gilson, USA
Pipette Aid	PIPETBOY, INTEGRA, Switzerland
Power Supplies	Power Pack P25 T, Biometra, Germany
Precision balance	EW 150-3M, Kern, Germany
PrintMate™ AS Cassette Printer	Thermo Fisher Scientific, USA
Real-Time PCR	7500 Fast & 7500 Real-Time PCR System, Applied Biosystems, USA
Safety Cabinet	Herasafe™, Heraeus, USA
	Tecnoflow, INTEGRA Biosciences, Switzerland
	Clean Air, Clean Air Systems, USA

Shaker	KS 260 basic, IKA, Germany
	Rocking Platform Shaker, VWR International, Germany
	Dual-Action Shaker KL 2, Edmund Bühler, Germany
SlideMateTM AS Slide Printer	Thermo Fisher Scientific, USA
Slide Scanner	Axio Scan.Z1, Zeiss, Germany
Sonicator	SONOPULS mini20, Bandelin, Germany
Spectrometer	NanoDrop 2000, PeQLab Biotechnologie GmbH, Germany
Thermocycler	TGRADIENT, Biometra, Germany
Tissue Drying Oven	TDO Sahara, Medite, Germany
Tissue Processor	STP120 embedding automate, Microm
Vacuum Pump	Diaphragm Vacuum Pump, Vacuumbrand, USA
Vortex	Testtube shaker, VWR International, Germany
Water purification systems	PURELAB® Ultra, ELGA, Germany
Waterbath	GFL 1083, Gesellschaft für Labortechnik, Germany

2.1.2 Consumables

Table 2. Overview of used consumables.

Equipment	Company
100 Sterican needles (26 G)	B. Braun, Germany
BD Microlance 3 TM needles (30 G)	BD, USA
Biosphere Filtered Tip, (1000μL, 200μL, 100μL, 20μL, 2.5μL)	Sarstedt AG&Co. KG, Germany
Cell scraper	Sarstedt AG&Co. KG, Germany

Corning™ 96-well Clear Flat Bottom	Thermo Fisher Scientific, USA
Corning® cell strainer size 70 µm	Sigma-Aldrich Corp, USA
Cotton swab (15 cm)	Careliv Produkte OHG, Germany
Cover Slips (24 x 32 mm)	Thermo Fisher Scientific, USA
Falcon (15 mL, 50 mL)	Sarstedt AG&Co. KG, Germany
Filter Paper	Marchery-Nagel, Germany
Gloves	TouchNTuff®, Ansell, Australia
Hypodermic Needle, 20G, 26G, 30G	BD Bioscience, USA
Injekt®-F syringes	B. Braun, Germany
MicroAmp Optical 96-well Reaction Plate	Applied Biosystems, USA
Microtome Blade A35	Feather, Japan
Omnifix Solo Luer 10 ml	B. Braun, Germany
Parafilm® M	Sigma-Aldrich Corp, USA
PCR SingleCap 8er-SoftStrips, 0.2 mL	Biozym, Germany
Pestle & microtube 1.5 mL	VWR International, Germany
Piccolo® Biochemistry Panel Plus	Abaxis, USA
RNase-Free 1.5 mL Microfuge Tues	Ambion, Germany
SafeSeal microtube (0.5 mL, 1.5 mL, 2 mL)	Sarstedt AG&Co. KG, Germany
Serologic pipette (5 mL, 10 mL, 25 mL, 50 mL)	Sarstedt AG&Co. KG, Germany
Sterile filter, Filtrapur S0.2	Sarstedt AG&Co. KG, Germany
Tips (1000 µl, 200 µl, 100 µL, 10 µl)	Sarstedt AG&Co. KG, Germany
Tissue-Loc™ HistoScreen Cassettes	Thermo Fisher Scientific, USA
Tissue Culture Plate Flat-Bottom 12-well Plate	Sarstedt AG&Co. KG, Germany
Vacuum Filtration Unit, 0.22 µm, 250 mL	Sarstedt AG&Co. KG, Germany

2.1.3 Chemicals

Table 3. List of used chemicals and kits.

Chemical	Company
Acetaminophen	Sigma-Aldrich Corp, USA
Acetic Acid	Carl Roth, Germany
ACK Lysing Buffer	Thermo Fisher Scientific, USA
Agarose	Biozym Scientific GmbH, Germany
Albumine Fraction V	Sigma-Aldrich Corp, USA
Amino acid solution	PAN Biotech GmbH, Germany
Anti-Asialo GM1	BioLegend, USA
Aspirin	Sigma-Aldrich Corp, USA
BD Cytofix	BD, USA
BD Permeabilization Solution 2	BD, USA
BioChemistry Panel Plus	Abaxis, USA
Calcium chloride	Sigma-Aldrich Corp, USA
Carbon Tetrachloride	Sigma-Aldrich Corp, USA
Collagenase from *Clostridium histolyticum*	Sigma-Aldrich Corp, USA
Collagenase type II	Sigma-Aldrich Corp, USA
Complete feed for Rats&Mice Maintenance	Sniff Spezialdiaeten, Germany
D09100301	Research Diets, USA
D-(+)- Glucose monohydrate	Sigma-Aldrich Corp, USA
Deoxyribonuclease I from bovine pancreas	Sigma-Aldrich Corp, USA
DEPC Treated Water	Invitrogen GmbH, USA
Dexamethason	Sigma-Aldrich Corp, USA
Dimethyl sulfoxide	Pan Biotech GmbH, Germany
DNA ladder, 2-log	New England Biolabs, USA
DNAZap™ PCR DNA Degradation Solutions	Invitrogen GmbH, USA
Dulbecco´s modified eagles medium (DMEM)	PAN Biotech GmbH, Germany

Dulbecco´s Phosphate Buffered Saline	Thermo Fisher Scientific, USA
EDTA	Thermo Fisher Scientific, USA
EGTA	Sigma-Aldrich Corp, USA
Eosin Y disodium salt	Sigma-Aldrich Corp, USA
Ethanol	Merck, Germany
Ethanol, 70%	Walter CMP, Germany
Ethidium Bromide	Invitrogen GmbH, USA
Fetal calf serum	Biochrom AG, Germany
FoxP3 Fixation/Permeabilization kit	eBioscience, USA
Gentamicin	PAN Biotech GmbH, Germany
HEPES	Carl Roth, Germany
High Capacity cDNA Reverse Transcription Kit	Applied Biosystems, USA
Hydrochloric acid 4 mol/L	Carl Roth, Germany
Insulin transferrin selenite supplement (ITS)	Sigma-Aldrich Corp, USA
Isoniazid	Sigma-Aldrich Corp, USA
Ketamin-ratiopharm® 50mg O.K Injection Solution	Ratiopharm, Germany
Ketoconazole	Sigma-Aldrich Corp, USA
KH Buffer (Krebs-Henseleit buffer)	Sigma-Aldrich Corp, USA
L-Glutamine	Sigma-Aldrich Corp, USA
Lipopolysaccharides from *E. Coli*	Sigma-Aldrich Corp, USA
Lyophilised rat collagen type I	Roche, Germany
Magnesium chloride	Carl Roth, Germany
Magnesium sulfate	Sigma-Aldrich Corp, USA
Mayer´s Hemalum solution	Merck, Germany
Microscopy Entellan	Merck, Germany
N-Acetyl-L-glutamic acid	Sigma-Aldrich Corp, USA
Olive Oil	Sigma-Aldrich Corp, USA
Paraffin Histowax Surgipath paraplast	Leica Microsystems, Germany

Penicillin/ Streptomycin (Pen/Strep)	PAN Biotech, Germany
Percoll®	Sigma-Aldrich Corp, USA
Phire Animal Tissue Direct PCR Kit	Thermo Fisher Scientific, USA
Picrosirius Red Stain Kit	Polysciences, USA
Potassium chloride	Sigma-Aldrich Corp, USA
Potassium dihydrogen phosphate	Sigma-Aldrich Corp, USA
Promethazine hydrochloride	Sigma-Aldrich Corp, USA
QIAzol Lysis Reagent	Qiagan, Germany
RNaseZap® RNase Decontamination Solution	Ambion, Germany
Rompun 2%	Bayer Health Care, Germany
Roti-Histofix 4%	Carl Roth, Germany
Roti-Histol	Carl Roth, Germany
RPMI-1640 medium	PAN Biotech GmbH, Germany
Sera Plus	PAN Biotech GmbH, Germany
Sodium chloride	Sigma-Aldrich Corp, USA
Stable L- Glutamine	Sigma-Aldrich Corp, USA
Taq DNA Polymerase kit	5-Prime, Germany
TaqMan® Universal Master Mix II, with UNG	Applied Biosystems, USA
Trypan Blue	Sigma-Aldrich Corp, USA
Valproic acid	Sigma-Aldrich Corp, USA
Williams´s E medium	PAN Biotech GmbH, Germany
Xylene	VWR International, Germany

2.1.4 Software

Table 4. List of used softwares.

Software	Company
FlowJo 10.8.0	FlowJo, LLC, Ashland, USA
FV10-ASW 4.1 Viewer	Olympus Europa SE & Co.KG, Hamburg, Germany
GraphPad PRISM 9.3.0	GraphPad, La Jolla, USA
LabWriter	Thermo Fisher Scientific, Waltham, USA
ZEN 3.1 (blue edition)	Zeiss, Jena, Germany

2.1.5 Flow cytometer antibodies

Table 5. Antibodies of Lymphocyte Panel for LSRFortessaTM Cell Analyzer, BD Bioscience.

Name	Conjugate	Dilution	Clone	Source
Zombie Red™ Fixable Viability Kit	Texas Red	1:1000		BioLegend, USA
Fc Block		1:200	93	BioLegend, USA
CD45	PerCP	1:400	30F11	BioLegend, USA
CD19	AmCyan510	1:50	6D5	BioLegend, USA
CD3	AF700	1:100	17A2	BioLegend, USA
CD4	FITC	1:800	RMA4-5	BioLegend, USA
CD8	PE	1:400	53-6.7	BioLegend, USA
NK1.1	BV421	1:25	PK136	BioLegend, USA

Table 6. Antibodies of Leukocyte Panel for LSRFortessaTM Cell Analyzer, BD Bioscience.

Name	Conjugate	Dilution	Clone	Source
Zombie Red™ Fixable Viability Kit	Texas Red	1:1000		BioLegend, USA
Fc Block		1:200	93	BioLegend, USA
CD45	PerCP	1:400	30F11	BioLegend, USA
CD115	AL488(FITC)	1:200	CSF-1R	BioLegend, USA
F4/80	PECy7	1:50	BM8	BioLegend, USA
CD11c	BV421	1:25	N418	BioLegend, USA
CD11b	AymCyan510	1:800	M1/70	BioLegend, USA
Ly6G	Al647	1:200	1A8	BioLegend, USA
Ly6C	Al700	1:800	HK1.4	BioLegend, USA

Table 7. Antibodies of NK cell Exhaustion Panel for LSRFortessaTM Cell Analyzer, BD Bioscience.

Name	Conjugate	Dilution	Clone	Source
Zombie Red™ Fixable Viability Kit	Texas Red	1:1000		BioLegend, USA
Fc Block		1:200	93	BioLegend, USA
CD45	PerCP	1:400	30F11	BioLegend, USA
CD3	AF700	1:100	17A2	BioLegend, USA
NK1.1	BV421	1:25	PK136	BioLegend, USA
CD49a	PE	1:50	HMα1	BioLegend, USA
KlrG1	PE-Cy7	1:100	2F1/KLRG1	BioLegend, USA
PD1	PE/Cy5.5	1:50	29F.1A12	BioLegend, USA

Table 8. Antibodies of NK cell Activation Panel for LSRFortessaTM Cell Analyzer, BD Bioscience.

Name	Conjugate	Dilution	Clone	Source
Zombie Red™ Fixable Viability Kit	Texas Red	1:1000		BioLegend, USA
Fc Block		1:200	93	BioLegend, USA
CD45	PerCP	1:400	30F11	BioLegend, USA
CD3	AF700	1:100	17A2	BioLegend, USA
NK1.1	BV421	1:25	PK136	BioLegend, USA
CD49a	PE	1:50	HMα1	BioLegend, USA
CD69	PE-Cy7	1:50	H1.2F3	BioLegend, USA
CD25	BV510	1:100	PC61	BioLegend, USA
CXCR6	FITC	1:50	SA051D1	BioLegend, USA

Table 9. Antibodies of intracellular NK cell Panel for LSRFortessaTM Cell Analyzer, BD Bioscience.

Name	Conjugate	Dilution	Clone	source
Zombie Red™ Fixable Viability Kit	Texas Red	1:1000		BioLegend, USA
Fc Block		1:200	93	BioLegend, USA
CD45	PerCP	1:400	30F11	BioLegend, USA
CD3	AF700	1:100	17A2	BioLegend, USA
NK1.1	BV421	1:25	PK136	BioLegend, USA
CD49a	PE	1:50	HMα1	BioLegend, USA
CD49b	FITC	1:800	DX5	BioLegend, USA

TNFα	AF647	1:200	MP6-XT22	BioLegend, USA
INFγ	PE-Cy7	1:200	XMG1.2	BioLegend, USA

Table 10. Antibodies of ILC Panel for LSRFortessaTM Cell Analyzer, BD Bioscience.

Name	Conjugate	Dilution	Clone	Source
Zombie Nir™ Fixable Viability Kit	AF700	1:1000		BioLegend, USA
Fc Block		1:200	93	BioLegend, USA
CD45	PerCP	1:400	30F11	BioLegend, USA
CD5	AF700	1:50	53-73	BioLegend, USA
Lin	AF700	1:50		BioLegend, USA
CD127	PE/Dazzle	1:100	A7R34	BioLegend, USA
Thy1.2	APC-Cy7	1:100	30-H12	BioLegend, USA
NKp46	BV510	1:100	29A1.4	BioLegend, USA
ST2	BV421	1:50	DIH9	BioLegend, USA
CD200r	FITC	1:200	OX2R	BioLegend, USA
PD1	PE/Cy5.5	1:50	29F.1A12	BioLegend, USA
CCR6	PE	1:25	29-2L17	BioLegend, USA
TNFα	AF647	1:200	MP6-XT22	BioLegend, USA
INFγ	PE-Cy7	1:200	XMG1.2	BioLegend, USA
GATA3	AF647	1:50	16E10A23	BioLegend, USA
T-Bet	PE-Cy7	1:200	4B10	BioLegend, USA

Table 11. Antibodies of new ILC1 Panel for Aurora, Cytek.

Name	Conjugate	Dilution	Clone	Source
Fixable Viability Dye eFluor® 780	APC - eF780	1:1500		eBioscience, USA
Fc Block		1:200	93	BioLegend, USA
CD45.2	BUV563	1:400	104	BD, USA
CD90-2	BUV496	1:400	30-H12	BD, USA
CD49a	BV605	1:200	Ha31/8	BD, USA
NK1.1	BV650	1:300	PK136	BioLegend, USA
NKp46	BV711	1:50		
CD127	BV421	1:200	A7R34	BioLegend, USA
cKit	APC	1:200	2B8	BioLegend, USA

IL18Rα	PE-Cy7	1:200	P3TUNYA	Thermo Fisher Scientific, USA
CD200r	FITC	1:50	OX2R	BioLegend, USA
CD3	biotinylated	1:200	145-2C11	BioLegend, USA
CD5	biotinylated	1:500	53-7.3	BioLegend, USA
CD19	biotinylated	1:300	6D5	BioLegend, USA
F4/80	biotinylated	1:300	Rat IgG2a,κ	BioLegend, USA
FcεR1α	biotinylated	1:300	MAR-1	BioLegend, USA
TCRγd	biotinylated	1:300	eBio-GL3	eBioscience
TCRβ	biotinylated	1:300	H57-597	BioLegend, USA
Ly6G	biotinylated	1:300	1A8	BioLegend, USA
Ter119	biotinylated	1:300	TER-119	BioLegend, USA
Streptavidin	V500	1:1000		BD, USA
INFγ	PE	1:200	XMG1.2	BioLegend, USA
T-Bet	PE	1:50	4B10	BioLegend, USA
RORγT	PECF594	1:500	Q31-378	BD, USA
Eomes	PerCP eF710	1:300	Dan11mag	eBioscience, USA
Ki-67	AF700	1:200	16A8	BioLegend, USA
Tcf7	AF700	1:200	C63D9	Cell Signalling, USA

2.1.5 Buffers and solutions

2.1.5.1 Buffer for liver perfusion

Table 12. List of buffers used for liver perfusion.

Buffer	Chemical	Amount
Collagenase Buffer	Glucose (9 g/L)	155 ml
	KH Buffer pH 7.4	25 ml
	HEPES pH 8.5	25 ml
	Amino acid solution	30 ml
	Calcium chloride (19 g/L)	10 ml
	L-Glutamin (7 g/L)	2.5 ml
	Collagenase from *Clostridium histolyticum*	100 mg
EGTA Buffer	Glucose (9 g/L)	248 ml
	KH Buffer pH 7.4	30 ml
	HEPES pH 8.5	30 ml
	Amino acid solution	60 ml
	L-Glutamin (7 g/L)	4 ml
	EGTA solution (47.5 g/l) pH 7.6	1.6 ml
Suspension Buffer	Albumin Fraction V	400 mg
	Amino Acid Solution	30 ml
	$CaCl_2$ (19 g/L)	1.6 ml
	Glucose (9 g/L)	124 ml
	L-Glutamin (7 g/L)	2 ml
	HEPES pH 7.6	20 ml
	KH buffer	20 ml
	Magnesium sulfate solution (24.6 g/l)	0.8 ml
KH Buffer	Potassium chloride (1.75 g/l)	1.75 g
	Potassium dihydrogen phosphate (60 g/l)	1.6 g
	Sodium chloride pH 7.4	60 g
	Fill up with distilled water	1 l
	adjust pH 7.4	

2.1.5.2 Other Buffers

Table 13. List of buffers and solutions.

Buffer	Chemical	Amount
10x PBS	Sodium chloride	80 g
	Potassium chloride	2 g
	Disodium phosphate	14.4 g
	Monopotassium phosphate	2.4 g
	Fill up with distilled water	1 l
	adjust to pH 7.4	
10x TAE	Tris-HCl	48.4 g
	Glacial acetic acid	11.4 ml
	EDTE disodium salt	3.7 g
	Fill up with distilled water	1 l

Anesthesia	0.9 % sodium chloride	1.8 ml
	Ketamine	200 µl
	Rompun	500 µl
EDTA solution	EDTA	32 mg
	Dissolved in distilled water	1 ml
Enzyme Solution	Collagenase type II	50 mg
	DNAse Type I	10.000 U
	0.15 M sodium cloride	500 µl
	5 mM magnesium chloride	101.65 mg
	FCS	10 ml
	Fill up with DPBS	100 ml
Eosin (1%)	Eosin	2 g
	Distilled water	200 ml
	Glacial acetic acid	2 drops
	Filtered before usage	
FACS Buffer	1x PBS	500 ml
	FCS	10 ml
	EDTA (0.5 M)	2 ml
Hematoxylin	Mayer´s Hemalum	40 ml
	Distilled water	160 ml
	Filtered before usage	
Percoll solution	Original Percoll Solution	18 ml
	10x sterile PBS	2 ml
	RPMI-1640 medium	27.7 ml
	Pen/Strep	0.3 ml
Sodium chloride (0.9%)	Sodium chloride	9 g
	Fill up with distilled water	1 l

2.1.6 Cell culture media

Table 14. Media for primary mouse hepatocytes culture.

Media	**Additives**	**Amount**
Plating Medium	William´s E medium	500 ml
	Sera Plus	50 ml
	Pen/Strep	5 ml
	Gentamicin	500 µl
	Dexamethasone	20 µl
	ITS supplements	5 µl
Culture Medium	William´s E medium	500 ml
	Pen/Strep	5 ml
	Gentamicin	500 µl
	Dexamethasone	20 µl
	ITS supplements	5 µl

Table 15. Media for immune cells.

Media	Additives	Amount
Wash Medium	RPMI-1640 medium	500 ml
	Pen/Strep	5 ml
Full Medium	RPMI-1640 medium	500 ml
	Pen/Strep	5 ml
	FCS	50 ml

2.1.7 Primers for Genotyping of B6;129-Ncr1^{tm10man}/J mice

Table 16. Primers for genotyping.

Primer	Sequence 5´-> 3´
Mutant Primer	ACC ACT ACC AGC AGA ACA CC
Wild type Primer	ACA ACC CAG AAT CTC ATT CG
Common Primer	TGC CAA ACT TGG TAA CAC TCC

2.1.8 TaqMan assays

Table 17. List of TaqMan assays.

Target gene	Company	Assay Catalog Number
GAPDH	Applied Biosystems, USA	4352932E
H60b	Applied Biosystems, USA	Mm04243254_m1
Klrk1	Applied Biosystems, USA	Mm0473603_m1
Rae1	Applied Biosystems, USA	Mm0558293_g1
Ulbp1 (MULT1)	Applied Biosystems, USA	Mm01180648_m1

2.2 Methods

In the following chapter, several different techniques are described, which have already been described in more detail in my master thesis: Studying of the function of WISP1 in the liver (Schlüter, 2018).

2.2.1 Animal models

In all experiments, male mice were used which were between eight and twelve weeks old at the start of the experiment. The mice were housed and treated in compliance with the animal welfare and laboratory animal regulations and the handling procedures were approved by the animal experimental committees. The mice were kept in a temperature-controlled room between 18°C to 23°C with a 12-hour light/ dark cycle and humidity between 30% and 70%. Furthermore, the mice had free access to water and were usually fed *ad libitum* with Ssniff R/M-H. 10mm standard diet (Ssniff, Soest, Germany). Changes in the feeding protocol for the

APAP and Western diet mouse models are described in the according chapters. Before the experiments started, all purchased mice had one week time to adjust to the new environment.

2.2.1.1 Acetaminophen mouse model

As one of the most investigated and well-established DILI mouse models, APAP was used. Male C57Bl/6N mice (Janvier Labs, France) were starved overnight but still had free access to water. On the next day, mice were treated intraperitoneally (i.p.) with 300 mg/kg APAP or with its vehicle control 1x PBS. Before APAP was injected, a solution of 14.9 g/l APAP was prepared in 1x PBS. In order to solubilize APAP, it was warmed up in a water bath at 55°C until it was dissolved. Afterwards, it was cooled down to room temperature, sterile filtered and subsequently injected. APAP was always freshly prepared before the injection.

2.2.1.2 Carbon tetrachloride mouse model

Another well-established and investigated mouse model is the CCl_4 mouse model. Within this mouse model, mice were i.p. treated with 1 g/kg CCl_4 dissolved in olive oil. As control, mice received the vehicle control olive oil. During the experiments, mice were fed *ad libitum*.
Several experiments were performed with CCl_4 and different mouse strains were included: C57Bl/6N mice (Janvier Labs, France), B6;129-Ncr1^{tm10man}/J mice (originally purchased from Jackson Laboratory and now bred in animal facility) and Hobit mice (received from Prof. Georg Gasteiger Würzburg). CCl_4 was always freshly prepared before the injection.

2.2.1.3 Hobit mice

Wild type and knock out Hobit mice were provided from Prof. Georg Gasteiger (Würzburg). The transcription factor gene Hobit, which is encoded by the gene *Zfp683*, is highly expressed on ILC1s and not on NK cells. But it is not exclusively expressed on ILC1s, it is also expressed by memory T cells and NKT cells and it is described to be required for the generation of ILC1s (Behr et al., 2020; Friedrich et al., 2021; Mackay et al., 2016). Due to the knockout of Hobit, these mice lack ILC1s but this knockout does not affect the NK cells.
In order to generate Hobit KO mice, Zfp683$^{tm1a(KOMP)Wtsi}$ ES cell clones were obtained from the KOMP repository and generated by the Wellcome Trust Sanger Institute (WTSI). Mice were generated by Laser assisted (XY-Clone Hamilton Thorne) injection of JM8A3.N cells into 8-cell-stage C57Bl/6NCrl embryos. All injections were done with Narishige manipulators in the Transgenic Core Facility (TCF) of the MPI-CBG. Chimeras were crossed to C57Bl/6NCrl mice, and their offspring was screened by PCR for germline transmission (Skarnes et al., 2011).

2.2.1.4 Homozygous NCR1 GFP mice

Heterozygous B6;129-Ncr1^{tm10man}/J (NCR1-GFP) mice were originally purchased from Jackson Laboratory and further bred in our animal facility to obtain homozygous NCR1-GFP mice. These mice lack the Ncr1 gene (NKp46 receptor). The basic strategy of generating

NCR1- green fluorescent protein (GFP) mice was to replace the exons 5 to 7 of the Ncr1 gene by a GFP cassette. Consequently, every cell which usually expresses NKp46 is labelled with GFP (Gazit et al., 2006) Originally, the idea was to specifically label NK cells, but during the last year, the activating receptor was found to be also expressed on ILC1s and some ILC3s. As a consequence of the GFP knock in into the NCR1 locus, the NCR1 gene is not functional anymore and the homozygous Ncr1-GFP mice are also NKp46 knock out mice.

2.2.1.4.1 Genotyping of NCR1 GFP mice

Genotyping is a commonly used technology to determine differences of an individual DNA sequence in comparison to a reference DNA sequence concerning their genetic information. In order to determine the genotype of the NCR1-GFP mice, the Phire Animal Tissue Direct PCR Kit (Thermo Scientific) was used. Therefore, ear punches from mice were collected in a 0.5 ml tube filled with 25 µl Dilution Buffer. To release the DNA from the tissue, a volume of 1.5 µl DNARelease Additive was pipetted to the ear punch containing tube and subsequently heated to 98°C for 25 minutes with gently shaking in a thermo block. After a short centrifugation step, the DNA concentration was measured using the NanoDrop2000 spectrometer. The measured concentrations should be between 200 ng/µl and 400 ng/µl to perform a successful PCR. The reaction mix for one PCR reaction is listed in table 18, containing three different primers for the detection of the different alleles (table 16). Finally, a volume of 20.4 µl of master mix was transferred to PCR-microtubes and 1 µl of isolated DNA were added. The PCR setup of the thermocycler is listed in table 19.

Table 18. PCR Master Mix for genotyping.

Phire Animal Tissue Direct PCR Kit	**Volume per reaction [µl]**
Phire Animal Tissue PCR Buffer	10
Mutant Primer	1
Wild type Primer	1
Common Primer	1
DEPC-treated water	7
Phire Hot Start II DNA Polymerase	0.4
Final Volume	**20.4 + 1 µl DNA-Sample**

Table 19. Setup of PCR reaction for genotyping using a thermocycler.

Step	Temperature [°C]	Time [sec]	Note
1	94	120	
2	94	20	
3	65	15	
4	68	10	Go back to step 2, repeat steps for 10 cycles
5	94	15	
6	60	15	
7	72	10	Go back to step 5, repeat steps for 28 cycles
8	72	120	
9	4		Pause, Hold on this temperature

To analyse the PCR products, a 1.5 % Agarose gel containing ethidium bromide was prepared. The PCR product was mixed with 5 µl of Gel loading dye, shortly spun and load onto the Agarose gel together with a DNA ladder. Gel electrophoresis was performed at 100 V for 60minutes in 1x TAE buffer. The genotyping results were obtained by visualizing the PCR product bands in the Agarose gel with E-BOW C5 (Vilber Lourmat, Germany) (Schlüter, 2018). Homozygous NCR1-GFP mice had one PCR product with a size of 550 base pairs (bp), while the PCR product of the wildtype mice possessed a size of 300 bp and heterozygous NCR1-GFP mice showed both bands.

2.2.1.5 Western-style diet mouse model

Within this mouse model, eight-week-old male C57Bl/6N mice (Janvier Labs, France) were fed *ad libitum* with either standard diet as control or western-style diet for twelve weeks. The standard diet group was fed with Ssniff R/M-H. 10mm standard diet (Ssniff, Soest, Germany). Western-style diet food contained 40 % kcal fat and carbohydrates, 20 % kcal fructose and proteins, and 2 % cholesterol (D09100301, Research Diets, New Brunswick, USA). Further ingredients are summarized in the given table:

Table 20. Ingredients of the used Western-style diet.

	grams	kcal
Casein, 80 mesh	200	800
L-cystine	3	12
Maltodextrin 10	100	400
Fructose	200	800
Sucrose	96	384
Cellulose (BW200)	50	0
Soybean oil	25	225
Primex shortening	135	1215
Lard	20	180
Mineral Mix S10026	10	0
Dicalcium phosphate	13	0
Calcium carbonate	5.5	0
Potassium citrate	16.5	0
Vitamin Mix (V10001)	10	40
Choline bitartrate	2	0
Cholesterol	18	0
FD&C Yellow dye	0.05	0
Total	**904.05**	**4056**

2.2.1.6 Valproic acid treatments

In order to investigate the NK cell activity against hepatocytes in response to a drug, the aim was to establish a mouse model in which the liver was damaged caused by VPA. For all described experiments, male C57Bl/6N mice (Janvier Labs, France) with an age between 8 and 12 weeks were used. Valproic acid salt (Sigma Aldrich) was dissolved in 1x PBS, subsequently sterile filtered and the doses were administered to mice orally by gavage.
In the first VPA experiment, a low dose (250 mg/kg) and a high dose (500 mg/kg) of VPA were daily applicated to the mice for 14 days.
Since the first experiment did not show any indication for a liver damage, in the second experiment, the mice were not only treated with 500 mg/kg VPA but also with lipopolysaccharide (LPS). LPS is usually found in the outer membrane of Gram-negative bacteria and causes a cytokine storm in the body. Therefore, 2 mg/kg LPS (Sigma Aldrich) in 1xPBS was first injected intravenously to mice and subsequently they orally received 500 mg/kg VPA.

2.2.1.7 Anti-Asialo GM1 Depletion Antibody

A commonly used approach to deplete NK cells *in vivo*, is the usage of a polyclonal antibody which specifically reacts with Asialo ganglio-N-tetraosylceramide (Anti-Asialo GM1). Asialo-GM1 is a glycolipid expressed by NK cells but also by basophils and some monocytes. In order

to deplete the NK cells, 50 µl of the depletion antibody Anti-Asialo GM1 (dissolved in 1 ml dH_2O, Biolegend) was i.p. injected into mice 24 hours before the collection.

2.2.2 Collection of blood samples and liver tissue

At the day of experiment, the mice were weighted and subsequently anaesthetised by i.p. injection with a mixture of 2 % sedative Rompun (20 mg/kg) and anaesthetic ketamine (120 mg/kg) in 0.9 % sodium chloride (NaCl) using a 1 ml syringe with a 26G cannula. To ensure that mice were anaesthetised and reflexes were fully suppressed, pain sensitivity was monitored by checking feet and eye reflexes. After the mice were fully anaesthetised and had no reflexes, they were fixed in a dorsal position on an operation stand and cleaned with 70 % ethanol to provide aseptic working conditions. In the next step, the abdominal cavity was opened.

2.2.2.1 Blood sampling and plasma separation

After the abdominal cavity was opened, the heart blood was collected. With the use of a 26G cannula in a 1 ml syringe containing 25 µl Ethylenediaminetetraacetic acid (EDTA) solution, the heart is directly punctured through the diaphragm. Due to the direct heart puncture, around 400 µl of blood was collected. The collected blood was immediatly centrifuged at 13.000 rpm for 10 minutes at 4°C and the separated plasma was stored in a 0.5 ml tube at -80°C for further biochemical analysis.

2.2.2.2 Biochemical analysis

In order to analyze the liver function, the Piccolo Xpress chemistry analyzer (Abaxis) and the Biochemistry Panel Plus discs (Abaxis) were used. The discs contained several dried reagents which enabled the determination of thirteen different substances such as alanine-aminotransferase (ALT), aspartate-aminotransaminases (AST) and albumin. For the analysis, the mouse plasma samples were diluted with 1x PBS at least in a 1:1 ratio. In case of liver damage, the samples needed to be higher diluted. In total, 100 µl of the diluted sample was pipetted into the sample chamber on the disc whereby bubbles needed to be avoided since they could influence the results. The disc was placed in the Piccolo Xpress chemistry analyzer in which the disc was spun automatically and the sample was able to reach the different dry reagents. Consequently, the reactions started and the signals were detected by the analyzer.

2.2.2.3 LC-MS-analysis of blood obtained from *vena facialis*

To analyze the kinetic of achieved plasma concentration of VPA, mice were treated with VPA and blood was taken from the *vena facialis* at different time points (5, 10, 15, 30, 60, 120, 240 and 480 minutes after VPA application). Therefore, the mouse was fixated so that at the same time, a stow of the vein takes place. The vein is located three mm dorsocaudal of the hair swirl

on the lower jaw. For the puncture of the *vena facialis*, a 20G needle is used and the obtained blood is collected in an Eppendorf tube filled with 25 µl EDTA solution. In order to obtain the plasma, the collected blood is centrifuged for ten minutes at 13.000 rpm and 4°C.
The following steps were performed by the analytical chemistry department. 10-20 µl of mouse plasma were diluted to 100 µL in ice-cold methanol containing internal standard (d6-valproic acid, Sigma Aldrich) for protein precipitation (resulting internal standard concentration: 50 µmol/L). Samples were centrifuged at 21.000x g for 3 minutes and the supernatant was frozen at -20°C until further use.
The analyses were conducted on a QExactive mass spectrometer coupled to a Vanquish Horizon UHPLC system (both Thermo Scientific). 5 µL of sample was applied to a 125 x 3 mm I.D., 2.7 µm NucleoShell Bluebird RP18 column (Macherey-Nagel) with a flow of 400 µL/min at 50% solvent B (solvent A: 0.1% formic acid in water; solvent B: 0.1% formic acid in acetonitrile). The mass spectrometer was operated in negative-ion targeted-SIM-mode at a resolution of 140.000 at 200 m/z using 2-fold MSX for 143.10775 Da (valproic acid) and 149.14541 Da (d6-valproic acid) with a 1 Da Q1 window. For quantification, the Skyline software (DOI:10.1093/bioinformatics/btq054) was used together with a linear calibration (0; 10; 25; 50; 75; 100; 200 µmol/l with 50 µmol/l internal standard).

2.2.2.4 Collection of tissue samples

After the final heart puncture, the gall bladder was removed. Next, the liver was flushed with RPMI 1640 medium (PAN Biotech) supplemented with 10% FBS and 1% Pen/Strep via the *portal vein* by using a 30G cannula and a 10 mL syringe to wash off the remaining blood. During the perfusion of the liver, the *vena cava* was cut to avoid a too high pressure and to allow the blood to get completely washed out of the liver. When the color of the liver turned beige, the liver was carefully excised, briefly rinsed in 1x PBS and weighted. One half of the left liver lobe was collected in Tissue-Loc™ HistoScreen Cassettes for paraffin embedding and histological analyses. Furthermore, two 0.5 cm^2 big pieces of the liver tissue was snap-frozen in liquid nitrogen and subsequently stored at -80°C for RNA isolation. The remaining liver tissue was weighted again and then used for the immune cell isolation.

2.2.2.4.1 Paraffin embedding of mouse liver

The left liver lobe, which was collected in Tissue-Loc™ HistoScreen Cassettes, was fixed in 4% PFA at 4°C. After 48 hours, the samples were washed with 1x PBS and stored at 4°C. In the next step, the tissues were embedded in paraffin by using the spin tissue processor STP120 embedding automate (Microm, Walldorf, Germany) as described in table 21. Lastly, the tissue samples were embedded in paraffin using the EC 350 – Modular tissue embedding center (CellPath, United Kingdom).

Table 21. Paraffin embedding program.

Solution	Time (min)
70 % Ethanol	30
70 % Ethanol	60
90 % Ethanol	30
90 % Ethanol	30
99 % Ethanol	30
99 % Ethanol	35
99 % Ethanol	60
Xylene	30
Xylene	35
Xylene	60
Paraffin	80
Paraffin	105

2.2.2.4.2 Immune cell isolation

After the remaining piece of the liver was weighted, the organ is roughly dissected. The tissue pieces were gently passed through a 70 µl strainer located on top of a 50 ml falcon tube on ice and washed with maximal 45 ml Roswell Park Memorial Institute (RPMI) 1640 medium supplemented with 10% FBS and 1% Pen/Strep. Next, the tissue suspension was centrifuged at 300x g for 10 minutes at 4°C. Afterwards, the supernatant was carefully aspirated, the remaining pellet was resuspended in 5 ml pre-warmed enzyme solution containing collagenase type II and DNAse type I and incubated at 37°C for 30 minutes in a gently shaking water bath. The digestion reaction was stopped by the addition of 40 ml cold 1x DPBS, a centrifugation step was performed at 300x g for five minutes at 4°C and the supernatant was gently removed. In order to remove the hepatocytes, the pellet was resuspended in 5 ml of 36 % Percoll containing solution, transferred to a 15 ml falcon tube and centrifuged at 1000x g for 15 minutes at room temperature. Importantly, the centrifugation needed to stop without the break otherwise the created phases would be destroyed. The top layer contains the hepatocytes which needed to be carefully removed with a clean cotton swab. In the next step, the interphase was aspirated and the pellet containing the immune cells was washed with 10 ml cold DPBS followed by a centrifugation step at 300x g for five minutes at 4°C. In the next step, the received pellet was resuspended in 3 ml Ammonium-Chloride-Potassium (ACK) buffer (Sigma Aldrich) and incubated for four minutes at room temperature with shaking. This step is necessary to remove the erythrocytes. To stop the reaction, 9 ml of 1x cold PBS was added and centrifuged at 300x g for five minutes at 4°C. The cell pellet was resuspended in 3 ml RPMI 1640 medium supplemented with 10% FBS and 1% Pen/Strep and kept on ice. To determine the immune cell number, a volume of 90 µl 0.4 % Trypan blue solution and 10 µl of cell suspension was mixed and applied to a Neubauer chamber and counted under a microscope.

2.2.3 Histopathology

In order to perform the two different histological analyses, formalin-fixed, paraffin embedded liver tissues were sliced in four µm-thick sections by using the HM 450 Sliding Microtome (Microm, Walldorf, Germany). In a next step, the slides were fixed on glass microscopy slides at 60°C for 20 minutes and then stored at 4°C for the following stainings.

2.2.3.1 Hematoxylin and eosin staining

Hematoxylin and Eosin (H&E) staining was performed to recognize various tissue types and morphologic changes. In this process, formalin-fixed, paraffin embedded liver slides were deparaffinized in Roti-Histol for three times ten minutes and subsequently rehydrated in a declining alcohol range (100 %, 90 %, 80 %, 70 % and dH_2O) for five minutes each. In the next step, the liver samples were incubated for five minutes with the basic dye Mayer's hematoxylin (1:5 diluted with destilled water) for staining of acidic or basophilic structures like DNA and RNA in a purplish blue. Subsequently, tissue slides were washed under running tap water for 15 minutes. Next, the samples were incubated with the acidic dye 1 % Eosin which binds to positively charged proteins achieving a pinkish color of the cytoplasm. After three minutes, the samples were dehydrated in an ascending ethanol series (dH_2O, 70%, 80 %, 90 % and 100 %) for 30 seconds each, followed by incubation in Roti-Histol for three minutes. Finally, the tissue samples were mounted with Entallan, dried overnight and images were acquired with whole slider scanner (Axio Scan Z1, Zeiss).

2.2.3.2 Sirius red staining

With the help of the Picrosirius red staining, collagen accumulation in the liver tissue can be visualized. This staining was performed by usage of a commercially available kit (Polyscience Europe GmbH). According to its manufacturer instructions, formalin-fixed, paraffin embedded liver slides were deparaffinized four-times for five minutes in Roti-Histol and rehydrated in descending ethanol series (100 %, 90 %, 80 %, 70 %, 50 %, 30 % and dH_2O) for five minutes each. Next, the liver tissues were incubated with phosphomolybdic acid for 2 minutes and subsequently rinsed in distilled H_2O for 90 seconds. Afterwards, the samples were stained with Picrosirius Red solution for 60 minutes, followed by two minutes rinsing in distilled H_2O. In the last incubation step, the tissues were washed in 0.01 % HCl for two minutes and then dehydrated in an ascending ethanol series (dH_2O, 70%, 80 %, 90 % and 100 %) for one minute each followed by incubation in Roti-Histol for three minutes. In the end, liver sections were preserved in Entallan, dried overnight and images were acquired with whole slider scanner (Axio Scan Z1, Zeiss).

2.2.4 Flow cytometry staining

In order to identify the different liver immune cells, the cells were stained intracellularly and extracellularly with different protocols and examined with the LSRFortessa^{TM} Cell Analyzer (BD Bioscience) or with the Aurora (Cytek). For all performed stainings, 200.000 immune cells were used for the extracellular and 1x10^6 cells for intracellular analyses. The appropriate number of cells were added in 96-well plates and spun at 1.500x g for 5 minutes at room temperature to remove the medium.

2.2.4.1 Extracellular staining protocols

All antibodies and dyes were individually titrated to determine the optimal dilution. All antibodies, dyes and dilutions are listed in the material part (table 5–11). The first staining step is to discriminate live and dead cells. Therefore, the cells were stained with the live/dead cell zombie dye (Biolegend, 1:1000 in 1x DPBS) and incubated in the dark at room temperature. After 15 minutes of incubation, the cells were washed with FACS buffer (2% FCS in PBS) and centrifuged at 1.500x g for 5 minutes at room temperature. In order to block CD16/CD32 interactions with the Fc domain of immunoglobulins, the cells were subsequently incubated with an Fc-block (Biolegend, 1:200 in FACS buffer) for 20 minutes on ice in the dark. Afterwards, the cells were again washed with FACS buffer and centrifuged at 1.500x g for 5 minutes at room temperature. Next, the cell surface was stained by resuspending the cells in a respective amount of antibodies and incubated for 10 minutes at room temperature in the dark. The different extracellular Panels and the containing antibodies are listed in the material part (table 5-11). As the last step of the extracellular staining, the cells were again washed with FACS buffer, centrifuged at 1.500x g for 5 minutes at room temperature and the stained cells were resuspended in 200 µL FACS buffer and examined with the BD LSR Fortessa^{TM} and analyzed with FlowJo.

2.2.4.2 Extracellular staining protocol for ILC1 characterization on Aurora

To characterize ILC1s, an already established staining protocol by Georg Gasteiger´s lab (Würzburg) with subsequent examination on the flow cytometer Aurora (Cytek) was used (table 11). The staining procedure is similar to the described protocol in the previous chapter 2.2.4.1. Similar to the previous protocol, the first step is the live/ dead cell discrimination which is performed with the fixable viability dye (eBioscience, 1:1500 in 1x DPBS). The cells were incubated for 30 minutes in the dark on ice and then washed with FACS buffer and centrifuged at 1.500x g for 5 minutes at room temperature. As already described before, the cells were next incubated with the Fc-Block, then washed and centrifuged, followed by the surface staining with the antibodies of the ILC1 Aurora Panel. After the followed washing and centrifugation steps, the cells are incubated with streptavidin which is conjugated with V500

(BD) for 10 minutes in the dark at room temperature. Again, the cells were washed and centrifuged and next intracellularly stained.

2.2.4.3 Intracellular staining of cytokines

After the extracellular staining and the subsequent washing and centrifugation steps, the cells were fixed with BD Cytofix (1:1 in FACS buffer, BD) for 10 minutes at room temperature in the dark. The fixed cells were washed and centrifuged and then permeabilized with BD Permeabilization Solution 2 (1:10 in dH_2O, BD) for 10 minutes at room temperature in the dark. Subsequently, the cells were washed, centrifuged and then intracellularly stained with the cytokine antibody mix (table 9-11). After 30 minutes incubation on ice in the dark, the cells were washed, centrifuged and resuspended in 200 µL FACS buffer and subsequently measured on one of the flow cytometers.

2.2.4.4 Intracellular staining of transcription factors

The other intracellular staining is performed in order to stain transcription factors. Therefore, the washed and centrifuged extracellularly stained cells are resuspended in FoxP3 Fixation/ Permeabilization buffer diluted in Fixation/ Permeabilization Diluent (1:4, eBioscience). The cells were fixed overnight at 4°C. On the next day, the fixed cells were washed twice in permeabilization buffer (1:10, in dH_2O, eBioscience) and centrifuged at 1.500x g for 5 minutes at room temperature. After the last centrifugation, the cells were resuspended in the transcription factor antibody mix and intracellularly stained for 2 hours on ice in the dark (table 10-11). Afterwards, the stained cells were again washed twice in permeabilization buffer (1:10, in dH_2O, eBioscience) and centrifuged at 1.500x g for 5 minutes at room temperature. Finally, the cells were resuspended in 200 µL FACS buffer and subsequently measured on one of the flow cytometers.

2.2.4.5 Identification of ILC1

As already described, the identification of ILC1s is difficult. Therefore, the two gating strategies, which were used to identify ILC1s, are presented in this chapter: ILC Panel measured on the LSRFortessa™ Cell Analyzer (table 10) and the examination of the ILC1 Panel on Aurora (Cytek) (table 11).

In general, both gating strategies start with identification of lymphocytes by the discrimination of their cell size via forward scatter (FSC) and granularity via the side scatter (SSC). Next, the identified lymphocytes are further gated on FSC-Height (FSC-H) against FSC-Area (FSC-A) to exclude doublets. The remaining single lymphocytes were gated on alive CD45 positive cells.

In case of the gating strategy of the ILC Panel measured on the LSRFortessa™ Cell Analyzer, the lineage markers had the same format as the dead cell marker Zombie NIR and therefore

included in the same gate. The alive Lin$^-$CD45$^+$ cells were further gate on the IL-7 receptor (CD127) positive and CD90 negative cells. With the help of this gate, it was possible to exclude NK cells and ILC3 cells. In the next gating step, the ILC2 cell were excluded. Therefore, the CD127$^+$CD90$^-$ cells were further gated on IL-33R (ST2) negative and NKp46 positive cells. To finally identify ILC1 cells in the liver, the CD127$^+$CD90$^-$ST2$^-$NKp46$^+$ cells were gated on the liver ILC1 marker CD200r. Based on this gating, the identified CD127$^+$NKp46$^+$CD200r$^+$ ILC1s were further characterized by the transcription factor T-Bet and the cytokines TNFα and IFNγ (Fig. 8).

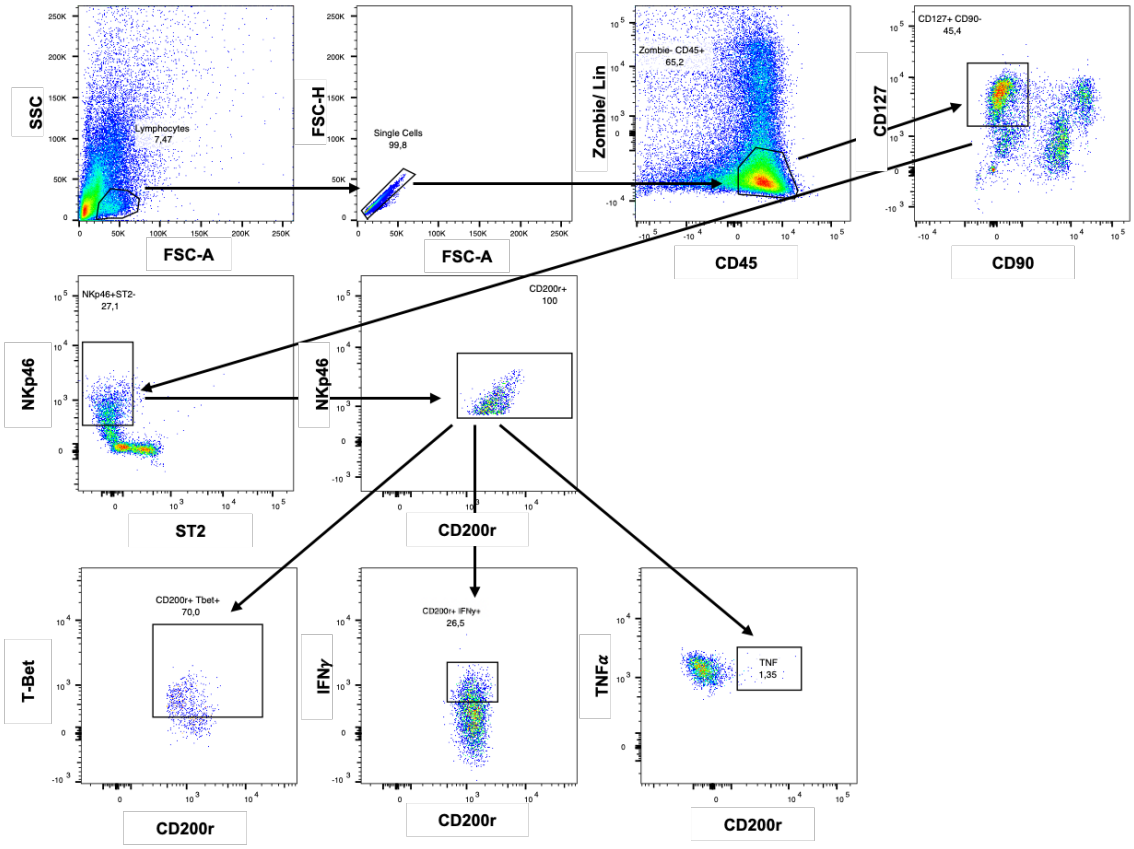

Figure 8. Gating strategy to identify ILC1s based on the ILC Panel measured on the LSRFortessaTM Cell Analyzer.
After the discrimination of the cell size, granularity and exclusion of doublets, the lymphocytes were gated on alive Lin$^-$CD45$^+$ cells. ILC1s were identified as CD127$^+$CD90$^-$NKp46$^+$ST2$^-$CD200r$^+$ cells. These cells were further quantified by their transcription actor T-Bet and the cytokines TNFα and IFNγ.

The second gating strategy to identify ILC1s were performed with the ILC1 Panel which was examined on Aurora (Cytek). After the identification of the alive CD45$^+$ cells, the cells were further gate on NK1.1$^+$Lin$^-$ cells. Within this gate, only ILC1, ILC3 and NK cells are included. In order to exclude the NK cells, the cells were further gate on CD49a$^+$Eomes$^-$ cells. In the next step, the ILC3s were excluded. Therefore, all RORγT positive cells were excluded. Additionally, the remaining NK1.1$^+$Lin$^-$ CD49a$^+$Eomes$^-$ RORγT$^-$ cells were gated on NKp46. The RORγT$^-$

NKp46^{+} cells were finally gate on CD127^{+}CD200r^{+} cells to identify liver ILC1s. Based on this gating, the ILC1 cells were further characterized (Fig 9).

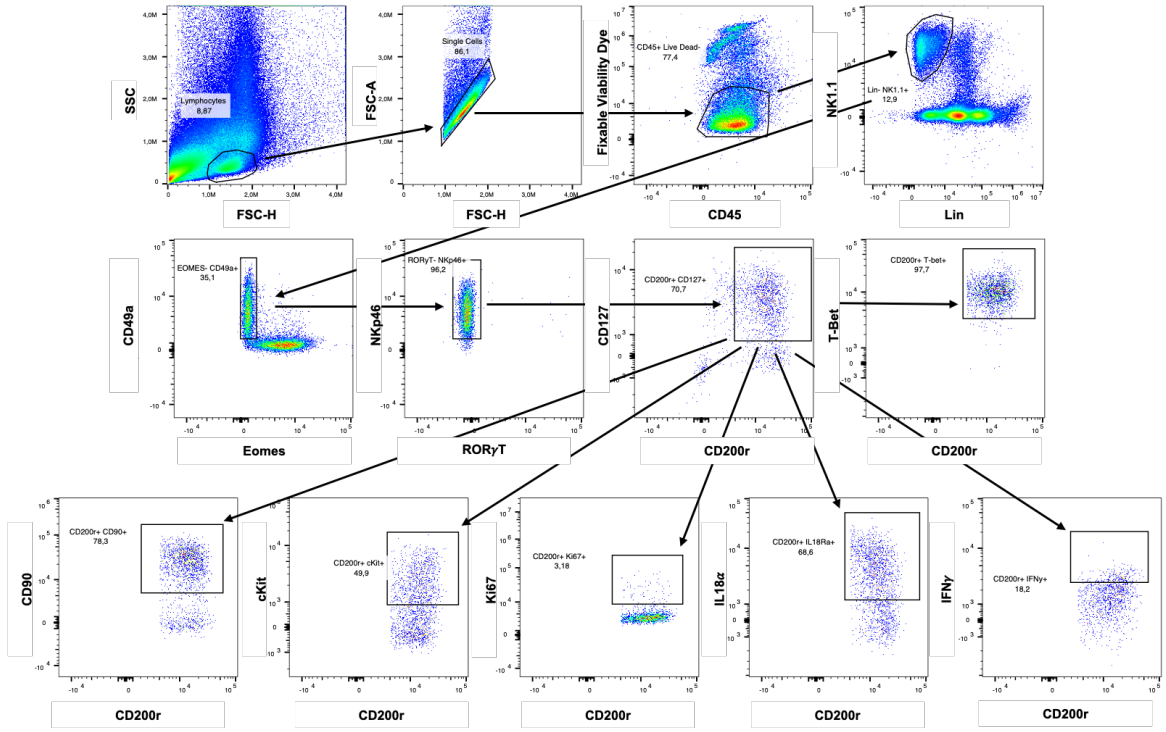

Figure 9. Identification of ILC1s based on the ILC1 Panel examined on Aurora (Cytek).
After the discrimination of the cell size, granularity and exclusion of doublets, the remaining cells were gated on alive CD45^{+} cells. ILC1s were identified as NK1.1^{+}Lin^{-}CD49a^{+}Eomes^{-}NKp46^{+}RORγT^{-}CD127^{+}CD200r^{+} cells. Based on this gating, these cells were further characterized.

2.2.5 Isolation and culture of primary mouse hepatocytes

2.2.5.1 Perfusion of mouse livers to isolate primary mouse hepatocytes

In order to obtain primary mouse hepatocytes, a two-step perfusion was performed by technicians. The perfusion was performed with C57Bl/6N mice aged between eight and fourteen weeks. At first, animals were weighted and subsequently anaesthetized by intraperitoneal injection with a mixture of 2 % sedative Rompun (20 mg/kg) and anaesthetic ketamine (120 mg/kg) in 0.9 % NaCl using a 1 ml syringe with a 26G cannula. To ensure that mice were narcotized and reflexes were fully suppressed, pain sensitivity was monitored by checking feet and eye reflexes. After the mice were fully narcotized and had no reflexes, they were fixed in a dorsal position on an operation stand and cleaned with 70 % ethanol to provide aseptic working conditions. In the next step, the abdominal cavity was open and the intestine was moved aside to be able to make an incision in the *vena cava inferior*. Therefore, a 24G cannula connected to a peristaltic pump with a flow rate of 15 ml/min was inserted into the open vein and different buffers were introduced to flush the liver (table 12). If the liver was successfully cannulated, the liver instantly changed the colour from red-brown to beige. To

avoid high pressure for the hepatocytes, the *venae portae* was cut and the buffers could flow out of the liver. The first used buffer to flush the liver is Ethylene glycol tetraacetic acid (EGTA) perfusion buffer, pre-warmed to 37°C for 15 minutes, in order to rinse the blood system, to complex and wash out blood cells and Ca^{2+} dependent adhesion factors. This complexation step is crucial for detachment and interruption of cell-cell connections which is necessary for the following step. In this following step, 37°C warm collagenase buffer is used to digest collagen in the extracellular matrix and disperse the tissue. Since collagenase is a Ca^{2+} dependent enzyme, new Ca^{2+} ions needed to be added. Depending on the enzymatic activity of collagenase, this step lasted around 5 to 15 minutes. After these different buffer treatments, the liver was excised from the mouse and under the sterile hood, the liver capsule was carefully opened to extract hepatocytes in the suspension buffer. This cell suspension was filtered through a 100 µm cell strainer to remove of tissue debris and centrifuged for 5 minutes at 50x g and 4°C. The hepatocytes were pelleted to separate them from non-parenchymal cells which were in the supernatant. The supernatant was discarded and the pelleted hepatocytes were resuspended in 10 ml cold suspension buffer by gently shaking and kept on ice. To determine the hepatocyte viability, a volume of 15 µl 0.4 % Trypan blue solution and 15 µl of cell suspension was mixed and applied to a Neubauer chamber. Stained dead cells as well as unstained live cells were counted and the cell viability was calculated with the following equation:

$$\text{viable cells (\%)} = \frac{\text{vital cells per quartile}}{\text{total number of cells per quartile}} \cdot 100\ \%$$

2.2.5.2 *In vitro* culture of primary mouse hepatocytes

Primary mouse hepatocytes were cultured in a sandwich culture. Therefore, a collagen stock solution of 1.11 mg/ ml was prepared by dissolving 10 mg lyophilised rat collagen type I (Roche) in 9 mL of 0.2 % sterile acetic acid at 4°C for at least 3 hours. After the collagen was dissolved, 9 parts of the 1.11 mg/ ml collagen solution was placed in a 50 ml falcon tube on ice together with 1 part of 10X DMEM which has an orange colour because of the pH indicator phenol red. In order to neutralise the acidity of the mixed collagen, 1M sodium hydroxide (NaOH) was drop-wise added by constantly shaking until the orange colour turns into fuchsia. This neutralized collagen was used to pre-coat the 12-well tissue culture plates by rinse the collagen solution until the well is completely covered with a thin, even and well distributed layer. The coated 12-well plates were carefully placed into a 37°C warm incubator for at least 45 minutes to allow to dry. After the gel polymerization, the plates were washed twice with pure William´s E medium and subsequently filled with pre-warmed William´s E medium with supplements and 10% Sera Plus. Afterwards, 400.000 hepatocytes were gently added to each

well to yield confluent conditions. Subsequently, the plates were carefully shaken to distribute the cells evenly and placed in the incubator at 37°C and 5 % CO_2. To ensure an even distribution of cells the plates were shaken twice in an interval of 5 minutes. After 3 hours of attachment the supernatant was discarded and the cells were washed three times with pure Williams E medium to remove cells that had not attached. In the next step, the second layer was added. Therefore, the same neutralized collagen was freshly prepared as described before and 300 µl were added to each well, gently shaken to distribute the collagen and subsequently transferred into a 37°C warm incubator for at least 40 minutes for drying. Afterwards, William´s E medium with additives were added and then placed overnight at 37°C and 5 % CO_2 in the incubator.

2.2.5.3 *In vitro* treatment of primary mouse hepatocytes with different drugs

After the addition and drying of the second layer, the PMH were directly treated with the drugs ketoconazole, isoniazid, promethazine, valproic acid or aspirin as a negative control. These drugs were dissolved in William´s E medium supplemented with additives, except for ketoconazole, which first needed to be dissolved in dimethyl sulfoxide (DMSO) and then diluted in William´s E medium with supplements. Afterwards, different concentrations of the drugs were added on the dry second layer and incubated for 24 hours at 37°C and 5 % CO_2 in the incubator.

2.2.5.4 Stimulation of primary mouse hepatocytes with TNFα

Primary mouse hepatocytes were stimulated with a concentration of 2 ng/µL TNFα (R&D Systems) for 24 hours. Recombinant human TNFα protein was reconstituted to a final concentration of 10 µg/ml in sterile PBS containing 0.1 % bovine serum albumin (BSA) and stored in aliquots at -20°C. On the day of experiment, an aliquot was thawed and a stock solution of TNFα was prepared with William´s E medium plus additives. This TNFα containing stock solution (2 ng/µl) was immediately added to the different wells after the second layer was dried. Subsequently, cells were incubated for 24 hours at 37°C and 5 % CO_2. On the next day, RNA was collected from the treated hepatocytes.

2.2.6 Gene Expression Analysis

There are several ways to isolate and analyze ribonucleic acid (RNA) which is transcribed in cells at the moment of isolation. The used protocol is based on the publication from Piotr Chomczynski (1986) in which the RNA needs to be collected with QIAzol lysis reagent (Qiagen) and isolated with phenol/chloroform followed by the synthesis of cDNA which has a higher stability than RNA. Qiazol lysis reagent contains phenol and guanidine thiocyanate which facilitate cell lysis and denaturation of proteins, especially RNases, because of its chaotropic properties. To finally quantify the expression levels of the targeted genes, real time

quantitative reverse transcription polymerase chain reaction (qRT-PCR) was performed (Schlüter, 2018).

2.2.6.1 RNA isolation

RNA was isolated from either the cultivated hepatocytes or from snap frozen liver tissues. In case of the cultivated hepatocytes, media was aspirated and 1 ml of QIAzol lysis reagent was added to each well. The cells in the wells were loosened with a cell scraper and subsequently transferred to a new 1.5 ml Eppendorf tube. Snap frozen liver sections with a size of around 0.5 cm^2 were homogenized on ice with a plastic pestle and 1 ml QIAzol in a 1.5 mL Eppendorf tube. After homogenization of snap frozen liver tissues and loosened cultivated hepatocytes, the samples were sonicated on ice for 30 seconds (5 seconds pulse/ 2 seconds break, 50 % amplitude) to break down the cell membrane and stored at -80°C until RNA isolation.
After sample thawing, to 1 ml QIAzol a volume of 200 µl chloroform were added under the fume hood and then strongly shaken for 15 seconds, incubated for two to three minutes at room temperature and centrifuged for 20 minutes at 12.000 rpm and 4°C. By the centrifugation, the samples were separated into different phases. The lower, organic phase which contained proteins, the interphase which contained DNA partitions and the upper, aqueous phase containing the RNA partitions. The upper, aqueous phase containing the RNA was carefully transferred to a new RNAse free 1.5 ml Eppendorf tube and gently mixed with 500 µl isopropanol for precipitation. The samples were incubated for ten minutes at room temperature followed by a centrifugation step for 20 minutes at 12.000 rpm and 4°C. The supernatant was carefully removed and the pellet was resuspended in 900 µl of 100 % ethanol, shortly vortexted and centrifuged at 12.000 rpm and 4°C for five minutes. This ethanol washing step was repeated twice with 80 % and 75 % ethanol. After the last ethanol washing step, the supernatant was removed and the pellet was air-dried under the fume hood. The dried pellet was dissolved in DEPC-treated water, the RNA concentration was measured using the NanoDrop 2000 spectrometer (Thermo Fisher Scientific). Extracted RNA samples were stored at -80°C (Schlüter, 2018).

2.2.6.2 cDNA synthesis

Double stranded cDNA synthesis was conducted from 2 µg of isolated RNA by using the reverse transcriptase polymerase chain reaction (RT-PCR) technique. The isolated RNA samples work as a template and by the reverse transcriptase (RT), the complementary DNA (cDNA) is generated. RT binds to the primers, which anneals to multiple sites along the RNA and adds complementary nucleotide bases to create the cDNA. In order to synthesize the second and complementary cDNA strand, RNA is digested by RNase H activity. The transcription was performed with the *High Capacity cDNA Reverse Transcription* Kit (Applied Biosystems). In table 22 the reaction mixture for one reaction is shown.

After the samples were prepared according to table 22, the PCR was performed by using the thermocycler TGRADIENT from Biometra. The qPCR program starts with an initial incubation at 25°C for 10 minutes. In the next phase, the reverse transcription is conducted at 37°C for 120 minutes followed by the inactivation phase at 85°C for five seconds. At the end of the program, the temperature is decreased to 4°C and the synthesis is completed. Afterwards, the obtained cDNA was diluted to a final concentration of 10 ng/µL with Diethylpyrocarbonate (DEPC)-treated water and stored at -20°C for qRT-PCR analysis (Schlüter, 2018).

Table 22. Preparation of master mix and reaction mixture for cDNA synthesis.

Compound	**Volume**
10x RT buffer	2 µl
25x dNTP mix (100mM)	0.8 µl
10x RT-Random Primer	2 µl
Reverse transcriptase	1 µl
DEPC-stimulated H_2O	4.2 µl
Volume 1	**10 µl**
RNA	2µg
DEPC-treated H_2O	up to 10 µl
Volume 2	**10 µl**
Final volume (Volume 1+2)	**20 µl**

2.2.6.3 Quantitative Real Time PCR (qRT-PCR)

Real-time quantitative polymerase chain reaction is used for determination of mRNA expression levels of target genes or DNA copy number measurements in genomic or viral DNAs. The qRT-PCR was performed based on the TaqMan-PCR technology with a 7500 Real-Time PCR System using a TaqMan® Universal Master Mix II with Uracil-N glycosylase (Applied Biosystems). For one PCR reaction, a volume of 10 µl TaqMan® Universal Master Mix II (Applied Biosystems), 6.5 µl DEPC-treated water, 1 µl of a specific TaqMan primer probe (Applied Biosystems) and 2.5 µl (25 ng) cDNA were pipetted to a 96-well plate. In table 17, the used TaqMan primer probes are listed. On every PCR reaction plate, a negative control was included in which the cDNA was exchanged to water as well as all samples with every primer probe were run in duplicates. In the end, the plate was covered with an adhesive foil for sealing, centrifuged for 1 minute at 1.500 rpm at room temperature, loaded to the machine and followed the qRT-PCR program setup (Table 23). The PCR products were analyzed with the 7500 Real-Time PCR System software and normalized to mouse glyceraldehyde-3-phosphate dehydrogenase (GAPDH) mRNA expression. For calculations of the relative gene

expressions, the comparative threshold method, which is also known as $2^{-\Delta\Delta Ct}$ method, was used (Schlüter, 2018).

Table 23. Overview of qRT-PCR program setup.

Stage	Temperature [°C]	Time	Repetitions
1	50	2 min	1
2	95	10 min	1
	94	15 s	
3	60	30 s	40
	72	35 s	
	95	15s	
	60	20 s	
4	95	15 s	1
	60	15 s	

2.2.7 Statistical analysis

All performed experiments were conducted with at least three or more biological replicates. To determine the significant differences between groups, the statistical analyses were performed with GraphPad Prism software version 9. Usually, one-way ANOVA and two-way ANOVA were used. P values of smaller than 0.05 were considered to be statistically significant.

3 RESULTS

3.1 Drug-induced liver damage

3.1.1 Induction of mouse NK cell ligands after drug exposure *in vitro*

Previous studies have shown an upregulation of several activating ligands for NK cell receptors like MICA and B7-H6 in primary human hepatocytes and human hepatocyte cell lines (Huh7 and HepG2) upon exposure to different drugs (Grinberg et al., 2014, Fasbender et al., 2020). Furthermore, the study of Fasbender et al., 2020 hypothesized a direct interaction of NK cells with hepatocytes resulting in cytotoxicity and IFNγ production. In order to investigate this modulation of drug-induced liver injury by NK cells, we wanted to establish a mouse model. However, since the activating ligands for NK cell receptors are not the same in mice as in humans, we first confirmed the effect of drugs on the upregulation of activating NK cell ligands on primary mouse hepatocytes (PMH) *in vitro*.

Therefore, PMH from three to four male C57Bl/6N mice were confluently plated in a sandwich culture and exposed to various concentrations of aspirin, isoniazid, ketoconazole, promethazine or valproic acid for 24 hours. Subsequently, cells were collected, RNA was isolated and transcript levels were measured by qRT-PCR for the expression of the NK cell ligands MULT1 and Rea1 and normalized to freshly isolated hepatocytes (Fig. 10). MULT1 and Rae1 are NKG2D ligands and are counterpart of the human ligands MICA, MICB and ULBP1-6 (Fu et al., 2017; Sheppard et al., 2018). Another NKG2D ligand, H60b, was also investigated but mRNA expression levels were below detection limits. It was already reported that H60b transcripts were limited *in vitro* (Diefenbach et al., 2001).

MULT1 expression levels were the highest with 10 mmol isoniazid (9.49-fold, Fig. 10D) and 10 mmol VPA (9.48-fold, Fig. 10B). After additional stimulation with 2 ng/ml TNFα for 24 hours, the expression of MULT1 was 22.83-fold induced with 7.5 mmol VPA compared to freshly isolated hepatocytes. The highest mRNA expression level for Rae1 was observed with TNFα stimulated hepatocytes which were treated with 10 mmol VPA (7.62-fold, Fig. 10B).

As a negative control, aspirin was chosen because it is not considered as a drug-induced liver injury compound and it did not show an effect on human activating NK cell ligands (Fasbender et al., 2020). In regard to the mouse NK cell ligands MULT1 and Rae1, both ligands showed a maximal increase of 2.99-fold (Fig. 10A). Furthermore, the same experiments were also performed with the murine hepatocyte cell line alpha mouse liver 12 (AML12, ATCC), but this cell line did not show any expression of NK cell ligands.

Based on the significantly higher mRNA expression levels of the NK cell ligands MULT1 and Rae1, VPA was chosen for further experiments *in vivo*.

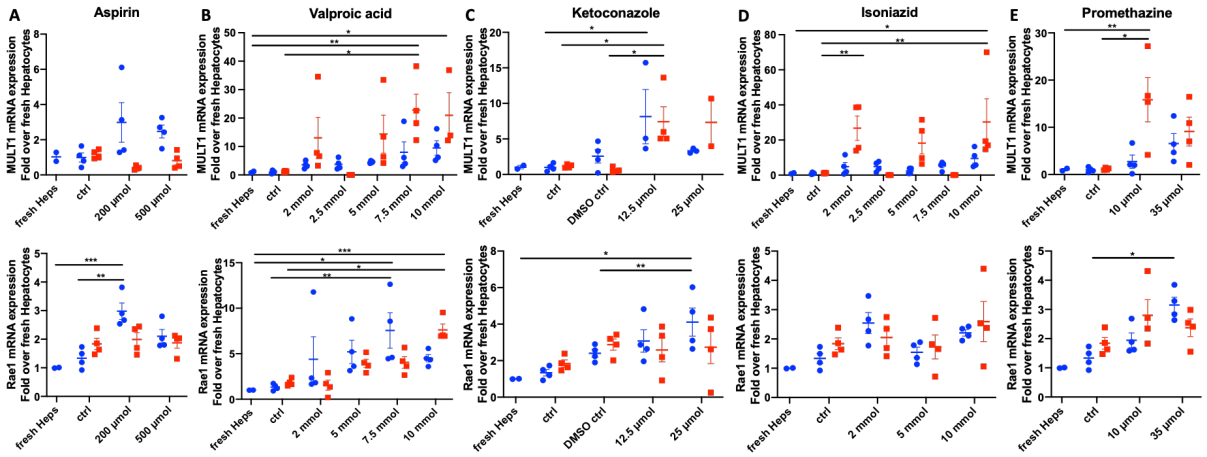

Figure 10. mRNA Expression levels of activating NK cell ligands after drug exposure to primary mouse hepatocytes.
Cultivation of primary mouse hepatocytes with **A.** aspirin, **B.** valproic acid, **C.** ketoconazole, **D.** isoniazid and **E.** promethazine without (blue) or with TNFα (red). After 24 hours of treatment, the expression of mouse NK cell ligands MULT1 (upper row) and Rae1 (lower row) were measured. Results are presented as means ± standard deviation of three to four biological replicates. Two-way ANOVA was used to calculate difference between groups. *P<0.05; **P<0.01; ***P<0.001.

3.1.2 Establishment of a VPA-induced liver injury mouse model

The aim of these experiments was to establish a mouse model that develops a liver damage caused by VPA and allows to investigate the question if there is a direct interaction of NK cells with hepatocytes resulting in cytotoxicity and IFNγ production *in vivo*.

In the first step, male C57Bl/6N mice were daily treated with a low (250 mg/kg) or a high (500 mg/kg) dose of VPA or with PBS as a control via oral gavage for 14 days. 24 hours after the last application, blood and liver tissue were collected (Fig. 11A). Gross pathology (Fig. 11B, left column) of the liver did not show any indications for a liver damage. Additionally, neither the staining of liver tissue with H&E, which visualize pericentral necrotic lesions (Fig. 11B, middle column), nor Sirius Red, picturing collagen deposition (Fig. 11B, right column), indicated a liver damage. In line with these first results, liver-weight-to-body-weight ratio and the liver enzymes ALT and AST showed no significant difference between control and treated group, indicating no hepatocyte death (Fig. 11C-E). After RNA isolation from the livers, the mRNA levels of the NK cell ligands were measured via qRT-PCR. Neither H60b, MULT1 nor Rae1 was elevated after VPA treatment in comparison to the control mice treated with PBS (Fig. 12).

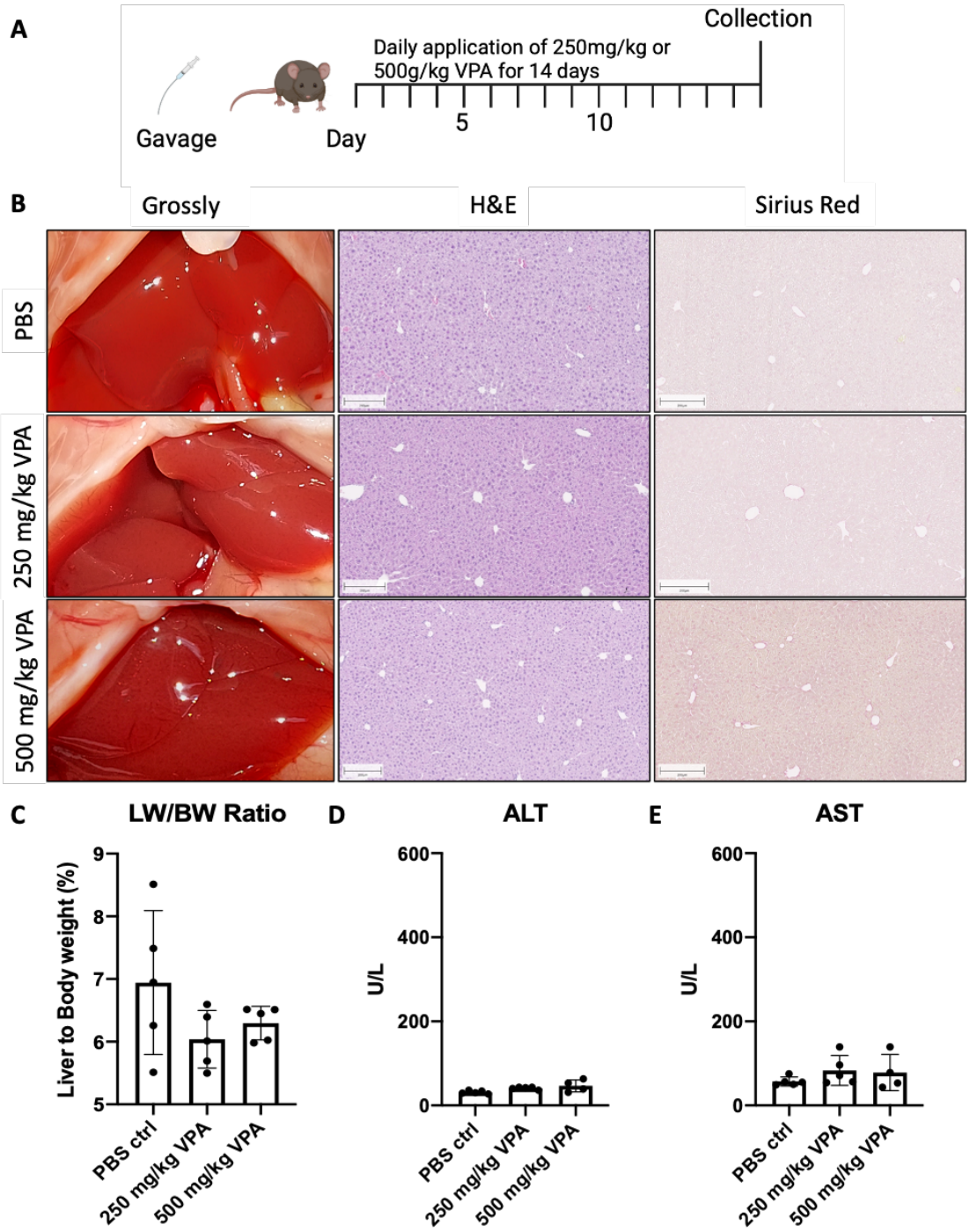

Figure 11. Application of VPA for 14 days does not lead to liver damage.
A. Experimental set up. **B.** Gross pathology (left column) and representative images of whole slide scans of H&E (middle column) and Sirius red (right column) stained liver paraffin embedded tissue sections of control mice treated with PBS (upper row) in comparison to 250 mg/kg VPA (middle row) and 500 mg/kg VPA do not show a change in the liver architecture (Scale bars: 200 μm). **C.** Liver-weight-to-body-weight ratio and plasma concentration of the liver enzymes **D.** ALT and **E.** AST are on the same levels indicating no liver damage. Data are presented as means ± standard deviation of 5 mice per group.

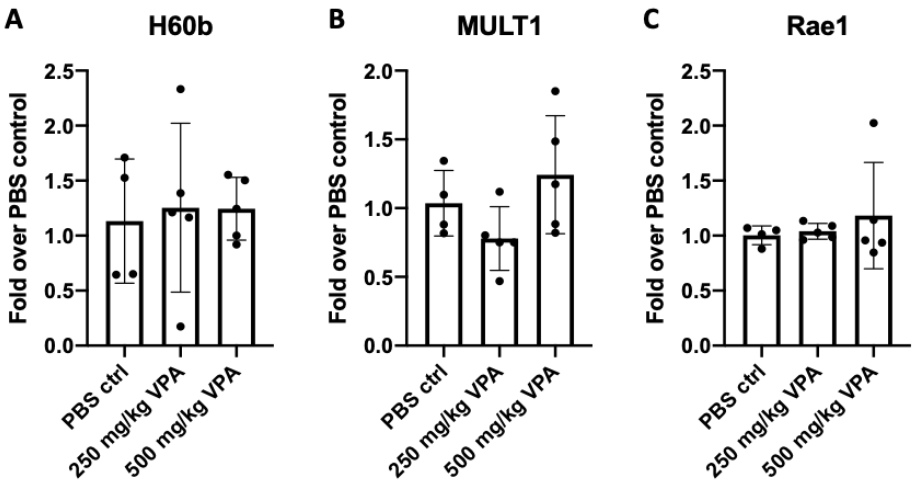

Figure 12. NK cell ligands are not induced after VPA treatment.
qRT-PCR analysis of liver tissues plotted as log-fold increase (ΔΔCt) does not show any upregulation of the NK cell ligands **A.** H60b, **B.** MULT1 and **C.** Rae1 after 250 mg/kg or 500 mg/kg VPA application. Data are presented as means ± standard deviation of five biological replicates.

To further investigate if the numbers and the function of NK cells shifted after VPA treatment, immune cells from the different livers were isolated, stained for phenotypic and activation markers and subsequently analyzed by flow cytometry. To identify the NK cells, all cells were stained extracellularly with NK1.1 as the general NK cell marker. For further characterization, the cells were also stained for CD49a to identify liver resident NK cells and intracellularly stained for their cytokines IFNγ and TNFα. The analysis of the different markers revealed a slight tendency for more NK cells in the liver after both VPA treatments (Fig. 13A), of which half of the NK cells were liver resident (Fig. 13B). However, the production of IFNγ (Fig. 13C) and TNFα (Fig. 13D) under the influence of VPA was in contrary decreased. These analyses underlined the previous results that with this mouse model the investigation of the direct effect of NK cells on hepatocytes was not possible.

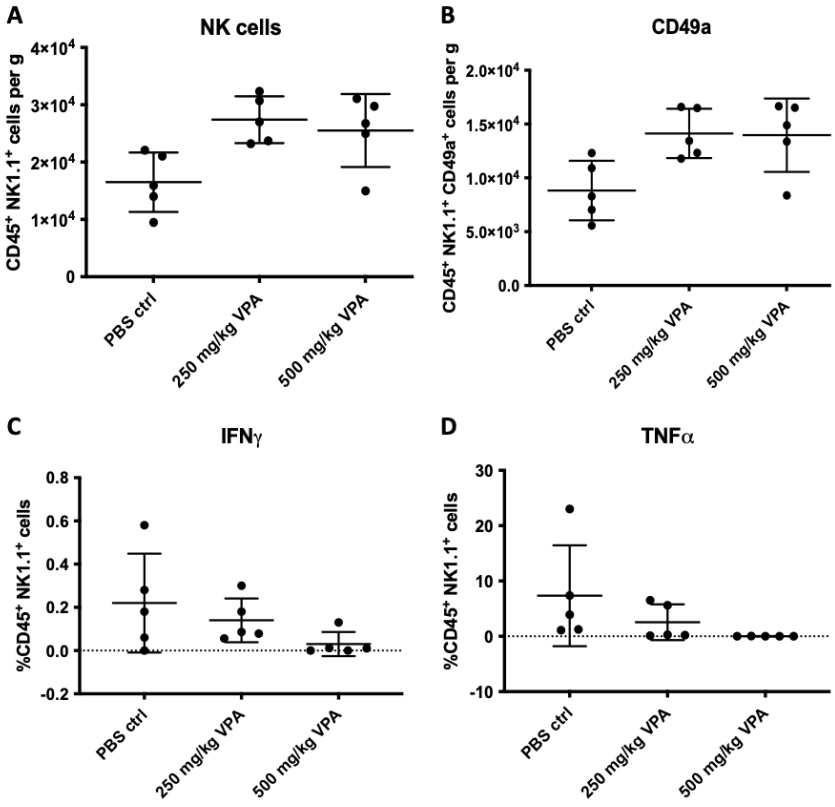

Figure 13. Characterization of NK cells after different doses of VPA for 14 days.
Freshly isolated immune cells from the livers were stained, measured via flow cytometry and analyzed with FlowJo to identify the number of **A**. NK cells which were identified as $CD45^+CD3^-NK1.1^+$, **B.** liver resident NK cells which express CD49a and the NK cell related cytokines **C.** IFNγ and **D.** TNFα. Data were analyzed from 5 biological replicates and are presented as means ± standard deviation.

Since this VPA mouse model did not cause a liver damage, the question was raised whether VPA enters the bloodstream and which maximal concentration can be reached. Therefore, the blood from mice treated for 14 days with a dose of 250 mg/kg VPA, was time-dependently collected through the submandibular vein after the last VPA application. To measure the VPA concentration in the blood plasma, analyses were conducted by mass spectrometry (Thermo Scientific). The results revealed that VPA could be measured in plasma already five minutes after drug application (Fig. 14). After eight hours, VPA was completely diminished from the bloodstream. The maximal concentration of 1 mM could be observed already 15 minutes after application. Nonetheless, the *in vitro* experiments (Fig. 10B) displayed that for significantly increase of NK cell ligands a concentration of at least 7.5 mM VPA was needed.

In summary the results from this mouse experiment showed no VPA-based liver damage and no higher activity of NK cells. Furthermore, the concentration of VPA was the highest at 1mM at 15 minutes after application indicating that the required concentration to upregulate the NK cell ligands will not be reached *in vivo*.

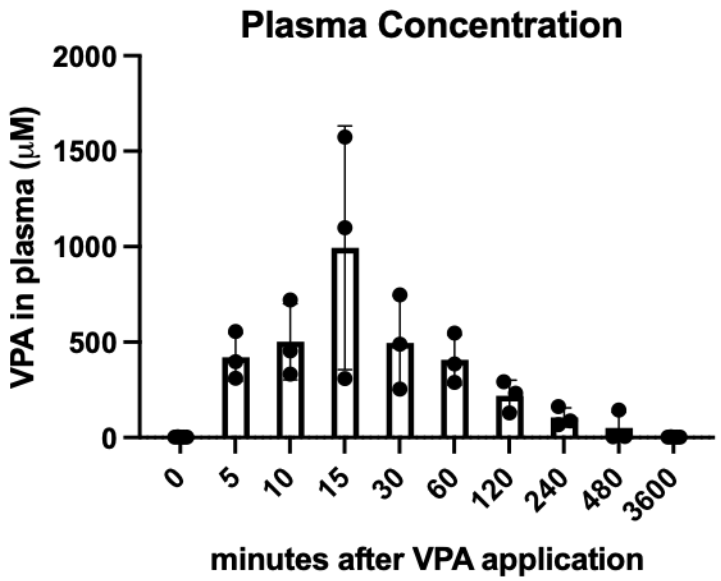

Figure 14. The highest plasma concentration of VPA was 15 minutes after the last application of 250 mg/kg VPA.
Blood samples were taken time-dependently from the submandibular vein and subsequently plasma was analyzed by mass spectrometry. Data are presented as means ± standard deviation of three biological replicates.

3.1.3 Establishment of an LPS-VPA-induced liver injury mouse model

The previously shown *in vitro* results (Fig. 10) demonstrated an even higher induction of the NK cell ligands MULT1 and Rae1 when the PMH were simultaneously treated with the drugs and 2 ng/ml TNFα for 24 hours. Treatment with TNFα and VPA induced a maximal change of 22.83-fold of MULT1 mRNA levels in comparison to freshly isolated hepatocytes. Thus, the next idea to establish a VPA-induced liver injury mouse model was to treat male C57Bl/6N mice with a substance resulting in a TNFα release in the liver. Since it is described that LPS leads to a release of different cytokines including high levels of TNFα within 90 minutes after injection (Tateda et al., 1996), male C57Bl/6N mice were first intravenously injected with 2 mg/kg LPS, and subsequently treated with 500mg/kg VPA via oral gavage. Twenty-four hours after the treatment, liver tissue and blood from these mice were collected (Fig. 15A). Gross pathology did not show a difference between PBS control, LPS, VPA or LPS+VPA group (Fig. 15B, left column). Neither H&E, Sirius red staining (Fig. 15B) nor the liver enzymes ALT (Fig. 15D) and AST (Fig. 15E) of the LPS+VPA treated livers indicated a damage of the liver in comparison to PBS and the LPS control. Further analysis of mRNA levels of the NK cell ligands H60b, MULT1 and Rae1 revealed no difference between the LPS+VPA and PBS control group (Fig. 16), although a single application of 500 mg/kg VPA seemed to result in a 6.34-fold induction of the H60b levels compared to the PBS control group (Fig. 16A).

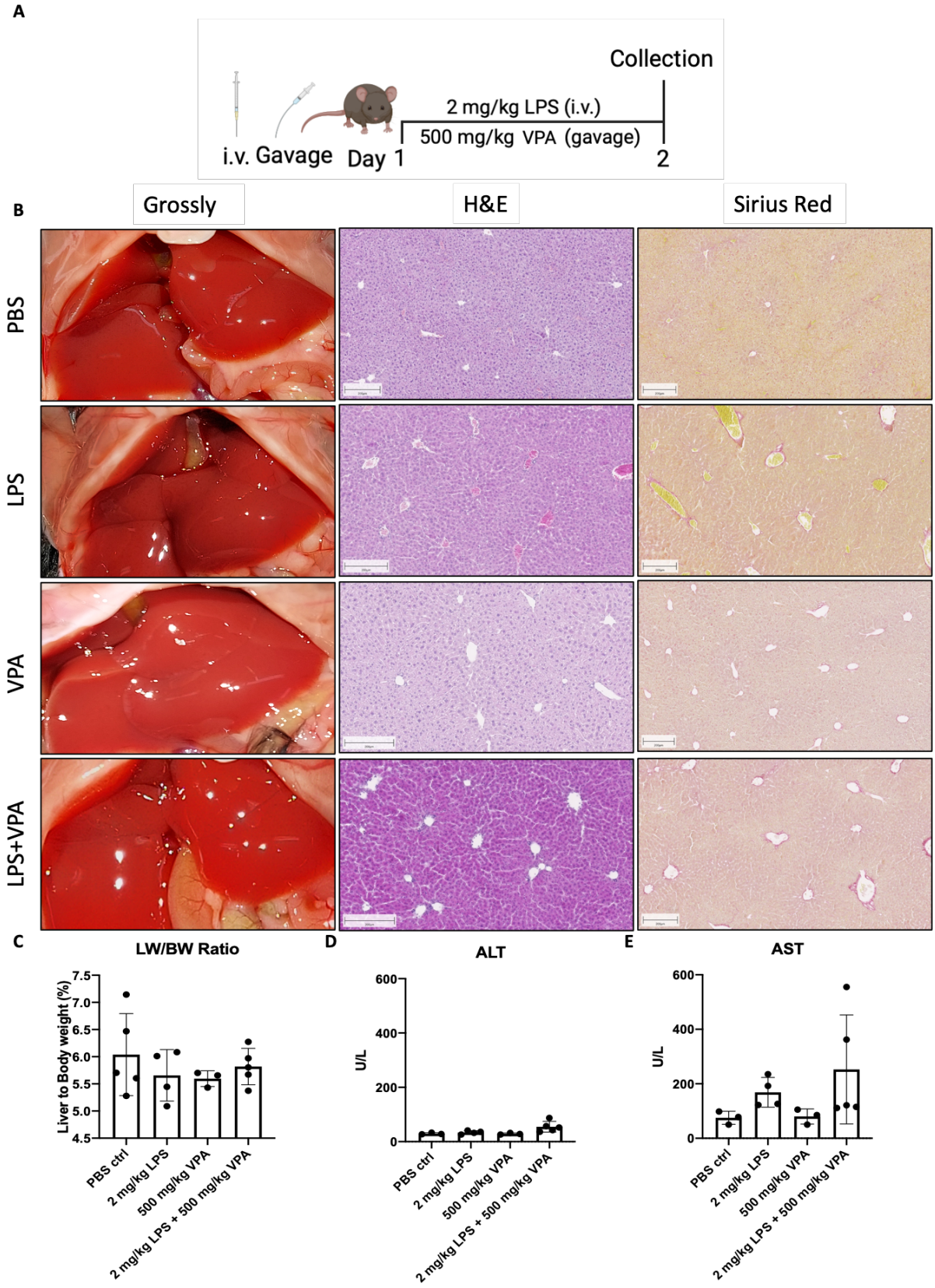

Figure 15. Simultaneous treatment with VPA and LPS does not lead to a liver damage.
A. Experimental design. **B.** Gross pathology (left column) and representative images of whole slide scans of H&E (middle column) and Sirius red (right column) stained liver paraffin embedded tissue sections of PBS control mice (upper row), 2 mg/kg LPS treated mice (second row), 500 mg/kg VPA treated mice (third row) and mice treated with 2 mg/kg LPS and 500 mg/kg VPA (lower row) do not show a change in the liver architecture (Scale bars: 200 μm). **C.** Liver-weight-to-body-weight ratio and plasma

analysis of the liver enzymes **D.** ALT and **E.** AST revealed no differences and are almost on the same level indicating no liver damage. Data are presented as means ± standard deviation of at least 5 mice per group.

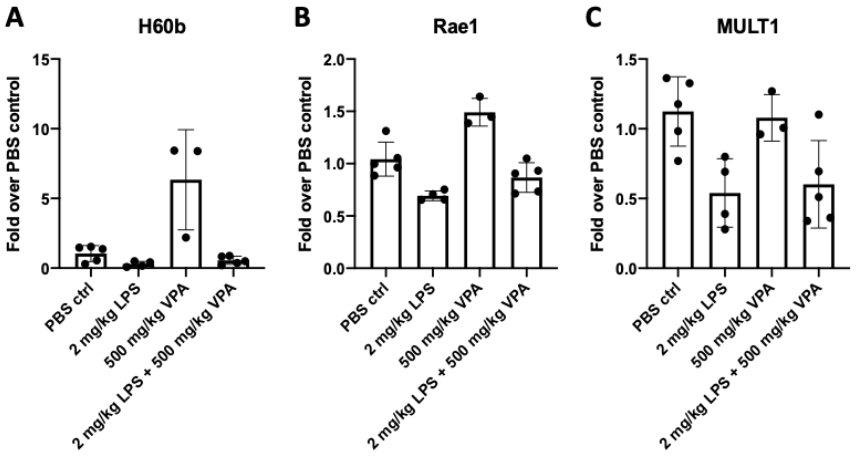

Figure 16. NK-cell ligands are not differently expressed after VPA and LPS treatment.
qRT-PCR analysis does not show any upregulation of the NK cell ligands after treatment with 2 mg/kg LPS + 500 mg/kg VPA in comparison to the PBS control group. **A.** The results for the NK cell ligand H60b display a slight induction after a single treatment with 500 mg/kg VPA. The other to NK cell ligands **B.** MULT1 and **C.** Rae1 show comparable levels in the four different groups. Data are presented as means ± standard deviation of at least three biological replicates.

After the isolation of immune cells from the different livers, the numbers and the function of NK cells were further characterized. Therefore, the isolated immune cells were stained extracellularly for NK1.1 (NK cells) and CD49a (liver resident NK cells), intracellularly for the produced cytokines IFNγ and TNFα and were subsequently analyzed by flow cytometry. The analysis of the flow cytometry data revealed a minimal tendency for more NK cells after the treatment with LPS+VPA in comparison to the other groups (Fig. 17A) while the numbers of liver resident NK cells remained nearly unchanged in relation to the LPS treated mice (Fig. 17B). More detailed analysis of the functionality of the NK cells showed an impaired cytokine production after the treatment with LPS+VPA, while the mean IFNγ production of the single treated mice with either 2 mg/kg LPS or 500 mg/kg VPA alone was slightly higher in comparison to the control group and the double treated mice (Fig. 17C). TNFα production was almost diminished after a single or the double treatment with the substances (Fig. 17D). Consequently, the absent effect on NK cells after treatment with 2 mg/kg LPS and 500 mg/kg VPA was in line with the results from the other experiments, demonstrating that a LPS-VPA-based liver injury mouse model could not be established and the investigation of the original question of the direct effect of NK cells on hepatocytes was not possible with this experimental set up.

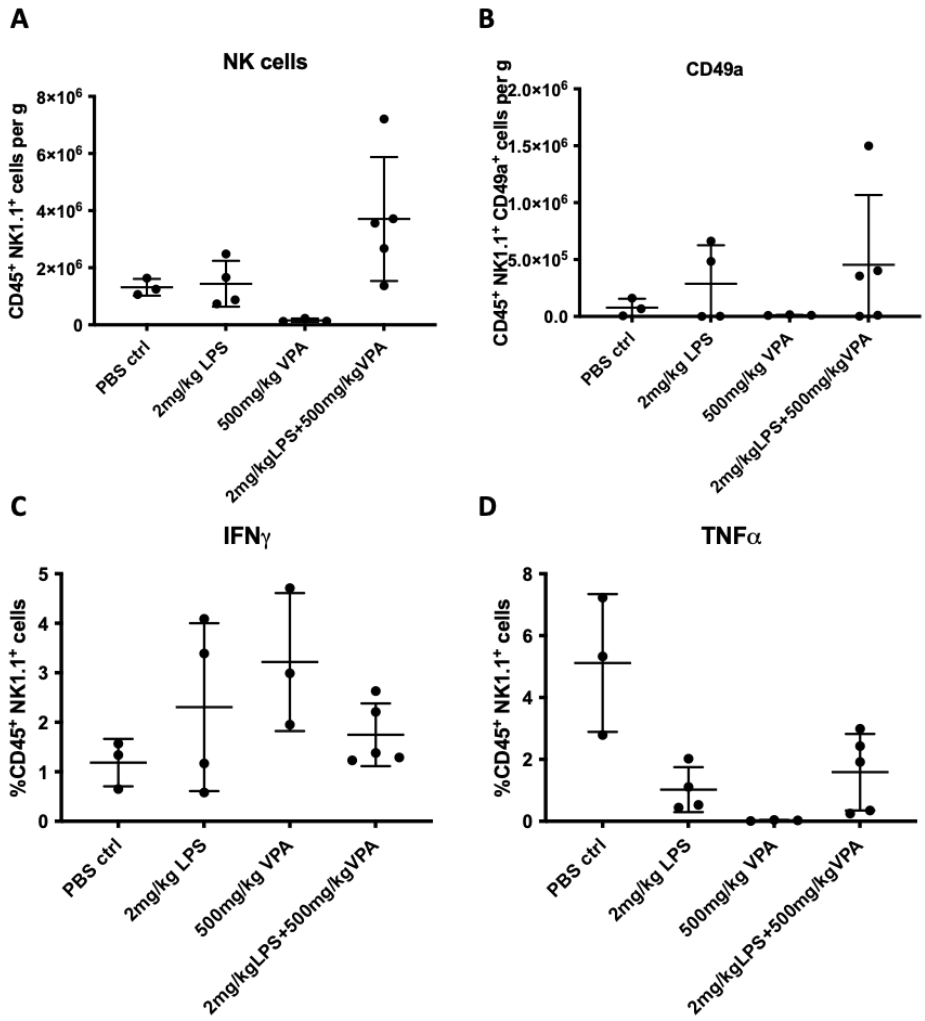

Figure 17. LPS and VPA treatment do not show an effect on NK cells and their function.
Freshly isolated immune cells from livers of PBS control mice, 2 mg/kg LPS treated mice, 500 mg/kg VPA treated mice and mice treated with 2 mg/kg LPS and 500 mg/kg VPA were stained for different markers, measured via flow cytometry and analyzed with FlowJo to identify the number of **A**. NK cells which were identified as $CD45^+CD3^-NK1.1^+$, **B.** liver resident NK cells expressing CD49a, and the NK cell related cytokines **C.** IFNγ and **D.** TNFα. Cells were analyzed from at least 3 mice.

As the first two experimental setups did not result in a liver damage caused by VPA, another approach was to daily apply VPA via oral gavage to 9 weeks old male C57Bl/6N mice starting with a daily dose of 500 mg/kg VPA. The daily VPA dose was slowly increased until the timepoint the mice developed a liver damage. To analyze the progression of the liver damage, blood was collected from the submandibular vein and subsequently the ALT levels were analyzed. Even though the concentration was increased to a daily dose of 1 g/kg VPA, the liver enzymes did not display any indication of liver damage. This high concentration of VPA resulted in neurological abnormalities for the mice and in the end two of the mice died.

In summary, the three experiments demonstrated that it was not possible to establish a VPA induced liver damage mouse model to investigate the direct effect of NK cells on hepatocytes or any other kind of effect on NK cells, which could have resulted in higher cytotoxicity or a

higher cytokine production. In the end, the project of VPA-induced liver injury and the impact of NK cells on hepatocytes was not pursued any further.

3.2 Role of liver immune cells in repeatedly induced liver damage

There are many different immune cells localized in the liver which have several tasks. Although the function of most immune cells during liver fibrosis and regeneration is described, we wanted to investigate their role during repeated liver damage induced by a drug and if the immune cells can possess a memory feature. To study the role of the different immune cells, an appropriate mouse model was needed. Therefore, the hepatotoxic compound CCl_4 was chosen because it was already established in house and the caused liver damage and the regeneration are well described in literature (D Weber et al., 2003).

3.2.1 NK cells in repeatedly induced liver injury

Since it had already been described that upon re-challenging with the same hapten, lrNK cells can possess a memory like feature, we closer investigated NK cells and a possible memory feature after repeated liver damage caused by CCl_4 *in vivo.* Therefore, nine weeks old male C57Bl/6N mice were treated with a single injection of CCl_4 (1.6 g/kg, i.p.) and the injection was repeated up to six times with 30 days recovery period between the injections. 24 hours after the third, fifth or sixth injection, blood and liver tissue of these mice were collected and analyzed (Fig. 18A).

Within these 30 days, the liver recovered from the CCl_4 caused damage, protein levels which were differently regulated during the CCl_4 injury had returned to control levels and the various activated immune cells became inactive again. In order to compare the treated mice, three different control groups were integrated. The first control group was treated with olive oil as vehicle control. The second control group was an age-matched untreated control group to evaluate the impact of olive oil on the liver and the immune cells. Furthermore, a third control group was included in which the mice received olive oil in the first injections and CCl_4 only once 24 hours before the collection. After the multiple injections of CCl_4, pericentral fibrosis was observed and it got more pronounced the more often the mice received CCl_4 (Fig. 18B, right column). Additionally, H&E staining revealed necrotic lesions around the central vein in all CCl_4 mice (Fig. 18B, middle column).

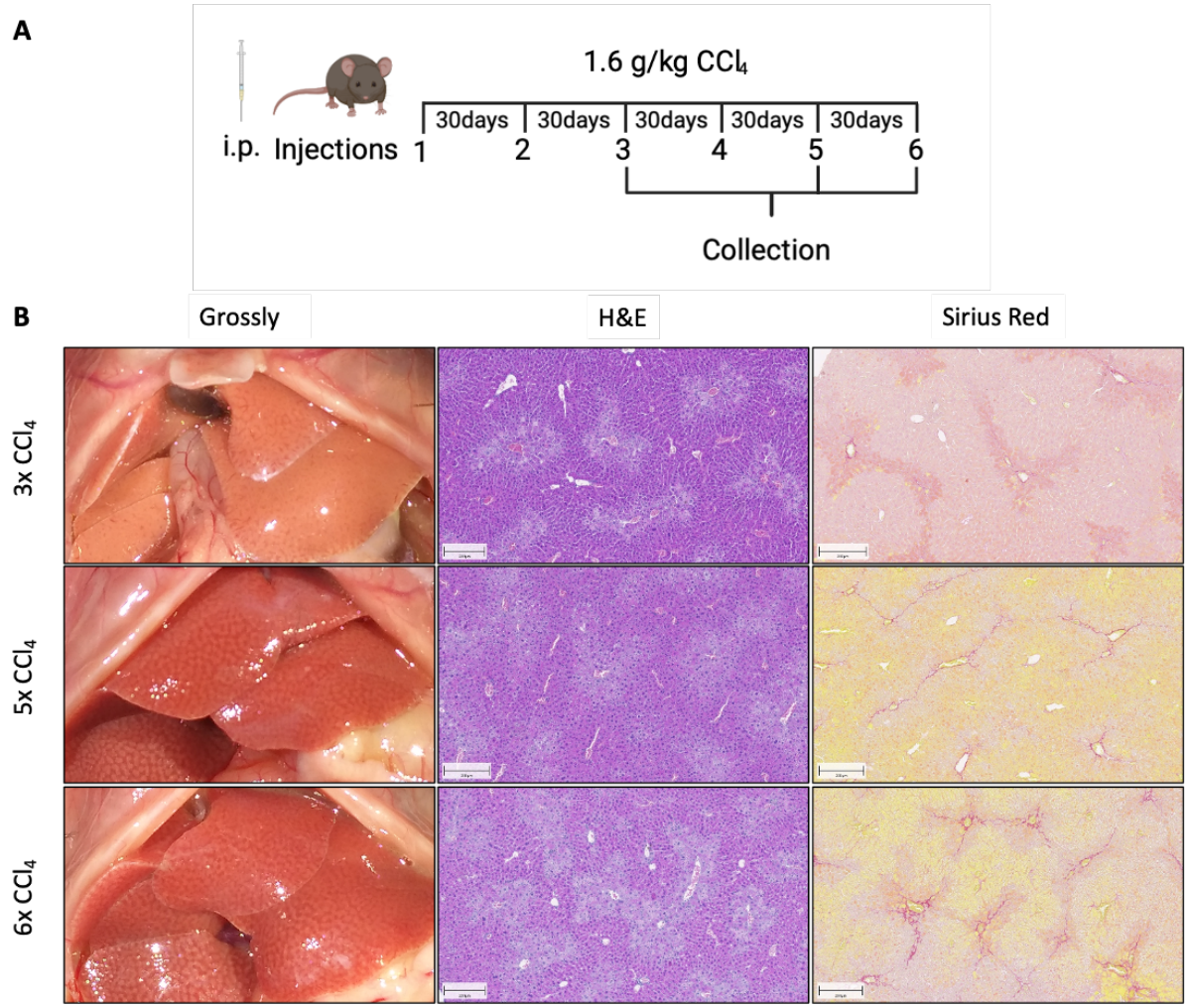

Figure 18. Multiple doses of CCl_4 aggravated the degree of liver fibrosis.
A. Experimental set up. **B.** Gross pathology (left column) and representative images of whole slide scans of H&E (middle column) and Sirius red (right column) stained liver paraffin embedded tissue sections of three times (upper row), five times (middle row) and six times (lower row) treated mice with 1.6 g/kg CCl_4 intraperitoneally from at least 3 mice per group (Scale bars: 200 μm).

Although it was not possible to observe a difference in the liver-weight-to-body-weight ratio between the untreated control group, the oil control group, one-time treated and the several times treated mice with CCl_4 (Fig. 19, left column), the death of hepatocytes indicating the liver damage caused by the CCl_4 injections was confirmed by the significantly increase of the two liver enzymes ALT and AST (Fig. 19, middle and right column). The plasma concentration of these two enzymes was higher after a single injection of CCl_4 than after multiple doses of CCl_4 which had been already described in literature (Scholten et al., 2015). As expected, the CCl_4 liver damage mouse model was successful.

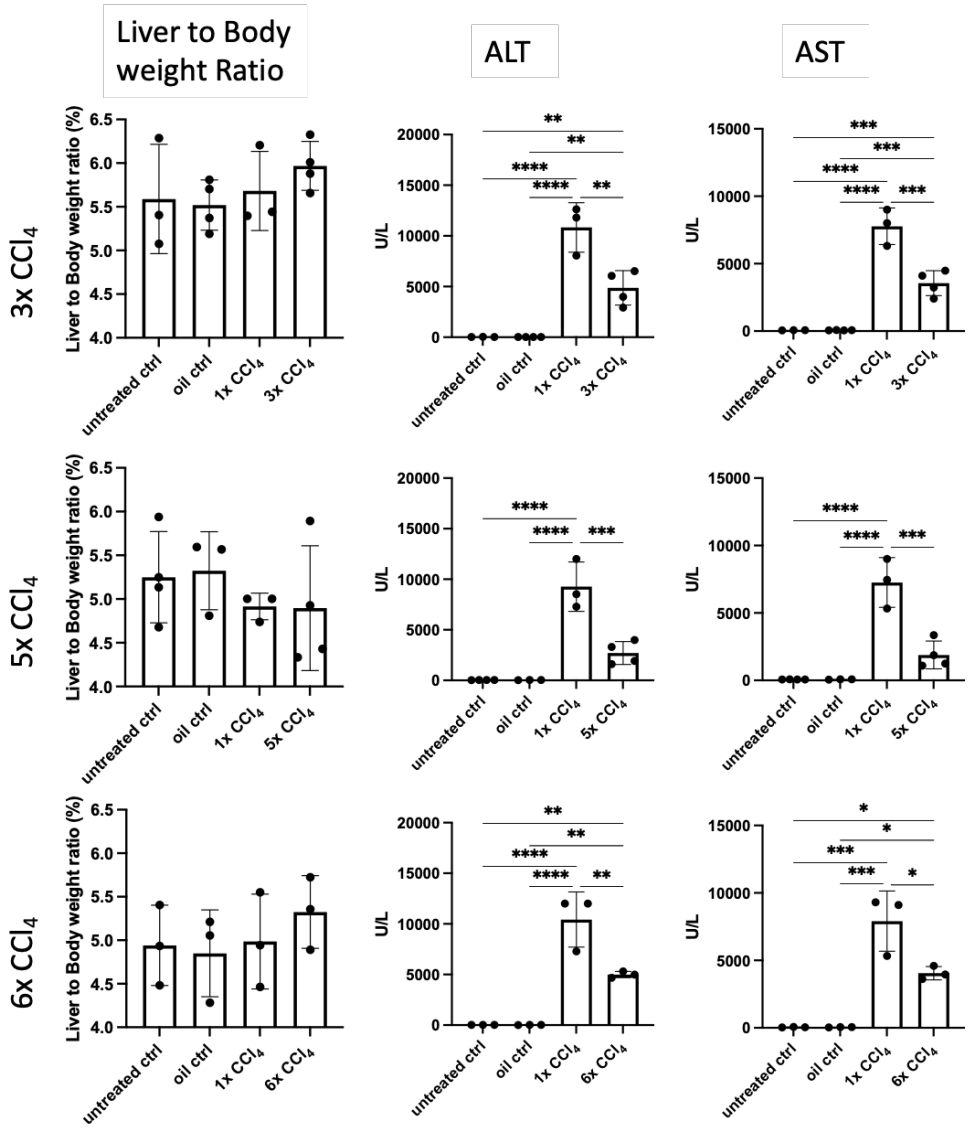

Figure 19. Multiple doses of CCl_4 lead to an increase of the liver enzymes in blood plasma. Liver-weight-to-body-weight ratio (left column) do not show any difference between the untreated and oil control groups and the CCl_4 treated mice despite the number of injections (3x CCl_4: upper row; 5x CCl_4: middle row; 6x CCl_4: lower row). Plasma analysis of the liver enzymes ALT (middle column) and AST (right column) revealed the highest levels after a single dose of CCl_4. The liver enzymes were also elevated after multiple doses of CCl_4. Data are presented as means ± standard deviation of at least three biological replicates. Calculation of differences between the groups was performed with one-way ANOVA. *P<0.05; **P<0.01; ***P<0.001, ****P<0.0001.

After the confirmation of the functional liver injury mouse model, immune cells were isolated from the liver, stained for different markers to characterize the NK cells, and subsequently measured by flow cytometry and analyzed. The analysis of NK cells showed no difference in the total numbers of NK cells (Fig. 20A) or $CD49a^+$ IrNK cells (Fig. 20B) per gram liver among the different groups. Also, the percentage of NK cells producing the cytokines IFNγ (Fig. 20C) or TNFα (Fig. 20D revealed no difference between a single and five injections of CCl_4. Further analysis of other NK cell markers like the activation markers CD69 (early activation marker ((Hood et al., 2019), Fig. 20E) and the chemokine receptor CXCR6 (Fig. 20F) or the exhausting marker programmed cell death protein 1 (PD1, Fig. 20H) did not show any differences. In case

of the exhausting marker KLRG1 a tendency of an opposite effect was observed since multiple injections of CCl_4 caused lower KLRG1 expression on NK cell surfaces in comparison to the other controls (Fig. 20G).

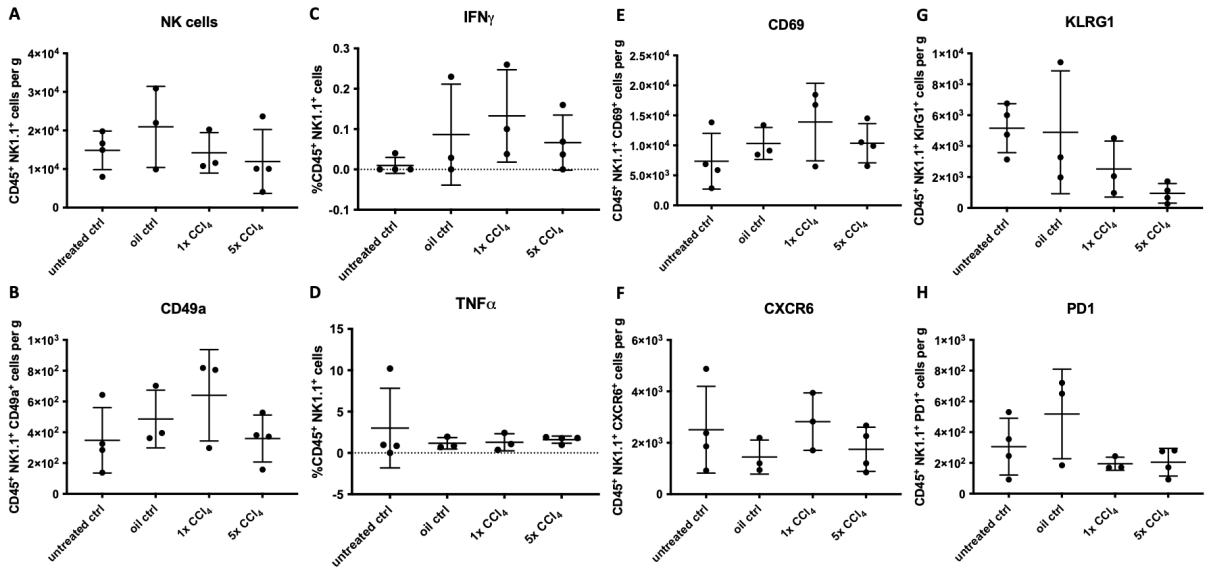

Figure 20. Analysis of different NK cell markers.
Freshly isolated immune cells of livers from untreated control, oil control, 1x CCl_4 treated and 5x CCl_4 treated mice were stained with different markers to identify the number of **A**. NK cells which were identified as $CD45^+CD3^-NK1.1^+$, **B.** liver resident NK cells expressing CD49a and the NK cell related cytokines **C.** IFNγ and **D.** TNFα. The NK cells were further characterized by the activation markers **E.** CD69 and **F.** CXCR6 and the exhaustion markers **G.** KLRG1 and **H.** PD1. Cells were isolated and analyzed from at least 3 biological replicates.

3.2.2 Other immune cells in repeatedly induced liver injury

These results demonstrated that the NK cells did not show a specific phenotype which were able produce more cytokines or express higher amounts of different markers in response to several doses of CCl_4 although the liver damage mouse model was working. Additionally to NK cells and their different markers, different lymphocytes and leukocyte markers were stained to obtain a general overview of the immune cells in this mouse model. In order to identify a shift in the numbers of the various immune cells in the liver, the ratio of the means of a single immune cell subset was calculated, comparing five times CCl_4 treated mice to mice injected with a single CCl_4 injection (Fig. 21). Figure 21 confirmed that there was no change in NK cell numbers (0.07) within the two groups. The biggest change between the CCl_4 treated groups occurred in the other ILC subsets especially in the ILC1 (0.89) population.

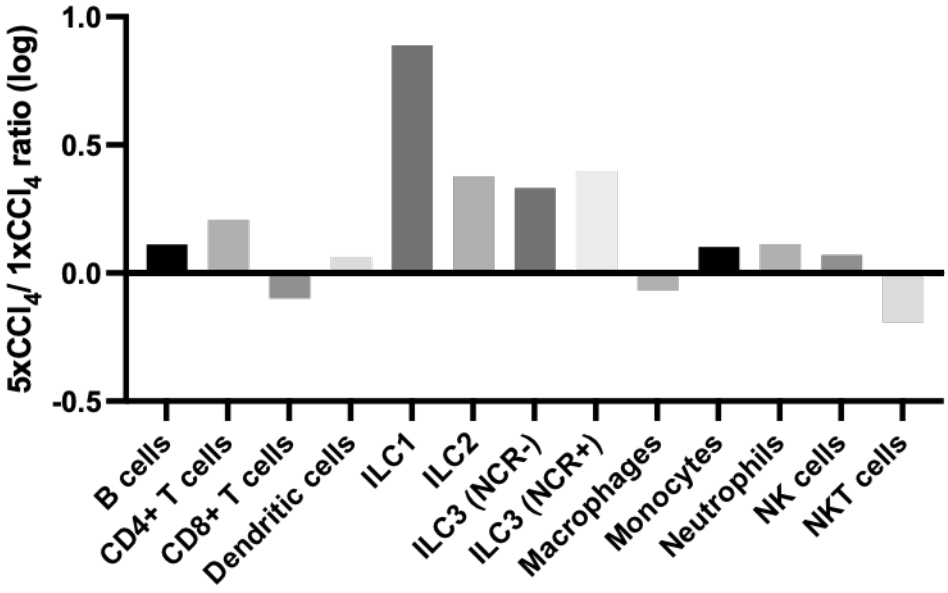

Figure 21. Shift in immune cell distribution in mice receiving five injections with CCl_4.
Bar graphs show the ratio of mean numbers of cells per gram liver from mice treated once or five times with CCl_4 plotted in a logarithmic scale. Cells were isolated and analyzed from three to four biological replicates.

In summary, these results clearly showed that the NK cells did not show a specific phenotype of for example a memory feature in this mouse model. Nevertheless, the repeatedly induced liver damage caused by CCl_4 enabled us to investigate another type of immune cells, in particular the ILC1s. Thus, we took advantage of this mouse model to study memory formation in ILC1s.

3.3 Identification of memory like ILC1s

Figure 21 shows that the biggest change occurs within the ILC1 population after several doses of CCl_4. Therefore, we decided to further analyze these cells and to investigate the question whether it was possible to identify memory like ILC1s with this mouse model. The phenotypical characterization of ILC1s is problematic, since some markers can be lost upon activation. Moreover, the differentiation between ILC1s and NK cells is difficult, because they have many markers in common like NK1.1 and expression of some markers is tissue specific, such as CD73 in salivary glands and CD160 in intestine (Seillet et al., 2021).
In order to identify liver ILC1s, the cells were stained for: (1) leukocyte marker CD45, (2) different lineage markers to exclude all other immune cells, (3) CD127 which is expressed on different ILC subsets, (3) NKp46 to identify NK cells, ILC1s and some ILC3s and (4) CD200r as the tissue specific marker for the liver ILC1s. Following this strategy to identify the ILC1s (Fig. 8), we observed significantly more ILC1s per gram liver after three (Fig. 22A, left column), five (Fig. 22A, middle column) and six (Fig. 22A, right column) doses of CCl_4 in comparison to one injection of CCl_4 or to the other control groups. Further characterization of the $CD200r^+$

ILC1s showed that all of the identified ILC1s are also positive for the transcription factor T-Bet (Fig. 22B).

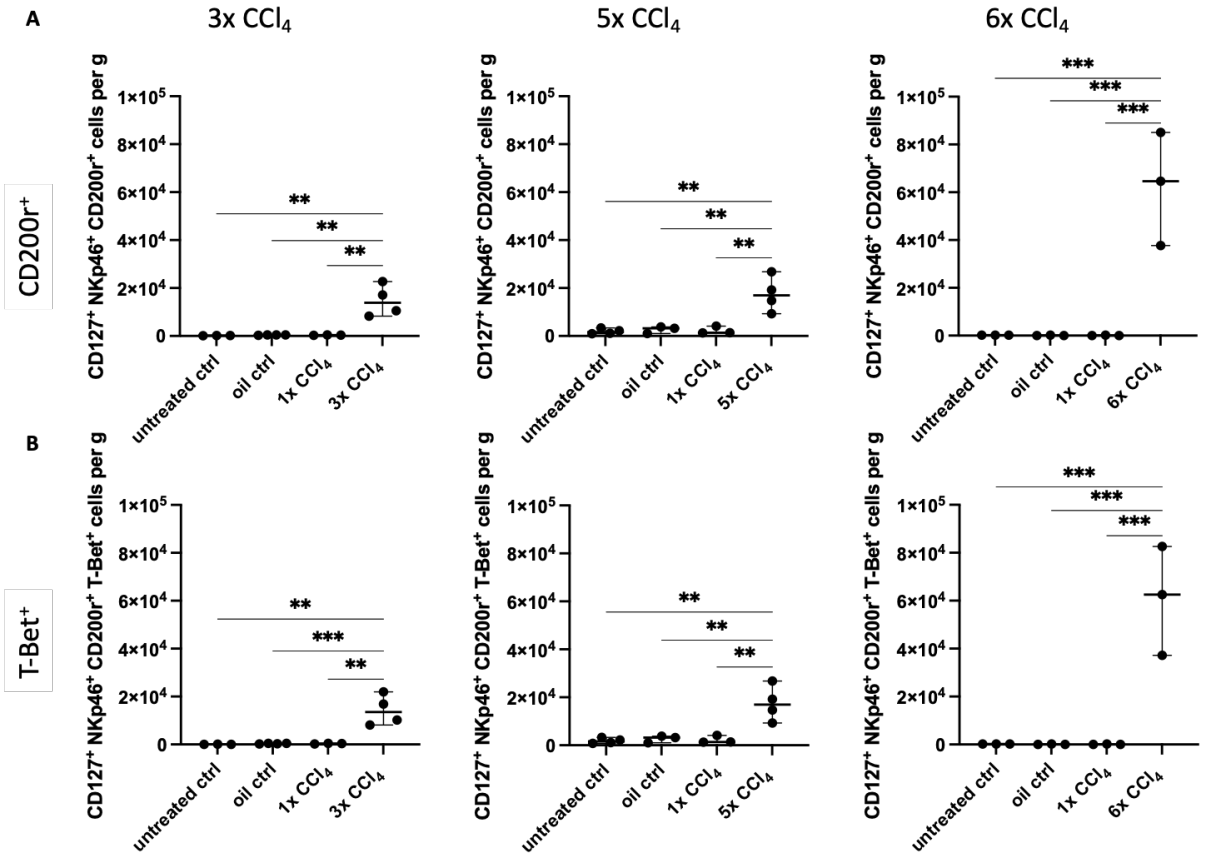

Figure 22. Multiple doses of CCl_4 caused higher numbers of ILC1s in the liver.
Freshly isolated immune cells of livers from the different groups of untreated control, oil control, 1x CCl_4 treated and 3x (left column), 5x (middle column) and 6x (right column) CCl_4 treated mice were stained for different markers, measured via flow cytometry and analyzed with FlowJo to identify the number of **A**. ILC1s which were identified as Zombie$^-$CD45$^+$Lin$^-$CD127$^+$CD90$^-$NKp46$^+$ST2$^-$CD200r$^+$, **B.** CD200r$^+$T-Bet$^+$ ILC1s. Data are presented as means ± standard deviation of at least three biological replicates. Calculation of differences between the groups was performed with one-way ANOVA. **P<0.01; ***P<0.001.

To further define the CD200r$^+$T-Bet$^+$ ILC1s and to answer the question, if these cells had a memory potential after multiple doses of CCl_4, the ILC1s were stained for the production of cytokines (Fig. 23). The results of the intracellular staining displayed a significantly higher IFNγ production in percentage (Fig. 23A) as well as significantly more IFNγ^+ cells per gram liver (Fig. 23B) after six times CCl_4 compared to other groups. In contrary, this increase was not observed for TNFα production (Fig. 23C-D). Consequently, these results are the proof for the memory potential of CD200r$^+$ ILC1s after multiple doses of CCl_4 which is defined by the higher IFNγ production.

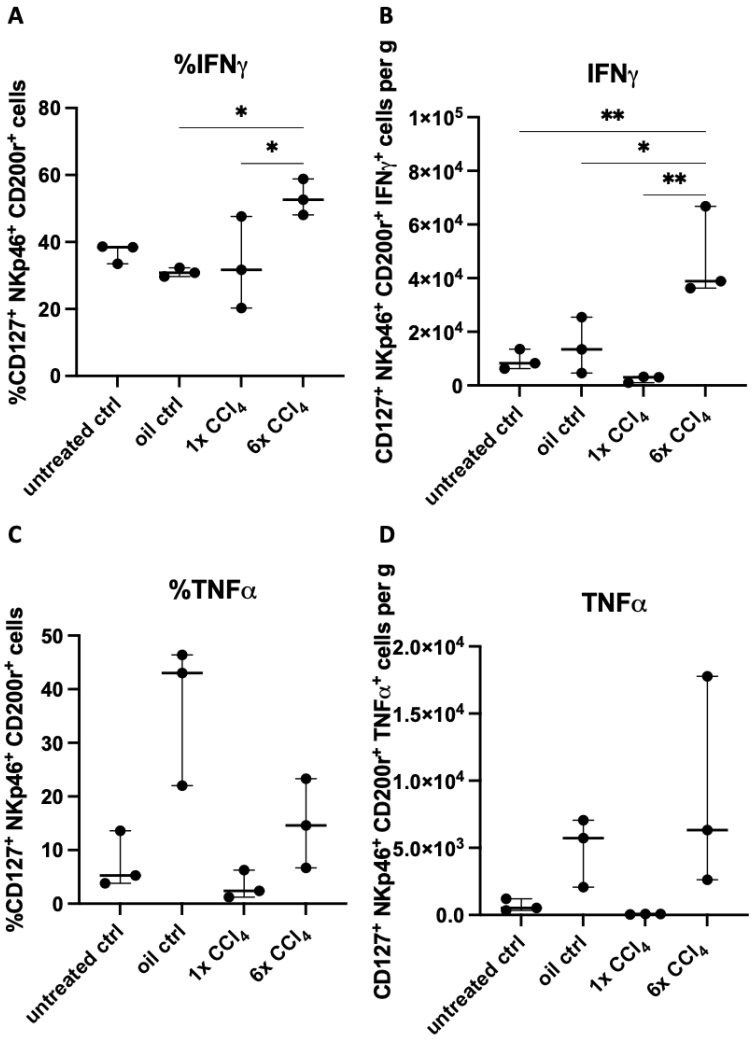

Figure 23. Higher numbers of CD200r+ ILC1s produce more IFNγ after six doses of CCl_4.
Freshly isolated immune cells of livers from the different groups of untreated control, oil control, 1x CCl_4 treated and 6x CCl_4 treated mice were stained with different markers, measured and analyzed to identify the **A**. the percentage of IFNγ producing cells, **B.** IFNγ$^+$ cell number per gram liver, **C.** the percentage of TNFα producing cells and **D.** TNFα$^+$ cell number per gram liver of Zombie$^-$CD45$^+$Lin$^-$CD127$^+$CD90$^-$ NKp46$^+$ST2$^-$CD200r$^+$ ILC1s. Data are presented as means ± standard deviation of at least three biological replicates. Calculation of differences between the groups was performed with one-way ANOVA. *P<0.05; **P<0.01.

3.4 Characterization of memory like ILC1s

As shown in the previous experiments, it was possible to successfully identify memory like ILC1s in the liver after multiple injections of CCl_4 with pauses of 30 days between the injections. The memory effect of these CD200r$^+$ ILC1s is identified by the higher IFNγ production in response to several CCl_4 injections. Based on these findings, we wanted to further characterize markers which are expressed on the surface of memory like ILC1s. Therefore, a new panel (Table 11) was designed to measure more markers on one cell at the same time on the flow cytometer Aurora (Cytek). Compared to the LSRFortessa^{TM} Cell Analyzer (BD), the Aurora has a better resolution and sensitivity.

Another goal was to clarify how the higher number of ILC1s after multiple doses of CCl_4 can be explained. To answer this, we included another control group which was injected twice with CCl_4 but the last injection before the collection was performed with olive oil (2xCCl_4+1xoil). With these mice, it was possible to evaluate if the high amounts of ILC1s were already in the liver and stayed there after the CCl_4 injections and just got activated by a new insult. Thus, the mice were injected three times with CCl_4 with 30-day waiting period between the injections (Fig. 24A). 24 hours after the last CCl_4 exposure (2xoil+1xCCl_4 or 3xCCl_4), gross pathology of these livers showed macroscopically altered patterns (small white spots on the liver; Fig. 24B, left column). The paraffin embedded liver tissue sections stained by H&E exhibited pericentral damaged areas and necrotic lesions in the three times treated group which could not be observed in the untreated and olive oil controls as well as the 2xCCl_4+1xoil treated mice (Fig. 24B, middle column). Furthermore, to visualize collagen deposition, Sirius red staining was performed. As expected, the untreated and olive oil control livers had a positive signal only in large blood vessels. This signal was also observed in the CCl_4 treated groups. In addition, the pericentral fibrosis was again observed in the 3xCCl_4 treated mice but also in the new group treated twice with CCl_4 and once with olive oil (Fig. 24B, right column). In line with the previous results, there was no difference between the different groups concerning the liver-weight-to-body-weight ratio (Fig. 24C) in contrast to the significant change in the two liver enzymes ALT (Fig. 24D) and AST (Fig. 24E) indicating the hepatocyte death and consequently liver damage. The high ALT and AST levels were only observed in plasma from mice that received CCl_4 24 hours ago. The 2xoil+1xCCl_4 group had comparable levels to the two control groups.

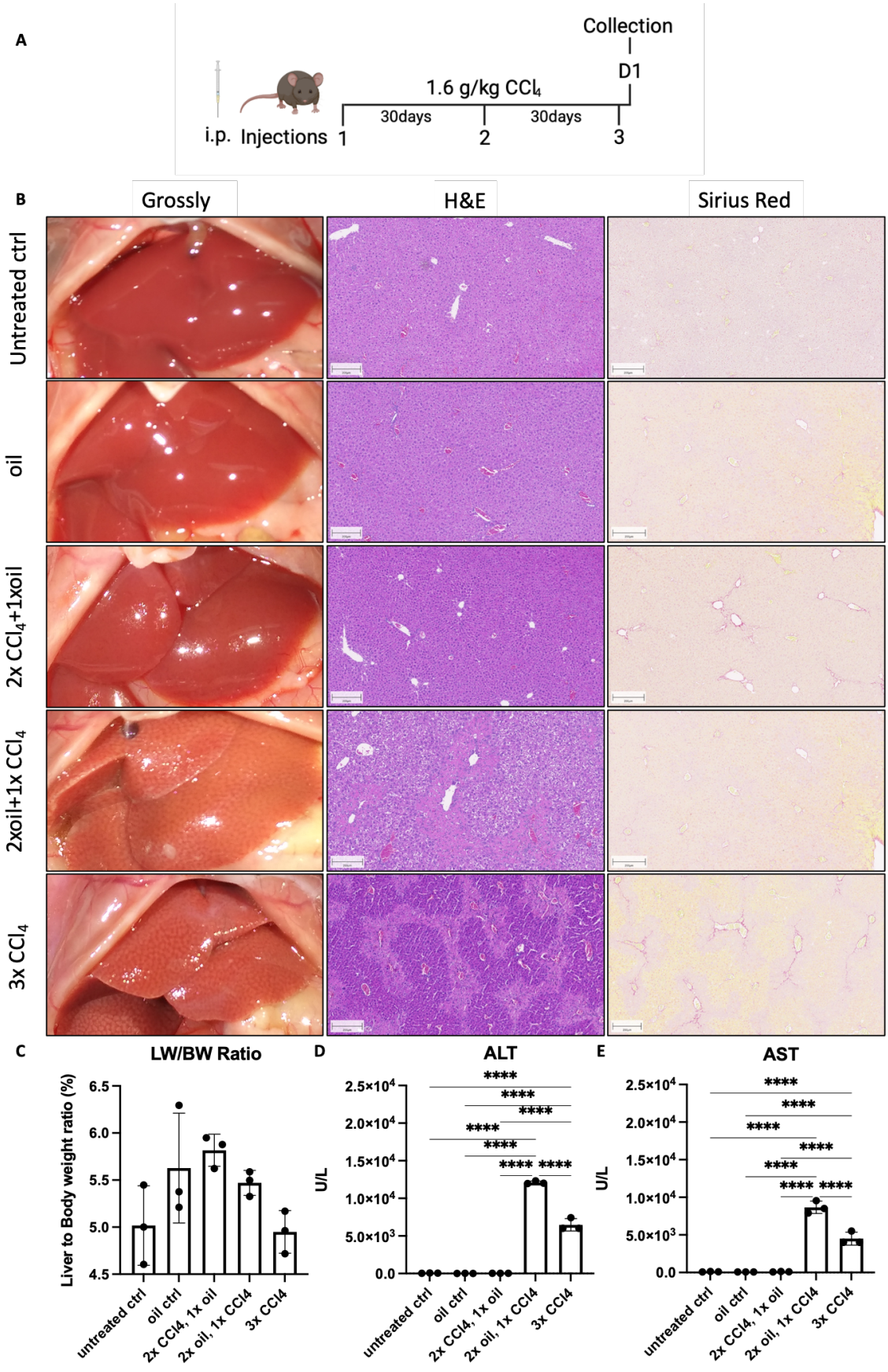

Figure 24. Three doses of CCl_4 cause liver damage with a mild fibrosis.
A. Experimental design of mice treatment. **B.** Gross pathology (left column) and representative images of whole slide scans of H&E (middle column) and Sirius red (right column) stained liver paraffin embedded tissue sections of untreated control (first row), olive oil control (second row), two times CCl_4

and one-time olive oil (third row), two times olive oil and one-time CCl_4 (forth row) and three times CCl_4 (fifth row) treated mice with 1.6 g/kg CCl_4 i.p. from 3 mice per group (Scale bars: 200 μm). **C.** Liver-weight-to-body-weight ratio. Plasma analysis of the liver enzymes **D.** ALT and **E.** AST revealed the highest levels after a single dose of CCl_4. Plasma levels of the liver enzymes are only elevated if the third injection was with CCl_4. Data are presented as means ± standard deviation of at least three biological replicates. Calculation of differences between the groups was performed with one-way ANOVA. ****P<0.0001.

To verify the memory effect after the third injection of CCl_4, the immune cells from the livers were isolated, stained with a newly arranged set of antibodies (Tabel 11) to clearly identify and characterize ILC1s (memory like ILC1 Panel) and subsequently analyzed on a flow cytometer. The ILC1s were now defined as fixable viability dye$^-$CD45$^+$Lin$^-$NK1.1$^+$EomesS$^-$CD49a$^+$RORγT$^-$CD127$^+$CD200r$^+$ cells (Fig. 9). Including these new markers, it was possible to exclude NK cells which would be Eomes$^+$ (Fig. 25E) and ILC3 which are dependent on the transcription factor RORγT. Additionally, to identify the ILC1s the tissue residency marker CD49a was also included (Seillet et al., 2021). This new gating for the ILC1s revealed a similar picture as with the previously used strategy: after three doses of CCl_4, the cell numbers of ILC1s per gram liver were significantly increased compared to all other groups (Fig. 25A). Furthermore, these CD200r$^+$ ILC1s were again positive for the transcription factor T-Bet (Fig. 25B) and produced significantly more IFNγ in comparison to the controls (Fig. 25C). Thus, the memory effect of the ILC1s was reproducible. Additionally, NK cell numbers were still not significantly different between the groups (Fig. 25E).

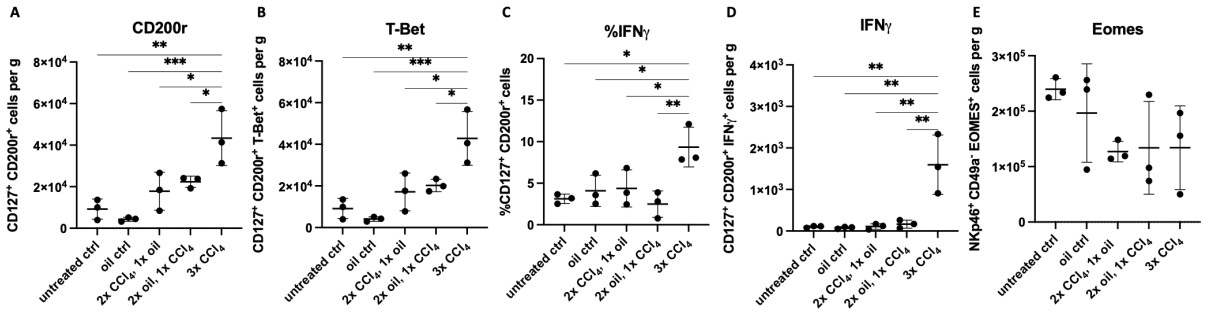

Figure 25. Reproducible memory effect of ILC1s after three injections of CCl_4.
Freshly isolated immune cells of livers of untreated control, olive oil control, two times CCl_4 and one-time olive oil, two times olive oil and one-time CCl_4 and three times CCl_4 treated mice were stained for different markers, measured on the flow cytometer Aurora and analyzed. Number of **A**. ILC1s which were identified as dead cell marker$^-$CD45$^+$Lin$^-$NK1.1$^+$EomesS$^-$CD49a$^+$RORγT$^-$CD127$^+$CD200r$^+$, **B.** T-Bet$^+$ ILC1s, **C.** the percentage of IFNγ producing cells, **D.** IFNγ$^+$ cells per gram liver and **E.** NK cells defined as dead cell marker$^-$CD45$^+$Lin$^-$NK1.1$^+$Eomes$^+$CD49a$^-$. Data are presented as means ± standard deviation of three biological replicates per group. Calculation of differences between the groups was performed with one-way ANOVA. *P<0.05, **P<0.01; ***P<0.001.

Another part of this experiment was to analyze more markers which could be expressed by the memory like ILC1s. Three markers were found which were also highly expressed on most of the CD200r$^+$ ILC1s: CD90.2, IL-18Rα and c-Kit (Fig. 26A-C). CD90.2, also known as Thy1.2, is a membrane GPI-anchored protein and has been described to be mainly expressed on T

cells and on different ILCs like ILC1s, too (di Censo et al., 2021; Sauzay et al., 2019). The second marker, IL-18Rα, belongs to the interleukin 1 receptor family and is expressed on endothelial cells and on several immune cells like NK cells, neutrophils, subsets of B and T cells as well as on ILC3s (Victor et al., 2017). Lastly, c-Kit is a receptor tyrosine kinase and is involved in intracellular signaling. It is detected on early lymphoid progenitors, on a subset of NK cells, $CD8^+$ T cells, ILC2 and ILC3s (Hochdörfer et al., 2019).

Additionally, the cells were stained for the proliferation marker Ki-67 (Fig. 26D) showing a low amount of Ki-67^+ ILC1s in the 3xCCl_4 mice. In general, the proportion of proliferating ILC1s in control mice or CCl_4 treated mice were low. Consequently, the increased $CD200r^+$ ILC1 in the liver was not caused by proliferation.

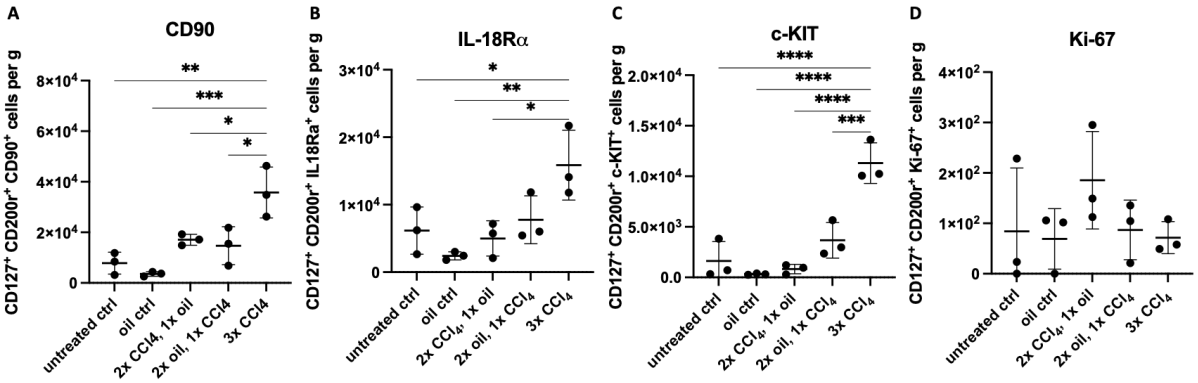

Figure 26. Memory like ILC1s do not proliferate within 24 hours.
Freshly isolated immune cells of livers from the different groups of untreated control, olive oil control, two times CCl_4 and one-time olive oil, two times olive oil and one-time CCl_4 and three times CCl_4 treated mice were stained, measured on a flow cytometer and analyzed with FlowJo to analyze the markers **A**. CD90, **B.** IL-18Rα, **C.** c-Kit and **D.** Ki-67 cells per gram liver of memory dead cell $marker^-CD45^+Lin^-$ $NK1.1^+EomesS^-CD49a^+ROR\gamma T^-CD127^+CD200r^+$ ILC1s. Data are shown as positive cells per gram liver and are presented as means ± standard deviation of three biological replicates per group. Calculation of differences between the groups was performed with one-way ANOVA. *P<0.05, **P<0.01; ***P<0.001; ****P<0.0001.

3.5 Presence of memory like ILC1s in the liver is transient

The previous experiments showed a successfully established mouse model to investigate memory like ILC1s which produce significantly more IFNγ in response to multiple doses of CCl_4 compared to control groups. Nevertheless, there are several questions which needed to be answered to further understand the memory like ILC1s. Previous results showed that the higher ILC1 numbers occurred 24 hours after the last CCl_4 treatment and in this section the focus was on how long these high numbers of memory like ILC1s persist in the liver. Therefore, the timepoints three, seven, fourteen and thirty days after the third CCl_4 injection were additionally investigated (Fig. 27A), as well as only one CCl_4 administration and oil controls. Macroscopically, gross pathology of the livers revealed alteration patterns especially on day one, while the small white spots were reduced on day three and were not visible by eye from

day seven on (Fig. 27B, left column). Comparably, H&E staining of liver tissue showed pericentral damaged areas and necrotic lesions on day one which ameliorated until day three and were completely diminished on day seven (Fig. 27B, middle column). Sirius red staining displayed pericentral fibrosis at day one after the third injection, and from day three until day fourteen a central-to-central bridging of fibrotic streets was clearly observed which was resolved until day thirty (Fig. 27B, right column). Although the liver-weight-to-body-weight ratio at the different days did not exhibit a change (Fig. 27C), plasma concentration of the liver enzymes confirmed the observation from the H&E staining. The highest amount of ALT (Fig. 27D) and AST (Fig. 27E) in plasma was found on day one and significantly decreased until day three, albeit the levels were still increased, indicating that the necrosis was not fully diminished. From day seven on, the increased plasma levels caused by CCl_4 were no longer detectable and the plasma levels of the treated mice were on the similar levels of the oil control mice.

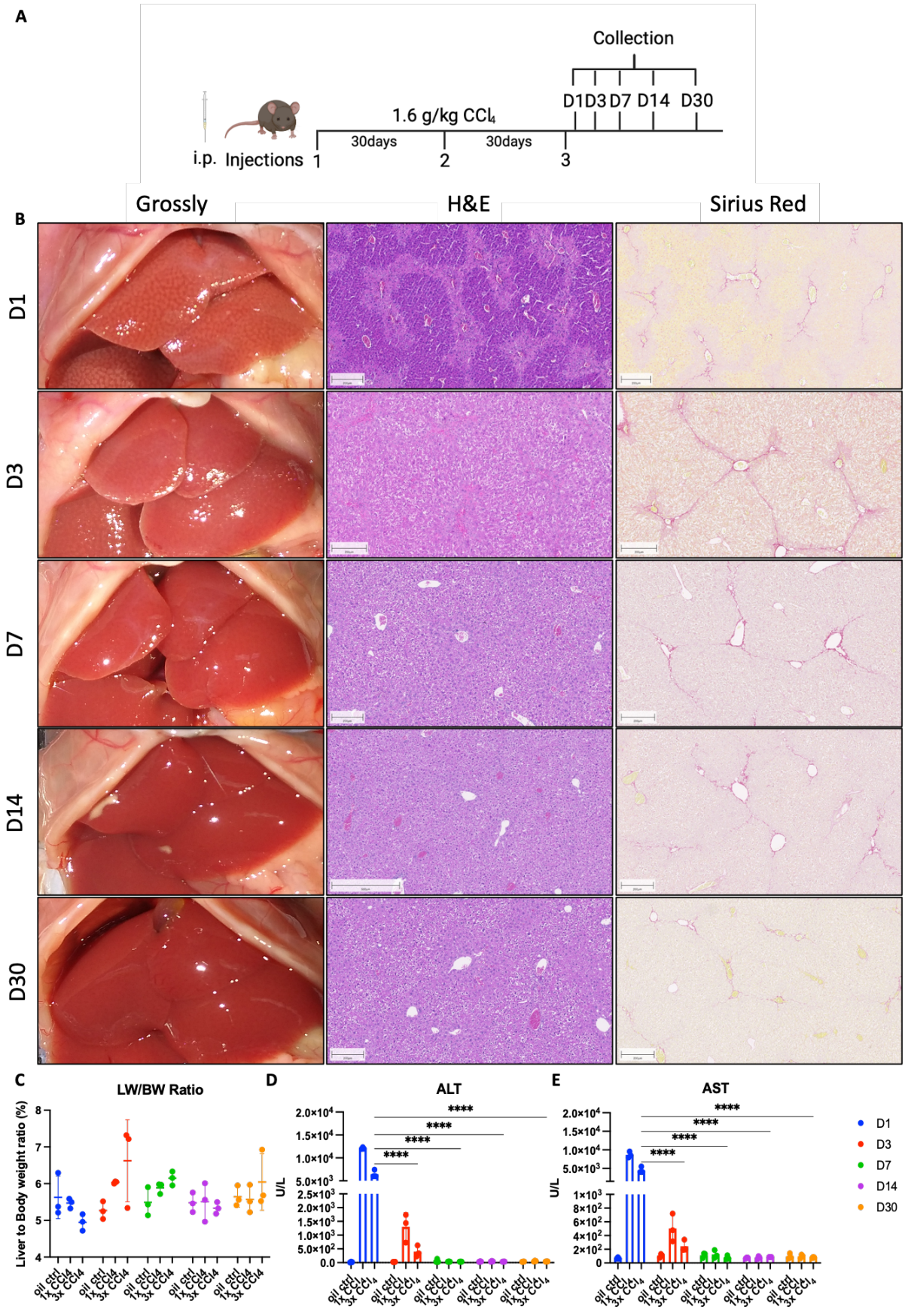

Figure 27. Time course of the liver regeneration after three doses of CCl_4.
A. Experimental design. **B.** Gross pathology (left column) and representative images of whole slide scans of H&E (middle column) and Sirius red (right column) stained liver paraffin embedded tissue sections of three times treated mice one day (first row), three days (second row), seven days (third row),

fourteen days (forth row) and thirty days (fifth row) after the last i.p. injection of 1.6 g/kg CCl_4 from 3 mice per group (Scale bars: 200 μm). **C.** Liver-weight-to-body-weight ratio do not show any difference between the groups. Plasma analysis of the liver enzymes **D.** ALT and **E.** AST revealed the highest plasma levels at day one. The enzymes were still increased on day three but from day seven on the plasma levels were comparable to the oil treated mice. Data are presented as means ± standard deviation of three biological replicates. Calculation of differences between the groups was performed with two-way ANOVA. ****P<0.0001.

In summary, the H&E staining as well as the liver enzymes demonstrated the recovery from necrosis in the liver. However, the initial question of this experiment remained of how long do the memory like ILC1s stay in the liver. After the isolation of the immune cells from the different livers, the staining with the memory like ILC1 Panel and the measurement on the flow cytometer, the received data were analyzed. The quantification revealed that the numbers of $CD200r^+$ ILC1s were significantly increased to 40.000 cells per gram liver only on day one in mice treated three times with the hepatotoxic compound (Fig. 28A). Almost all of these cells were also positive for the transcription factor T-Bet (Fig. 28B). In contrast, the elevated numbers of $CD200r^+$ ILC1s were not found on the other days; the number of ILC1s after the third injection was comparable to their oil control (Fig. 28A). The increased IFNγ production and higher numbers of IFNγ positive ILC1s per gram liver were only observed at day one (Fig. 28C, D). In conclusion, the significantly increased numbers of memory like ILC1s producing more IFNγ in response to the third CCl_4 dose were only observed on day one. At day three, the numbers of these cells were reduced to a comparable level of the oil control mice. To see if the memory like ILC1s die in the liver after day one until day three, the cells were stained with a fixable viability dye (eBioscience) to identify dead cells. The quantification of the dead memory like ILC1s did not reveal an increased number of dead ILC1s in the liver at day three, meaning that the reduced number of these cells cannot be explained by dying memory like ILC1s (Fig. 28E).

In summary, the kinetic experiment of memory like ILC1s showed that a significantly increased number of these cells was observed only on day one but it was a transient effect since until day three the numbers of these cells were reduced to the level of the oil controls.

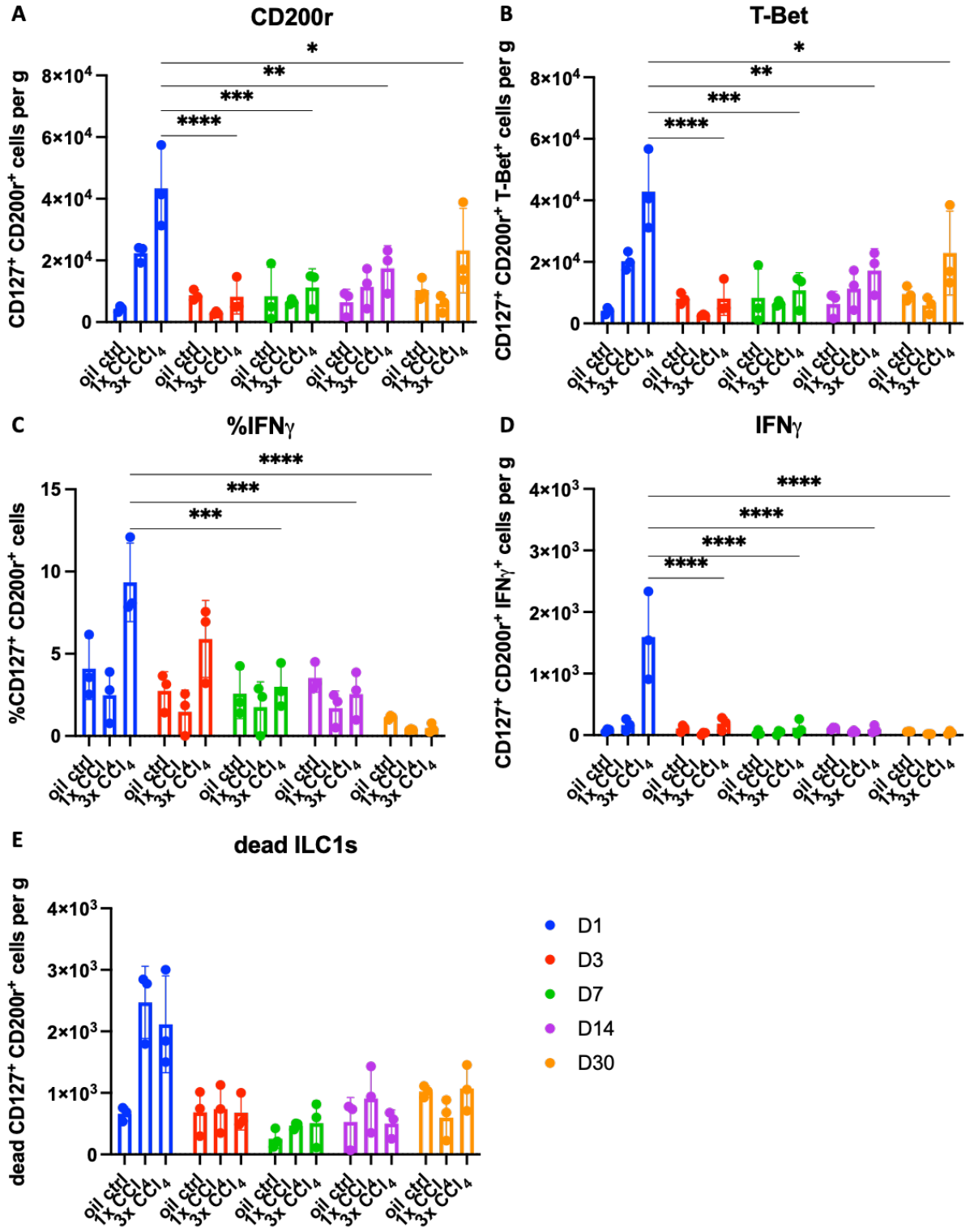

Figure 28. Transient effect of memory like ILC1s in the liver after three injections of CCl_4. Freshly isolated immune cells from livers of olive oil control, two times olive oil and one-time CCl_4 and three times CCl_4 treated mice were analyzed to identify the number of **A**. ILC1s which were identified as dead cell marker$^-$CD45$^+$Lin$^-$NK1.1$^+$EomesS$^-$CD49a$^+$RORγT$^-$CD127$^+$CD200r$^+$, **B.** T-Bet$^+$ ILC1s, **C.** the percentage of IFNγ producing cells, **D.** IFNγ$^+$ cells per gram liver and **E.** dead ILC1s which were gated as CD45$^+$Lin$^-$NK1.1$^+$EomesS$^-$CD49a$^+$RORγT$^-$CD127$^+$CD200r$^+$fixable viability dye$^+$. Data are presented as means ± standard deviation of three biological replicates per group. Calculation of differences between the groups was performed with two-way ANOVA. *P<0.05, **P<0.01; ***P<0.001; ****P<0.0001.

3.6 Recall of memory like ILC1s in the liver

The previous figures showed the successful identification of the memory potential of ILC1s after repeated injections of the hepatotoxic compound CCl_4. Furthermore, the increased numbers of memory like ILC1s which produce more IFNγ was shown to be in the liver only on day one but until day three this increase could not be observed anymore. Since the transient effect of the $CD200r^+$ ILC1s was observed, the question was raised whether the memory potential of these cells is long lasting.

Therefore, the same experimental set up was chosen as in figure 15A but instead of collecting the liver and blood 24 hours after the third injection, the mice were kept for additional 90 days before they received a fourth time CCl_4. Twenty-four hours after this fourth injection, liver and blood were collected (Fig. 29A). As control groups, untreated age matched mice which were untreated were included as well as the olive oil control and mice which received the first two injections olive oil and the third and fourth injection CCl_4. Macroscopically, mice receiving four times CCl_4 had a pale and damaged liver. Additionally, alteration patterns were also observed in the livers of mice treated with CCl_4 twice, while the livers of the two control groups looked healthy (Fig. 29B, left column). In line with these macroscopic results, paraffin embedded liver tissue sections stained with H&E exhibited necrotic areas around the central veins of the two groups treated with CCl_4 (Fig. 29B, middle column). These two groups also showed a positive signal in the Sirius red staining but it was more pronounced after four CCl_4 injections showing the beginning of the central-to-central vein bridging of the fibrotic streets (Fig. 29B. left column). Contrarily, both control groups did not show a damage either in H&E or Sirius red staining, as expected. To confirm these results, the liver enzymes ALT (Fig. 29D) and AST (Fig. 29E) were measured. The ALT and AST values underlined the liver damage after the CCl_4 administration with significantly higher plasma levels of these enzymes while in the control groups the enzymes were not detected. The comparison of the liver-weight-to-body-weight ratio of the four groups did not indicate any difference (Fig. 29C).

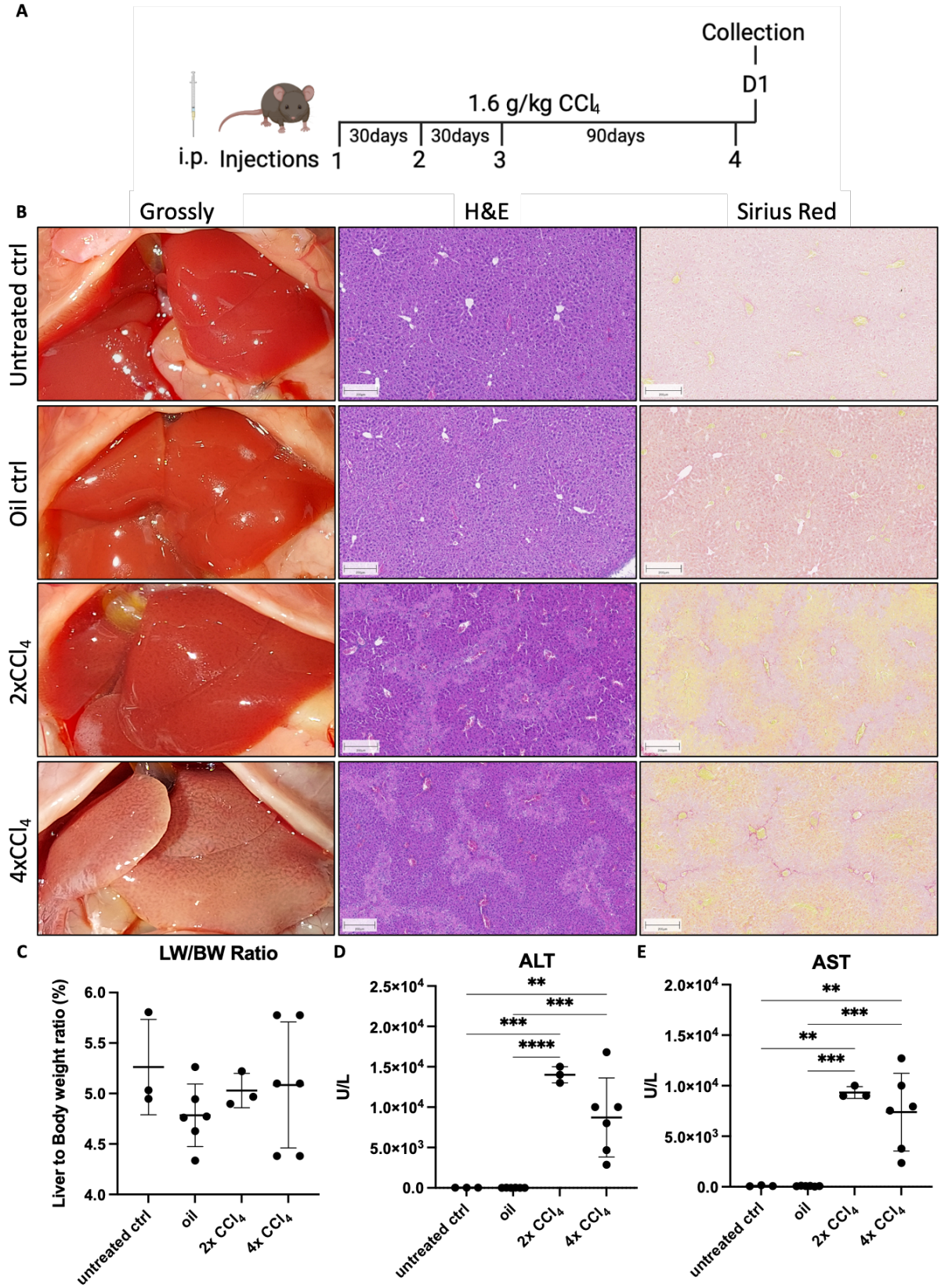

Figure 29. Rechallenge with a fourth CCl_4 dose after a break of 90 days causes liver damage. **A.** Experimental design. **B.** Gross pathology (left column) and representative images of whole slide scans of H&E (middle column) and Sirius red (right column) stained liver sections of untreated control mice (first row), oil control mice (second row), two times treated mice (third row) and four times treated mice (forth row) with intraperitoneal injections of 1.6 g/kg CCl_4 from at least 3 mice per group (Scale bars: 200 μm). **C.** Liver-weight-to-body-weight ratio does not show any difference between the groups.

Plasma analysis of the liver enzymes **D.** ALT and **E.** AST revealed the significantly higher plasma levels in response to CCl_4. Data are presented as means ± standard deviation of at least three biological replicates. Calculation of differences between the groups was performed with one-way ANOVA. **P<0.01; ***P<0.001; ****P<0.0001.

After the isolation, staining and measurement of the immune cells, the memory effect of ILC1s after a break of 90 days was observed again. The comparison of the untreated and olive oil control to the fourth dose of CCl_4 showed significantly more $CD200r^+$ ILC1s (Fig. 30A). The ILC1s from the group of four times treated mice were also positive for the transcription factor T-Bet (Fig. 30B) and were able to produce significantly and in total more IFNγ in relation to all other groups (Fig. 30C, D). Although the rechallenge of the liver still caused the memory effect of ILC1s, the total number of ILC1s per gram liver was reduced by half reduced compared to the numbers of ILC1s after three doses of CCl_4 without a break (Fig. 30A).

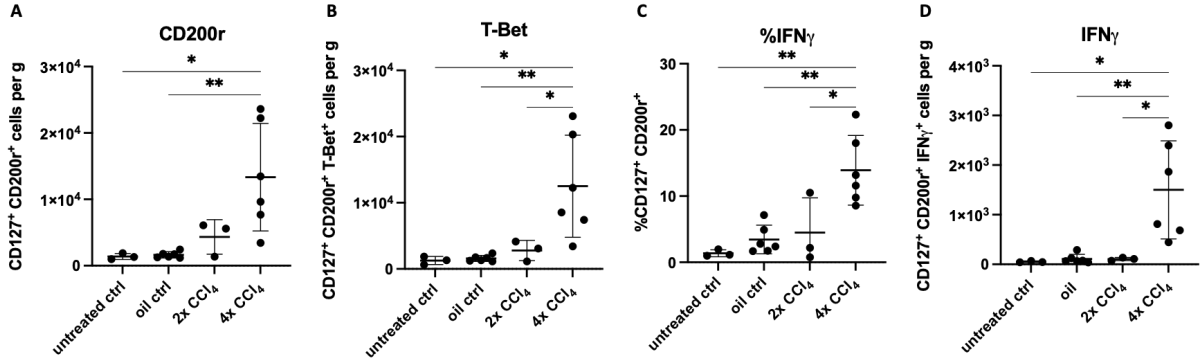

Figure 30. Long lasting effect and recall response of memory like ILC1s to additional injection of CCl_4 after a break of 90 days.
Freshly isolated immune cells of livers from the different groups of untreated control, olive oil control, two times CCl_4 and four times CCl_4 treated mice were measured on a flow cytometer and analyzed with FlowJo to identify the number of **A**. ILC1s which were identified as dead cell $marker^-CD45^+Lin^-NK1.1^+EomesS^-CD49a^+ROR\gamma T^-CD127^+CD200r^+$, **B.** $T\text{-}Bet^+$ ILC1s, **C.** the percentage of IFNγ producing cells and **D.** $IFN\gamma^+$ cells per gram liver. Data are presented as means ± standard deviation of three biological replicates per group. Calculation of differences between the groups was performed with one-way ANOVA. *P<0.05, **P<0.01.

3.7 Two injections of CCl_4 are not enough to cause a memory effect of ILC1s

Since two CCl_4 injections in the re-challenge experiment with 90 days break were not enough to generate memory like ILC1s with higher IFNγ production (Fig. 30), we wanted to investigate if a shorter period would lead to a memory effect of ILC1s. The same experimental setup was chosen as in figure 24 but the liver and blood were already collected 24 hours after the second injections of CCl_4 (Fig. 31A). Gross pathology of the livers treated once or twice with CCl_4 showed the typical macroscopic alteration patterns which were more pronounced after the second CCl_4 application while the olive oil control livers did not exhibit any indications of damage (Fig. 31B, left column). Paraffin embedded liver tissue sections stained with H&E staining exhibited pericentral damaged area and necrotic lesions after CCl_4 treatment which was not observed in the olive oil controls (Fig. 31B, middle column). To visualize collagen

deposition in the livers, Sirius red staining was performed. As already seen in the other olive oil control livers, these livers had a positive signal only around large blood vessels. The same positive signal was also observed in the CCl_4 treated groups, whereas in mice which received CCl_4 twice, the livers had some small, thin and short fibrotic streets. These small fibrotic streets could not be found in the one-time treated mice (Fig. 31B, right column). The liver-weight-to-body-weight ratio revealed no difference between the groups (Fig. 31C). Analysis of the liver enzymes in plasma showed that ALT (Fig. 31D) as well as AST (Fig. 31E) were significantly elevated after CCl_4 exposure. The comparison of the two CCl_4 groups revealed that higher enzyme levels in plasma were detected after two injections.

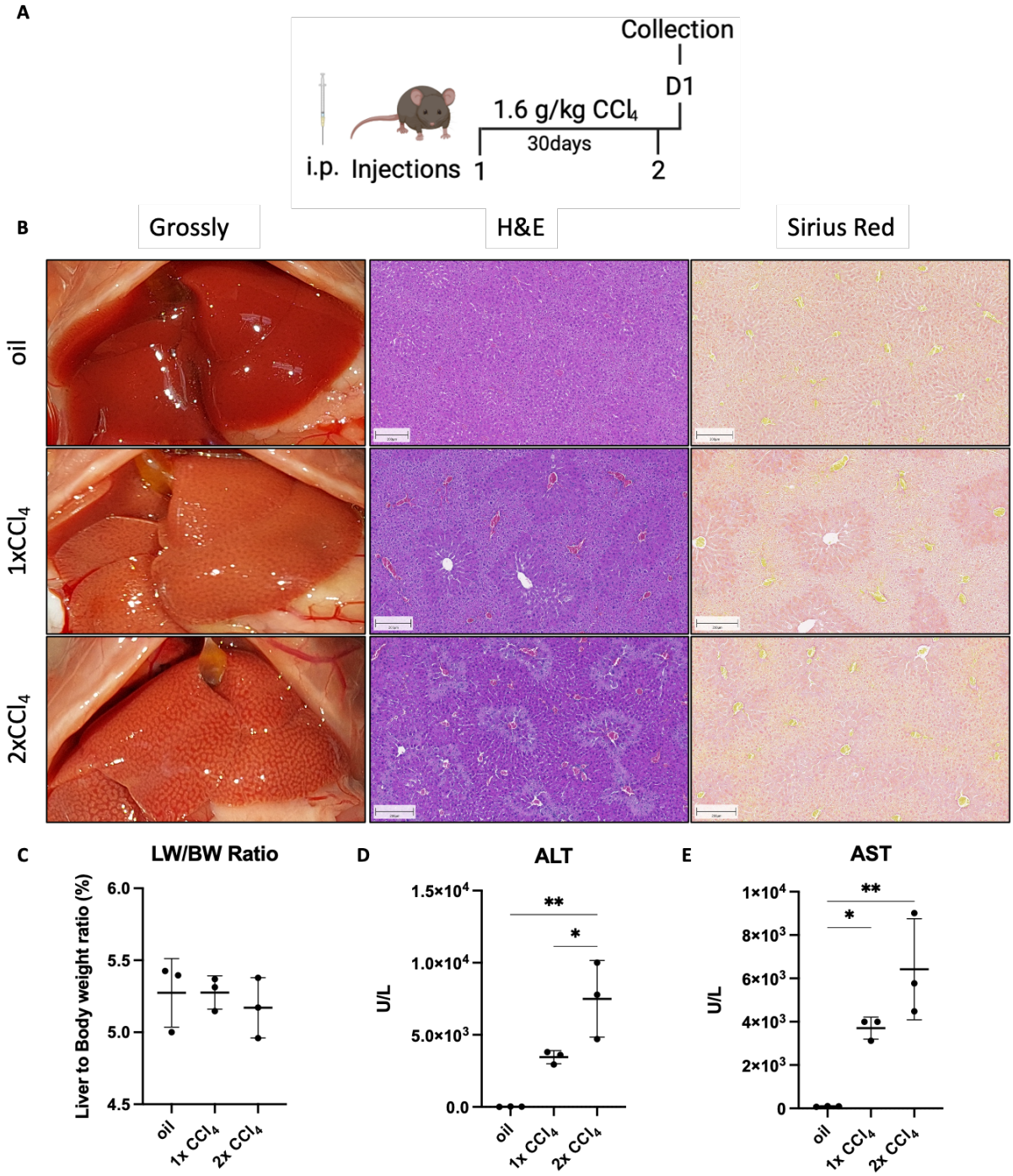

Figure 31. Treatment with only two CCl_4 injections does not cause collagen deposition.

A. Experimental design. **B.** Gross pathology (left column) and representative images of whole slide scans of H&E (middle column) and Sirius red (right column) stained liver paraffin embedded tissue sections of oil control mice (first row), one-time treated mice (second row) and two times treated mice (third row) with intraperitoneal injections of 1.6 g/kg CCl_4 from 3 mice per group (Scale bars: 200 μm). **C.** Liver-weight-to-body-weight ratio do not show any alterations. Analysis of the liver enzymes **D.** ALT and **E.** AST revealed the significantly higher plasma levels in response to CCl_4 which are more pronounced after the second application of CCl_4. Data are presented as means ± standard deviation of three biological replicates. Calculation of differences between the groups was performed with one-way ANOVA. *P<0.05; **P<0.01; ***P<0.001.

In order to identify the memory potential of ILC1s after the second injection of CCl_4, the immune cells from the different livers were isolated, stained, measured on a flow cytometer and analyzed by FlowJo. The analysis of the data testified significantly higher numbers of $CD200r^+$ ILC1s per gram liver after two CCl_4 applications (Fig. 32A) although the numbers were lower than in figure 25A. Furthermore, these $CD200r^+$ ILC1s were still positive for the transcription factor T-Bet (Fig. 32B). Despite the fact that these $CD200r^+$ ILC1s contained significantly more IFNγ positive cells per gram liver after the second injection of CCl_4 (Fig. 32D), these cells only showed a non-significant tendency to produce more IFNγ compared to the other groups (Fig. 32C). Thus, there was no memory effect of $CD200r^+$ ILC1s after the second injection of CCl_4. This finding clearly underlined that it is necessary to inject at least three times CCl_4 to generate the phenotype of IFNγ producing memory like ILC1s in the liver.

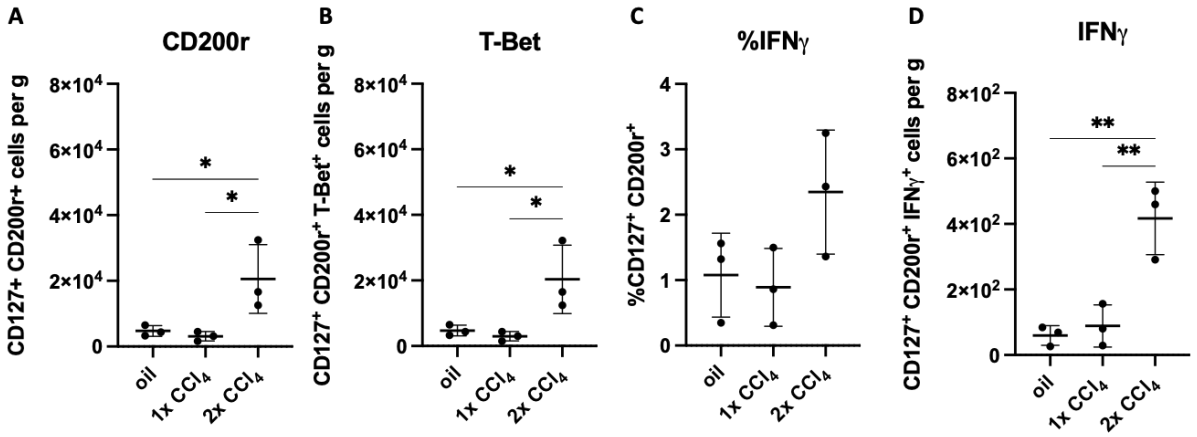

Figure 32. Two injections of CCl_4 already lead to an increase of CD200r+ ILC1s in the liver.
Freshly isolated immune cells of livers from olive oil control, one-time CCl_4 and two times CCl_4 treated mice were analyzed to identify the number of **A**. ILC1s which were identified as dead cell marker$^-$ $CD45^+Lin^-NK1.1^+EomesS^-CD49a^+ROR\gamma T^-CD127^+CD200r^+$, **B.** T-$Bet^+$ ILC1s, **C.** the percentage of IFNγ producing cells and **D.** IFNγ^+ cells per gram liver. Data are presented as means ± standard deviation of three biological replicates per group. Calculation of differences between the groups was performed with one-way ANOVA. *P<0.05, **P<0.01.

3.8 ILC1 deficient mice

The memory effect of ILC1s with higher production of IFNγ after at least three doses of CCl_4 was reproducibly shown. Additionally, their phenotype and the transient effect was shown. Nevertheless, there are still a lot of unknown features of the memory like ILC1s unknown which needed to be further analyzed. Thus, in the next experiment we wanted to see what would

happen if the mice lack ILC1s. To answer this question ILC1 deficient Hobit knock out mice were received from Georg Gasteiger´s lab (Würzburg).

In the following experiment, these Hobit knock out mice were treated three times either with olive oil or with CCl_4 in the same manner as described in figure 24A. As further controls, Hobit WT mice and C57Bl/6J mice, which are the background of the Hobit mice, were also treated three times with CCl_4. 24 hours after the third injection, liver and blood of these mice were collected. Gross pathology of all mice receiving three doses of CCl_4 showed a pale liver with alteration patterns indicating a damage of the organ (Fig. 33A, left column). In line with the macroscopic observation, H&E staining of the paraffin embedded liver tissue sections also confirmed a damage of the liver. Especially the CCl_4 treated Hobit KO mice and the C57BL/6J mice exhibited large necrotic areas around the central veins whereas the Hobit WT mice seemed to have less pericentral damaged area and necrotic lesions (Fig. 33A, middle column). Similar to the H&E results, the CCl_4 treated Hobit KO mice and the C57Bl/6J mice exhibited pericentral fibrosis with central-to-central vein bridging of the fibrotic streets. In contrast to these mice, the Hobit WT mice did only show a weak signal in the Sirius red staining indicating a mild collagen deposition in the pericentral area (Fig. 33A, right column). The olive oil Hobit KO control did not reveal any indication of a liver damage as expected. While the liver-weight-to-body-weight ratio did not reveal any differences between the four groups (Fig. 33B), the two measured liver enzymes ALT (Fig. 33C) and AST (Fig. 33D) were higher expressed in the plasma of all CCl_4 treated mice compared to the olive oil treated Hobit KO mice.

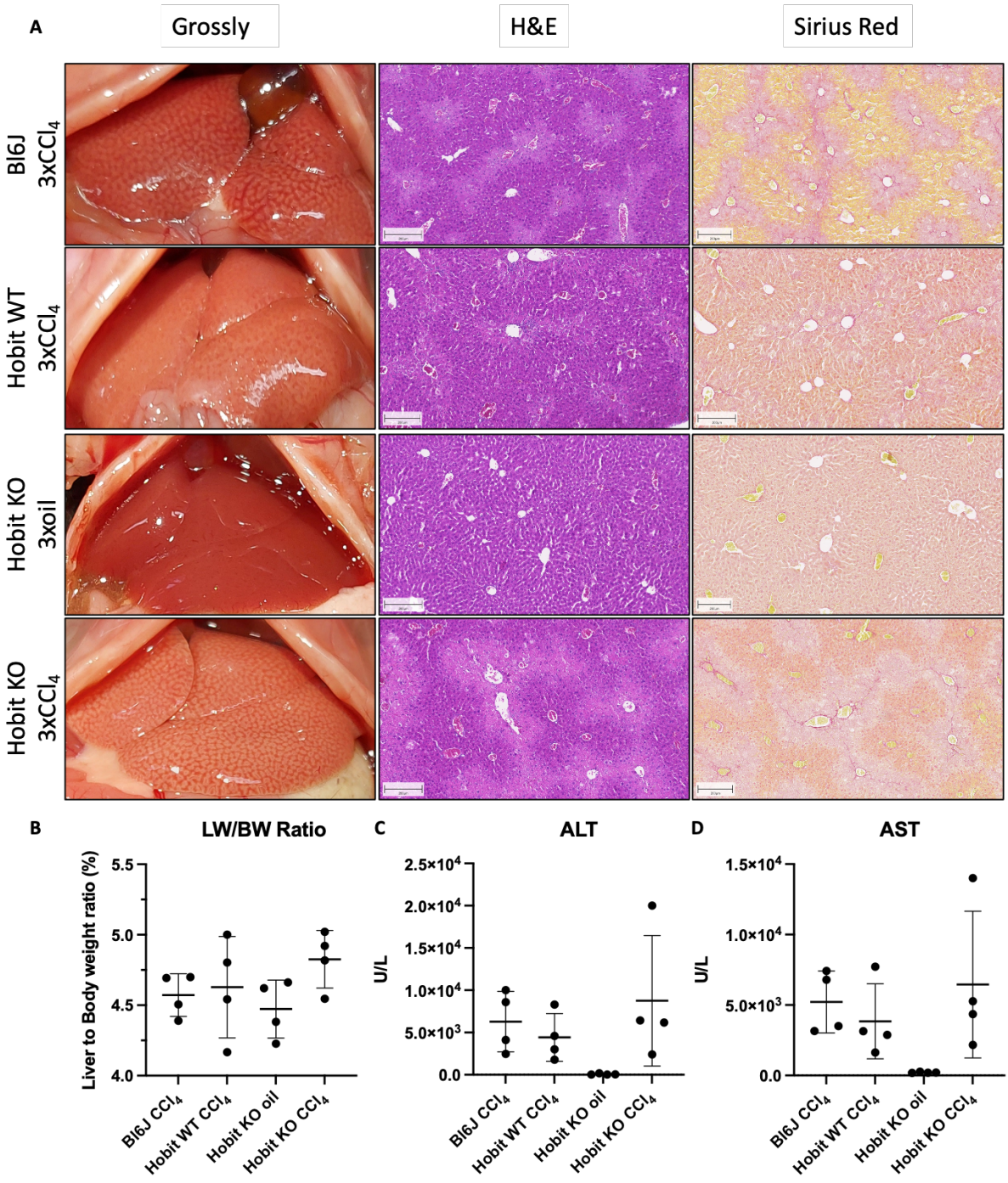

Figure 33. Hobit KO mice exhibit a liver damage after three doses of CCl_4.
A. Gross pathology (left column) and representative images of whole slide scans of H&E (middle column) and Sirius red (right column) stained liver paraffin embedded tissue sections C57Bl/6J mice treated three times with CCl_4 (first row), Hobit WT mice treated three times with CCl_4 (second row), Hobit KO control mice treated with olive oil (third row) and Hobit KO mice treated three times with CCl_4 (forth row) with intraperitoneally injections of 1.6 g/kg CCl_4 of 4 mice per group (Scale bars: 200 μm). **B.** Liver-weight-to-body-weight ratio did not show any alterations between the different mice. Plasma analysis of the liver enzymes **C.** ALT and **D.** AST revealed statistically non-significant increased plasma levels in response to CCl_4 in comparison to olive oil treated mice. Data are presented as means ± standard deviation of four biological replicates per group.

In the next step the immune cells were isolated, stained, measured and analyzed. The analysis of the stained ILC1s showed that the background controls C57Bl/6J had in average 60.000 CD200r$^+$ ILC1s per gram liver (Fig. 34A) and they also expressed the transcription factor T-Bet (Fig. 34B). This high number of CD200r$^+$ ILC1s after three doses of CCl_4 in C57Bl/6J is comparable to the number of CD200r$^+$ ILC1s after six doses of CCl_4 in C57Bl/6N in the previous experiment (Fig. 22A). In the CCl_4 treated Hobit WT mice, the numbers of CD200r$^+$ ILC1s were variable, however their ILC1s were still able to produce more IFNγ, as well as did the other CCl_4 treated mice (Fig. 34C). In comparison to the C57Bl/6J and Hobit WT mice, the olive oil and CCl_4 treated Hobit mice had significant decreased ILC1 cells per gram liver. Nevertheless, the repeated CCl_4 injections of Hobit KO mice still caused a small increase of ILC1s per gram liver compared to the Hobit oil control (Fig. 34A). Interestingly, the ILC1 cells of the CCl_4 treated Hobit KO mice were able to produce significantly more IFNγ compared to the olive oil control and to the Hobit WT mice, although their total number per gram liver of CD200r$^+$IFNγ$^+$ was not significantly higher compared to the olive control and was even significantly reduced compared to the C57Bl/6J mice (Fig. 34D).

Even though these Hobit KO mice should not have any ILC1s, the results demonstrated that after the CCl_4 treatment the mice had more CD200r$^+$ ILC1s which were able to produce more IFNγ compared to the olive oil control. Thus, these results show a memory effect of ILC1s in Hobit KO mice although the numbers of CD200r$^+$ ILC1s were not as high as their C57Bl/6J background control.

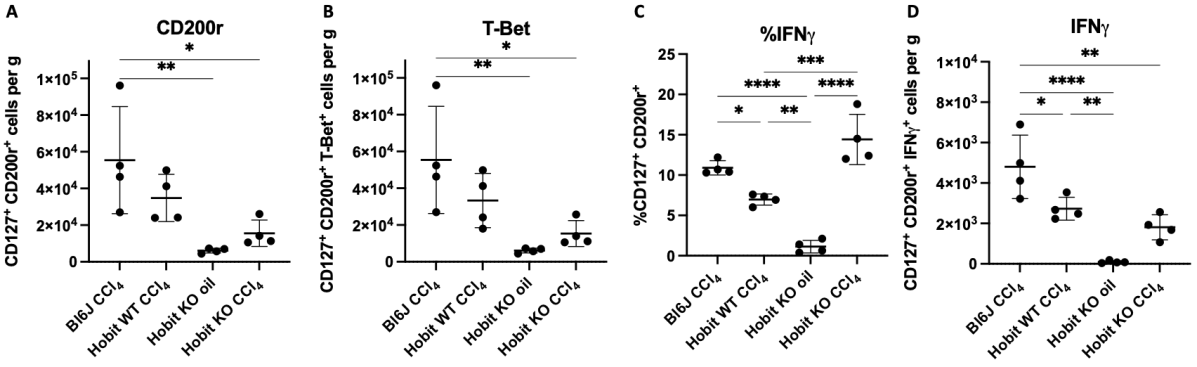

Figure 34. Hobit KO mice have lower numbers of memory like ILC1s in the liver.
Freshly isolated immune cells of livers from the different groups of olive oil control, one-time CCl_4 and two times CCl_4 treated mice were stained with the different markers, measured via the flow cytometer Aurora and analyzed with FlowJo to identify the number of **A**. ILC1s which were identified as dead cell marker$^-$CD45$^+$Lin$^-$NK1.1$^+$EomesS$^-$CD49a$^+$RORγT$^-$CD127$^+$CD200r$^+$, **B.** T-Bet$^+$ ILC1s, **C.** the percentage of IFNγ producing cells and **D.** IFNγ$^+$ cells per gram liver. Data are presented as means ± standard deviation of three biological replicates per group. Calculation of differences between the groups was performed with one-way ANOVA. *P<0.05, **P<0.01; ***P<0.001; ****P<0.0001.

3.9 Depletion of NK cells

The previous results showed that although the Hobit KO mice should be ILC1 deficient, they could still develop memory like ILC1s after three CCl_4 injections (Fig. 34). Furthermore, we could already show that the increased number of ILC1s is not caused by proliferation (Fig. 26D). Thus, until now, we cannot explain the increased ILC1 numbers in response to multiple CCl_4 injections resulting in a memory effect. During the last years, several researcher groups published papers about the phenomenon that, under certain circumstances, such as changes in the microenvironment, the innate lymphoid cells can change their phenotype and associated function into another ILC subset. This phenomenon is called plasticity (Bal et al., 2020; Vivier et al., 2018). One example for the ILC plasticity is the change of cytotoxic NK cells to ILC1s which requires an enhanced TGF-β signaling (Cortez et al., 2017; Gao et al., 2017). Thus, the next step was to investigate whether the increased number of ILC1s is caused by NK cell plasticity. Therefore, the idea was to specifically deplete NK cells and see if the higher numbers of ILC1s are still observable. However, NK cells and ILC1s are quite similar and have many markers in common. Nabekura et al., 2020 could show that the polyclonal antibody Anti-Asialo GM1 specifically depletes the NK cells but not the ILC1s (Nishikado et al., 2011). With this antibody, we performed two experiments. In the first experiment, male C57Bl/6N mice were used to evaluate the function of the depletion antibody and if the NK cells contribute to the increased numbers of ILC1s after three applications of CCl_4. The second experiment was performed with B6;129-Ncr1^{tm10man}/J mice, short NCR1-GFP, in order to further investigate the function of ILC1s and to show where they are localized in the liver.

For the first experiment, male C57Bl/6N mice were treated intraperitoneally three times with 1.6 g/kg CCl_4 with a break of 30 days between the injections. Together with the third injection, the depletion antibody Anti-Asialo GM1 (50 µL) was also intraperitoneally injected. As controls, mice were injected intraperitoneally three times with olive oil or the first two times with olive oil and the third time with CCl_4 and together with the third injection, they also received the depletion antibody. 24 hours after the third injection, blood plasma and livers were collected from the mice (Fig. 35A). Macroscopically, the livers looked similar to the ones without NK cell depletion (Fig. 24B). The one-time treated liver exhibited the typical CCl_4 alteration patterns which were more prominent after the third CCl_4 application while the olive oil controls did not show any indications for a damage (Fig. 35B, left column). H&E staining of paraffin embedded liver tissue sections displayed necrotic lesions around the central vein after CCl_4 exposure (Fig. 35B, middle column) while in the Sirius red staining no fibrotic streets were observed in livers with three doses of CCl_4 although the signal was stronger in these livers compared to one-time CCl_4 treated mice (Fig. 35B, right column). As expected, olive oil controls did not have any necrotic areas nor any collagen deposition. The liver-weight-to-body-weight ratio was nearly

similar in the three groups whereas the plasma levels of the liver enzymes ALT (Fig. 35D) as well as AST (Fig. 35E) were elevated after CCl_4 exposure.

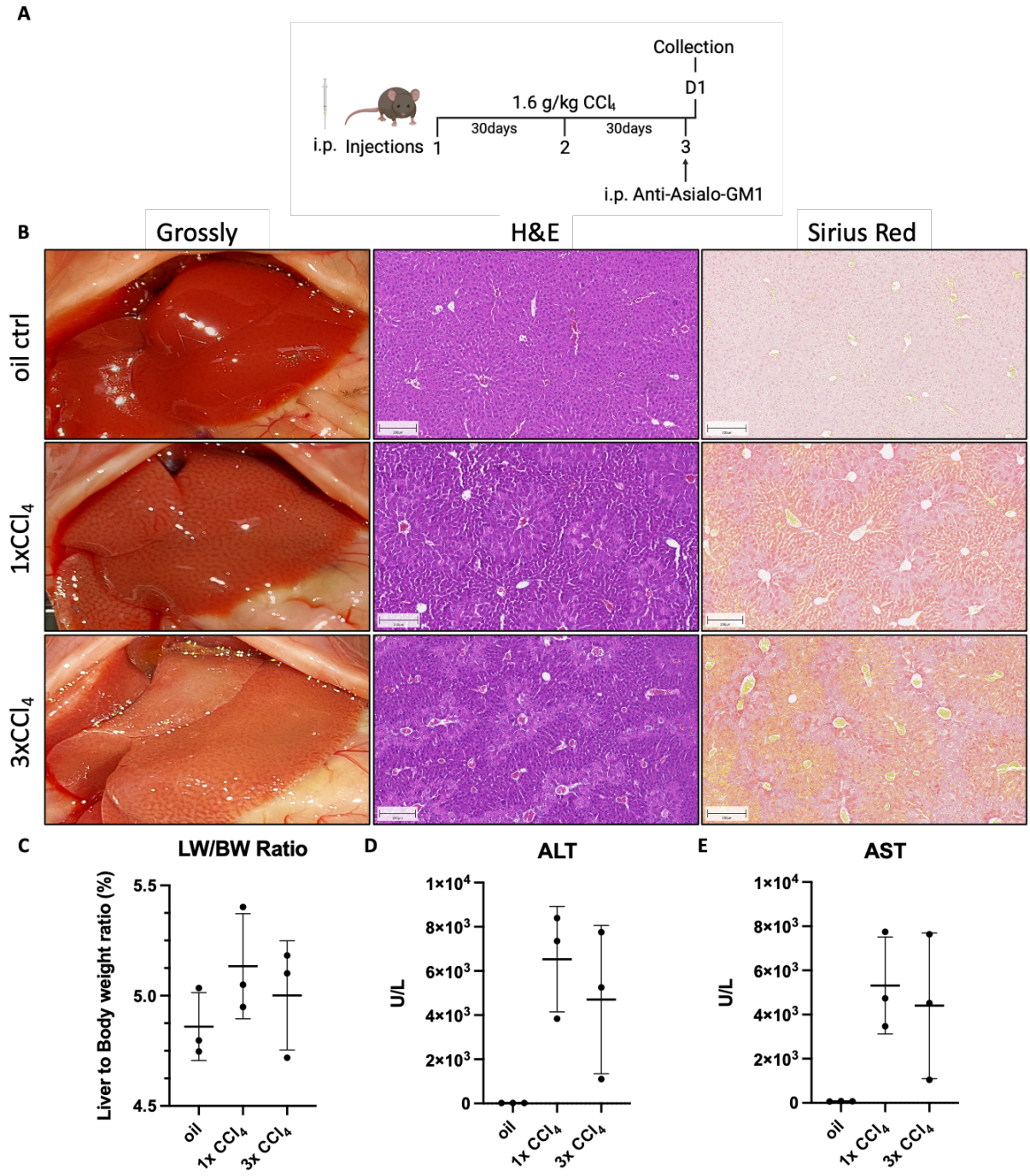

Figure 35. Treatment with the depletion antibody Anti-Asialo GM1 has no effect on the liver damage after the third injection of CCl_4.
A. Experimental design. **B.** Gross pathology (left column) and representative images of whole slide scans of H&E (middle column) and Sirius red (right column) stained liver sections of oil control mice (first row), one-time treated mice (second row) and two times treated mice (third row) with intraperitoneal injections of 1.6 g/kg CCl_4 and 50 µL Anti-Asialo GM1 from 3 mice per group (Scale bars: 200 µm). **C.** Liver-weight-to-body-weight ratio did not show any alterations. Plasma analysis of the liver enzymes **D.** ALT and **E.** AST revealed the higher plasma levels in response to CCl_4. Data are presented as means ± standard deviation of three biological replicates per group.

The analysis of the isolated and stained immune cells revealed that the Anti-Asialo GM1 worked since the NK cell numbers per gram liver were reduced (Fig. 36E) compared to C57Bl/6N mice which were not treated with the depletion antibody (Fig. 25E). But not only was the NK cell number reduced, but there were also less ILC1 per gram liver. After the third CCl_4 dose there were only around 2.000 $CD200r^+$ ILC1s per gram liver while the single injection of CCl_4 lead to 1.000 $CD200r^+$ ILC1s per gram liver (Fig. 36A). Only few of these cells were expressing the transcription factor T-Bet. Nevertheless, the ILC1s of the three times treated mice were still able to significantly produce more IFNγ (Fig. 36C) and also the number of $IFN\gamma^+$ cells (Fig. 36D) were significantly higher in relation to the two other groups. However, the experiment did not help to answer the question if the higher numbers of ILC1s can be explained by the plasticity effect from NK cells to ILC1s or if Anti-Asialo GM1 antibody also depletes ILC1s.

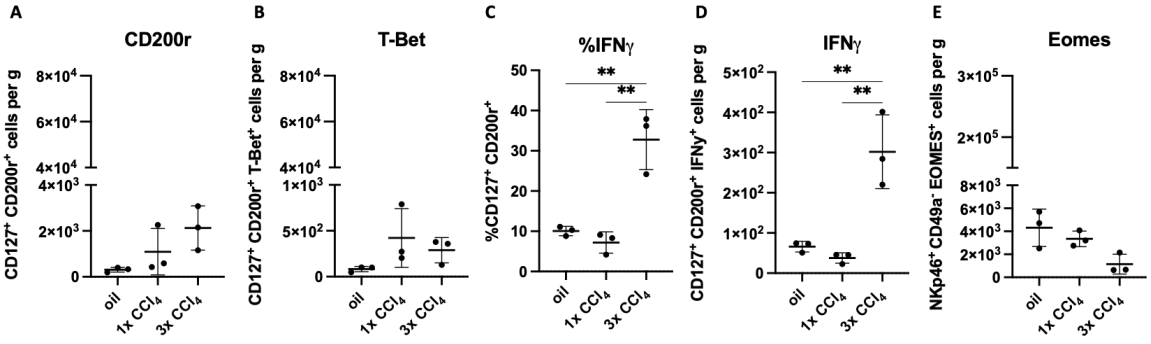

Figure 36. Depletion antibody Anti-Asialo GM1 causes reduced NK cell numbers but also reduced numbers of ILC1s.
Freshly isolated immune cells of livers from the mice treated with Anti-Asialo GM1 and olive oil, one time CCl_4 and three times CCl_4 were stained with the different markers, measured via the flow cytometer Aurora and analyzed with FlowJo to identify the number of **A**. ILC1s which were identified as dead cell marker$^-$CD45$^+$Lin$^-$NK1.1$^+$EomesS$^-$CD49a$^+$RORγT$^-$CD127$^+$CD200r$^+$, **B.** T-Bet$^+$ ILC1s, **C.** the percentage of IFNγ producing cells, **D.** $IFN\gamma^+$ cells per gram liver and **E.** NK cells defined as dead cell marker$^-$ CD45$^+$Lin$^-$NK1.1$^+$Eomes$^+$CD49a$^-$. Data are presented as means ± standard deviation of three biological replicates per group. Calculation of differences between the groups was performed with one-way ANOVA. **P<0.01.

Next, we performed the second experiment in order to evaluate if the Anti-Asialo GM1 also depleted ILC1s, and to see if the depletion of NK cells helps to investigate the function of ILC1s and their localization in the liver.

Therefore, the same experimental set up with the same controls was chosen as in the previous experiment (Fig. 35A). But instead of using C57Bl/6N mice, in this experiment homozygous Ncr1-GFP mice were chosen. 24 hours after the Ncr1-GFP labelled mice received their last injection of CCl_4 and one group was injected with Anti-Asialo GM1 intraperitoneally, liver and blood were collected. Grossly, the livers revealed no difference between the mice injected with or without the depletion antibody in the olive oil, once or three times with CCl_4 treated group. As already seen before, the only one-time treated liver exhibited the typical alteration patterns while after the third dose of CCl_4 the livers were in both cases pale and the alteration patterns

were more pronounced (Fig. 37A, left column of both panels). Immunohistochemistry of the paraffin embedded liver tissue sections displayed in the H&E staining again necrotic lesions around the central vein after CCl_4 exposure (Fig. 37A, middle column of both panels). Additionally, the Sirius red staining displayed in both groups some thin fibrotic streets after the third CCl_4 doses whereas the liver tissues of mice treated with one dose CCl_4 and depletion antibody showed a stronger signal of the staining, indicating more collagen depositions than in the mice without Anti-Asialo GM1 (Fig. 37A, right column of both panels). The olive oil control groups did not indicate any liver damage, neither macroscopically nor in the immunohistochemistry stainings. Further analysis showed that liver-weight-to-body-weight ratio was nearly similar independent of the Anti-Asialo GM1 treatment, but again the liver enzymes in the plasma were elevated after CCl_4 exposure. Especially the mice treated with the depletion antibody had significantly elevated ALT (Fig. 37F) and AST (Fig. 37G) levels, while the other group of mice showed non-significantly higher plasma levels of ALT (Fig. 37C) and AST (Fig. 37D) after CCl_4 application.

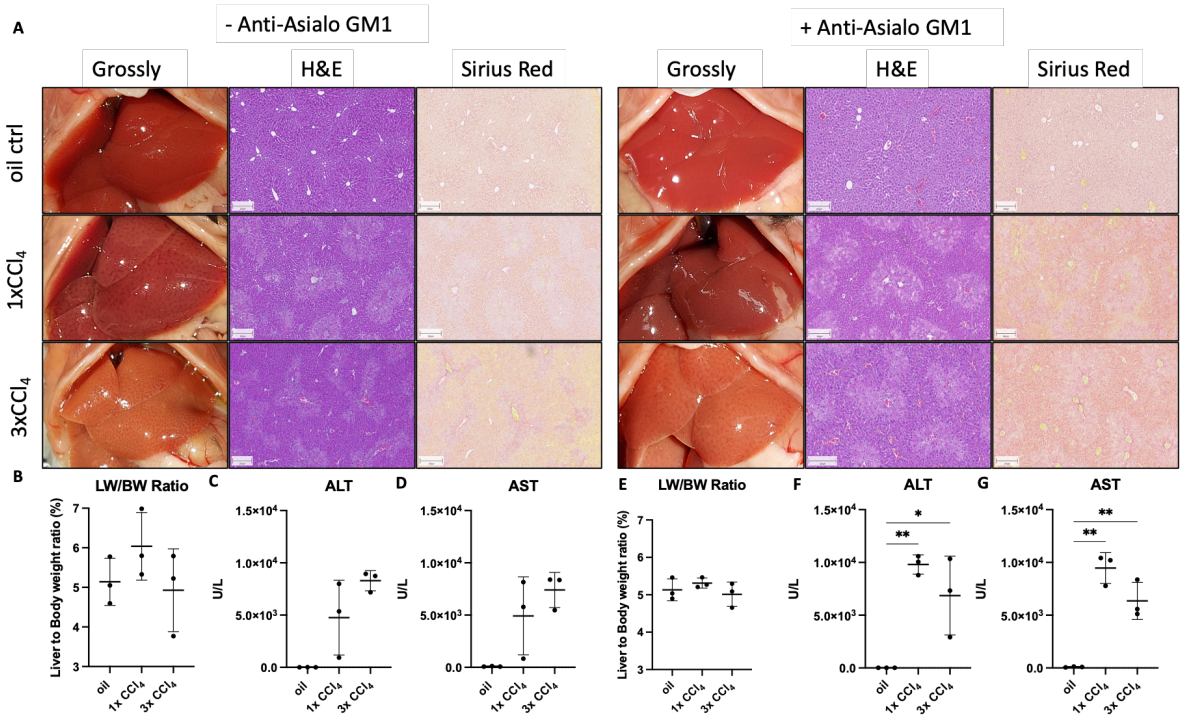

Figure 37. NCR1-GFP mice treated with or without the depletion antibody Anti-Asialo GM1 show both a liver damage in response to the third injection of CCl_4.
A. Gross pathology (left column) and representative images of whole slide scans of H&E (middle column) and Sirius red (right column) stained liver paraffin embedded tissue sections of oil control mice (first row), one-time treated mice (second row) and two times treated mice (third row) with intraperitoneally injections of 1.6 g/kg CCl_4 (left panel) and additional treatment with 50 µL Anti-Asialo GM1 (right panel) from 3 mice per group (Scale bars: 200 µm). **B.** Liver-weight-to-body-weight ratio does not show any alterations in NCR1-GFP mice after the CCl_4 treatment. Plasma analysis of the liver enzymes **C.** ALT and **D.** AST revealed the higher plasma levels in response to CCl4. **E.** Teatment of NCR1-GFP mice with Anti-Asialo GM1 do not show a difference in the liver-weight-to-body-weight-ratio. **F.** ALT and **G.** AST revealed significantly higher plasma levels in response to CCl_4 in comparison to olive oil treated mice. Data are presented as means ± standard deviation of three biological replicates

per group. Calculation of differences between the groups was performed with one-way ANOVA *P<0.05, **P<0.01.

In the next step, the isolated immune cells were stained and analyzed. The analysis of the NCR1-GFP mice showed that the mice which were not treated with the depletion antibody had significantly more ILC1s in the liver after the third CCl_4 injection (Fig. 38A), although the numbers were clearly reduced compared to C57Bl/6N mice (Fig. 25A). Nevertheless, the CD200r$^+$ ILC1s of three times treated CCl_4 mice also expressed T-Bet (Fig. 38B) and were able to produce significantly more IFNγ (Fig. 38E) and also the number of IFNγ^+ cells (Fig. 38F) was significantly higher in relation to the two other groups. Furthermore, the calculated number of NK cells per gram liver revealed that the CCl_4 application led to a slightly increase of NK cells in the NCR1-GFP mice (Fig. 38I). The comparison between the Anti-Asialo GM1 treated mice and the mice which were not treated with the depletion antibody revealed a dramatic reduction of NK cells caused by Anti-Asialo GM1 (Fig. 38J). Interestingly, numbers of CD200r$^+$ ILC1s per gram liver were also reduced. After the depletion of NK cells, the CD200r$^+$ ILC1s were reduced to around 1.500 cells per gram liver (Fig. 38C) whereas the number in the not depleted mice was around 5.000 cells per gram liver after the third CCl_4 exposure (Fig. 38A). Moreover, most of the CD200r$^+$ ILC1s in the Anti-Asialo GM1 treated mice were also T-Bet$^+$ (Fig. 38D), and in total produced significantly more IFNγ (Fig. 38G, H)

With this experiment we wanted to answer several questions and to track the ILC1s. However, already due to the reduced numbers of ILC1s in the NCR1-GFP mice, it was not possible to localize these few ILC1s in the liver in this mouse model nor to answer the question if NK cell plasticity to ILC1 cells causes the increased cell numbers in the liver after multiple CCl_4 injections.

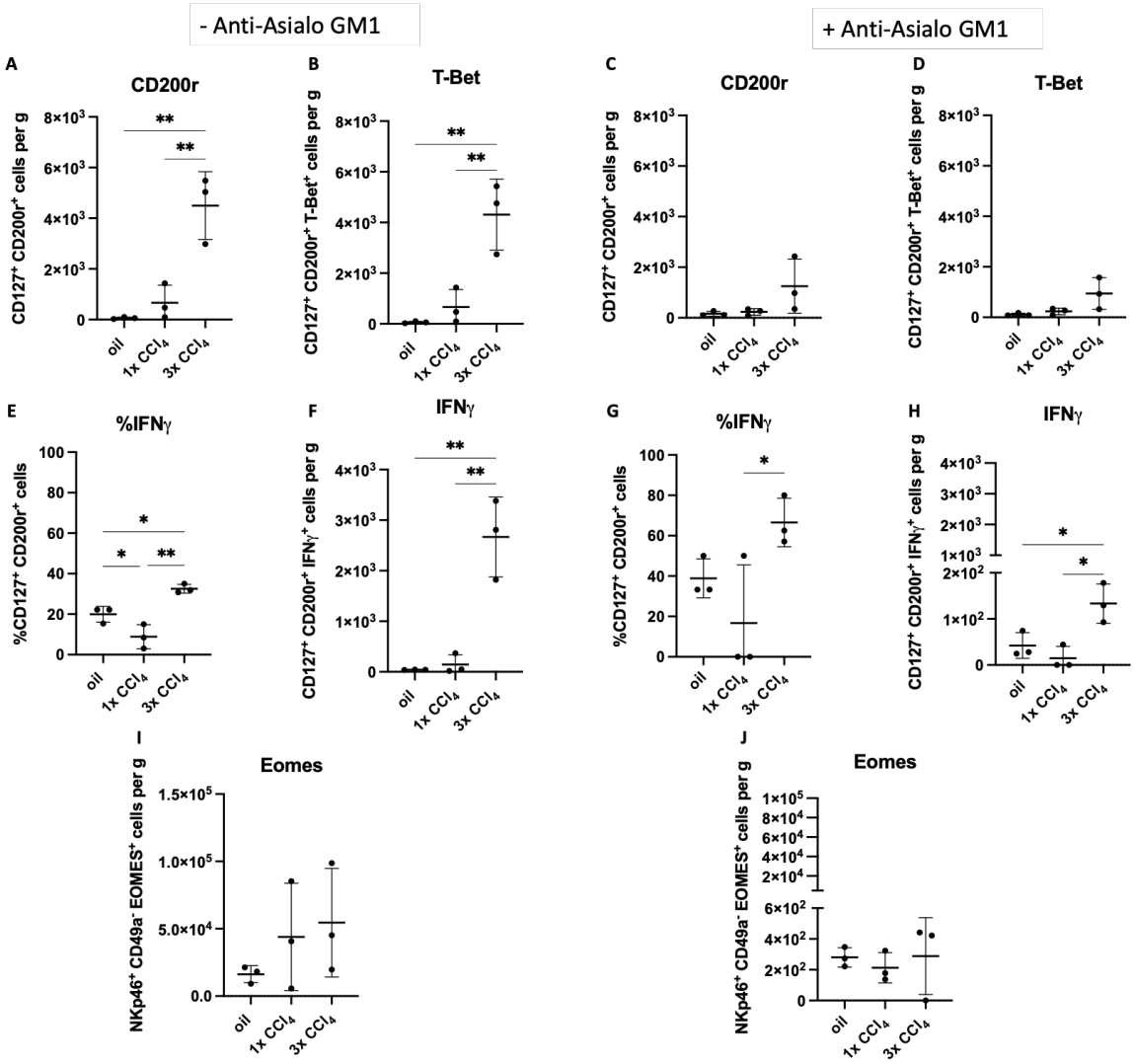

Figure 38. Depletion antibody Anti-Asialo GM1 causes reduced NK cell numbers but also reduced numbers of ILC1s.
Freshly isolated immune cells of livers from the mice treated without (left panel) or with (right panel) Anti-Asialo GM1 additionally to olive oil, one-time CCl_4 and three times CCl_4 treatment. Cells were stained with the new ILC1 panel, measured and analyzed to identify the number of **A**. and **C.** ILC1s which were identified as dead cell marker$^-$CD45$^+$Lin$^-$NK1.1$^+$EomesS$^-$CD49a$^+$RORγT$^-$CD127$^+$CD200r$^+$, **B. and D.** T-Bet$^+$ ILC1s, **E. and G.** the percentage of IFNγ producing cells, **F. and H.** IFNγ$^+$ cells per gram liver and **I. and J.** NK cells defined as dead cell marker$^-$CD45$^+$Lin$^-$NK1.1$^+$Eomes$^+$CD49a$^-$. Data are presented as means ± standard deviation of three biological replicates per group. Calculation of differences between the groups was performed with one-way ANOVA. **P<0.01.

3.10 Memory potential of ILC1s in other liver damage mouse models

To investigate the memory potential of ILC1s in the liver, the CCl_4 liver damage mouse model was used for all of the experiments. But there are several other liver damage mouse models described in the literature and we wanted to investigate whether the phenomenon of the formation of memory potential of ILC1s is restricted to the CCl_4 mouse model, or whether it can it be also observed in other mouse models. Therefore, western-style diet and Acetaminophen (APAP) mouse models were chosen to investigate this question.

The first experiment was performed with the western diet mouse model. Therefore, male Bl6N mice were fed either with a standard diet (SD) or a calorie-rich western-style diet (WD). After 12 weeks of standard and western diet, two groups of each diet mice were injected intraperitoneally with either olive oil or 1.6 g/kg CCl_4 and the third group remained untreated and was the diet control group (Fig. 39A). The CCl_4 injection was included since the previous results showed that the memory potential of ILC1s was created after an acute and fresh insult of the liver. Gross pathology of the livers showed that the WD livers displayed alteration patterns and the organs were pale which was even more prominent after the CCl_4 treatment. In comparison to the SD controls, only the CCl_4 treatment caused the alteration patterns and a less reddish liver which was not as pale as after 12 weeks WD (Fig. 39B, left column). Another big difference between the two diet groups could be observed in the stainings of the paraffin embedded liver tissue sections. In all WD livers, H&E as well as the Sirius red staining displayed lipid droplets especially in the midzonal and periportal hepatocytes for the diet and olive oil control, but the CCl_4 treated mice seemed to have more lipid droplets in particular in the pericentral area. Furthermore, H&E staining also showed necrotic cells around the central vein after CCl_4 exposure in both diet groups whereas the necrosis was not observed in the other two groups (Fig. 39B, middle column). The similar observation was made in the Sirius red staining in which only the CCl_4 treated mice had some small and thin pericentral fibrotic streets with a stronger signal in the WD CCl_4 treated mice. As expected, the control mice of both diets did not display any collagen depositions (Fig. 39B, right column). The comparison of the liver-weight-to-body-weight ratio revealed that the WD mice had increased ratios in relation to the SD, independent of the CCl_4 treatment. Further analysis of the blood plasma showed that the ALT (Fig. 39D) as well as AST (Fig. 39E) levels were significantly elevated after CCl_4 exposure compared to the other groups. The WD CCl_4 treated mice had significantly higher ALT and AST plasma levels compared to the SD CCl_4 treated mice. In general, the plasma levels of the WD mice were higher than the SD.

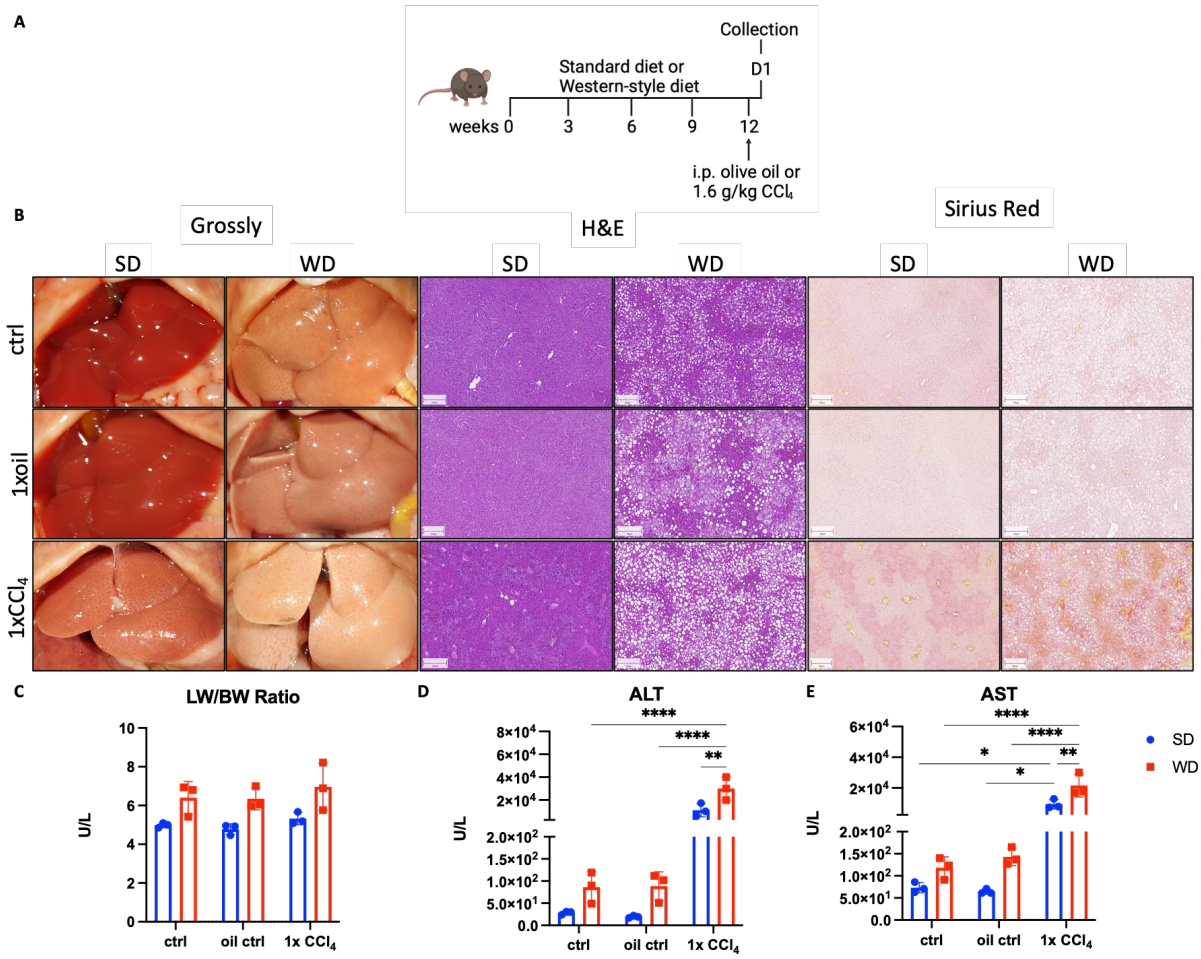

Figure 39. Comparison of twelve weeks standard diet and western-style-diet plus one injection of CCl_4.
A. Experimental design. **B.** Comparison of standard diet (SD, left side) and western-style-diet (WD, right side) in gross pathology (left column) and representative images of whole slide scans of H&E (middle column) and Sirius red (right column) stained liver paraffin embedded tissue sections of diet control mice (first row), oil control mice (second row) and CCl_4 treated mice (third row) with intraperitoneal injections of 1.6 g/kg CCl_4 from 3 mice per group (Scale bars: 200 μm). **C.** Liver-weight-to-body-weight ratio do not show any difference between treatments and SD (red) and WD (blue). Plasma analysis of the liver enzymes **D.** ALT and **E.** AST revealed the higher plasma levels in response to CCl_4. There is no difference between the diets. Data are presented as means ± standard deviation of three biological replicates per group. *P<0.05; **P<0.01; ****P<0.0001.

The results showed a difference between the SD and WD CCl_4 treated mice. In the next step, the immune cells were isolated, stained, measured and analyzed. In general, the SD mice had twice as many CD200r$^+$ ILC1s per gram liver compared to the WD mice and the numbers of CD200r$^+$ ILC1s were increased after additional CCl_4 treatment (Fig. 40A) and most of the observed CD200r$^+$ ILC1s expressed the transcription factor T-Bet (Fig. 40B). The functional analysis of the CD200r$^+$ ILC1s showed that the cells from all CCl_4 treated mice were able to significantly produce more IFNγ (Fig. 40C) and had in total significantly more IFNγ (Fig. 40C). However, ILC1 cells from WD fed CCl_4 mice showed slightly higher percentage of IFNγ producing cells. In contrast, SD fed CCl_4 mice had slightly more IFNγ$^+$ ILC1s per gram liver compared to WD.

In summary, the WD mouse model was not able to generate a memory potential in CD200r$^+$ ILC1s.

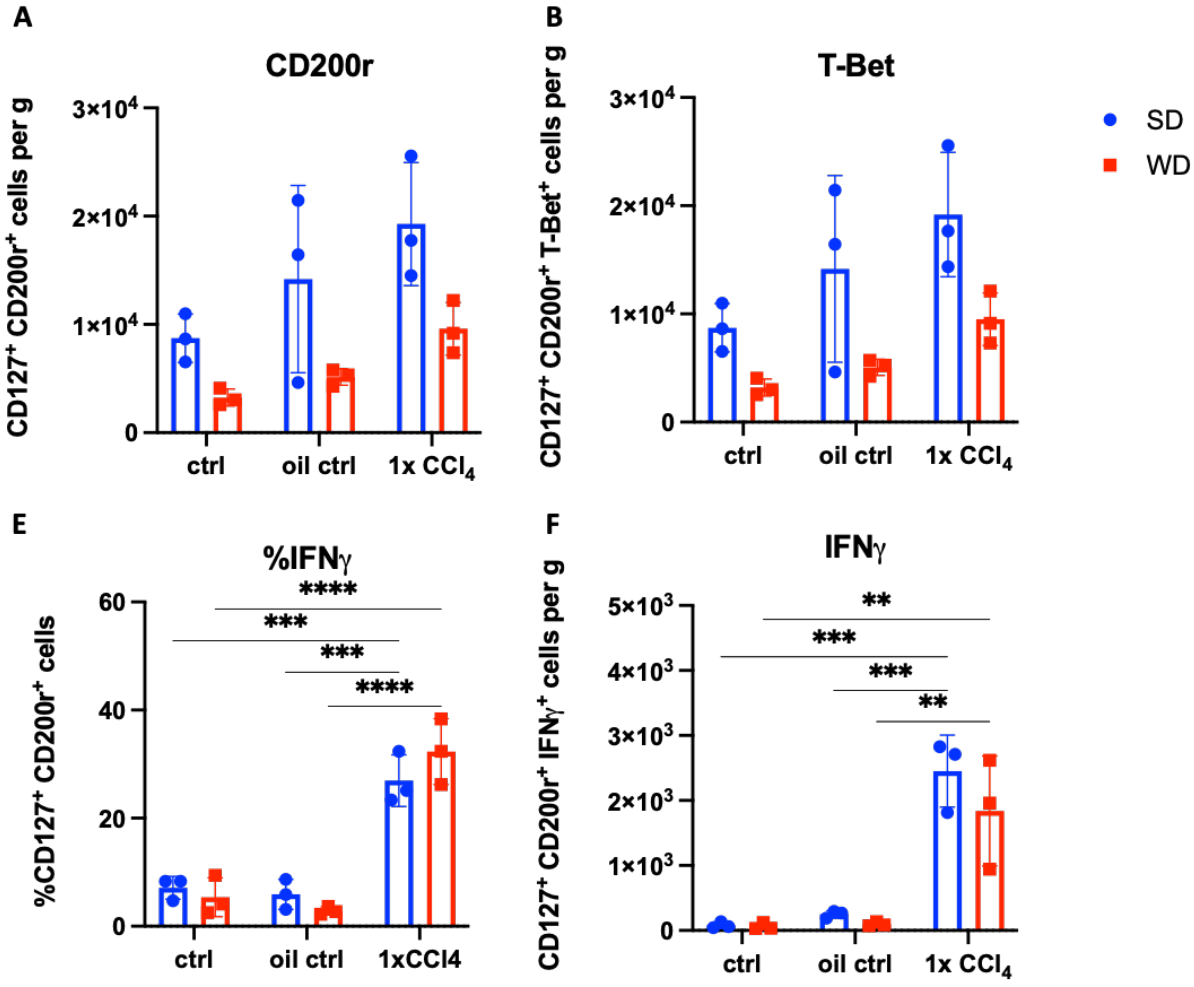

Figure 40. Western-style diet mice have less CD200r+ ILC1 after the CCl_4 injection in comparison to the standard diet.
Freshly isolated immune cells of livers from the different groups of diet, control, olive oil control and one-time CCl_4 treated mice were stained for the different markers, measured on the flow cytometer Aurora and analyzed with FlowJo to identify the number of **A**. ILC1s which were identified as dead cell marker$^-$ CD45$^+$Lin$^-$NK1.1$^+$EomesS$^-$CD49a$^+$RORγT$^-$CD127$^+$CD200r$^+$, **B.** T-Bet$^+$ ILC1s, **C.** the percentage of IFNγ producing cells and **D.** IFNγ$^+$ cells per gram liver. Data are presented as means ± standard deviation of three biological replicates per group. Calculation of differences between the groups was performed with two-way ANOVA. **P<0.01; ***P<0.001; ****P<0.0001. Standard-diet (SD, blue), Western-style-diet (WD, red).

Although memory like ILC1s could not be observed in the WD mouse model, the second mouse model was nevertheless verified. Here, 300 mg/kg APAP was intraperitoneally injected into male C57Bl/6N mice and after a break of 30 days, APAP was again injected for up to three times (Fig. 41A). Since APAP is dissolved in PBS, a PBS control group was included as well as a group of mice receiving the first two injections PBS and the last injection APAP. In order to directly compare the APAP mouse model with the previous results, three times treated CCl_4 mice were included. Furthermore, another group of mice were included to the analysis which

received the first two injections APAP and with the third injection CCl_4 and their control group (2xPBS, 1xolive oil) were investigated to learn if the combination of two different hepatotoxic compounds APAP and CCl_4 could also lead to an induction of a memory potential of ILC1s. As usual, all livers and plasma samples were collected 24 hours after the last injection. Grossly, alteration patterns were observed in all mice which were treated with either APAP or CCl_4, whereas the livers only after three CCl_4 injections were pale (Fig. 41, left column). In line with the observed macroscopical changes, H&E staining revealed dead cell areas around the central vein in the after APAP or CCl_4 treatment, however, after the three CCl_4 exposures, the damaged area occurred smaller compared to all APAP groups (Fig. 41B, middle column). Sirius red staining visualized collagen deposition in the pericentral zone in mice treated with two APAP and one CCl_4 injection whereas three injections of the same compound resulted in some small and thin pericentral fibrotic streets (Fig. 41B, right column). Both control groups did not show any indication for a liver damage neither macroscopically nor in H&E staining and the collagen deposition was only observed around blood vessels. Calculation of the liver-weight-to-body-weight ratio revealed only small variations between the control and treated groups (Fig. 41C). The plasma levels of the liver enzymes ALT (Fig. 41D) and AST (Fig. 41E) were significantly increased in all treated mice compared to the two control groups. However, the differently treated groups had similar levels of plasma liver enzymes.

Next, the immune cells were isolated from the livers and subsequently stained, measured and analyzed. The analysis of the isolated liver immune cells showed that all mice receiving in total three injections with either APAP or CCl_4 had significantly increased numbers of $CD200r^+$ ILC1s per gram liver (Fig. 42A). Most of these $CD200r^+$ ILC1s also expressed the T-Bet transcription factor (Fig. 42B). In order to investigate the memory potential of the increased numbers of $CD200r^+$ ILC1s, the IFNγ production was quantified. Higher IFNγ production was found not only after the third CCl_4 dose, but also after three injections of APAP and after two APAP and one CCl_4 injection. Furthermore, these three groups had significantly more $CD200r^+$ $IFN\gamma^+$ ILC1 per gram liver compared to both control groups and mice treated only once with APAP (Fig. 42C).

The APAP mouse model was able to create the memory potential of $CD200r^+$ ILC1s. These $CD200r^+$ ILC1s also produce more $IFN\gamma^+$. In conclusion, the APAP experiment clearly showed that the memory effect of ILC1s is not restricted to the CCl_4 mouse model.

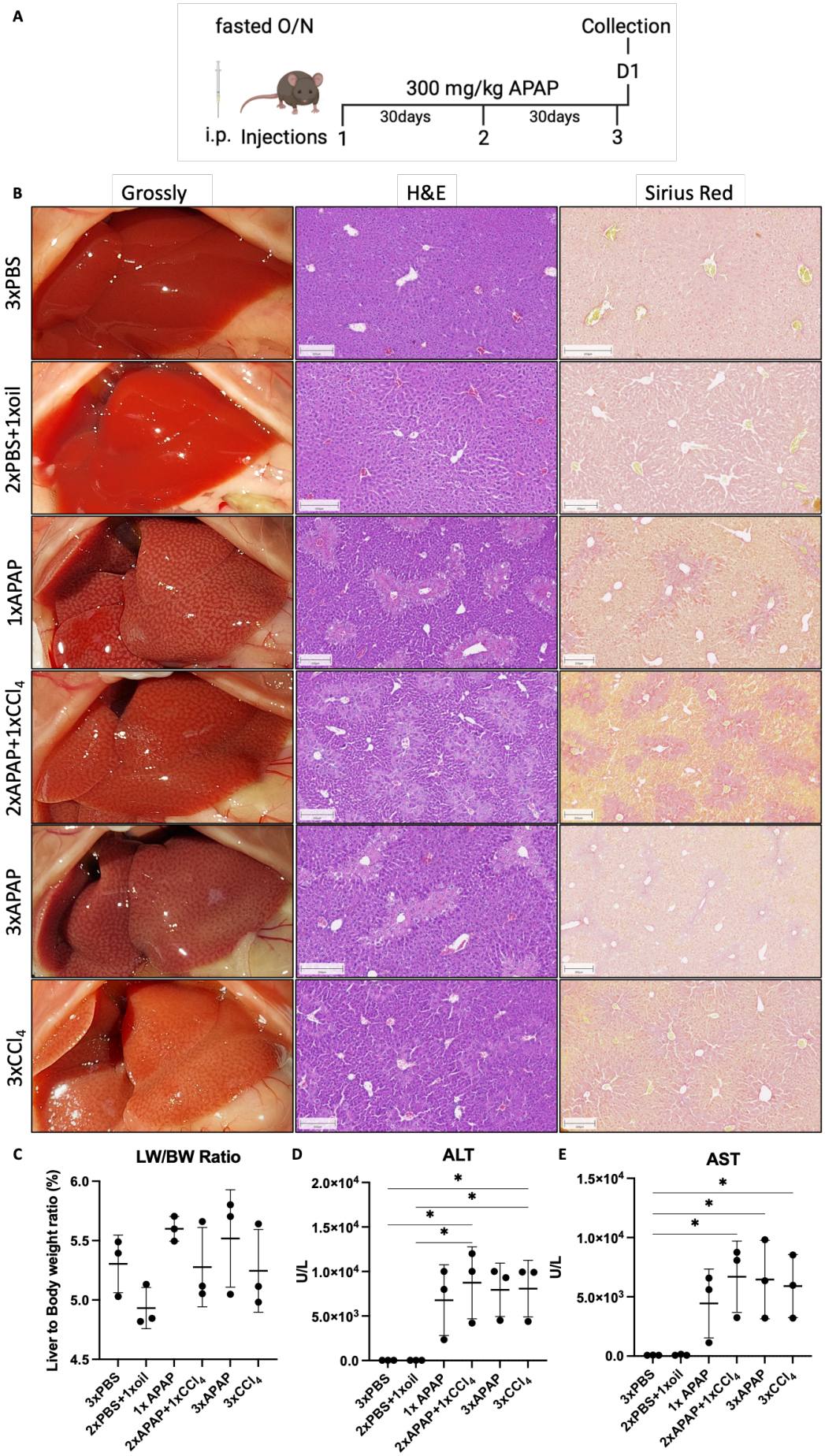

Figure 41. Three doses of APAP cause a liver damage.

A. Experimental design. **B.** Gross pathology (left column) and representative images of whole slide scans of H&E (middle column) and Sirius red (right column) stained liver paraffin embedded tissue sections of PBS control (first row), two times PBS and one time olive oil control (second row), one time 300 mg/kg APAP (third row), two times 300 mg/kg APAP and one-time 1.6 g/kg CCl_4 (forth row), three times 300 mg/kg APAP (fifth row) and three times 1.6 g/kg CCl_4 (sixth row) treated mice from 3 mice per group (Scale bars: 200 μm). **C.** Liver-weight-to-body-weight ratio did not show any difference between the groups. Plasma analysis of the liver enzymes **D.** ALT and **E.** AST revealed the highest levels after APAP and CCl_4 treatment. Data are presented as means ± standard deviation of at least three biological replicates. Calculation of differences between the groups was performed with one-way ANOVA. *P<0.05.

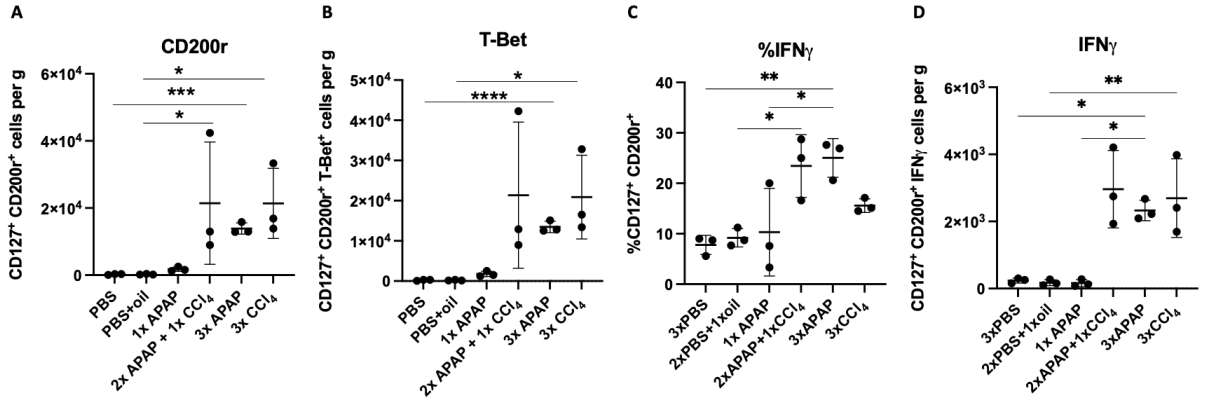

Figure 42. Three injections of APAP induce memory like ILC1s.
Freshly isolated immune cells of livers from the different groups of PBS control, two times PBS and one time olive oil control, one-time 300 mg/kg APAP, two times 300 mg/kg APAP and one-time 1.6 g/kg CCl_4, three times 300 mg/kg APAP and three times 1.6 g/kg CCl_4 treated mice were stained for different markers, measured on the flow cytometer Aurora and analyzed with FlowJo to qunatify the number of **A**. ILC1s which were identified as dead cell marker$^-$CD45$^+$Lin$^-$NK1.1$^+$EomesS$^-$CD49a$^+$RORγT$^-$CD127$^+$CD200r$^+$, **B.** T-Bet$^+$ ILC1s, **C.** the percentage of IFNγ producing cells and **D.** IFNγ$^+$ cells per gram liver. Data are presented as means ± standard deviation of three biological replicates per group. Calculation of differences between the groups was performed with one-way ANOVA. *P<0.05, **P<0.01; ***P<0.001; ****P<0.0001.

4 DISCUSSION

This thesis focused on two main projects: VPA-induced liver injury, and the memory potential of liver ILC1s after multiple applications of a hepatotoxic compound. The results of the first part clearly demonstrate that it is possible to stimulate the expression of activating NK cell ligands on PMH upon drug exposure and to further enhance their expression by TNFα *in vitro*, but the transfer to a mouse model was not successful. The second part of the thesis is focused on the discovery of IFNγ producing memory like ILC1s in the liver after multiple doses of CCl_4 and further characterization of these cells.

4.1 VPA induced liver injury

Between 1990 and 2010, 27% of withdrawals of drugs from the marketplace were due to hepatotoxicity (Craveiro et al., 2020). Although these drugs passed all steps of drug approval, such as routine animal toxicology and pharmacological tests, these tests failed to identify the risk of DILI causing symptoms of acute and chronic liver diseases (Babai et al., 2021; Katarey & Verma, 2016). Multiple risk factors were identified to favor DILI, such as age, gender, CYP polymorphisms and drug-drug interactions, but the underlying mechanism are still unclear and therefore the prediction of DILI remains challenging (Chalasani et al., 2008; Davern, 2012; Koch, 2010; Song et al., 2021). As one possible mechanism causing DILI, Grinberg et al., 2014 and Fasbender et al., 2020 found, that activating NK cell ligands were upregulated in primary human hepatocytes upon drug exposure. Furthermore, they showed a NK cell mediated killing of hepatocytes treated with isoniazid, promethazine, ketoconazole and valproic acid and their IFNγ release by NK cells. The aim of this thesis was to generate a DILI mouse model to investigate the impact of NK cells on hepatocytes, and to identify the mechanism causing DILI. Since not all activating receptors on human NK cell are also expressed on mouse NK cells and therefore the ligands are different (Krueger et al., 2011), the first step was to confirm if there is a higher expression of activating NK cell ligands on mouse hepatocytes upon drug exposure. Therefore, primary mouse hepatocytes as well as the immortalized AML12 cell line were treated with the different drugs for different exposure times.

The drug treatment of PMH for 24 hours showed elevated mRNA expression levels of especially MULT1, which in most cases was even more increased after TNFα stimulation. In contrast, the cell line AML12 did not upregulate NK cell ligands on the surfaces after stimulation with isoniazid, ketoconazole, promethazine and valproic acid and TNFα. There are several possible explanations why the AML12 cell line does not express Rae1 and MULT1. Actually, cell lines should maintain the features of primary cells. However, the company ATCC itself warned that the expression of proteins in AML12 cells decreases over time in culture. Furthermore, not only genetic manipulation but also the serial passages of the cell lines can cause an alteration of functions, phenotype and responsiveness to stimuli or also

contaminations could have an impact on the results (Hay et al., 1989; Kaur & Dufour, 2012). Since all mycoplasma tests were negative, it might be more likely that the AML12 cells are epigenetically changed, have changed transcription factors or lost the genetic information to express the NK cell ligands due to the passages or the genetic manipulation.

Since VPA caused a dose dependent increase of the NK cell ligands in PMH, the drug was chosen to test *in vivo*. The mice in the first VPA *in vivo* experiment, in which the mice were treated with a low and high VPA dose for 14 days, developed neither liver damage nor elevated mRNA levels of the different NKG2D ligands. Analysis of the plasma VPA concentration detected a maximal concentration of 1 mM 15 minutes after VPA application. In comparison to the *in vitro* data, Rae1 mRNA levels in PMH were increased after treatment with 5 mM VPA for 24 hours. As a consequence, male mice were also treated for a longer period while the applied VPA doses were slowly increased to avoid neurological damage. Nevertheless, before these mice could develop a liver damage, they died after receiving 950 mg/kg VPA. Considering the fact that gender can also be a risk factor for DILI, the same experiment was repeated with female C57Bl/6N mice. Female mice were not more susceptible to the increased VPA doses, the highest applied dose of VPA was 1.1 g/kg before they also died.

In the second *in vivo* experiment, mice were additionally treated with LPS to cause a TNFα release in the liver. The mice were not susceptible to VPA nor did they upregulate the NK cell ligands in the liver. Additionally, the *in vitro* data demonstrated that even with the TNFα stimulation, a high dose of VPA was needed to induce the NKG2D ligands. Usually, patients with bipolar disorders are treated with 750 mg to 2000 mg per day to achieve a therapeutic level of around 80 to 125 μg/mL in plasma (Bennett & Shad, 2021) corresponding to a maximal concentration of 0.87 mM which is similar to the maximal plasma concentration observed in VPA treated mice. Although the concentration is in a similar range, there is the challenge of mice to human translation, as well as the *in vitro* to *in vivo* translation.

The direct translation of the *in vitro* generated results to *in vivo* models was not possible. Although freshly isolated primary cells were used, the isolation and cultivation of hepatocytes leads to a loss or an addition of information for example the loss of environment, loss of the lobular architecture, the difference of periportal and pericentral hepatocytes which is diminished in culture, or down- and upregulation of several genes caused by isolation and culture protocols. Furthermore, impurities of other cells as well as the culture system itself, like monolayer or sandwich culture, can also change the hepatocyte response and could cause false results (Mattes, 2020; Smith et al., 2018). Additionally, the hepatocytes in culture are directly in touch with the different drugs while *in vivo*, the drug could have been already converted to an intermediate and so the applied drug is possibly never in touch with the hepatocytes. Another possible reason could be a different drug metabolism in human and mouse, resulting in different metabolites. Thus, a 2D-culture system can never recapitulate the

multicellular and three-dimensional organization of the tissue, nor the situation in the whole body. One possibility to overcome the limitations of the 2D-culture system are the organoids. Organoids are three-dimensional structures containing multiple cell types. They enable to rebuild the situation in the organ and have become more important for DILI predictions (Mattes, 2020; Steger-Hartmann & Raschke, 2020). Nevertheless, 3D-systems also lack important features, for example a complete immune system or all other organs which shows that animal model are still indispensable (McGill & Jaeschke, 2019).

Although animal models are still necessary for research and drug development, these models also have limitations in translating to humans as demonstrated by the *in vivo* VPA results. In response to chemical compounds, human and mice can react differently regarding the timing, immune related reactions as inflammation or immune cell recruitment and pathogenicity or the mouse and human metabolism forms different intermediates of these drugs. Furthermore, some diseases like hepatitis C only exist in humans and are not reported in rodents. Some researchers criticized that the main reason for DILI mouse model not being successful established, is linked to a suboptimal experimental design (Bolker, 2017; Denayer et al., 2014; Leenaars et al., 2019; Martić-Kehl et al., 2012). Nevertheless, it is reported in literature that drugs that cause DILI in human do not necessarily lead to an animal model with consistent liver damage, even when high doses were applied and with a good experimental design (Delire et al., 2015; Tasnim et al., 2021; Uetrecht, 2019). One prominent example is the alcohol liver disease (ALD). Despite their aversion to alcohol, rodents have a fast alcohol metabolism preventing high blood alcohol levels. Even chronic alcohol application does not result in severe liver damage indicating a differential susceptibility between humans and rodents (Iimuro et al., 1996). Another point is that the liver of rodents has a high immune tolerance which is essential since it is exposed to various substances like inflammatory molecules, although it is doubted that it plays a role for DILI patients (Uetrecht, 2019). Thus, in combination with alternative mechanism it could be one reason why it is so difficult to establish a DILI mouse model.

4.2 Liver immune cells in repeatedly induced liver damage

Since the liver is exposed to different compounds like harmless dietary products but also to toxic substances, it is a requirement that the liver is appropriately equipped with different immune cells. During the last decades, the role of liver immune cells in an acute or a chronic liver injury have been investigated. However, the repeatedly induced liver damage and the impact of immune cells have not been investigated closely. In order to study the role of the different immune cells, mice were repeatedly injected with CCl_4 with 30 days recovery period between the injections.

In the first step, we concentrated on NK cells, since the repeated challenge with chemical haptens causes memory like NK cells in the liver (Min-Oo et al., 2013; Pahl et al., 2018). However, the repeated CCl_4 exposure in mice did not cause a memory like phenotype of NK cells. The investigation of activating or exhaustion receptors like CXCR6, which is necessary for hapten induced memory like NK cell formation, did not reveal any differences nor could be observed a higher cytokine production (Fig. 20).

There are several explanations for the lack of memory like NK cells. One possible reason could be that the treatment intervals were too long. Although it is reported that MCMV induced memory NK cells have a stable memory phenotype for more than 28 days, the cytokine induced memory response persists for 3 weeks. In contrast, it was also reported that cytokine induced memory functionality can last for at least 12 weeks (Romee et al., 2012).

Another possible explanation could be that the timepoint of collection was too early and should be shifted to a later timepoint. Sun et al., 2009 described that memory like NK cells expand until day seven after MCMV infection and that at this day the highest numbers of memory like NK cells were observed. Also, the NK cells in the hapten studies were analyzed earliest 48 hours after the last sensitization (O'Leary et al., 2006).

A further reason for the lack of memory like NK cells after CCl_4 exposure could be that the hepatotoxic compound does not directly interact with the NK cells. All mechanisms of generating memory like NK cells include receptors on the NK cell surface which directly recognize the virus protein (Ly49H), the cytokines (IL-12R, IL-15R, IL-18R) or haptens possibly through Ly49C/I-sensitive peptides (X. Wang et al., 2019; Wight et al., 2018).

Even though the chosen CCl_4 mouse model did not induce a memory phenotype in NK cells or alterations in leukocytes and most lymphocytes, it resulted in a memory response of another subset of innate lymphoid cells which are similar to NK cells: group 1 innate lymphoid cells (Fig 21).

ILC1s are also described to develop a memory response after hapten sensitization (X. Wang et al., 2018). These hapten induced memory like ILC1s are recruited from skin-draining lymph nodes in a CXCR3-dependent manner and reside in the liver via CXCR6-CXCL16 interaction (X. Wang et al., 2018). Additionally, these memory cells also express CD127 and CD49a and the cytokine IL-7 is necessary for their longevity (X. Wang et al., 2018). Comparable to the hapten induced memory ILC1s, the identified memory like ILC1s after repeated exposure to hepatotoxic compounds APAP and CCl_4 were also expressed CD127 and CD49a, whereas CXCR6 was not included in our investigation. Nevertheless, one main finding of this current thesis is the identification of memory like $CD127^+CD200r^+$ ILC1s after repeated liver injury. Furthermore, we could show that the numbers of memory like ILC1s in the liver were transiently increased only on day one after repeated CCl_4 treatment.

In order to explain this short term effect, the cells were first stained with the proliferation marker Ki-67. However, the staining did not reveal a higher proliferation of the memory like ILC1s (Fig 26D). Ki-67 only stains the cells during the cell cycle and not the cells which already divided and are back in the resting phase G_0. As a confirmation of the Ki-67 results, a 5-bromo-2´-deoxyuridine (BrdU) cell proliferation assay could be performed. With the help of the BrdU assay, it would be possible to track already proliferated cells, since BrdU is a thymidine analogue and can be incorporated into a newly synthesized DNA during the S phase (Kee et al., 2002). Furthermore, the possibility of a wrongly chosen timepoint of 24 hours after CCl_4 injection could be excluded. Reports in the literature described, that the cell cycle time of lymphocytes lasts between six and eight hours (Lawrence & Braciale, 2004; H. Yoon et al., 2010). Interestingly, after a potent stimulus, the cell cycle time can be even shortened to two up to four hours (H. Yoon et al., 2007, 2010). However, as a proof that the Ki-67 staining works in general, the proliferation of other immune cell populations in the same sample was examined showing high numbers of proliferating NK cells and Lin^+ cells per gram liver (data not shown). This result confirms not only the functionality of the Ki-67 staining but also the finding, that the increased number of memory like ILC1s after 24 hours cannot be explained by proliferation.

A possible explanation for the decreased number of ILC1s at day three, could be apoptosis, but the dead cell staining revealed no higher numbers of dead ILC1s on day three (Fig.28E). Of course, we have to take into account that the cells could have died on day two and been phagocytosed until day three, since phagocytosis of dead cells is the initial step for tissue recovery (Scott et al., 2001; K. W. Yoon, 2017). In order to investigate the possible apoptosis and phagocytosis, the time-point of 48 hours should be closer investigated and possible upregulation of different apoptosis related genes should also be checked. Although one possible explanation for the transient increase of ILC1s after several stimuli with CCl_4 could have been proliferation within 24 hours followed by apoptosis of these cells until day three, this hypothesis was rejected based on the Ki-67 results.

Another explanation for the increased ILC1 numbers could have been that the $CD200r^+$ ILC1s have already been in the liver due to by the previous injections and only get activated. If this would have been the case, they would have the same number of $CD200r^+$ ILCs in the liver as the $3xCCl_4$ treated mice, because the $2xCCl_4$+1xoil mice had received their last CCl_4 injection 31 days before the collection (Fig. 25). Since these control mice only showed half of the number of ILC1s in the liver compared to the mice which received three injections of CCl_4, this hypothesis was rejected.

A third hypothesis to explain the transient ILC1 numbers in the liver could be the plasticity of NK cells to helper ILC1s. In general, there is a high number of circulating NK cells which could transdifferentiate to ILC1s and therefore could explain the increase of ILC1s within 24 hours. The transdifferentiation of NK cells to helper ILC1 is driven by IL-12 and TGFβ which

downregulates Eomes and upregulates T-Bet (Almeida & Belz, 2016; Vivier et al., 2018a). Possible sources of TGFβ could be the deposits in the extracellular matrix or platelets (Dewidar et al., 2019; Ghafoory et al., 2018). Until day three, the helper ILC1s could transdifferentiate back to NK cells, but until now, the mechanism of the transformation back to NK cells is not understood (Bal et al., 2020; Colonna, 2018; Meininger et al., 2020). In order to analyze the impact of NK cells plasticity on the increased ILC1 numbers and to possibly visualize this process and the ILC1s, C57Bl/6N and homozygous NCR1-GFP mice were treated with olive oil, one time CCl_4 or three times CCl_4 and additionally with the depletion antibody Anti-Asialo GM1. Nabekura et al., 2020 showed that the injection of Anti-Asialo GM1 results in a dramatically reduced number of NK cells, while the numbers of ILC1s were similar compared to the vehicle control. Although our findings also showed reduced NK cell numbers, we could observe a strong reduction of memory like ILC1s per gram liver (Fig. 36 and Fig. 38). Furthermore, they could show that Anti-Asialo GM1 did not affect the ALT level nor the amount of IFNγ in comparison to the vehicle control (Nabekura et al., 2020). In contrast to Nabekura´s results, we observed in both mouse strains less IFNγ after Anti-Asialo GM1 injection in comparison to mice without depletion antibody treatment (Fig. 36D, Fig. 38F, H). These reduced memory like ILC1 numbers further supported the hypothesis of the NK cell to helper ILC1 transdifferentiation. However, the experiment performed with the Hobit KO mice did not show highly increased numbers of ILC1s after the third CCl_4 injection, although the NK cells were not impaired in these mice. If the transdifferentiation of NK cells to ILC1s would be the reason for the increased ILC1 numbers in the liver after repeated CCl_4 injections, we would have expected a similar amount of ILC1s in the liver as the controls C57Bl/6J and Hobit WT mice had (Fig. 34). This low ILC1 cell number in the CCl_4 treated Hobit KO mice clearly showed that the increased numbers of memory like ILC1s after repeated liver injury was not caused by NK cell plasticity and the hypothesis was rejected.

Another hypothesis, explaining the transiently altered ILC1 cell numbers, could be the migration of ILC1s from other organs into the liver. Originally, a main feature of ILCs is their tissue-residency in lymphoid and non-lymphoid organs during homeostasis and infection (Gasteiger et al., 2015). However, our data showed, that in response to several doses of CCl_4, the numbers of ILC1s increase 24 hours after injection, and until day three, the ILC1 numbers are decreased to numbers comparable to the olive oil control, indicating a hit and run situation in the liver. Caused by the repeated insult of the liver, ILC1s could migrate into the liver, producing more IFNγ, and leave the liver until day three. Possible sources of the additional $CD127^+$ ILC1 could be for example the small intestine or the spleen in which the ILC1s can also express CD200r on their surface (Meininger et al., 2020; Nabekura & Shibuya, 2021). Recently, a researcher group identified a cellular differentiation state of ILC1s in which the $CD127^+CD200r^+$ ILC1s express c-Kit as well as IL-18Rα and had a slightly increased IFNγ

production. These so called early ILC1s were not only found in the liver, but also in salivary glands, kidneys, lymph nodes and in the small intestine. Furthermore, these cells are TCF-1^{hi}, which is a transcription factor in the early maturation states of ILC1s (Friedrich et al., 2021). We also observed an increase in the mean fluorescence intensity after three injections of APAP and CCl_4 showing that they have more TCF-1 in the inside of the cells (data not shown). However, due to the multiple CCl_4 treatments, the liver is not the only organ being damaged. Additionally, the microbiota and the immune system in the gut are altered, leading to an impaired intestinal barrier (Muñoz et al., 2019; J. Zhang et al., 2018). The altered immune system is characterized by the expansion and activation of gut lymphocytes (Muñoz et al., 2019). Until now, it has not been investigated, if also the ILC1s are expanded and activated in the intestine. Since these early $CD127^{+}CD200r^{+}$ ILC1s were also found in the small intestine and were also expressing c-Kit as well as IL-18Rα and had an altered IFNγ production, there could be the possibility that the CCl_4 activated intestine ILC1s migrate through the portal vein into the liver within 24 hours and leave the liver through the biliary tract until day three. This described circulation is known as gut-liver axis (Tripathi et al., 2018). This hypothesis should be further investigated.

The fifth hypothesis to explain the transient ILC1 numbers in the liver could be the plasticity of ILC3s to so called ex-ILC3/ILC1 like cells. $NKp46^{+}$ ILC3s expressing RORγT and T-Bet can translate to ILC1s and produce IFNγ in response to the pro-inflammatory cytokines IL-1β and IL-12 (Bal et al., 2020; Colonna, 2018; Vivier et al., 2018). Although these proinflammatory cytokines are present after CCl_4 exposure (Pan et al., 2018; ZHAO et al., 2015), there are only few ILC3s in the liver. In contrast, there are high numbers of ILC3s in the intestine (Meininger et al., 2020; Vivier et al., 2018). Furthermore, the plasticity from ILC3s to ILC1s is well described in the intestine and is regulated by an inflammatory signal (Almeida & Belz, 2016; Colonna, 2018; Domingues & Hepworth, 2020). As already mentioned before, it could be that ILC3s in the intestine are translated to ILC1s through signals from the inflamed epithelium which releases IL-1β, and dendritic cells releasing IL-12 (Bal et al., 2020). After transition to ILC1s, they subsequently migrate via the gut-liver axis into the liver (Colonna, 2018; Domingues & Hepworth, 2020; Tripathi et al., 2018). Additionally, the ILC3s in the intestine do also express CD90, IL-18Rα and c-Kit on their surfaces, which were also present on the ILC1s in the liver (Colonna, 2018; Meininger et al., 2020). Additionally to the hypothesis of the migrating ILC1s, also the migration of ex-ILC3s via the gut-liver axis into the liver should be further investigated in order to explain the transient effect of memory like ILC1s after repeated liver damage.

Since the transient nature of memory like ILC1s was now well described, the question of their function remained. In order to answer this question, in the first step, we wanted to investigate

whether lack of ILC1s has an impact on the liver damage. Although the Hobit KO mice were no full knockout mice, they showed significantly reduced numbers compared to the treated C57Bl/6J and Hobit WT mice and therefore still suitable to investigate the question. Nevertheless, these few remaining ILC1s in Hobit KO mice were increased in numbers after repeated CCl_4 treatment and produced significantly more IFNγ compared to oil treated Hobit KO mice (Fig. 34). Notwithstanding that it was surprising that the Hobit KO mice still had some ILC1s, it was not caused by an artefact. Then recently, it was published that the maturation of some subtypes of ILC1s can be dependent of Hobit but this transcription factor itself is not as crucial for the development of ILC1s as T-Bet and NFIL3 (Almeida & Belz, 2016; Friedrich et al., 2021; Yomogida et al., 2021). Because of the Hobit independent developmental pathway of ILC1s, the knockout of Hobit does not lead to the complete absence of ILC1s and therefore confirms our results (Ducimetière et al., 2021; Friedrich et al., 2021; Yomogida et al., 2021). The few observed ILC1s in Hobit KO mice are not ex-ILC3s which has been proven by a RORγT fate mapping mouse (Friedrich et al., 2021). Additionally, Friedrich et al., 2021a could also show that the early $CD127^+$c-Kit^+IL18R^+ ILC1s, which seem to have a similar phenotype to the identified memory like ILC1s, are not dependent on Hobit since they were present at normal numbers in the different organs of naive Hobit-deficient mice compared to naive wildtype mice (Friedrich et al., 2021). However, our results reveal a heterogeneity of the identified memory like ILC1s in C57Bl/6J mice after multiple CCl_4 injections. Although most of the cells seem to express Hobit, the transcription factor is not necessarily needed to form the memory potential and the increased numbers of ILC1s.

Nevertheless, with the help of these mice we were still able to create a first idea of a possible function of memory like ILC1s in repeated liver damage. Visual analysis of H&E and Sirius red stained paraffin embedded liver tissue sections suggests that the CCl_4 treated Hobit KO mice had a more damaged liver compared to the control mice (Fig. 33A). This could indicate a protective function of memory like ILC1s in the liver, although the ALT and AST plasma levels of the CCl_4 treated C57Bl/6J, Hobit WT and KO mice revealed no difference 24 hours after the last injection (Fig. 33C, D). Nabekura et al., 2020, also treated Hobit deficient mice with a higher single dose of CCl_4 (10 μL per gram body weight) observing significantly higher ALT levels compared to the wildtype mice which was most pronounced on day two. In contrast, we could not identify higher ALT levels in Hobit KO mice after multiple doses of CCl_4, which can be justified by the investigation day. Nabekura et al. investigated ILC1s on day two after a single dose of CCl_4 whereas our chosen investigation timepoint was 24 hours after three CCl_4 injections in Hobit KO mice. Additionally, it has to take into consideration that on day two, other immune cells are already recruited to the site of injury whereas on day one the damage is still new and the liver is in the beginning of the inflammation phase which could also explain the

different findings about the ALT levels. Furthermore, Nabekura et al identified the ILC1s as either NK1.1^{+}TCRβ^{-}B220^{-}DX5^{-}CD49a^{+}CD200r^{+} or NK1.1^{+}NKp46^{+}DX5^{-}CD49a^{+}CD200r^{+}. Since CD200r is also expressed on macrophages, neutrophiles and subsets of T- and B-cells, it has to be considered that their gating strategy may also include other immune cells and not only ILC1s. Nevertheless, they concluded a protective effect of IFNγ producing ILC1s during acute liver damage supporting our hypothesis regarding the function of memory like ILC1s (Nabekura et al., 2020).

In order to further examine the hypothesis of the protection effect of memory like ILC1s in repeatedly induced liver damage, the experiments with the depletion antibody Anti-Asialo GM1 could have been included in the analysis since they also showed decreased ILC1 numbers. Both mice strains, C57Bl/6N and homozygous NCR1-GFP mice, treated with Anti-Asialo GM1 did not show a significant increase of memory like ILC1 cells in the liver after the third dose of CCl_4. Nevertheless, these few ILC1 cells were still able to produce more IFNγ after the third CCl_4 injection (Fig.36, Fig. 38). Visual analysis of the stained paraffin embedded liver tissue sections showed maybe slightly bigger necrotic areas around the central vein in the Anti-Asialo GM1 treated mice compared to mice without depletion antibody treatment. The Sirius red staining in the depletion antibody and CCl_4 treated livers showed in general a higher signal whereas the scaring of the liver is not as pronounced as in the mice which were not treated with the depletion antibody (Fig. 35A, Fig 37A). However, especially the Anti-Asialo GM1 treated homozygous NCR1-GFP mice had significantly elevated ALT and AST levels (Fig. 37F, G) which were also slightly higher compared to the not treated with Anti-Asialo GM1 NCR1-GFP mice (Fig. 37C, D). This result would further promote the hypothesis of the protective effect of memory ILC1s in the liver. Additionally, the H&E and Sirius red stainings should be quantified to verify the hypothesis.

The treatment with Anti-Asialo GM1 revealed significant lower numbers of memory like ILC1s in the liver (Fig. 36, Fig. 38). It has to be considered that Anti-Asialo GM1 is able to not only deplete NK cells but also to deplete ILC1s as well. During the last decades, several reports were published showing that Asialo GM1 is not exclusively expressed on NK cells but also on subpopulations of NKT cells, T cells, eosinophils and macrophages. Consequently, the depletion with Anti-Asialo GM1 causes off-target effects (Kataoka et al., 2004; Nishikado et al., 2011; Slifka et al., 2000; Stitz et al., 1986; Wiltrout et al., 1985). Furthermore, researchers showed that the antibody does mainly deplete tissue resident NK1.1^{+}CD49a^{+} NK cells and not the circulating NK1.1^{+}CD49b^{+} NK cells (Victorino et al., 2015). Furthermore, in their classification of tissue resident NK1.1^{+}CD49a^{+} NK cells, the ILC1s were not excluded.

Therefore, the results show the reduction of ILC1s, which was probably caused by the depletion of Asialo-GM1.
Moreover, the experiments performed with the NCR1-GFP mice revealed, that after Anti-Asialo GM1 treatment just a few ILC1s were present in the liver and these few cells were still able to produce more IFNγ although the numbers were quite low (Fig. 38). Nevertheless, the ILC1 numbers are in general reduced in the NCR1-GFP mice independent of the Anti-Asialo GM1 treatment suggesting that the receptor NKp46 is important for ILC1s. Y. Wang et al., 2018 observed similar results and showed that ILC1 development also depends cell-intrinsically on NKp46. Furthermore, they also showed that the insertion of GFP causes a strong reduction of ILC1s in homozygous NCR1-GFP mice, while heterozygous NCR1-GFP mice still have reduced numbers compared to wildtype mice (Y. Wang et al., 2018).

However, the previous results demonstrated that repeated injection of the hepatotoxic compounds CCl_4 and APAP are able to generate ILC1s which produce more IFNγ than controls. On the other hand, the western-style diet mouse model did not cause a memory phenotype of liver ILC1s (Fig. 40). Although the twelve weeks western-style diet mice were additionally treated with an acute insult, it caused a reduced presence of $CD200r^{+}T\text{-}Bet^{+}$ ILC1s in the WD liver compared to standard diet fed mice. Furthermore, we could not identify a difference in the IFNγ production. There are some reasons why a memory effect of ILC1s was not observable.
One possible explanation could be that the chosen time of WD was wrong. Different publications used mice which were fed with WD for maximal 8 weeks. Within these studies, researchers found a contribution of ILC1s to obesity-associated insulin resistance and that IFNγ production of ILC1s leads to the polarization of M1 macrophages in adipose tissue during early WD consumption (O'Sullivan et al., 2016; Saetang & Sangkhathat, 2017). Furthermore, a positive correlation of ILC1s and fibrogenesis in adipose tissue was identified (H. Wang et al., 2019). Despite these findings, we could show that the memory effect of the ILC1s is long-lasting in other mouse models and therefore it is not likely that a shorter period of WD feeding would lead to the formation of memory like ILC1s.
On the other hand, an extended period of WD feeding could be necessary for inducing a memory effect of ILC1s. The longer period of WD feeding would cause a severe fibrosis with more proliferated and activated hepatic stellate cells and the accumulation of collagen (Myllys, 2021). Hence, extended periods of WD feeding could be further investigated to identify the impact of adiposity, fibrosis and memory like ILC1s in WD mice.
Anyway, the most likely explanation why the WD mice did not cause a memory phenotype of liver ILC1s could be the experimental setup itself. We could observe memory like ILC1s producing more IFNγ only after several insults of the liver including a regeneration phase

between the liver injuries. In contrast, the WD mouse model is a chronic mouse model without a regeneration phase. Although an additional acute insult with CCl_4 was included, memory like ILC1s could not be observed since there was no recovery phase between the different treatments. Therefore, memory like ILC1s are not a phenomenon of the chronic induced liver injury.

Thus, a repeated acute liver damage including a recovery phase between the injections is necessary to generate a memory potential of ILC1s. This hypothesis is further promoted by the fact that a single injection of a hepatotoxic compound is not enough to generate a memory potential (Fig. 22, Fig. 25, Fig. 42). Furthermore, we could also show that that it is necessary to inject at least three times CCl_4 to generate the phenotype of IFNγ producing memory like ILC1s in the liver since two injections of CCl_4 did not cause a memory effect of CD200r$^+$ ILC1s (Fig. 32). Additionally, the control mice treated the two times with CCl_4 and the third time with olive oil (2xCCl_4 +1xoil) support these findings that the recovery phase between the liver damaging injections as well as the third acute insult are obligated to generate the phenotype of memory like ILC1s (Fig. 25).

These results clearly showed that the regeneration phase is obligated between repeatedly induced acute liver injuries in order to create memory like ILC1s which produce more IFNγ.

4.3. Conclusion and further perspectives

In summary, the data of this current thesis showed that it is not possible to establish a VPA-induced liver injury mouse model, although different strategies were followed. Additionally, this thesis further presented the identification of memory like ILC1s after repeated treatment with the hepatotoxic compounds APAP and CCl_4. This phenotype of memory like ILC1s were only generated after repeatedly induced acute liver damage including a regeneration phase between the injections. Further characterization of these memory like ILC1s revealed a long-lasting memory effect and a transient increase in the liver. The two most likely hypotheses explaining the transiently altered ILC1 cell numbers, are the migration of ILC1s or ex-ILC3/ILC 1 like cells from the intestine into the liver through the gut-liver axis. Additionally, the results showed that memory like ILC1s might possess a liver protective role, since the stained paraffin embedded liver tissue sections showed a tendency for greater liver damage when less memory like ILC1s were present in the liver.

In order to closer investigate the migration hypotheses, the function and the localization of memory like ILC1s in the liver after repeatedly induced liver damage, the original idea was to specifically deplete NK cells with the depletion antibody Anti-Asialo GM1 in NCR1-GFP mice to enable the visualization of ILC1s. However, the presented data demonstrated that the depletion antibody not only depleted NK cells but also ILC1s. Therefore, the use of the depletion Anti-Asialo GM1 and the NCR1-GFP mice are not the right approaches to investigate

the three remaining. In order to verify the protective function and to investigate the migration hypotheses and the localization in of memory like ILC1s the liver, other mice strains which completely lack ILC1s or fate mapping ILC1 mice should be considered for further research. In addition, possible interactions with other immune cells require further investigation which could reveal further functions of memory like ILC1s.

5. REFERENCES

Abdel-Misih, S. R. Z., & Bloomston, M. (2010). Liver Anatomy. *Surgical Clinics of North America*, *90*(4), 643–653. https://doi.org/10.1016/j.suc.2010.04.017

Almeida, F. F., & Belz, G. T. (2016). Innate lymphoid cells: models of plasticity for immune homeostasis and rapid responsiveness in protection. *Mucosal Immunology*, *9*(5), 1103–1112. https://doi.org/10.1038/mi.2016.64

Amaral, S. S., Oliveira, A. G., Marques, P. E., Quintão, J. L. D., Pires, D. A., Resende, R. R., Sousa, B. R., Melgaço, J. G., Pinto, M. A., Russo, R. C., Gomes, A. k C., Andrade, L. M., Zanin, R. F., Pereira, R. V. S., Bonorino, C., Soriani, F. M., Lima, C. X., Cara, D. C., Teixeira, M. M., … Menezes, G. B. (2013). Altered responsiveness to extracellular ATP enhances acetaminophen hepatotoxicity. *Cell Communication and Signaling*, *11*(1), 10. https://doi.org/10.1186/1478-811X-11-10

An, Z., Flores-Borja, F., Irshad, S., Deng, J., & Ng, T. (2020). Pleiotropic Role and Bidirectional Immunomodulation of Innate Lymphoid Cells in Cancer. *Frontiers in Immunology*, *10*. https://doi.org/10.3389/fimmu.2019.03111

Andrade, R. J., Chalasani, N., Björnsson, E. S., Suzuki, A., Kullak-Ublick, G. A., Watkins, P. B., Devarbhavi, H., Merz, M., Lucena, M. I., Kaplowitz, N., & Aithal, G. P. (2019). Drug-induced liver injury. *Nature Reviews Disease Primers*, *5*(1), 58. https://doi.org/10.1038/s41572-019-0105-0

Arteta, B., Lasuen, N., Lopategi, A., Sveinbjörnsson, B., Smedsrød, B., & Vidal-Vanaclocha, F. (2010). Colon carcinoma cell interaction with liver sinusoidal endothelium inhibits organ-specific antitumor immunity through interleukin-1-induced mannose receptor in mice. *Hepatology*, *51*(6), 2172–2182. https://doi.org/10.1002/hep.23590

Aumüller, G. A. G. D. A. et al. (2010). *Anatomie* (Vol. 2). Georg Thieme Verlag.

Babai, S., Auclert, L., & Le-Louët, H. (2021). Safety data and withdrawal of hepatotoxic drugs. *Therapies*, *76*(6), 715–723. https://doi.org/10.1016/j.therap.2018.02.004

Bal, S. M., Golebski, K., & Spits, H. (2020a). Plasticity of innate lymphoid cell subsets. *Nature Reviews Immunology*, *20*(9), 552–565. https://doi.org/10.1038/s41577-020-0282-9

Bal, S. M., Golebski, K., & Spits, H. (2020b). Plasticity of innate lymphoid cell subsets. *Nature Reviews Immunology*, *20*(9), 552–565. https://doi.org/10.1038/s41577-020-0282-9

Bandyopadhyay, K., Marrero, I., & Kumar, V. (2016). NKT cell subsets as key participants in liver physiology and pathology. *Cellular & Molecular Immunology*, *13*(3), 337–346. https://doi.org/10.1038/cmi.2015.115

Barrow, A. D., Martin, C. J., & Colonna, M. (2019). The Natural Cytotoxicity Receptors in Health and Disease. *Frontiers in Immunology*, *10*. https://doi.org/10.3389/fimmu.2019.00909

Barthel, G. (1998). *Hepatotoxizität von Valproinsäure in isolierten Rattenhepatozyten: Einfluß von Prooxidantien und Hungern*.

Behr, F. M., Parga-Vidal, L., Kragten, N. A. M., van Dam, T. J. P., Wesselink, T. H., Sheridan, B. S., Arens, R., van Lier, R. A. W., Stark, R., & van Gisbergen, K. P. J. M. (2020). Tissue-resident memory CD8+ T cells shape local and systemic secondary T cell responses. *Nature Immunology*, *21*(9), 1070–1081. https://doi.org/10.1038/s41590-020-0723-4

Bennett, S., & Shad, M. U. (2021). Valproic acid autoinduction: a case-based review. *International Journal of Bipolar Disorders*, *9*(1), 27. https://doi.org/10.1186/s40345-021-00232-6

Ben-Shachar, R., Chen, Y., Luo, S., Hartman, C., Reed, M., & Nijhout, H. F. (2012). The biochemistry of acetaminophen hepatotoxicity and rescue: a mathematical model. *Theoretical Biology and Medical Modelling*, *9*(1), 55. https://doi.org/10.1186/1742-4682-9-55

Beraza, N., Malato, Y., Sander, L. E., Al-Masaoudi, M., Freimuth, J., Riethmacher, D., Gores, G. J., Roskams, T., Liedtke, C., & Trautwein, C. (2009). Hepatocyte-specific NEMO

deletion promotes NK/NKT cell– and TRAIL-dependent liver damage. *Journal of Experimental Medicine*, *206*(8), 1727–1737. https://doi.org/10.1084/jem.20082152
Berhani, O., Glasner, A., Kahlon, S., Duev-Cohen, A., Yamin, R., Horwitz, E., Enk, J., Moshel, O., Varvak, A., Porgador, A., Jonjic, S., & Mandelboim, O. (2019). Human anti-NKp46 antibody for studies of NKp46-dependent NK cell function and its applications for type 1 diabetes and cancer research. *European Journal of Immunology*, *49*(2), 228–241. https://doi.org/10.1002/eji.201847611
Böhm, F., Köhler, U. A., Speicher, T., & Werner, S. (2010). Regulation of liver regeneration by growth factors and cytokines. *EMBO Molecular Medicine*, *2*(8), 294–305. https://doi.org/10.1002/emmm.201000085
Bolker, J. A. (2017). Animal Models in Translational Research: Rosetta Stone or Stumbling Block? *BioEssays*, *39*(12), 1700089. https://doi.org/10.1002/bies.201700089
Brempelis, K. J., & Crispe, I. N. (2016). Infiltrating monocytes in liver injury and repair. *Clinical & Translational Immunology*, *5*(11), e113. https://doi.org/10.1038/cti.2016.62
Brillantes, M., & Beaulieu, A. M. (2020). Memory and Memory-Like NK Cell Responses to Microbial Pathogens. *Frontiers in Cellular and Infection Microbiology*, *10*. https://doi.org/10.3389/fcimb.2020.00102
Campana, L., & Iredale, J. (2017). Regression of Liver Fibrosis. *Seminars in Liver Disease*, *37*(01), 001–010. https://doi.org/10.1055/s-0036-1597816
Campos, G., Schmidt-Heck, W., Ghallab, A., Rochlitz, K., Pütter, L., Medinas, D. B., Hetz, C., Widera, A., Cadenas, C., Begher-Tibbe, B., Reif, R., Günther, G., Sachinidis, A., Hengstler, J. G., & Godoy, P. (2014). The transcription factor CHOP, a central component of the transcriptional regulatory network induced upon CCl4 intoxication in mouse liver, is not a critical mediator of hepatotoxicity. *Archives of Toxicology*, *88*(6), 1267–1280. https://doi.org/10.1007/s00204-014-1240-8
Caparrós, E., Juanola, O., Gómez-Hurtado, I., Puig-Kroger, A., Piñero, P., Zapater, P., Linares, R., Tarín, F., Martínez-López, S., Gracia-Sancho, J., González-Navajas, J. M., & Francés, R. (2020). Liver Sinusoidal Endothelial Cells Contribute to Hepatic Antigen-Presenting Cell Function and Th17 Expansion in Cirrhosis. *Cells*, *9*(5), 1227. https://doi.org/10.3390/cells9051227
Cardoso, C. C., Matiollo, C., Pereira, C. H. J., Fonseca, J. S., Alves, H. E. L., da Silva, O. M., de Souza Menegassi, V., dos Santos, C. R., de Moraes, A. C. R., de Lucca Schiavon, L., & Santos-Silva, M. C. (2021). Patterns of dendritic cell and monocyte subsets are associated with disease severity and mortality in liver cirrhosis patients. *Scientific Reports*, *11*(1), 5923. https://doi.org/10.1038/s41598-021-85148-y
Chalasani, N., Fontana, R. J., Bonkovsky, H. L., Watkins, P. B., Davern, T., Serrano, J., Yang, H., Rochon, J., & Drug Induced Liver Injury Network (DILIN). (2008). Causes, clinical features, and outcomes from a prospective study of drug-induced liver injury in the United States. *Gastroenterology*, *135*(6), 1924–1934, 1934.e1-4. https://doi.org/10.1053/j.gastro.2008.09.011
Chen, Y., & Tian, Z. (2021). Innate lymphocytes: pathogenesis and therapeutic targets of liver diseases and cancer. *Cellular & Molecular Immunology*, *18*(1), 57–72. https://doi.org/10.1038/s41423-020-00561-z
Cheng, M. L., Nakib, D., Perciani, C. T., & MacParland, S. A. (2021). The immune niche of the liver. *Clinical Science*, *135*(20), 2445–2466. https://doi.org/10.1042/CS20190654
Clemens, M. M., McGill, M. R., & Apte, U. (2019). *Mechanisms and biomarkers of liver regeneration after drug-induced liver injury* (pp. 241–262). https://doi.org/10.1016/bs.apha.2019.03.001
Colonna, M. (2018). Innate Lymphoid Cells: Diversity, Plasticity, and Unique Functions in Immunity. *Immunity*, *48*(6), 1104–1117. https://doi.org/10.1016/j.immuni.2018.05.013
Colucci, F., di Santo, J. P., & Leibson, P. J. (2002). Natural killer cell activation in mice and men: different triggers for similar weapons? *Nature Immunology*, *3*(9), 807–813. https://doi.org/10.1038/ni0902-807
Cortez, V. S., Ulland, T. K., Cervantes-Barragan, L., Bando, J. K., Robinette, M. L., Wang, Q., White, A. J., Gilfillan, S., Cella, M., & Colonna, M. (2017). SMAD4 impedes the

conversion of NK cells into ILC1-like cells by curtailing non-canonical TGF-β signaling. *Nature Immunology*, *18*(9), 995–1003. https://doi.org/10.1038/ni.3809
Craveiro, N. S., Lopes, B. S., Tomás, L., & Almeida, S. F. (2020). Drug Withdrawal Due to Safety: A Review of the Data Supporting Withdrawal Decision. *Current Drug Safety*, *15*(1), 4–12. https://doi.org/10.2174/1574886314666191004092520
Crespo Yanguas, S., Cogliati, B., Willebrords, J., Maes, M., Colle, I., van den Bossche, B., de Oliveira, C. P. M. S., Andraus, W., Alves, V. A., Leclercq, I., & Vinken, M. (2016). Experimental models of liver fibrosis. *Archives of Toxicology*, *90*(5), 1025–1048. https://doi.org/10.1007/s00204-015-1543-4
Cuff, A. O., Sillito, F., Dertschnig, S., Hall, A., Luong, T. V., Chakraverty, R., & Male, V. (2019). The Obese Liver Environment Mediates Conversion of NK Cells to a Less Cytotoxic ILC1-Like Phenotype. *Frontiers in Immunology*, *10*. https://doi.org/10.3389/fimmu.2019.02180
D Weber, L. W., Boll, M., & Stampfl, A. (2003). Hepatotoxicity and Mechanism of Action of Haloalkanes: Carbon Tetrachloride as a Toxicological Model. In *Critical Reviews in Toxicology* (Vol. 33, Issue 2).
Davern, T. J. (2012). Drug-induced liver disease. *Clinics in Liver Disease*, *16*(2), 231–245. https://doi.org/10.1016/j.cld.2012.03.002
Delire, B., Stärker P, & Leclercq I. (2015). Animal Models for Fibrotic Liver Diseases: What We Have, What We Need, and What Is under Development. *Journal of Clinical and Translational Hepatology*, *3*(1), 53–66. https://doi.org/10.14218/JCTH.2014.00035
Denayer, T., Stöhr, T., & Roy, M. van. (2014). Animal models in translational medicine: Validation and prediction. *European Journal of Molecular & Clinical Medicine*, *2*(1), 5. https://doi.org/10.1016/j.nhtm.2014.08.001
Dewidar, Meyer, Dooley, & Meindl-Beinker. (2019). TGF-β in Hepatic Stellate Cell Activation and Liver Fibrogenesis—Updated 2019. *Cells*, *8*(11), 1419. https://doi.org/10.3390/cells8111419
di Censo, C., Marotel, M., Mattiola, I., Müller, L., Scarno, G., Pietropaolo, G., Peruzzi, G., Laffranchi, M., Mazej, J., Hasim, M. S., Asif, S., Russo, E., Tomaipitinca, L., Stabile, H., Lee, S. H., Vian, L., Gadina, M., Gismondi, A., Shih, H. Y., … Sciumè, G. (2021). Granzyme A and CD160 expression delineates ILC1 with graded functions in the mouse liver. *European Journal of Immunology*, *51*(11), 2568–2575. https://doi.org/10.1002/eji.202149209
Diefenbach, A., Colonna, M., & Koyasu, S. (2014). Development, Differentiation, and Diversity of Innate Lymphoid Cells. *Immunity*, *41*(3), 354–365. https://doi.org/10.1016/j.immuni.2014.09.005
Diefenbach, A., Jamieson, A. M., Liu, S. D., Shastri, N., & Raulet, D. H. (2000). Ligands for the murine NKG2D receptor: expression by tumor cells and activation of NK cells and macrophages. *Nature Immunology*, *1*(2), 119–126. https://doi.org/10.1038/77793
Diefenbach, A., Jensen, E. R., Jamieson, A. M., & Raulet, D. H. (2001). Rae1 and H60 ligands of the NKG2D receptor stimulate tumour immunity. *Nature*, *413*(6852), 165–171. https://doi.org/10.1038/35093109
Ding, B.-S., Cao, Z., Lis, R., Nolan, D. J., Guo, P., Simons, M., Penfold, M. E., Shido, K., Rabbany, S. Y., & Rafii, S. (2014). Divergent angiocrine signals from vascular niche balance liver regeneration and fibrosis. *Nature*, *505*(7481), 97–102. https://doi.org/10.1038/nature12681
Domingues, R. G., & Hepworth, M. R. (2020). Immunoregulatory Sensory Circuits in Group 3 Innate Lymphoid Cell (ILC3) Function and Tissue Homeostasis. *Frontiers in Immunology*, *11*. https://doi.org/10.3389/fimmu.2020.00116
Ducimetière, L., Lucchiari, G., Litscher, G., Nater, M., Heeb, L., Nuñez, N. G., Wyss, L., Burri, D., Vermeer, M., Gschwend, J., Moor, A. E., Becher, B., van den Broek, M., & Tugues, S. (2021). Conventional NK cells and tissue-resident ILC1s join forces to control liver metastasis. *Proceedings of the National Academy of Sciences*, *118*(27), e2026271118. https://doi.org/10.1073/pnas.2026271118
Dufour, J. F., & Clavien, P. A. (2015). *Signaling Pathways in Liver Disease* (Vol. 3). WILEY Blackwell.

Farber, D. L., Yudanin, N. A., & Restifo, N. P. (2014). Human memory T cells: generation, compartmentalization and homeostasis. *Nature Reviews Immunology*, *14*(1), 24–35. https://doi.org/10.1038/nri3567

Fasbender, F., Obholzer, M., Metzler, S., Stöber, R., Hengstler, J. G., & Watzl, C. (2020). Enhanced activation of human NK cells by drug-exposed hepatocytes. *Archives of Toxicology*, *94*(2), 439–448. https://doi.org/10.1007/s00204-020-02668-8

Fernández-Álvarez, S., Gutiérrez-de Juan, V., Zubiete-Franco, I., Barbier-Torres, L., Lahoz, A., Parés, A., Luka, Z., Wagner, C., Lu, S. C., Mato, J. M., Martínez-Chantar, M. L., & Beraza, N. (2015). TRAIL-producing NK cells contribute to liver injury and related fibrogenesis in the context of GNMT deficiency. *Laboratory Investigation*, *95*(2), 223–236. https://doi.org/10.1038/labinvest.2014.151

Forbes, S. J., & Rosenthal, N. (2014). Preparing the ground for tissue regeneration: from mechanism to therapy. *Nature Medicine*, *20*(8), 857–869. https://doi.org/10.1038/nm.3653

Freitas-Lopes, M., Mafra, K., David, B., Carvalho-Gontijo, R., & Menezes, G. (2017). Differential Location and Distribution of Hepatic Immune Cells. *Cells*, *6*(4), 48. https://doi.org/10.3390/cells6040048

Friedman, S. L., Neuschwander-Tetri, B. A., Rinella, M., & Sanyal, A. J. (2018). Mechanisms of NAFLD development and therapeutic strategies. *Nature Medicine*, *24*(7), 908–922. https://doi.org/10.1038/s41591-018-0104-9

Friedrich, C., Taggenbrock, R. L. R. E., Doucet-Ladevèze, R., Golda, G., Moenius, R., Arampatzi, P., Kragten, N. A. M., Kreymborg, K., Gomez de Agüero, M., Kastenmüller, W., Saliba, A. E., Grün, D., van Gisbergen, K. P. J. M., & Gasteiger, G. (2021a). Effector differentiation downstream of lineage commitment in ILC1s is driven by Hobit across tissues. *Nature Immunology*, *22*(10), 1256–1267. https://doi.org/10.1038/s41590-021-01013-0

Friedrich, C., Taggenbrock, R. L. R. E., Doucet-Ladevèze, R., Golda, G., Moenius, R., Arampatzi, P., Kragten, N. A. M., Kreymborg, K., Gomez de Agüero, M., Kastenmüller, W., Saliba, A.-E., Grün, D., van Gisbergen, K. P. J. M., & Gasteiger, G. (2021b). Effector differentiation downstream of lineage commitment in ILC1s is driven by Hobit across tissues. *Nature Immunology*, *22*(10), 1256–1267. https://doi.org/10.1038/s41590-021-01013-0

Fu, Q., Yan, S., Wang, L., Duan, X., Wang, L., Wang, Y., Wu, T., Wang, X., An, J., Zhang, Y., Zhou, Q., & Zhan, L. (2017). Hepatic NK cell-mediated hypersensitivity to ConA-induced liver injury in mouse liver expressing hepatitis C virus polyprotein. *Oncotarget*, *8*(32), 52178–52192. https://doi.org/10.18632/oncotarget.11052

Fuhrmann G. (2006). *Toxikologie für Naturwissenschaftler- Einführung in die Theoretische und Spezielle Toxikologie*. B. G. Teubner Verlag.

Gang, M., Wong, P., Berrien-Elliott, M. M., & Fehniger, T. A. (2020). Memory-like natural killer cells for cancer immunotherapy. *Seminars in Hematology*, *57*(4), 185–193. https://doi.org/10.1053/j.seminhematol.2020.11.003

Gao, Y., Souza-Fonseca-Guimaraes, F., Bald, T., Ng, S. S., Young, A., Ngiow, S. F., Rautela, J., Straube, J., Waddell, N., Blake, S. J., Yan, J., Bartholin, L., Lee, J. S., Vivier, E., Takeda, K., Messaoudene, M., Zitvogel, L., Teng, M. W. L., Belz, G. T., … Smyth, M. J. (2017). Tumor immunoevasion by the conversion of effector NK cells into type 1 innate lymphoid cells. *Nature Immunology*, *18*(9), 1004–1015. https://doi.org/10.1038/ni.3800

Gasteiger, G., Fan, X., Dikiy, S., Lee, S. Y., & Rudensky, A. Y. (2015). Tissue residency of innate lymphoid cells in lymphoid and nonlymphoid organs. *Science*, *350*(6263), 981–985. https://doi.org/10.1126/science.aac9593

Gazit, R., Gruda, R., Elboim, M., Arnon, T. I., Katz, G., Achdout, H., Hanna, J., Qimron, U., Landau, G., Greenbaum, E., Zakay-Rones, Z., Porgador, A., & Mandelboim, O. (2006). Lethal influenza infection in the absence of the natural killer cell receptor gene Ncr1. *Nature Immunology*, *7*(5), 517–523. https://doi.org/10.1038/ni1322

Gebhardt, R. (1992). Metabolic zonation of the liver: Regulation and implications for liver function. *Pharmacology & Therapeutics*, *53*(3), 275–354. https://doi.org/10.1016/0163-7258(92)90055-5

Ghafoory, S., Varshney, R., Robison, T., Kouzbari, K., Woolington, S., Murphy, B., Xia, L., & Ahamed, J. (2018). Platelet TGF-β1 deficiency decreases liver fibrosis in a mouse model of liver injury. *Blood Advances*, *2*(5), 470–480. https://doi.org/10.1182/bloodadvances.2017010868

Greim H, & Dem E. (1996). *Toxikologie – Eine Einführung für Naturwissenschaftler und Mediziner*. VHC Verlagsgesellschaft mbH Weinheim.

Grinberg, M., Stöber, R. M., Edlund, K., Rempel, E., Godoy, P., Reif, R., Widera, A., Madjar, K., Schmidt-Heck, W., Marchan, R., Sachinidis, A., Spitkovsky, D., Hescheler, J., Carmo, H., Arbo, M. D., van de Water, B., Wink, S., Vinken, M., Rogiers, V., … Hengstler, J. G. (2014). Toxicogenomics directory of chemically exposed human hepatocytes. *Archives of Toxicology*, *88*(12), 2261–2287. https://doi.org/10.1007/s00204-014-1400-x

Guia, S., & Narni-Mancinelli, E. (2020). Helper-like Innate Lymphoid Cells in Humans and Mice. *Trends in Immunology*, *41*(5), 436–452. https://doi.org/10.1016/j.it.2020.03.002

Gur, C., Doron, S., Kfir-Erenfeld, S., Horwitz, E., Abu-tair, L., Safadi, R., & Mandelboim, O. (2012). NKp46-mediated killing of human and mouse hepatic stellate cells attenuates liver fibrosis. *Gut*, *61*(6), 885–893. https://doi.org/10.1136/gutjnl-2011-301400

Hammer, Q., Rückert, T., Borst, E. M., Dunst, J., Haubner, A., Durek, P., Heinrich, F., Gasparoni, G., Babic, M., Tomic, A., Pietra, G., Nienen, M., Blau, I. W., Hofmann, J., Na, I.-K., Prinz, I., Koenecke, C., Hemmati, P., Babel, N., … Romagnani, C. (2018). Peptide-specific recognition of human cytomegalovirus strains controls adaptive natural killer cells. *Nature Immunology*, *19*(5), 453–463. https://doi.org/10.1038/s41590-018-0082-6

Hay, R. J., Macy, M. L., & Chen, T. R. (1989). Mycoplasma infection of cultured cells. *Nature*, *339*(6224), 487–488. https://doi.org/10.1038/339487a0

Hochdörfer, T., Winkler, C., Pardali, K., & Mjösberg, J. (2019). Expression of c-Kit discriminates between two functionally distinct subsets of human type 2 innate lymphoid cells. *European Journal of Immunology*, *49*(6), 884–893. https://doi.org/10.1002/eji.201848006

Hoehme, S., Brulport, M., Bauer, A., Bedawy, E., Schormann, W., Hermes, M., Puppe, V., Gebhardt, R., Zellmer, S., Schwarz, M., Bockamp, E., Timmel, T., Hengstler, J. G., & Drasdo, D. (2010). Prediction and validation of cell alignment along microvessels as order principle to restore tissue architecture in liver regeneration. *Proceedings of the National Academy of Sciences*, *107*(23), 10371–10376. https://doi.org/10.1073/pnas.0909374107

Hood, S. P., Foulds, G. A., Imrie, H., Reeder, S., McArdle, S. E. B., Khan, M., & Pockley, A. G. (2019). Phenotype and function of activated natural killer cells from patients with prostate cancer: Patient-dependent responses to priming and IL-2 activation. *Frontiers in Immunology*, *10*(JAN). https://doi.org/10.3389/fimmu.2018.03169

Iimuro, Y., Ikejima, K., Rose, M. L., Bradford, B. U., & Thurman, R. G. (1996). Nimodipine, a dihydropyridine-type calcium channel blocker, prevents alcoholic hepatitis caused by chronic intragastric ethanol exposure in the rat. *Hepatology*, *24*(2), 391–397. https://doi.org/10.1002/hep.510240217

Iorga, A., Dara, L., & Kaplowitz, N. (2017). Drug-Induced Liver Injury: Cascade of Events Leading to Cell Death, Apoptosis or Necrosis. *International Journal of Molecular Sciences*, *18*(5), 1018. https://doi.org/10.3390/ijms18051018

Iredale, J. P. (2007). Models of liver fibrosis: exploring the dynamic nature of inflammation and repair in a solid organ. *Journal of Clinical Investigation*, *117*(3), 539–548. https://doi.org/10.1172/JCI30542

Ishibashi, H., Nakamura, M., Komori, A., Migita, K., & Shimoda, S. (2009). Liver architecture, cell function, and disease. *Seminars in Immunopathology*, *31*(3), 399–409. https://doi.org/10.1007/s00281-009-0155-6

Jacquelot, N., Seillet, C., Souza-Fonseca-Guimaraes, F., Sacher, A. G., Belz, G. T., & Ohashi, P. S. (2021). Natural Killer Cells and Type 1 Innate Lymphoid Cells in Hepatocellular Carcinoma: Current Knowledge and Future Perspectives. *International Journal of Molecular Sciences*, *22*(16), 9044. https://doi.org/10.3390/ijms22169044

Jaeschke, H., Williams, C. D., McGill, M. R., Xie, Y., & Ramachandran, A. (2013a). Models of drug-induced liver injury for evaluation of phytotherapeutics and other natural products. *Food and Chemical Toxicology*, *55*, 279–289. https://doi.org/10.1016/j.fct.2012.12.063

Jaeschke, H., Williams, C. D., McGill, M. R., Xie, Y., & Ramachandran, A. (2013b). Models of drug-induced liver injury for evaluation of phytotherapeutics and other natural products. *Food and Chemical Toxicology*, *55*, 279–289. https://doi.org/10.1016/j.fct.2012.12.063

Jenne, C. N., & Kubes, P. (2013). Immune surveillance by the liver. *Nature Immunology*, *14*(10), 996–1006. https://doi.org/10.1038/ni.2691

Jeong, W.-I., Park, O., Suh, Y.-G., Byun, J.-S., Park, S.-Y., Choi, E., Kim, J.-K., Ko, H., Wang, H., Miller, A. M., & Gao, B. (2011). Suppression of innate immunity (natural killer cell/interferon-γ) in the advanced stages of liver fibrosis in mice. *Hepatology*, *53*(4), 1342–1351. https://doi.org/10.1002/hep.24190

Jiang, Y. (2004). Changes in the Gene Expression Associated with Carbon Tetrachloride-Induced Liver Fibrosis Persist after Cessation of Dosing in Mice. *Toxicological Sciences*, *79*(2), 404–410. https://doi.org/10.1093/toxsci/kfh120

Kalra, A., Yetiskul, E., Wehrle, C. J., & Tuma, F. (2022). *Physiology, Liver*.

Karimzadeh Toosi, A. E. (2015). Liver Fibrosis: Causes and Methods of Assessment, A Review. *Romanian Journal Of Internal Medicine*, *53*(4), 304–314. https://doi.org/10.1515/rjim-2015-0039

Kataoka, S., Konishi, Y., Nishio, Y., Fujikawa-Adachi, K., & Tominaga, A. (2004). Antitumor Activity of Eosinophils Activated by IL-5 and Eotaxin against Hepatocellular Carcinoma. *DNA and Cell Biology*, *23*(9), 549–560. https://doi.org/10.1089/dna.2004.23.549

Katarey, D., & Verma, S. (2016). Drug-induced liver injury. *Clinical Medicine (London, England)*, *16*(Suppl 6), s104–s109. https://doi.org/10.7861/clinmedicine.16-6-s104

Kaur, G., & Dufour, J. M. (2012). Cell lines. *Spermatogenesis*, *2*(1), 1–5. https://doi.org/10.4161/spmg.19885

Kee, N., Sivalingam, S., Boonstra, R., & Wojtowicz, J. M. (2002). The utility of Ki-67 and BrdU as proliferative markers of adult neurogenesis. *Journal of Neuroscience Methods*, *115*(1), 97–105. https://doi.org/10.1016/S0165-0270(02)00007-9

Kietzmann, T. (2017). Metabolic zonation of the liver: The oxygen gradient revisited. *Redox Biology*, *11*, 622–630. https://doi.org/10.1016/j.redox.2017.01.012

Kisseleva, T., & Brenner, D. (2021). Molecular and cellular mechanisms of liver fibrosis and its regression. *Nature Reviews Gastroenterology & Hepatology*, *18*(3), 151–166. https://doi.org/10.1038/s41575-020-00372-7

Knolle, P. A., & Wohlleber, D. (2016). Immunological functions of liver sinusoidal endothelial cells. *Cellular & Molecular Immunology*, *13*(3), 347–353. https://doi.org/10.1038/cmi.2016.5

Koch, L. (2010). Therapy: Propylthiouracil use associated with severe hepatotoxicity in children. *Nature Reviews. Endocrinology*, *6*(8), 416. https://doi.org/10.1038/nrendo.2010.96

Konjević, G., Vuletić, A., Martinović, K. M., & Džodić, R. (2017). The Role of Activating and Inhibitory NK Cell Receptors in Antitumor Immune Response. In *Natural Killer Cells*. InTech. https://doi.org/10.5772/intechopen.69729

Krstic, R. v. (1997). *Human Microscopic Anatomy: An Atlas for Students of Medicine and Biology* (Vol. 3). Springer-Verlag.

Krueger, P. D., Lassen, M. G., Qiao, H., & Hahn, Y. S. (2011). Regulation of NK Cell Repertoire and Function in the Liver. *Critical Reviews™ in Immunology*, *31*(1), 43–52. https://doi.org/10.1615/CritRevImmunol.v31.i1.40

Lawrence, C. W., & Braciale, T. J. (2004). Activation, Differentiation, and Migration of Naive Virus-Specific CD8 $^{+}$ T Cells during Pulmonary Influenza Virus Infection. *The Journal of Immunology*, *173*(2), 1209–1218. https://doi.org/10.4049/jimmunol.173.2.1209

LeCluyse, E. L., Witek, R. P., Andersen, M. E., & Powers, M. J. (2012). Organotypic liver culture models: Meeting current challenges in toxicity testing. *Critical Reviews in Toxicology*, *42*(6), 501–548. https://doi.org/10.3109/10408444.2012.682115

Leenaars, C. H. C., Kouwenaar, C., Stafleu, F. R., Bleich, A., Ritskes-Hoitinga, M., de Vries, R. B. M., & Meijboom, F. L. B. (2019). Animal to human translation: a systematic scoping review of reported concordance rates. *Journal of Translational Medicine*, *17*(1), 223. https://doi.org/10.1186/s12967-019-1976-2

Li, N., & Hua, J. (2017). Immune cells in liver regeneration. *Oncotarget*, *8*(2), 3628–3639. https://doi.org/10.18632/oncotarget.12275

Liaskou, E., Wilson, D. v., & Oo, Y. H. (2012). Innate Immune Cells in Liver Inflammation. *Mediators of Inflammation*, *2012*, 1–21. https://doi.org/10.1155/2012/949157

Liedtke, C., Luedde, T., Sauerbruch, T., Scholten, D., Streetz, K., Tacke, F., Tolba, R., Trautwein, C., Trebicka, J., & Weiskirchen, R. (2013). Experimental liver fibrosis research: update on animal models, legal issues and translational aspects. *Fibrogenesis & Tissue Repair*, *6*(1), 19. https://doi.org/10.1186/1755-1536-6-19

Lin, S.-Z., & Fan, J.-G. (2022). Peripheral immune cells in NAFLD patients: A spyhole to disease progression. *EBioMedicine*, *75*, 103768. https://doi.org/10.1016/j.ebiom.2021.103768

Liu, M., & Zhang, C. (2017). The Role of Innate Lymphoid Cells in Immune-Mediated Liver Diseases. *Frontiers in Immunology*, *8*. https://doi.org/10.3389/fimmu.2017.00695

Long, E. O., Sik Kim, H., Liu, D., Peterson, M. E., & Rajagopalan, S. (2013). Controlling Natural Killer Cell Responses: Integration of Signals for Activation and Inhibition. *Annual Review of Immunology*, *31*(1), 227–258. https://doi.org/10.1146/annurev-immunol-020711-075005

Luci, C., Vieira, E., Perchet, T., Gual, P., & Golub, R. (2019). Natural Killer Cells and Type 1 Innate Lymphoid Cells Are New Actors in Non-alcoholic Fatty Liver Disease. *Frontiers in Immunology*, *10*. https://doi.org/10.3389/fimmu.2019.01192

Lüllmann-Rauch, R. (2009). *Taschenlehrbuch Histologie* (Vol. 3). Georg Thieme Verlag.

Mackay, L. K., Minnich, M., Kragten, N. A. M., Liao, Y., Nota, B., Seillet, C., Zaid, A., Man, K., Preston, S., Freestone, D., Braun, A., Wynne-Jones, E., Behr, F. M., Stark, R., Pellicci, D. G., Godfrey, D. I., Belz, G. T., Pellegrini, M., Gebhardt, T., … van Gisbergen, K. P. J. M. (2016). Hobit and Blimp1 instruct a universal transcriptional program of tissue residency in lymphocytes. *Science*, *352*(6284), 459–463. https://doi.org/10.1126/science.aad2035

Markose, D., Kirkland, P., Ramachandran, P., & Henderson, N. C. (2018). Immune cell regulation of liver regeneration and repair. *Journal of Immunology and Regenerative Medicine*, *2*, 1–10. https://doi.org/10.1016/j.regen.2018.03.003

Martić-Kehl, M. I., Schibli, R., & Schubiger, P. A. (2012). Can animal data predict human outcome? Problems and pitfalls of translational animal research. *European Journal of Nuclear Medicine and Molecular Imaging*, *39*(9), 1492–1496. https://doi.org/10.1007/s00259-012-2175-z

Martinez-Gonzalez, I., Mathä, L., Steer, C. A., Ghaedi, M., Poon, G. F. T., & Takei, F. (2016). Allergen-Experienced Group 2 Innate Lymphoid Cells Acquire Memory-like Properties and Enhance Allergic Lung Inflammation. *Immunity*, *45*(1), 198–208. https://doi.org/10.1016/j.immuni.2016.06.017

Mattes, W. B. (2020). In vitro to in vivo translation. *Current Opinion in Toxicology*, *23–24*, 114–118. https://doi.org/10.1016/j.cotox.2020.09.001

McGill, M. R., & Jaeschke, H. (2013). Metabolism and Disposition of Acetaminophen: Recent Advances in Relation to Hepatotoxicity and Diagnosis. *Pharmaceutical Research*, *30*(9), 2174–2187. https://doi.org/10.1007/s11095-013-1007-6

McGill, M. R., & Jaeschke, H. (2019). Animal models of drug-induced liver injury. *Biochimica et Biophysica Acta (BBA) - Molecular Basis of Disease*, *1865*(5), 1031–1039. https://doi.org/10.1016/j.bbadis.2018.08.037

Mehendale, H. M. (2010). Halogenated Hydrocarbons. In *Comprehensive Toxicology* (pp. 459–474). Elsevier. https://doi.org/10.1016/B978-0-08-046884-6.00824-1

Meininger, I., Carrasco, A., Rao, A., Soini, T., Kokkinou, E., & Mjösberg, J. (2020). Tissue-Specific Features of Innate Lymphoid Cells. *Trends in Immunology*, *41*(10), 902–917. https://doi.org/10.1016/j.it.2020.08.009

Metushi, I., Uetrecht, J., & Phillips, E. (2016). Mechanism of isoniazid-induced hepatotoxicity: then and now. *British Journal of Clinical Pharmacology*, *81*(6), 1030–1036. https://doi.org/10.1111/bcp.12885

Mikulak, J., Bruni, E., Oriolo, F., di Vito, C., & Mavilio, D. (2019). Hepatic Natural Killer Cells: Organ-Specific Sentinels of Liver Immune Homeostasis and Physiopathology. *Frontiers in Immunology*, *10*. https://doi.org/10.3389/fimmu.2019.00946

Min-Oo, G., Kamimura, Y., Hendricks, D. W., Nabekura, T., & Lanier, L. L. (2013). Natural killer cells: walking three paths down memory lane. *Trends in Immunology*, *34*(6), 251–258. https://doi.org/10.1016/j.it.2013.02.005

Muñoz, L., Borrero, M., Úbeda, M., Conde, E., del Campo, R., Rodríguez-Serrano, M., Lario, M., Sánchez-Díaz, A., Pastor, O., Díaz, D., García-Bermejo, L., Monserrat, J., Álvarez-Mon, M., & Albillos, A. (2019). Intestinal Immune Dysregulation Driven by Dysbiosis Promotes Barrier Disruption and Bacterial Translocation in Rats With Cirrhosis. *Hepatology*, *70*(3), 925–938. https://doi.org/10.1002/hep.30349

Myllys, M. K. (2021). *Identification of a novel mechanism driving NAFLD progression and therapeutic strategies*. http://hdl.handle.net/2003/40573 http://dx.doi.org/10.17877/DE290R-22442

Nabekura, T., Riggan, L., Hildreth, A. D., O'Sullivan, T. E., & Shibuya, A. (2020). Type 1 Innate Lymphoid Cells Protect Mice from Acute Liver Injury via Interferon-γ Secretion for Upregulating Bcl-xL Expression in Hepatocytes. *Immunity*, *52*(1), 96-108.e9. https://doi.org/10.1016/j.immuni.2019.11.004

Nabekura, T., & Shibuya, A. (2021). Type 1 innate lymphoid cells: Soldiers at the front line of immunity. *Biomedical Journal*, *44*(2), 115–122. https://doi.org/10.1016/j.bj.2020.10.001

Narni-Mancinelli, E., Gauthier, L., Baratin, M., Guia, S., Fenis, A., Deghmane, A.-E., Rossi, B., Fourquet, P., Escalière, B., Kerdiles, Y. M., Ugolini, S., Taha, M.-K., & Vivier, E. (2017). Complement factor P is a ligand for the natural killer cell–activating receptor NKp46. *Science Immunology*, *2*(10). https://doi.org/10.1126/sciimmunol.aam9628

Nishikado, H., Mukai, K., Kawano, Y., Minegishi, Y., & Karasuyama, H. (2011a). NK Cell-Depleting Anti-Asialo GM1 Antibody Exhibits a Lethal Off-Target Effect on Basophils In Vivo. *The Journal of Immunology*, *186*(10), 5766–5771. https://doi.org/10.4049/jimmunol.1100370

Nishikado, H., Mukai, K., Kawano, Y., Minegishi, Y., & Karasuyama, H. (2011b). NK Cell-Depleting Anti-Asialo GM1 Antibody Exhibits a Lethal Off-Target Effect on Basophils In Vivo. *The Journal of Immunology*, *186*(10), 5766–5771. https://doi.org/10.4049/jimmunol.1100370

O'Leary, J. G., Goodarzi, M., Drayton, D. L., & von Andrian, U. H. (2006). T cell– and B cell–independent adaptive immunity mediated by natural killer cells. *Nature Immunology*, *7*(5), 507–516. https://doi.org/10.1038/ni1332

O'Sullivan, T. E., Rapp, M., Fan, X., Weizman, O.-E., Bhardwaj, P., Adams, N. M., Walzer, T., Dannenberg, A. J., & Sun, J. C. (2016). Adipose-Resident Group 1 Innate Lymphoid Cells Promote Obesity-Associated Insulin Resistance. *Immunity*, *45*(2), 428–441. https://doi.org/10.1016/j.immuni.2016.06.016

O'Sullivan, T. E., Sun, J. C., & Lanier, L. L. (2015). Natural Killer Cell Memory. *Immunity*, *43*(4), 634–645. https://doi.org/10.1016/j.immuni.2015.09.013

Pahl, J. H. W., Cerwenka, A., & Ni, J. (2018). Memory-Like NK Cells: Remembering a Previous Activation by Cytokines and NK Cell Receptors. *Frontiers in Immunology*, *9*. https://doi.org/10.3389/fimmu.2018.02796

Pan, Y., Long, X., Yi, R., & Zhao, X. (2018). Polyphenols in Liubao Tea Can Prevent CCl4-Induced Hepatic Damage in Mice through Its Antioxidant Capacities. *Nutrients*, *10*(9), 1280. https://doi.org/10.3390/nu10091280

Patel, A. M., Liu, Y. S., Davies, S. P., Brown, R. M., Kelly, D. A., Scheel-Toellner, D., Reynolds, G. M., & Stamataki, Z. (2021). The Role of B Cells in Adult and Paediatric Liver Injury. *Frontiers in Immunology*, *12*. https://doi.org/10.3389/fimmu.2021.729143

Paul, S., & Lal, G. (2017). The Molecular Mechanism of Natural Killer Cells Function and Its Importance in Cancer Immunotherapy. *Frontiers in Immunology*, *8*. https://doi.org/10.3389/fimmu.2017.01124

Paust, S., Senman, B., & von Andrian, U. H. (2010). Adaptive immune responses mediated by natural killer cells. *Immunological Reviews*, *235*(1), 286–296. https://doi.org/10.1111/j.0105-2896.2010.00906.x

Pellicoro, A., Ramachandran, P., Iredale, J. P., & Fallowfield, J. A. (2014). Liver fibrosis and repair: immune regulation of wound healing in a solid organ. *Nature Reviews Immunology*, *14*(3), 181–194. https://doi.org/10.1038/nri3623

Peng, H., & Sun, R. (2017). Liver-resident NK cells and their potential functions. *Cellular & Molecular Immunology*, *14*(11), 890–894. https://doi.org/10.1038/cmi.2017.72

Peng, H., & Tian, Z. (2016). Tissue-resident natural killer cells in the livers. *Science China Life Sciences*, *59*(12), 1218–1223. https://doi.org/10.1007/s11427-016-0334-2

Peng, H., & Tian, Z. (2017). Natural Killer Cell Memory: Progress and Implications. *Frontiers in Immunology*, *8*. https://doi.org/10.3389/fimmu.2017.01143

Peng, H., Wisse, E., & Tian, Z. (2016). Liver natural killer cells: subsets and roles in liver immunity. *Cellular & Molecular Immunology*, *13*(3), 328–336. https://doi.org/10.1038/cmi.2015.96

Petrasek, J., Csak, T., & Szabo, G. (2013). *Toll-Like Receptors in Liver Disease* (pp. 155–201). https://doi.org/10.1016/B978-0-12-405211-6.00006-1

Phiel, C. J., Zhang, F., Huang, E. Y., Guenther, M. G., Lazar, M. A., & Klein, P. S. (2001). Histone Deacetylase Is a Direct Target of Valproic Acid, a Potent Anticonvulsant, Mood Stabilizer, and Teratogen. *Journal of Biological Chemistry*, *276*(39), 36734–36741. https://doi.org/10.1074/jbc.M101287200

Puengel, T., & Tacke, F. (2018). Repair macrophages in acute liver failure. *Gut*, *67*(2), 202–203. https://doi.org/10.1136/gutjnl-2017-314245

Radaeva, S., Sun, R., Jaruga, B., Nguyen, V. T., Tian, Z., & Gao, B. (2006). Natural Killer Cells Ameliorate Liver Fibrosis by Killing Activated Stellate Cells in NKG2D-Dependent and Tumor Necrosis Factor–Related Apoptosis-Inducing Ligand–Dependent Manners. *Gastroenterology*, *130*(2), 435–452. https://doi.org/10.1053/j.gastro.2005.10.055

Ramachandran, A., & Jaeschke, H. (2018). Acetaminophen Toxicity: Novel Insights Into Mechanisms and Future Perspectives. *Gene Expression*, *18*(1), 19–30. https://doi.org/10.3727/105221617X15084371374138

Ramachandran, A., & Jaeschke, H. (2020). A mitochondrial journey through acetaminophen hepatotoxicity. *Food and Chemical Toxicology*, *140*, 111282. https://doi.org/10.1016/j.fct.2020.111282

Robinson, M. W., Harmon, C., & O'Farrelly, C. (2016). Liver immunology and its role in inflammation and homeostasis. *Cellular & Molecular Immunology*, *13*(3), 267–276. https://doi.org/10.1038/cmi.2016.3

Romee, R., Schneider, S. E., Leong, J. W., Chase, J. M., Keppel, C. R., Sullivan, R. P., Cooper, M. A., & Fehniger, T. A. (2012). Cytokine activation induces human memory-like NK cells. *Blood*, *120*(24), 4751–4760. https://doi.org/10.1182/blood-2012-04-419283

Saetang, J., & Sangkhathat, S. (2017). Role of innate lymphoid cells in obesity and metabolic disease (Review). *Molecular Medicine Reports*. https://doi.org/10.3892/mmr.2017.8038

Sauzay, C., Voutetakis, K., Chatziioannou, A. A., Chevet, E., & Avril, T. (2019). CD90/Thy-1, a cancer-associated cell surface signaling molecule. In *Frontiers in Cell and Developmental Biology* (Vol. 7, Issue APR). Frontiers Media S.A. https://doi.org/10.3389/fcell.2019.00066

Schlüter, S. (2018). *Studying of the function of WISP1 in the liver*.

Scholten, D., Trebicka, J., Liedtke, C., & Weiskirchen, R. (2015). The carbon tetrachloride model in mice. *Laboratory Animals*, *49*, 4–11. https://doi.org/10.1177/0023677215571192

Scott, R. S., McMahon, E. J., Pop, S. M., Reap, E. A., Caricchio, R., Cohen, P. L., Earp, H. S., & Matsushima, G. K. (2001). Phagocytosis and clearance of apoptotic cells is mediated by MER. *Nature*, *411*(6834), 207–211. https://doi.org/10.1038/35075603

Seillet, C., Brossay, L., & Vivier, E. (2021a). Natural killers or ILC1s? That is the question. *Current Opinion in Immunology*, *68*, 48–53. https://doi.org/10.1016/j.coi.2020.08.009
Seillet, C., Brossay, L., & Vivier, E. (2021b). Natural killers or ILC1s? That is the question. In *Current Opinion in Immunology* (Vol. 68, pp. 48–53). Elsevier Ltd. https://doi.org/10.1016/j.coi.2020.08.009
Shen, K., Chang, W., Gao, X., Wang, H., Niu, W., Song, L., & Qin, X. (2011). Depletion of activated hepatic stellate cell correlates with severe liver damage and abnormal liver regeneration in acetaminophen-induced liver injury. *Acta Biochimica et Biophysica Sinica*, *43*(4), 307–315. https://doi.org/10.1093/abbs/gmr005
Shen, Y., Li, J., Wang, S.-Q., & Jiang, W. (2018). Ambiguous roles of innate lymphoid cells in chronic development of liver diseases. *World Journal of Gastroenterology*, *24*(18), 1962–1977. https://doi.org/10.3748/wjg.v24.i18.1962
Sheppard, S., Ferry, A., Guedes, J., & Guerra, N. (2018). The Paradoxical Role of NKG2D in Cancer Immunity. *Frontiers in Immunology*, *9*. https://doi.org/10.3389/fimmu.2018.01808
Sheppard, S., & Sun, J. C. (2021). Virus-specific NK cell memory. *Journal of Experimental Medicine*, *218*(4). https://doi.org/10.1084/jem.20201731
Skarnes, W., Rosen, B., West, A., & et al. (2011). A conditional knockout resource for the genome-wide study of mouse gene function. *Nature*, *474*, 337–342.
Slifka, M. K., Pagarigan, R. R., & Whitton, J. L. (2000). NK Markers Are Expressed on a High Percentage of Virus-Specific CD8 $^{+}$ and CD4 $^{+}$ T Cells. *The Journal of Immunology*, *164*(4), 2009–2015. https://doi.org/10.4049/jimmunol.164.4.2009
Smith, A. K., Xu, Y., Ropella, G. E. P., & Hunt, C. A. (2018). A Model Mechanism-Based Explanation of an In Vitro-In Vivo Disconnect for Improving Extrapolation and Translation. *Journal of Pharmacology and Experimental Therapeutics*, *365*(1), 127–138. https://doi.org/10.1124/jpet.117.245019
Song, Y., Li, C., Liu, G., Liu, R., Chen, Y., Li, W., Cao, Z., Zhao, B., Lu, C., & Liu, Y. (2021). Drug-Metabolizing Cytochrome P450 Enzymes Have Multifarious Influences on Treatment Outcomes. *Clinical Pharmacokinetics*, *60*(5), 585–601. https://doi.org/10.1007/s40262-021-01001-5
Spits, H., Artis, D., Colonna, M., Diefenbach, A., di Santo, J. P., Eberl, G., Koyasu, S., Locksley, R. M., McKenzie, A. N. J., Mebius, R. E., Powrie, F., & Vivier, E. (2013). Innate lymphoid cells — a proposal for uniform nomenclature. *Nature Reviews Immunology*, *13*(2), 145–149. https://doi.org/10.1038/nri3365
Stamataki, Z., & Swadling, L. (2020). The liver as an immunological barrier redefined by single-cell analysis. *Immunology*, *160*(2), 157–170. https://doi.org/10.1111/imm.13193
Steger-Hartmann, T., & Raschke, M. (2020). Translating in vitro to in vivo and animal to human. *Current Opinion in Toxicology*, *23–24*, 6–10. https://doi.org/10.1016/j.cotox.2020.02.003
Stitz, L., Baenziger, J., Pircher, H., Hengartner, H., & Zinkernagel, R. M. (1986). Effect of rabbit anti-asialo GM1 treatment in vivo or with anti-asialo GM1 plus complement in vitro on cytotoxic T cell activities. *Journal of Immunology (Baltimore, Md. : 1950)*, *136*(12), 4674–4680.
Sun, J. C., Beilke, J. N., & Lanier, L. L. (2009). Adaptive immune features of natural killer cells. *Nature*, *457*(7229), 557–561. https://doi.org/10.1038/nature07665
Takeda, K., Cretney, E., Hayakawa, Y., Ota, T., Akiba, H., Ogasawara, K., Yagita, H., Kinoshita, K., Okumura, K., & Smyth, M. J. (2005). TRAIL identifies immature natural killer cells in newborn mice and adult mouse liver. *Blood*, *105*(5), 2082–2089. https://doi.org/10.1182/blood-2004-08-3262
Tarannum, M., & Romee, R. (2021). Cytokine-induced memory-like natural killer cells for cancer immunotherapy. *Stem Cell Research & Therapy*, *12*(1), 592. https://doi.org/10.1186/s13287-021-02655-5
Tasnim, F., Huang, X., Lee, C. Z. W., Ginhoux, F., & Yu, H. (2021). Recent Advances in Models of Immune-Mediated Drug-Induced Liver Injury. *Frontiers in Toxicology*, *3*. https://doi.org/10.3389/ftox.2021.605392

Tateda, K., Matsumoto, T., Miyazaki, S., & Yamaguchi, K. (1996). Lipopolysaccharide-Induced Lethality and Cytokine Production in Aged Mice. In *INFECTION AND IMMUNITY* (Vol. 64, Issue 3). https://journals.asm.org/journal/iai

Taub, R. (2004). Liver regeneration: from myth to mechanism. *Nature Reviews Molecular Cell Biology*, *5*(10), 836–847. https://doi.org/10.1038/nrm1489

Tian, Z., Chen, Y., & Gao, B. (2013). Natural killer cells in liver disease. *Hepatology*, *57*(4), 1654–1662. https://doi.org/10.1002/hep.26115

Tortora, G., & Derrickson, B. (2014). *Principles of Anatomy and Physiology* (14th Revised edition). John Wiley & Sons Inc.

Tosello-Trampont, A., Surette, F. A., Ewald, S. E., & Hahn, Y. S. (2017). Immunoregulatory Role of NK Cells in Tissue Inflammation and Regeneration. *Frontiers in Immunology*, *8*. https://doi.org/10.3389/fimmu.2017.00301

Triantafyllou, E., Woollard, K. J., McPhail, M. J. W., Antoniades, C. G., & Possamai, L. A. (2018). The Role of Monocytes and Macrophages in Acute and Acute-on-Chronic Liver Failure. *Frontiers in Immunology*, *9*. https://doi.org/10.3389/fimmu.2018.02948

Tribble, D. L., Aw, T. Y., & Jones, D. P. (1987). The pathophysiological significance of lipid peroxidation in oxidative cell injury. *Hepatology*, *7*(2), 377–386. https://doi.org/10.1002/hep.1840070227

Tripathi, A., Debelius, J., Brenner, D. A., Karin, M., Loomba, R., Schnabl, B., & Knight, R. (2018). The gut–liver axis and the intersection with the microbiome. *Nature Reviews Gastroenterology & Hepatology*, *15*(7), 397–411. https://doi.org/10.1038/s41575-018-0011-z

Trittel, S., Chambers, B. J., Heise, U., Guzmán, C. A., & Riese, P. (2019). Key features and homing properties of NK cells in the liver are shaped by activated iNKT cells. *Scientific Reports*, *9*(1), 16362. https://doi.org/10.1038/s41598-019-52666-9

Uetrecht, J. (2019). Mechanistic Studies of Idiosyncratic DILI: Clinical Implications. *Frontiers in Pharmacology*, *10*. https://doi.org/10.3389/fphar.2019.00837

Ulfig, N. (2011). *Kurzlehrbuch Histologie* (Vol. 3). Georg Thieme Verlag.

Vancells Lujan, P., Viñas Esmel, E., & Sacanella Meseguer, E. (2021). Overview of Non-Alcoholic Fatty Liver Disease (NAFLD) and the Role of Sugary Food Consumption and Other Dietary Components in Its Development. *Nutrients*, *13*(5), 1442. https://doi.org/10.3390/nu13051442

Vernon, H., Wehrle, C. J., & Kasi, A. (2022). *Anatomy, Abdomen and Pelvis, Liver*.

Victor, A. R., Nalin, A. P., Dong, W., McClory, S., Wei, M., Mao, C., Kladney, R. D., Youssef, Y., Chan, W. K., Briercheck, E. L., Hughes, T., Scoville, S. D., Pitarresi, J. R., Chen, C., Manz, S., Wu, L.-C., Zhang, J., Ostrowski, M. C., Freud, A. G., … Yu, J. (2017). IL-18 Drives ILC3 Proliferation and Promotes IL-22 Production via NF-κB. *The Journal of Immunology*, *199*(7), 2333–2342. https://doi.org/10.4049/jimmunol.1601554

Victorino, F., Sojka, D. K., Brodsky, K. S., McNamee, E. N., Masterson, J. C., Homann, D., Yokoyama, W. M., Eltzschig, H. K., & Clambey, E. T. (2015). Tissue-Resident NK Cells Mediate Ischemic Kidney Injury and Are Not Depleted by Anti–Asialo-GM1 Antibody. *The Journal of Immunology*, *195*(10), 4973–4985. https://doi.org/10.4049/jimmunol.1500651

Vivier, E., Artis, D., Colonna, M., Diefenbach, A., di Santo, J. P., Eberl, G., Koyasu, S., Locksley, R. M., McKenzie, A. N. J., Mebius, R. E., Powrie, F., & Spits, H. (2018). Innate Lymphoid Cells: 10 Years On. *Cell*, *174*(5), 1054–1066. https://doi.org/10.1016/j.cell.2018.07.017

Vliegenthart, A., Kimmitt, R., Seymour, J., Homer, N., Clarke, J., Eddleston, M., Gray, A., Wood, D., Dargan, P., Cooper, J., Antoine, D., Webb, D., Lewis, S., Bateman, D., & Dear, J. (2017). Circulating acetaminophen metabolites are toxicokinetic biomarkers of acute liver injury. *Clinical Pharmacology & Therapeutics*, *101*(4), 531–540. https://doi.org/10.1002/cpt.541

Vohr, H.-W. (2010). *Toxikologie – Band 1: Grundlage der Toxikologie*. WILEYVCH Verlag GmbH & Co KGaA Weinheim.

Walzer, T., Bléry, M., Chaix, J., Fuseri, N., Chasson, L., Robbins, S. H., Jaeger, S., André, P., Gauthier, L., Daniel, L., Chemin, K., Morel, Y., Dalod, M., Imbert, J., Pierres, M.,

Moretta, A., Romagné, F., & Vivier, E. (2007). Identification, activation, and selective *in vivo* ablation of mouse NK cells via NKp46. *Proceedings of the National Academy of Sciences*, *104*(9), 3384–3389. https://doi.org/10.1073/pnas.0609692104

Wang, H., Shen, L., Sun, X., Liu, F., Feng, W., Jiang, C., Chu, X., Ye, X., Jiang, C., Wang, Y., Zhang, P., Zang, M., Zhu, D., & Bi, Y. (2019). Adipose group 1 innate lymphoid cells promote adipose tissue fibrosis and diabetes in obesity. *Nature Communications*, *10*(1), 3254. https://doi.org/10.1038/s41467-019-11270-1

Wang, X., Peng, H., Cong, J., Wang, X., Lian, Z., Wei, H., Sun, R., & Tian, Z. (2018). Memory formation and long-term maintenance of IL-7Rα+ ILC1s via a lymph node-liver axis. *Nature Communications*, *9*(1), 4854. https://doi.org/10.1038/s41467-018-07405-5

Wang, X., Peng, H., & Tian, Z. (2019). Innate lymphoid cell memory. *Cellular & Molecular Immunology*, *16*(5), 423–429. https://doi.org/10.1038/s41423-019-0212-6

Wang, X., Tian, Z., & Peng, H. (2020). Tissue-resident memory-like ILCs: innate counterparts of TRM cells. *Protein & Cell*, *11*(2), 85–96. https://doi.org/10.1007/s13238-019-0647-7

Wang, Y., Dong, W., Zhang, Y., Caligiuri, M. A., & Yu, J. (2018). Dependence of innate lymphoid cell 1 development on NKp46. *PLOS Biology*, *16*(4), e2004867. https://doi.org/10.1371/journal.pbio.2004867

Wang, Y., & Zhang, C. (2019). The Roles of Liver-Resident Lymphocytes in Liver Diseases. *Frontiers in Immunology*, *10*. https://doi.org/10.3389/fimmu.2019.01582

Watzl, C. (2014). *How to Trigger a Killer* (pp. 137–170). https://doi.org/10.1016/B978-0-12-800147-9.00005-4

Weber, L. W. D., Boll, M., & Stampfl, A. (2003). Hepatotoxicity and Mechanism of Action of Haloalkanes: Carbon Tetrachloride as a Toxicological Model. *Critical Reviews in Toxicology*, *33*(2), 105–136. https://doi.org/10.1080/713611034

Welsch. (2010). *Lehrbuch Histologie* (Vol. 3). Urban & Fischer Verlag.

Wight, A., Mahmoud, A. B., Scur, M., Tu, M. M., Rahim, M. M. A., Sad, S., & Makrigiannis, A. P. (2018). Critical role for the Ly49 family of class I MHC receptors in adaptive natural killer cell responses. *Proceedings of the National Academy of Sciences*, *115*(45), 11579–11584. https://doi.org/10.1073/pnas.1722374115

Williams, M. A., & Bevan, M. J. (2007). Effector and Memory CTL Differentiation. *Annual Review of Immunology*, *25*(1), 171–192. https://doi.org/10.1146/annurev.immunol.25.022106.141548

Wiltrout, R. H., Santoni, A., Peterson, E. S., Knott, D. C., Overton, W. R., Herberman, R. B., & Holden, H. T. (1985). Reactivity of Anti-Asialo GM $_1$ Serum With Tumoricidal and Non-Tumoricidal Mouse Macrophages. *Journal of Leukocyte Biology*, *37*(5), 597–614. https://doi.org/10.1002/jlb.37.5.597

Woolbright, B. (2017). The impact of sterile inflammation in acute liver injury. *Journal of Clinical and Translational Research*. https://doi.org/10.18053/jctres.03.2017S1.003

Woolbright, B. L., & Jaeschke, H. (2015). Sterile inflammation in acute liver injury: myth or mystery? *Expert Review of Gastroenterology & Hepatology*, *9*(8), 1027–1029. https://doi.org/10.1586/17474124.2015.1060855

Yamashita, Y., Imai, K., Mima, K., Nakagawa, S., Hashimoto, D., Chikamoto, A., & Baba, H. (2017). Idiosyncratic drug-induced liver injury: A short review. *Hepatology Communications*, *1*(6), 494–500. https://doi.org/10.1002/hep4.1064

Yang, P., Wang, Y., Tang, W., Sun, W., Ma, Y., Lin, S., Jing, J., Jiang, L., Shi, H., Song, Z., & Yu, L. (2020). Western diet induces severe nonalcoholic steatohepatitis, ductular reaction, and hepatic fibrosis in liver CGI-58 knockout mice. *Scientific Reports*, *10*(1), 4701. https://doi.org/10.1038/s41598-020-61473-6

Yang, S., Tian, Z., Wu, Y., van Velkinburgh, J. C., & Ni, B. (2015). Pivotal Roles of ILCs in Hepatic Diseases. *International Reviews of Immunology*, *34*(6), 509–522. https://doi.org/10.3109/08830185.2015.1008631

Yomogida, K., Bigley, T. M., Trsan, T., Gilfillan, S., Cella, M., Yokoyama, W. M., Egawa, T., & Colonna, M. (2021). Hobit confers tissue-dependent programs to type 1 innate lymphoid cells. *Proceedings of the National Academy of Sciences*, *118*(50), e2117965118. https://doi.org/10.1073/pnas.2117965118

Yoon, H., Kim, T. S., & Braciale, T. J. (2010). The Cell Cycle Time of CD8+ T Cells Responding In Vivo Is Controlled by the Type of Antigenic Stimulus. *PLoS ONE*, *5*(11), e15423. https://doi.org/10.1371/journal.pone.0015423

Yoon, H., Legge, K. L., Sung, S. J., & Braciale, T. J. (2007). Sequential Activation of CD8 $^{+}$ T Cells in the Draining Lymph Nodes in Response to Pulmonary Virus Infection. *The Journal of Immunology*, *179*(1), 391–399. https://doi.org/10.4049/jimmunol.179.1.391

Yoon, K. W. (2017). Dead cell phagocytosis and innate immune checkpoint. *BMB Reports*, *50*(10), 496–503. https://doi.org/10.5483/BMBRep.2017.50.10.147

Yu, J., Freud, A. G., & Caligiuri, M. A. (2013). Location and cellular stages of natural killer cell development. *Trends in Immunology*, *34*(12), 573–582. https://doi.org/10.1016/j.it.2013.07.005

Zhang, C.-Y., Yuan, W.-G., He, P., Lei, J.-H., & Wang, C.-X. (2016). Liver fibrosis and hepatic stellate cells: Etiology, pathological hallmarks and therapeutic targets. *World Journal of Gastroenterology*, *22*(48), 10512. https://doi.org/10.3748/wjg.v22.i48.10512

Zhang, J., Wang, Z., Huo, D., & Shao, Y. (2018). Consumption of Goats' Milk Protects Mice From Carbon Tetrachloride-Induced Acute Hepatic Injury and Improves the Associated Gut Microbiota Imbalance. *Frontiers in Immunology*, *9*. https://doi.org/10.3389/fimmu.2018.01034

Zhang, Y., Tang, J., Tian, Z., van Velkinburgh, J. C., Song, J., Wu, Y., & Ni, B. (2016). Innate Lymphoid Cells: A Promising New Regulator in Fibrotic Diseases. *International Reviews of Immunology*, *35*(5), 399–414. https://doi.org/10.3109/08830185.2015.1068304

ZHAO, X., QIAN, Y., LI, G.-J., & TAN, J. (2015). Preventive effects of the polysaccharide of Larimichthys crocea swim bladder on carbon tetrachloride (CCl4)-induced hepatic damage. *Chinese Journal of Natural Medicines*, *13*(7), 521–528. https://doi.org/10.1016/S1875-5364(15)30046-7

Zhou, W.-C. (2014). Pathogenesis of liver cirrhosis. *World Journal of Gastroenterology*, *20*(23), 7312. https://doi.org/10.3748/wjg.v20.i23.7312

Zuñiga-Aguilar, E., & Ramírez-Fernández, O. (2022). Fibrosis and hepatic regeneration mechanism. *Translational Gastroenterology and Hepatology*, *7*, 9–9. https://doi.org/10.21037/tgh.2020.02.21

6. LIST OF FIGURES

7. LIST OF TABLES

8. ACKNOWLEDGEMENT

The time as a PhD student and working on this thesis were challenging and would not have been possible without the support and guidance of many people.

First and foremost, I must thank my supervisors **Prof. Dr. Carsten Watzl** and **Prof. Dr. Jan Hengstler** for their outstanding support, both professional and personal. They constantly enable unremitting work on different projects by connecting the two disciplines of Immunology and Toxicology. They always lent an ear to listen to my results and asked critical questions to support me. Their ideas, guidance, support and suggestions did not only contribute significantly to the completion of this thesis, but also to my personal growth and development as a scientist.
Dear Carsten, thank you for giving me the opportunity to work in your laboratory. Your encouragement, trust in my abilities, patience, and advices helped me to navigate through difficult times of the projects and to never loose trust in my abilities. The meaning of an advisor highly fits to you.
Dear Prof. Hengstler, without your support, guidance and contagious enthusiasm for research during my bachelor and master thesis, I would never have considered to start my PhD. You taught me to think out of the box, and what it means to deliver excellent research. Thank you!

Furthermore, I would like to address special thanks to **Katharina Belgasmi** who did not only stand up early to help me with the mice collection and performing perfusions, but also provided answers to nearly every problem. Without her, I would probably still stand in the laboratory. Together with **Dr. Daniela González** and **Dr. Maiju Myllys**, we are not only colleagues, but also friends. Thank you for all the shared moments of laughter and fun, for listening, supporting, helping and for simply being there. In addition, I would like to thank the LivTox guys, **David Feuerborn** and **Dr. Patrick Nell** for the helpful discussions, inspirations and especially their sense of humor.

Moreover, I am grateful to **Dr. Maren Claus** for the careful proof-reading of this thesis and in general for her help. Thanks for the support, research advices and the help with technical problems. If she would not have laid her magical hands on the flow cytometers, I am not sure if they would still remain in the laboratory.

Special thanks to **Lea Picard**, **Martin Obholzer**, **Vivian Bönnemann** and **Dr. Isabel Uhlenbrock** for all your help, advices, sarcasm and your careful proof-reading.

I would also like to show gratitude to the collaboration partners **Prof. Dr. Georg Gasteiger** and **Dr. Christin Friedrich** who enabled the work with the Hobit mice and helped me to look from a different perspective and interpreted some of the wired ILC1 results.

Many thanks to **Elmar Kriek** for his support regarding the mice handling, organization and taking good care.

During my time at the IfADo, I got to know and worked with a lot of people. They did not only help and support me; they also created a good working atmosphere. Therefore, my gratitude to the members of the Watzl lab and the toxicology department.

Most importantly, none of this could have happened without my family and friends.
I would especially like to thank my parents and my husband for their endless love, support, courage, assistance, strength, patience and all their motivating, cheering and sometimes clear words. You are always there for me and always have my back. Thank you!